Human population history and its interplay with natural selection

Veronika Siska

Department of Zoology

University of Cambridge

This dissertation is submitted for the degree of

Doctor of Philosophy

Trinity College 2018 September

Human population history and its interplay with natural selection

Veronika Siska

Summary

The complex demographic changes that underlie the expansion of anatomically modern humans out of Africa have important consequences on the dynamics of natural selection and our ability to detect it. In this thesis, I aimed to refine our knowledge on human population history using ancient genomes, and then used a climate-informed, spatially explicit framework to explore the interplay between complex demographies and selection.

I first analysed a high-coverage genome from Upper Palaeolithic Romania from ~37.8 kya, and demonstrated an early diversification of multiple lineages shortly after the out-of-Africa expansion (Chapter 2). I then investigated Late Upper Palaeolithic (~13.3ky old) and Mesolithic (~9.7 ky old) samples from the Caucasus and a Late Upper Palaeolithic (~13.7ky old) sample from Western Europe, and found that these two groups belong to distinct lineages that also diverged shortly after the out of Africa, ~45-60 ky ago (Chapter 3). Finally, I used East Asian samples from ~7.7ky ago to show that there has been a greater degree of genetic continuity in this region compared to Europe (Chapter 4).

In the second part of my thesis, I used a climate-informed, spatially explicit demographic model that captures the out-of-Africa expansion to explore natural selection. I first investigated whether the model can represent the confounding effect of demography on selection statistics, when applied to neutral part of the genome (Chapter 5). Whilst the overlap between different selection statistics was somewhat underestimated by the model, the relationship between signals from different populations is generally well-captured. I then modelled natural selection in the same framework and investigated the spatial distribution of two genetic variants associated with a protective effect against malaria, sickle-cell anaemia and β^0 thalassemia (Chapter 6). I found that although this model can reproduce the disjoint ranges of different variants typical of the former, it is incompatible with overlapping distributions characteristic of the latter. Furthermore, our model is compatible with the inferred single origin of sickle-cell disease in most regions, but it can not reproduce the presence of this disorder in India without long-distance migrations.

Declaration

This dissertation is the result of my own work and includes nothing which is the outcome of work done in collaboration except as declared in the Preface and specified in the text.

It is not substantially the same as any that I have submitted, or, is being concurrently submitted for a degree or diploma or other qualification at the University of Cambridge or any other University or similar institution except as specified in the text.

I further state that no substantial part of my dissertation has already been submitted, or, is being concurrently submitted for any such degree, diploma or other qualification at the University of Cambridge or any other University or similar institution.

The main text does not exceed the prescribed word limit for the relevant Degree Committee (School of Biology).

Veronika Siska

2018 September

Acknowledgements

I would like to give my thanks to the many people in many countries who I met through my PhD journey and without whom the work presented in this thesis would not have been possible.

First and foremost, I would like to thank my supervisor, Andrea Manica. Thank you for your continuous support, your understanding and your advice in both academic matters and regarding general life issues. Thank you also for your trust and for giving me the freedom to explore my ideas. I am also grateful for the continuous support of the postdocs in our group – without them, this PhD would have been a very lonely experience. Thank you, Eppie, for your guidance on ancient DNA, for my first, fully positive experience about collaborative research, and for your incredible support when I was searching for my path. I also want to thank Anders for creating the model I could build on; Pier for his warm support (especially in the last, frantic period) and the many useful discussions and Mario and Robert for their effort on modelling. I would like to also thank my advisors, Chris Jiggins and John Welch for insightful comments on my project. Another warm thank goes to those who have given their time to read through my thesis and make sure it is actually in English: to Philipp, Eppie, Pier, Anne-Sophie and Riva.

I am also grateful for all of the organisations who supported me. The Gates Cambridge Trust provided the financial basis that enabled me to conduct this research and attend conferences. Even more importantly, the Trust provided a stimulating environment through workshops on general humanitarian and personal development topics and by acting as a platform to meet with like-minded scholars. I also would like to thank the Cambridge Philosophical Society for their financial help in the last year of my PhD studies. Lastly, living in Cambridge would not have been such an incredible, unique experience without my college, Trinity, who not only helped me financially, but was also my home for over three years. In particular, the support of my college tutor, David Spring, the lively discussions over dinner on the Trinity Biology Seminars and the warmth and helpfulness of every member of the college staff made me feel welcome in Cambridge and at Trinity College.

The Department of Zoology and the Evolutionary Ecology Lab provided the basis of all of my academic work. The frequent coffee breaks, happy hours, talks showcasing various animals and the odd lunch meeting created a lovely working space. I am grateful for the staff to make all of our work possible and feel honoured to have met so many incredible people at Zoology: Riva, Anne-Sophie, Eppie, Pier, Anahit, Robert, Mario, Tim, Anders, Maddie, Maanasa, Lizzie, Alison, James, Jim, Arne and so many others. Such an environment made it possible to keep focused and bounce back at the inevitable downs - I will miss everyone!

I also would like to thank my friends who had my back through these exciting, but often challenging years. In Cambridge, Anne-Sophie helped me manage my own expectations and demonstrated that work-life balance is possible, Riva showed what being passionate about a research topic really is like and Young Mi was always there when things were not going according to plan. Another warm thanks goes to David for his support; Konrad for helping me find a job; Daniel, Tim and Lawrence, my climbing companions, and to all the friendly Trinitarians, Zoologists and other Cambridge residents I've met. Special thanks to all of my friends in Budapest who made the effort to keep in touch with me through my ever-changing life, visited me and met with me at home: Péter, Szilvi, Laura, Bence and Bálint kept me in touch with "real life" beyond Cambridge. Finally, I am eternally grateful for my family for supporting me in a foreign environment and for giving me the strong roots that I could rely on.

This PhD was an incredible journey leading to new destinations. I would like to dedicate my thesis to those closest to me who helped me find my own way: to my parents, Éva and Péter, and to my partner, Philipp.

Contents

Contents vi

Chapter 1 General introduction 11

1.1 History of anatomically modern humans 11

1.1.1 Evolution of anatomically modern humans 11

1.1.2 The expansion of anatomically modern humans out of Africa 13

1.1.3 Neolithic transition 15

1.2 Genome sequencing 16

1.2.1 Introduction to genome sequencing 16

1.2.2 Ancient DNA 17

1.3 Modelling 19

1.3.1 Demography 19

1.3.2 Genetics 20

1.4 Natural selection 22

1.4.1 Introduction to natural selection 22

1.4.2 Confounding effects 23

1.5 Bibliography 24

Chapter 2 Palaeolithic Oase genome implies diversification and extinction events across Eurasia 32

2.1 Abstract 32

2.2 Contribution 33

2.3 Introduction 33

2.4 Results 36

2.4.1 DNA extraction, sequencing and authentification 36

2.4.2 Mitochondrial haplogroup assignment 38

2.4.3 Comparison of Oase 1 and Oase 2 39

2.4.4 Neanderthal ancestry 42

2.4.5 Comparison of Oase 2 and other modern and ancient samples 44

2.4.6 African origins 45

2.4.7 Demographic analysis on high-quality Upper Palaeolithic genomes 47
2.5 Conclusions 50
2.6 Methods 52
2.6.1 DNA extraction and library preparation 52
2.6.2 Processing and mapping of NGS data 54
2.6.3 Mitochondrial DNA 55
2.6.4 Authenticity of ancient DNA molecules 55
2.6.5 SNP calling and merging with reference panel 56
2.6.6 Calculating statistics 56
2.6.7 G-PhoCS analysis for Oase 58
2.7 Bibliography 63
Chapter 3 Upper Palaeolithic genomes reveal deep roots of modern Eurasians 69
3.1 Abstract 69
3.2 Contribution 70
3.3 Introduction 70
3.4 Results 72
3.4.1 Samples, sequencing and authenticity 72
3.4.2 Continuity across the Palaeolithic-Mesolithic boundary 72
3.4.3 Deep coalescence of early Holocene lineages 75
3.4.4 Caucasus hunter-gatherer contribution to subsequent populations 80
3.4.5 CHG origins of migrating Early Bronze Age herders 82
3.4.6 Modern impact of CHG ancestry 84
3.5 Conclusions 84
3.6 Methods 86
3.6.1 Sample preparation and DNA sequencing 86
3.6.2 Sequence processing and alignment 86
3.6.3 Authenticity of results 87
3.6.4 Molecular sex and uniparental haplogroups 90
3.6.5 Merging ancient data with published data 92
3.6.6 Population genetic analyses 95
3.6.7 Dating split times using G-PhoCS. 100
3.6.8 Runs of homozygosity 105
3.6.9 Phenotypes of interest 107
3.7 Bibliography 109

Chapter 4 Genome-wide data from two early Neolithic East Asian individuals dating to 7,700 years ago 119
4.1 Abstract 119
4.2 Contribution 120
4.3 Introduction 120
4.4 Results 121
4.4.1 Samples, sequencing and authenticity 121
4.4.2 Relation to modern populations 123
4.4.3 Relation to ancient genomes from Asia 128
4.4.4 Continuity between Devil's Gate and the Ulchi 128
4.4.5 Southern and Northern genetic material in the Japanese and the Korean........130
4.4.6 Phenotypic prediction 133
4.5 Conclusions 133
4.6 Methods 134
4.6.1 Experimental Design 134
4.6.2 Statistical Analysis 137
4.7 Bibliography 144
Chapter 5 Behaviour of selection statistics in a spatially explicit, neutral demographic model 153
5.1 Abstract 153
5.2 Contribution 154
5.3 Introduction 154
5.4 Methods 157
5.4.1 Spatially explicit demographic model 157
5.4.2 Refitting the model 160
5.4.3 Overlap between different statistics 169
5.5 Results 173
5.5.1 Refitting the model 173
5.5.2 Overlap between different statistics and populations 175
5.6 Discussion 183
5.7 Bibliography 184
Chapter 6 Explaining spatial patterns of adaptation against malaria....................188
6.1 Abstract 188
6.2 Contribution 189
6.3 Introduction 189

6.3.1 Malaria and protective genetic disorders 189
6.3.2 Variants of protective disorders 190
6.3.3 Aim of this study 191
6.4 Methods 192
6.4.1 Model 192
6.4.2 Data 195
6.4.3 Inferring haplotype origins 202
6.4.4 Single-origin hypothesis of sickle-cell disease 203
6.5 Results 204
6.5.1 Inferring haplotype origins 204
6.5.2 Qualitative spatial patterns 209
6.5.3 Single-origin hypothesis of sickle-cell anaemia 212
6.6 Discussion 213
6.6.1 Results 213
6.6.2 Limitations 214
6.6.3 Perspectives 216
6.6.4 Summary 216
6.7 Bibliography 217
Chapter 7 Epilogue 222
7.1 Introduction 222
7.2 aDNA and its use in uncovering demographic processes 223
7.2.1 Introduction 223
7.2.2 Broad and deep sampling 223
7.2.3 Increase in data volume and issues of compatibility 225
7.2.4 Data-driven projects 225
7.3 Continuity and extinctions in human evolution 226
7.3.1 Introduction 226
7.3.2 Extinctions and lineages 226
7.3.3 Definition of continuity 227
7.4 Importance of space in modelling 228
7.4.1 Advantages 228
7.4.2 Disadvantages 228
7.5 Concluding remarks 229
7.6 Bibliography 230

Appendix A Appendix for Chapter 2 ... 234
A.1 NGS sequencing statistics ... 234
A.2 Mitochondrial genome ... 237
A.3 Outgroup f_3 statistics for Oase 1 using modern populations ... 238
A.4 Outgroup f_3 statistics for Oase 2 on SNPs called in Oase 1 ... 239
A.5 African origins ... 241
A.6 Comparison of Upper Palaeolithic genomes using D statistics ... 248
A.7 Convergence of G-PhoCS Monte Carlo chains ... 250
A.8 Detailed G-PhoCS results ... 254
Appendix B Appendix for Chapter 3 ... 260
B.1 Archaeological context ... 260
B.1.1 Kotias Klde ... 260
B.1.2 Satsurblia ... 262
B.1.3 Grotte du Bichon ... 263
B.2 Supplementary figures ... 265
B.3 Supplementary tables ... 272
Appendix C Appendix for Chapter 4 ... 292
C.1 Osteology ... 292
C.2 Archaeology ... 293
C.3 Phenotypic prediction ... 294
C.4 Supplementary figures ... 297
C.5 Supplementary tables ... 311
Appendix D Appendix for Chapter 5 ... 346
D.1 Relationship between potential ABC summary statistics ... 346
Appendix E Appendix for Chapter 6 ... 353
E.1 Fit using SSE for thalassemia ... 353
E.2 Sensitivity analysis ... 356
E.2.1 Selection coefficient ... 357
E.2.2 Demographic parameters ... 358
E.2.3 Starting time of selection ... 360

Chapter 1 General introduction

1.1 History of anatomically modern humans

1.1.1 Evolution of anatomically modern humans

Anatomically modern humans evolved through a long and non-linear process, starting with the separation of the hominins (species closer to humans than to the closest relative, the chimpanzee). The current, widely accepted model of hominin origins is termed “Out of Asia”: according to this, apes evolved in Africa and then dispersed over Eurasia in the Middle Miocene, once a landbridge was established. Climate change then lead to the disappearance of primitive apes from Africa (by roughly 9 million years ago), until its recolonization in the Late Miocene (roughly 4-8 million years ago)[1,2]. These modern apes then evolved into diverse groups through a so-called adaptive dispersal, since they were faced with a new, heterogeneous environment following climate change (e.g. forest cover breaking up)[3]. In this view, hominins were just one of the resulting groups, together with other African apes like gorillas or chimpanzees.

A combination of fossil evidence, genetics and paleoclimate reconstructions support this “Out of Asia” model of hominin origins[1,2]. Palaeontology provides evidence for when different clades appeared and how they were related morphologically, genetics establishes their phylogenetic relation, and past climate dates when the necessary land-bridge existed and when the climate changed. Genetics was crucial to disentangle the relationship between hominins and African apes, supporting that hominins and chimpanzees form a clade, as opposed to earlier models that placed all non-hominin apes into one clade based on their morphology.

However, the timing and process of the separation of hominins and other apes is far from clear. Palaeontology struggles with a combination of sparsity and unclear classification of fossil specimens, carrying a mosaic of archaic and modern morphological features. Regarding genetics, we can only rely on the difference between living species due to a lack of genetic data from ancient hominins[1,2]. Based on modern genetic data, the separation occurred around 6 million years ago, but a large variation of estimated divergence times between humans and chimpanzees across the genome and a shorter divergence time on the X chromosome was inferred[4]. This could be due to incomplete lineage sorting[5], the different mutation rate of the X chromosome[5,6] and/or natural selection acting differentially[6], but could also be the sign of a complex speciation-hybridisation process as opposed to a clean split[4] ().

After the separation of the hominin clade, a long and winding evolutionary road leads to the genus Homo, following the same pattern of complex relationships among different taxa. There is no clear definition of the genus Homo, but broadly speaking, members of the family are those either ancestral to or closely related to modern humans. There is an observed, continual increase in cranial capacity throughout the evolution of the genus, which is also associated with the advent of tool use[2]. These signs separate them from their ancestors, the early hominins and Australopithecines, as well as the robust Australopithecines who took an alternative evolutionary path and did not leave any present-day descendants.

Classification of the Homo genus into species and subspecies is challenging, due to incomplete information and complex relationships within the genus; I here present the summary of a widely accepted view[1,2]. The first accepted species is *Homo habilis*, the initiators of tool use, with an evolutionary history in Africa. This species is followed by the more human-like *Homo ergaster* in Africa and the *Homo erectus* inside and outside Africa, with even more derived features. According to the currently most accepted view, *Homo erectus* evolved through a radiation out of Africa, where *Homo ergaster* was its ancestral or sister species. *Homo erectus* then spread over Eurasia and separated into diverse groups with different variants inhabiting different areas, from Spain and Georgia all the way to South-East Asia. However, the classification of these variants is still debated: whether they are separate species, ancestral to each other, or simply regional variants originating from the same dispersal event remains unclear. What we know for certain is that they represent a wide range of morphological variation, but due to the limited number of remains in each group, it is difficult to judge the level of differentiation.

Homo heidelbergensis appeared around 700kya[2]. They reached the range of cranial capacity of anatomically modern humans and possessed material culture hardly distinguishable from that of early *Homo sapiens*, including tool use and even signs of social structures, such as care of the old or infirm or interpersonal violence. The evolution and classification of *Homo heidelbergensis* mimic that of *Homo erectus*, with unclear boundaries between groups, a plausible origin in Africa, a successive spread over Eurasia and divergent evolution in geographically different areas. Neanderthals and Denisovans in Eurasia, and *Homo sapiens*, also called anatomically modern humans (AMHs) in Africa are all thought to have evolved from *Homo heidelbergensis*, with African and Eurasian groups possibly separated due to climatic changes (an arid phase in the Near East)[2].

1.1.2 The expansion of anatomically modern humans out of Africa

Evidence for the African origin of *Homo sapiens* comes from a combination of archaeology and genetics. The earliest fossils classified as Homo sapiens all originate from Africa Omo Valley, Ethiopia ~190kya[7], Herto, Ethiopia ~160kya[8] and Pinnacle Point, South Africa ~164kya[9]). However, the recent dating to ~300kya of a *Homo sapiens* fossil from Jebel Irhoud, Morocco[10,11], implies that modern humans may have evolved earlier and could have had a wider distribution than previously thought. In contrast, the earliest fossils outside Africa is only 92kya (Skuhl & Quafzeh, Israel[2]), but even those have archaic features and are regarded by many scholars as not directly ancestral to present-day non-Africans. The first finding from outside the Near East is from China (Daoxian teeth ~80kya[12]), followed by archaeological and palaeontological evidence showing that anatomically modern humans spread out from Africa from 60kya onwards, reaching all corners of Eurasia by about 45kya[13–15] and crossing into the Sahul somewhere between 60kya and 40kya[14].

Genetics played a crucial role in establishing the African origin of anatomically modern humans. The first line of evidence comes from the present-day diversity of uniparental haplotypes (mtDNA[16,17] and Y-chromosome[17,18]), which date last common ancestor to between 200 and 130kya, before the appearance of modern human fossils outside Africa. These dates rely heavily on estimates of the mutation rate, which provide the conversion between mutational distance and time. However, by now, accurate estimates are available using Next-Generation Sequencing data for the Y chromosome[19] and ancient data for mtDNA[20]. Second, the modern-day non-African genetic diversity lies within that of Africans, both regarding uniparental markers and the nuclear genome. Therefore, populations within Africa carry the deepest separations, with the oldest (more than 100kya) separating the South African Khoe San people from all other populations[19]. Last, genetic diversity on mtDNA[21] and nuclear markers[22,23], but even phenotypic diversity estimated based on cranial metrics[22,24], decreases with distance from Africa. This pattern of decreasing diversity with distance from the origin is typical after the expansion of a species.

Many aspects of the exit out of Africa are well understood. The most commonly accepted timing is around 50-60 kya, supported by the appearance of unambiguously classified *Homo sapiens* fossils outside of Africa[2], the times to the common origin of non-African mtDNA[25] haplogroups, as well as estimated exit times based on modelling using nuclear genetic diversity[26,27]. Furthermore, this period coincides with a window of climate favourable for humans in the otherwise arid and impassable Arabian peninsula around 60-70kya[27].

However, there are also several aspects of the so-called Out-of-Africa event that remain unclear. First, there is a possibility of earlier exit(s) out of Africa, which are difficult to detect if they were overwhelmed by a subsequent larger wave. There was a favourable climatic window about 130kya, accompanied by a similarity in lithics inside and outside of Africa[28] and some genetic studies also point to a small amount of genetic material from such an early wave in Papuans[29]. However, other studies, also including samples from the same region, failed to reject the single-wave scenario[30,31], and the broad pattern of diversity in non-African populations is also consistent with a single expansion wave[22,27]. This implies that anatomically modern humans (AMHs) mainly originate from a single wave, which could have been preceded by a smaller one. Chapter 2 explores the diversity of AMHs in Eurasia shortly after the main wave out of Africa in light of a ~37.8 ky old genome from present-day Romania.

The relationship between modern and archaic humans (Neanderthals and Denisovans, the latter only known by its DNA) is an additional debated point in the early evolution of AMHs. Certain modern-day non-Africans show an increased affinity to Neanderthals[32,33] and Denisovans[34]. Neanderthal ancestry is estimated at roughly 1.5-2.1 in all non-Africans[33], whereas Denisovan ancestry is estimated at around 2-4% in Oceania[35] and Melanesia[36]. However, it is also possible that substructure within Africa[37] or a difference in mutation rates between modern Africans and non-Africans[38] can explain at least part of this signal.

1.1.3 Neolithic transition

After the spread of humans out of Africa, a structured population of hunter-gatherers existed all over Eurasia. In addition to their cultural relations from archaeological studies, we are now starting to understand their genetic composition, with the help of ancient genomes. There is genetic material available from Eurasia in the Upper Paleolithic, the period stretching from the dispersal of anatomically modern humans out of Africa until the advent of the Holocene roughly 10 kya. Some samples are associated with different groups of modern populations (e.g. Europeans[39–41], East Asians[42], Native Americans[43] or Central Asians from the Caucasus[40]), but others did not seem to contribute substantially to extant populations

(Ust'Ishim from Asia[44] and several European samples from 40-30,000 years ago[41,45]). Chapter 3 explores data from one of the early European lineages that appear to be a dead end, whereas Chapter 4 presents an Upper Paleolithic lineage that left its footprint on modern populations across Eurasia.

The next large shift in the history of anatomically modern humans was brought by the so-called Neolithic transition, coinciding with the beginning of the Holocene in West Eurasia and characterised by the advent of agriculture, industrial developments (pottery, textile) and a sedentary lifestyle. The transition is well-studied in archaeology, but genetic data is necessary to determine the extent to which the Neolithic spread through cultural transmission or the movement of people. Ancient genomes have revealed a major population replacement in West Eurasia during the transition from hunting-gathering to agriculture from ~10.5 kya onwards, followed by a progressive "resurgence" of local hunter-gatherer population ancestry and later, coinciding with the advent of the Bronze age ~5.5 kya, a major contribution from the Asian Steppe[39,46]. The process in Asia is less well-known: archaeology shows multiple origins of the Neolithic and a lack of the strong association between its components (pottery, farming and animal husbandry) that was observed in Europe, but ancient DNA is still missing from the relevant time period in the region. In Chapter 5, I analyse such data and explore its implications on the Neolithic transition on the northern periphery of East Asia.

1.2 Genome sequencing

1.2.1 Introduction to genome sequencing

One of the main sources of information on human population history is genetic data. The genetic data used in this thesis is mainly the sequence of DNA from the 22 nuclear chromosomes, the sex chromosomes and the mitochondrial chromosome, encoded in a four-letter alphabet of base pairs. In the case of whole-genome sequencing, we are interested in all positions, but one can also focus on only single nucleotides at given polymorphic positions (single nucleotide polymorphisms or SNPs).

The process of determining the DNA sequence is called sequencing. The most common technology used nowadays is Next-Generation Sequencing (NGS)[47], where the target sequence is broken up into pieces and then amplified before the base pairs are determined (in other words, the sequence is read). These short, generally 50-100 base pair long segments (reads) are then mapped (aligned) to the sequence of the organism in question (the reference sequence), according to where they fit well. Finally, the bases that the sample most likely had at locations of interest (genotypes) can be determined.

1.2.2 Ancient DNA

Sequencing ancient DNA (aDNA), that is, DNA from specimens not preserved for DNA analysis (e.g. bones from archaeological sites, mummies, hair, tissues from the permafrost) is technologically challenging. The first such study in 1984 reported DNA traces from an ancient horse species, the Quagga, sampled over 150 years after the organism's death[48]. Unfortunately several early ancient DNA studies proved to be only contamination, including claims of obtaining DNA from a dinosaur[49]. These false positives, together with the laborious process of sequencing DNA at the time before NGS, hindered advances in the field[50–52]. However, with technological progress and rigorous laboratory procedures, it became possible to routinely sequence ancient DNA; first from the abundantly available mitochondria and later also from the nuclear genome. The age of sequenced samples is continuously pushed back: the oldest sequenced sample to date is a horse from the permafrost that lived over half a million years ago[53], but several modern[44] and ancient[33,35] hominins over 40,000 years-old have also been sequenced.

There are three main families of problems that make the sequencing of ancient DNA challenging[50–52]. First, as DNA breaks down, the segments get shorter. With NGS, these segments can be sequenced, but the difficulty of alignment increases with decreasing segment length. Even intermediate read lengths make de novo assembly impossible, and parts of the genome that are particularly difficult to align to (e.g. repetitive regions) become inaccessible. At even shorter read lengths, any kind of alignment becomes infeasible. Second, chemical processes, deamination in particular, can change the sequence and cause spurious mutations, especially at the end of the fragments. Third, contamination leads to only a small proportion of the DNA originating from the ancient specimen. Including these fragments in the analysis can lead to erroneous conclusions, and they are especially difficult to filter out if the ancient sample is contaminated by modern DNA of the same or similar species.

There are several ways to assess the quality of ancient genomes and to deal with the challenges described above. Both fragment length and the presence of deaminated bases at the end of fragments can be used to assess the authenticity of the sample. Afterwards, a minimum read length is usually imposed and the (likely damaged) ends are clipped before further processing. It is also possible to chemically reverse deamination, in which case a small portion of the DNA is kept in its original form for authenticity assessment. Regarding contamination, sequences from organisms different from the sample (e.g. soil bacteria on a human sample) can be separated during alignment on the basis of their low similarity to the target reference sequence. Contamination from modern sources of the same or closely related organism (e.g. humans handling an ancient human sample) is more challenging to handle. In addition to authenticity based on damage patterns, the level of such contamination can be estimated using uniparental markers (by looking at the proportion of sequencing not matching the consensus haplotype) or, for male specimens, using the X chromosome (by looking at polymorphisms).

1.3 Modelling

1.3.1 Demography

The goal of demographic modelling is to provide a simplified framework of demographic processes, such as natural birth and death or population admixture. Such models track the size of populations over time, given the rules governing its change. These models can be discrete or continuous in how they represent population size, space and time. Discrete and continuous models can be each other's approximation and the choice of framework depends on the system studied and the features of its behaviour that one is trying to capture. For instance, a discrete-time model is more suited for a system with separate generations, whereas one with overlapping generations with incremental changes is easier to represent using a continuous-time framework.

Deterministic and stochastic demographic models are fundamentally different in terms of their mathematics, but can be used to model similar systems. Just like with continuous and discrete models, deterministic and stochastic models can be equivalent under certain conditions, and the choice between them depends on the system. Deterministic models are usually easier to handle mathematically and often have a smaller computational footprint, but the effects of stochasticity can be important for certain systems. Natural systems are usually stochastic by nature, but in the case of large systems, where fluctuations even out, a deterministic approximation can be sufficient. However, when the population sizes are low or changes are abrupt (e.g. large fluctuations or small subpopulations), stochastic effects have to be taken into account explicitly.

Population substructure can further complicate demographic models. Real systems are usually not completely homogeneous, but it depends on the level of inhomogeneity whether such substructure can be neglected. There are numerous ways to represent substructure, from toy models consisting of a few separate populations through metapopulation models where populations are connected in a network all the way to complex, spatially explicit frameworks that attempt to capture geographical substructure. However, in addition to the obvious trade-off between simplicity and computational time, fitting the model to the real system also has to be considered. Often there is not enough data to set all parameters in a structured model, even if it is clear that the structure exists. In such cases there are two possibilities: one can either use a simplified model (e.g. only a few populations) or make assumptions about the underlying structure (e.g. assume that inhomogeneities and/or connectivity are a function of a measurable quantity). Simple tree-like models (Chapters 2 and 3) are examples for the former, whereas spatially explicit models with environment-dependent carrying capacities and connectivity (Chapters 5 and 6) for the latter.

1.3.2 Genetics

Once we have a demographic model, we can use it to also study the genetic composition of samples from the population, that is, the DNA sequences of each sample. Depending on the organism, a single individual can contain one (haploid) or two (diploid) sequences, which can change from generation to generation through mutation and recombination. Tracking a certain variant or sequence is equivalent to differentiating between different types of individuals in the population. In addition to the sequences, the relationship between different samples can also be relevant. For instance, for analysis based on genealogical trees (the ancestry tree of sampled genetic markers), we need to track the ancestry of individuals in our demographic model.

The simplest genetic models assume that there are no new mutations and individuals randomly mate with each other (no selection) in an infinite population, with non-overlapping generations. A diploid organism with two alleles in such a model is described by the Hardy-Weinberg model, where frequencies of the three possible diploid genotypes will be constant and only dependent on the frequencies of the two alleles[54].

One of the simplest deviations from the above model is to relax the assumption of an infinite population and instead work with a finite number of discrete individuals. Such a system can be described in a simple stochastic framework, where individuals are still mating randomly within a population, with each offspring originating from two randomly chosen ancestors in the previous generation[54]. The case with non-overlapping populations is described by the Wright-Fisher model, where the whole population is replaced by a new set of individuals in each generation. The other extreme is the Moran model, where generations overlap and only a single individual is replaced by a new one in each step. In both of these models, the change in the number of alleles from generation to generation can be described by a random walk on a bounded interval, and the corresponding mathematical results (time to fixation, diffusion approximation, etc.) apply.

Once we have a model to describe the dynamics of different alleles in a population and a set of samples we are interested in at a given generation, we can build the ancestral relationship between these (genealogical tree). The genealogy can then be used to calculate when the most recent common ancestor between any two samples lived, or to track where a certain mutation occurred and which samples it affects. Observed data generally comes in the form of a set of samples, which can be used to estimate the corresponding genealogies and through that, to make inferences about past population history.

A further complication in a diploid population comes from recombination. Recombination is when the two ancestral sequences are combined to form a diploid sample in the next generation, but with both sequences in the new sample containing material from both of the two ancestral sequences. The process mixes up the genealogical trees from the sequences, resulting in a genealogical network. Furthermore, since recombination only occurs through a set of breakpoints along a sequence, it takes time to de-couple nearby section of the sequence. As a consequence, mutations close to each other on the sequence will occur more frequently together, forming linked sections or haplotypes. Patterns of such haplotypes can also be used to infer the population history of the sample, and are particularly informative on the timing and extent of admixture events between populations[55,56].

1.4 Natural selection

1.4.1 Introduction to natural selection

Natural selection is the main process behind evolution, where individuals better adapted to their environment tend to be more successful in survival and reproducing, thus changing the distribution of heritable biological traits in the population. By studying the dynamics of adaptation to different environments, it is possible to uncover population history, speciation and demonstrate evolution at work (e.g. spread of lactase persistence in humans in response to consuming dairy products[57] or change in pigmentation of peppered moths in response to industrial development[58]). Detecting signals of selection also has important implications for medical applications. Since selection acts on the phenotype, segments under selection are often of functional importance, associated for instance with resistance against pathogens or genetic diseases (e.g. sickle cell trait offering partial protection against malaria[59], deleterious mutation in Siberians originally providing an advantage to a high-fat diet or cold environment[60]). Strong signals of selection in the genome thus have the potential to guide association studies looking for the underlying genetic causes of medical conditions.

There are several different modes in which selection can act. It can be simply directional, where an allele is either advantageous and increases in frequency (positive selection) or the opposite (negative selection). Most new mutations are disadvantageous, leading to constant negative selection against new variants, called background or purifying selection. In non-haploid organisms, selection can also act in more complex ways. Balancing selection favours intermediate frequencies of multiple alleles, for example when the heterozygote is favoured in a diploid organism. The signature of selection in the genome also depends on whether a newly arisen mutation is quickly increasing in frequency (hard sweep) or whether it is an existing variant, part of standing variation, that is becoming favoured (soft sweep). In humans, the spread of lactase persistence in humans in response to pastorialism[57] is a typical example of a sweep, while the HLA locus has long been shown to be under balancing selection[61].

The availability of dense genetic data has made it possible to detect signals of natural selection. Selection can be studied either by directly investigating the time series of occurrence of traits and/or genetic composition (e.g. from experiments or ancient DNA), looking for associations with certain environments, or by studying signatures of past selection in the genome. For humans, long-term experiments are unavailable and the quantity and quality of ancient DNA is just now becoming sufficient to study selection. Two successful examples for the study of selection using ancient DNA are the detection of derived immune and ancestral pigmentation alleles in a single 7,000 year old European hunter-gatherer[62] and direct evidence for selection acting on pigmentation in Europeans during the last 5,000 years[63]. Associations with the environment provide strong indicators (e.g. between latitude and skin pigmentation in humans[64]), but require assumptions about what the important environmental factors are, as well as about past climate and the selected population's history. Furthermore, spatial boundaries between different genetically incompatible variants (alleles neutral on the native background, but disadvantageous when occurring together) tend to become trapped by environmental boundaries even without any kind of selection[65]. Therefore, for humans, most effort has been dedicated to the indirect method of looking for signals of past selection in the genomes from present-day genomes.

1.4.2 Confounding effects

Interpreting the results of indirect methods can be challenging, as they are influenced by the demographic history of the studied populations, including changes in population size, population substructure or admixture[66]. Neutral demographic events can create signals similar to those left by natural selection, making it difficult to assess the significance of any given finding. There are two strategies commonly adopted to deal with this issue: to use a simple demographic model to define the null distribution of the signal of interest in the absence of selection[57,63] or to focus on a fixed quantile (e.g. top 1%) of the loci with strongest signal[60,67–70]. Each of these solutions can be problematic, since simple demographic models often fail to fully capture the confounding processes of interest, and defining a quantile of how much of the genome is under strong selection is arbitrary (and does not really solve the confounding effect of demography). A strong warning of the lack of precision in these methods comes from the low congruence in the sites detected as under selection by different methods – although we also have to keep in mind that some methods are sensitive for different kinds of selection and/or on different timescales than others.

To mitigate the confounding effects, some researchers combine multiple metrics into composite measures to look for regions consistently scoring highly using different methods (e.g. composite likelihood ratio[71]). However, without knowing the correlations between the individual measures and how they relate to different cases of selection, statistical significance still cannot be calculated. In order to disentangle signals of selection from false positives caused by demographic events and assess significance, we would ideally need a more realistic demographic model.

1.5 Bibliography

1. Boyd, R. & Silk, J. B. *How Humans Evolved: Seventh Edition*. (W. W. Norton & Company, 2014).

2. Foley, R. A. & Lewin, R. *Principles of Human Evolution*. (John Wiley & Sons, 2013).

3. Kürschner, W. M., Kvaček, Z. & Dilcher, D. L. The impact of Miocene atmospheric carbon dioxide fluctuations on climate and the evolution of terrestrial ecosystems. *Proc. Natl. Acad. Sci. U. S. A.* **105,** 449–453 (2008).

4. Patterson, N., Richter, D. J., Gnerre, S., Lander, E. S. & Reich, D. Genetic evidence for complex speciation of humans and chimpanzees. *Nature* **441,** 1103–1108 (2006).

5. Barton, N. H. Evolutionary Biology: How Did the Human Species Form? *Curr. Biol.* **16,** R647–R650 (2006).

6. Wakeley, J. Complex speciation of humans and chimpanzees. *Nature* **452,** E3 (2008).

7. McDougall, I., Brown, F. H. & Fleagle, J. G. Stratigraphic placement and age of modern humans from Kibish, Ethiopia. *Nature* **433,** 733–736 (2005).

8. White, T. D. *et al.* Pleistocene Homo sapiens from Middle Awash, Ethiopia. *Nature* **423,** 742–747 (2003).

9. Marean, C. W. *et al.* Early human use of marine resources and pigment in South Africa during the Middle Pleistocene. *Nature* **449,** 905 (2007).

10. Hublin, J.-J. *et al.* New fossils from Jebel Irhoud, Morocco and the pan-African origin of *Homo sapiens*. *Nature* **546,** 289 (2017).

11. Richter, D. *et al.* The age of the hominin fossils from Jebel Irhoud, Morocco, and the origins of the Middle Stone Age. *Nature* **546,** 293 (2017).

12. Liu, W. *et al.* The earliest unequivocally modern humans in southern China. *Nature* **526,** 696 (2015).

13. Mellars, P. Why did modern human populations disperse from Africa ca. 60,000 years ago? A new model. *Proc. Natl. Acad. Sci.* **103,** 9381 (2006).

14. Mellars, P. Going East: New Genetic and Archaeological Perspectives on the Modern Human Colonization of Eurasia. *Science* **313,** 796–800 (2006).

15. Barker, G. *et al.* The ‘human revolution’ in lowland tropical Southeast Asia: the antiquity and behavior of anatomically modern humans at Niah Cave (Sarawak, Borneo). *J. Hum. Evol.* **52,** 243–261 (2007).

16. Cann, R. L., Stoneking, M. & Wilson, A. C. Mitochondrial DNA and human evolution. *Nature* **325,** 31–36 (1987).

17. Poznik, G. D. *et al.* Sequencing Y Chromosomes Resolves Discrepancy in Time to Common Ancestor of Males Versus Females. *Science* **341,** 562–565 (2013).

18. Francalacci, P. *et al.* Low-Pass DNA Sequencing of 1200 Sardinians Reconstructs European Y-Chromosome Phylogeny. *Science* **341,** 565–569 (2013).

19. Helgason, A. *et al.* The Y-chromosome point mutation rate in humans. *Nat. Genet.* **47,** 453 (2015).

20. Rieux, A. *et al.* Improved Calibration of the Human Mitochondrial Clock Using Ancient Genomes. *Mol. Biol. Evol.* **31,** 2780–2792 (2014).

21. Balloux, F., Handley, L.-J. L., Jombart, T., Liu, H. & Manica, A. Climate shaped the worldwide distribution of human mitochondrial DNA sequence variation. *Proc. R. Soc. Lond. B Biol. Sci.* **276,** 3447–3455 (2009).

22. Manica, A., Amos, W., Balloux, F. & Hanihara, T. The effect of ancient population bottlenecks on human phenotypic variation. *Nature* **448,** 346–348 (2007).

23. Prugnolle, F., Manica, A. & Balloux, F. Geography predicts neutral genetic diversity of human populations. *Curr. Biol.* **15,** R159–R160 (2005).

24. Betti, L., Balloux, F., Amos, W., Hanihara, T. & Manica, A. Distance from Africa, not climate, explains within-population phenotypic diversity in humans. *Proc Biol Sci* **276,** 809–14 (2009).

25. Soares, P. *et al.* Correcting for Purifying Selection: An Improved Human Mitochondrial Molecular Clock. *Am. J. Hum. Genet.* **84,** 740–759 (2009).

26. Liu, H., Prugnolle, F., Manica, A. & Balloux, F. A Geographically Explicit Genetic Model of Worldwide Human-Settlement History. *Am. J. Hum. Genet.* **79,** 230–237 (2006).

27. Eriksson, A. *et al.* Late Pleistocene climate change and the global expansion of anatomically modern humans. *Proc. Natl. Acad. Sci.* **109,** 16089–16094 (2012).

28. Groucutt, H. S. *et al.* Rethinking the dispersal of Homo sapiens out of Africa. *Evol. Anthropol. Issues News Rev.* **24,** 149–164 (2015).

29. Pagani, L. *et al.* Genomic analyses inform on migration events during the peopling of Eurasia. *Nature* **538,** 238–242 (2016).

30. Malaspinas, A.-S. *et al.* A genomic history of Aboriginal Australia. *Nature* **538,** nature18299 (2016).

31. Mallick, S. *et al.* The Simons Genome Diversity Project: 300 genomes from 142 diverse populations. *Nature* **538,** 201–206 (2016).

32. Green, R. E. *et al.* A Draft Sequence of the Neandertal Genome. *Science* **328,** 710–722 (2010).

33. Prüfer, K. *et al.* The complete genome sequence of a Neanderthal from the Altai Mountains. *Nature* **505,** 43–49 (2014).

34. Meyer, M. *et al.* A High-Coverage Genome Sequence from an Archaic Denisovan Individual. *Science* **338,** 222–226 (2012).

35. Meyer, M. *et al.* A High-Coverage Genome Sequence from an Archaic Denisovan Individual. *Science* **338,** 222–226 (2012).

36. Vernot, B. *et al.* Excavating Neandertal and Denisovan DNA from the genomes of Melanesian individuals. *Science* **352,** 235–239 (2016).

37. Eriksson, A. & Manica, A. Effect of ancient population structure on the degree of polymorphism shared between modern human populations and ancient hominins. *Proc. Natl. Acad. Sci.* **109,** 13956–13960 (2012).

38. Amos, W. The quantity of Neanderthal DNA in modern humans: a reanalysis relaxing the assumption of constant mutation rate. *bioRxiv* 065359 (2016). doi:10.1101/065359

39. Lazaridis, I. *et al.* Ancient human genomes suggest three ancestral populations for present-day Europeans. *ArXiv13126639 Q-Bio* (2013).

40. Jones, E. R. *et al.* Upper Palaeolithic genomes reveal deep roots of modern Eurasians. *Nat. Commun.* **6,** 8912 (2015).

41. Fu, Q. *et al.* The genetic history of Ice Age Europe. *Nature* **534,** 200–205 (2016).

42. Yang, M. A. *et al.* 40,000-Year-Old Individual from Asia Provides Insight into Early Population Structure in Eurasia. *Curr. Biol.* **27,** 3202–3208.e9 (2017).

43. Raghavan, M. *et al.* Upper Palaeolithic Siberian genome reveals dual ancestry of Native Americans. *Nature* **505,** 87–91 (2014).

44. Fu, Q. *et al.* Genome sequence of a 45,000-year-old modern human from western Siberia. *Nature* **514,** 445–449 (2014).

45. Fu, Q. *et al.* An early modern human from Romania with a recent Neanderthal ancestor. *Nature* **524,** 216–219 (2015).

46. Haak, W. *et al.* Massive migration from the steppe was a source for Indo-European languages in Europe. *Nature* **522,** 207–211 (2015).

47. Schuster, S. C. Next-generation sequencing transforms today’s biology. *Nature Methods* (2007). Available at: https://www.nature.com/articles/nmeth1156. (Accessed: 21st April 2018)

48. Wilson, A. C., Bowman, B., Freiberger, M., Ryder, O. A. & Higuchi, R. DNA sequences from the quagga, an extinct member of the horse family. *Nature* **312,** 282 (1984).

49. Woodward, S. R., Weyand, N. J., Bunnell, M. & others. DNA sequence from Cretaceous period bone fragments. *Sci.-N. Y. THEN Wash.-* 1229–1229 (1994).

50. Poinar, H. N. & Cooper, A. Ancient DNA: do it right or not at all. *Science* **5482,** 416 (2000).

51. Ancient DNA Comes of Age. Available at: http://journals.plos.org/plosbiology/article?id=10.1371/journal.pbio.0030056#pbio-0030056-b2. (Accessed: 21st December 2017)

52. Hagelberg, E., Hofreiter, M. & Keyser, C. Ancient DNA: the first three decades. *Phil Trans R Soc B* **370,** 20130371 (2015).

53. Velazquez, A. M. V. *et al.* Recalibrating *Equus* evolution using the genome sequence of an early Middle Pleistocene horse. *Nature* **499,** 74 (2013).

54. Hartl, D. L., Clark, A. G. & Clark, A. G. *Principles of population genetics*. **116,** (Sinauer associates Sunderland, 1997).

55. Li, H. & Durbin, R. Inference of human population history from individual whole-genome sequences. *Nature* **475,** 493–496 (2011).

56. Lawson, D. J., Hellenthal, G., Myers, S. & Falush, D. Inference of Population Structure using Dense Haplotype Data. *PLOS Genet.* **8,** e1002453 (2012).

57. Tishkoff, S. A. *et al.* Convergent adaptation of human lactase persistence in Africa and Europe. *Nat. Genet.* **39,** 31–40 (2007).

58. Cook, L. M. The Rise and Fall of the Carbonaria Form of the Peppered Moth. *Q. Rev. Biol.* **78,** 399–417 (2003).

59. Hanchard, N. *et al.* Classical sickle beta-globin haplotypes exhibit a high degree of long-range haplotype similarity in African and Afro-Caribbean populations. *BMC Genet.* **8,** 52 (2007).

60. Clemente, F. J. *et al.* A Selective Sweep on a Deleterious Mutation in CPT1A in Arctic Populations. *Am. J. Hum. Genet.* (2014). doi:10.1016/j.ajhg.2014.09.016

61. Hedrick, P. W. & Thomson, G. Evidence for Balancing Selection at Hla. *Genetics* **104,** 449–456 (1983).

62. Olalde, I. *et al.* Derived immune and ancestral pigmentation alleles in a 7,000-year-old Mesolithic European. *Nature* **507,** 225–228 (2014).

63. Wilde, S. *et al.* Direct evidence for positive selection of skin, hair, and eye pigmentation in Europeans during the last 5,000 y. *Proc. Natl. Acad. Sci.* **111,** 4832–4837 (2014).

64. Norton, H. L. *et al.* Genetic Evidence for the Convergent Evolution of Light Skin in Europeans and East Asians. *Mol. Biol. Evol.* **24,** 710–722 (2007).

65. Bierne, N., Welch, J., Loire, E., Bonhomme, F. & David, P. The coupling hypothesis: why genome scans may fail to map local adaptation genes. *Mol. Ecol.* **20,** 2044–2072 (2011).

66. Li, J. *et al.* Joint analysis of demography and selection in population genetics: where do we stand and where could we go? *Mol. Ecol.* **21,** 28–44 (2012).

67. Scheinfeldt, L. B. *et al.* Genetic adaptation to high altitude in the Ethiopian highlands. *Genome Biol.* **13,** R1 (2012).

68. Xu, S. *et al.* A Genome-Wide Search for Signals of High-Altitude Adaptation in Tibetans. *Mol. Biol. Evol.* **28,** 1003–1011 (2011).

69. Tekola-Ayele, F. *et al.* Novel genomic signals of recent selection in an Ethiopian population. *Eur. J. Hum. Genet.* **23,** 1085–1092 (2015).

70. Metspalu, M. *et al.* Shared and Unique Components of Human Population Structure and Genome-Wide Signals of Positive Selection in South Asia. *Am. J. Hum. Genet.* **89,** 731–744 (2011).

71. Kim, Y. & Nielsen, R. Linkage Disequilibrium as a Signature of Selective Sweeps. *Genetics* **167,** 1513–1524 (2004).

Chapter 2 Palaeolithic Oase genome implies diversification and extinction events across Eurasia

2.1 Abstract

We sequenced to high coverage (~20X) the genome of Oase 2, a ~34-38 ky old individual from the Pestera cu Oase cave in Romania, where a specimen (Oase 1) with a recent Neanderthal ancestor was found. Oase 2 has a lower Neanderthal contribution than Oase 1, and is from a related, but not identical population. Oase 2 is highly divergent from modern day populations, but more related to modern and ancient East Asian and Native American populations than to Western Eurasians. A joint analysis with other high-quality Upper Palaeolithic samples from Eurasia (~32ky old Sunghir and ~45ky old Ust'Ishim from Siberia) shows that the genetic affinity of these populations does not follow present-day geographical patterns. Furthermore, coalescent modelling implies that the populations that these three genomes belong to separated around the same time, around 45-60ky ago. This is consistent with temporally close diversifications between early Upper Palaeolithic populations across Eurasia shortly after the exit out of Africa, followed by population extinctions and the establishment of structured genetic landscape seen in modern-day populations only later on.

2.2 Contribution

I performed all population genetics analysis and wrote the manuscript, except for the sections detailed below. Gloria González Fortes conducted DNA extraction, sequencing, mapping and mitochondrial haplogroup analysis and wrote the corresponding sections (2.4.1, 2.4.2 and 2.6.1 to 2.6.4). Michi Hofreiter helped provide the archaeological context and also contributed to the writing process. Serena Tucci gave comments on the text. Neutral windows for the G-PhoCS analysis were extracted using a modified version of scripts written by Anders Eriksson for Jones et al. 2015[1].

2.3 Introduction

The dynamics of how anatomically modern humans expanded out of Africa and colonised Eurasia is still highly debated[2]. Genetic evidence, such as the age of the most recent common ancestor of non-African mtDNA[3] haplogroups and estimated exit times from models using nuclear genetic diversity[4,5], point to a relatively recent out of Africa expansion around 50-60kya. This timing is supported by the appearance of morphologically distinct *Homo sapiens* fossils outside of Africa[6], and it coincides with a window of favourable climate around 60-70kya in the otherwise arid and impassable Arabian peninsula[5]. Based on early fossil remains from the Arabian Peninsula and China, an earlier exit has also been suggested, possibly taking advantage of a favourable climatic window about 130kya. This early exit is also supported by the similarity of lithics inside and outside of Africa[5] during this period. Whilst some genetic studies have found signals compatible with a small amount of genetic material from such an early wave in Papuans[7], other studies, also including samples from the same region, failed to reject the single-wave scenario[8,9]. Whilst the extent of this earlier wave is unclear, all genetic lines of evidence point to a major expansion wave about 50-60kya, from which all modern populations derive the majority or entirety of their ancestry.

Chapter 2 Palaeolithic Oase genome implies diversification and extinction events across Eurasia

After the spread of humans out of Africa during this recent exit, a structured population of hunter-gatherers existed all over Eurasia by about 50-40kya[10–12]. Based on the nearly synchronous appearance of fossils all over Eurasia, stretching from Europe to South-East Asia and Australia, archaeologists postulated a fast expansion in all directions[2]. The sparsity of the fossil record, however, prevents us from reconstructing the dynamics of expansion in any detail. Genetic data from this era are also limited to a handful of anatomically modern humans, mostly captured rather than shotgun-sequenced (thus preventing accurate timing of the splits among these populations). Some, such as 40kya Tianyuan[13] from China, samples from 37kya onwards in Europe[14] or 13kya Satsurblia[1] from Georgia are associated with modern populations of the same region. Other, especially older, samples, are either not directly related to any modern population (37-42kya Oase 1[15] and 45kya Ust'Ishim[16] from Central Siberia) or their closest relationship is not to populations currently living in the same area (24kya MA1[17] from Central Siberia). In modern genetic data, there is a clear separation into a European and an Asian major lineage[18], with estimated split times shortly after the exit out of Africa[7,9]. However, the origin of these lineages and how they became so diverged is unclear, since there is no clear geographic barrier leading to such a separation.

To shed light on the population history of anatomically modern humans in Eurasia in the Upper Palaeolithic and their relationship to modern lineages, we sequenced to high coverage (~20X, Figure 2.2) an anatomically modern human (Oase 2) from the Upper Palaeolithic (~34-38 ky old, based on association with directly dated finds from the site[19–21]) from Pestera cu Oase in Romania[19–21]. A sample from the same cave and of a similar age (Oase 1), dated to ~37.8kya[20] was captured using an enrichment strategy with a panel of ~2.2 million SNPs (2.2M panel), to extract information on sites informative about its relationship to Neanderthals and present-day humans[15]. However, the low coverage and high contamination of this sample did not allow for detailed demographic analysis. The high quality of Oase 2 enabled us to conduct haplotype-based demographic analysis and to compare it to other high-quality Upper Palaeolithic genomes. I also conducted a SNP-based analysis using a panel consisting of modern populations from the Human Origins panel[14], as well as ancient African[22] and Eurasian[16,17,14,13] samples (Figure 2.1 for key ancient samples).

Upper Palaeolithic genomes also inform us on the extent of Neanderthal admixture. Neanderthal ancestry in modern living individuals has been mostly ascribed to one pulse of admixture at a very early stage of the out of Africa expansion, with possible minor events later on. The observed relationship of decreasing Neanderthal ancestry with time is attributed to negative selection acting on such genetic segments[14,16], although the topic is still debated. So far, Oase 1 is the only sample that stands out in this regard: it had an unusually high proportion of its genome derived from Neanderthals DNA: 6-9%, more than expected given its age (up to ~6%)[15]. Furthermore, this ancestry was distributed in very long segments, indicative of a Neanderthal ancestor as recent as 4-6 generations back[15]. Whether Oase 2 is also special in this extent can inform us on the dynamics of Neanderthal interbreeding in early humans.

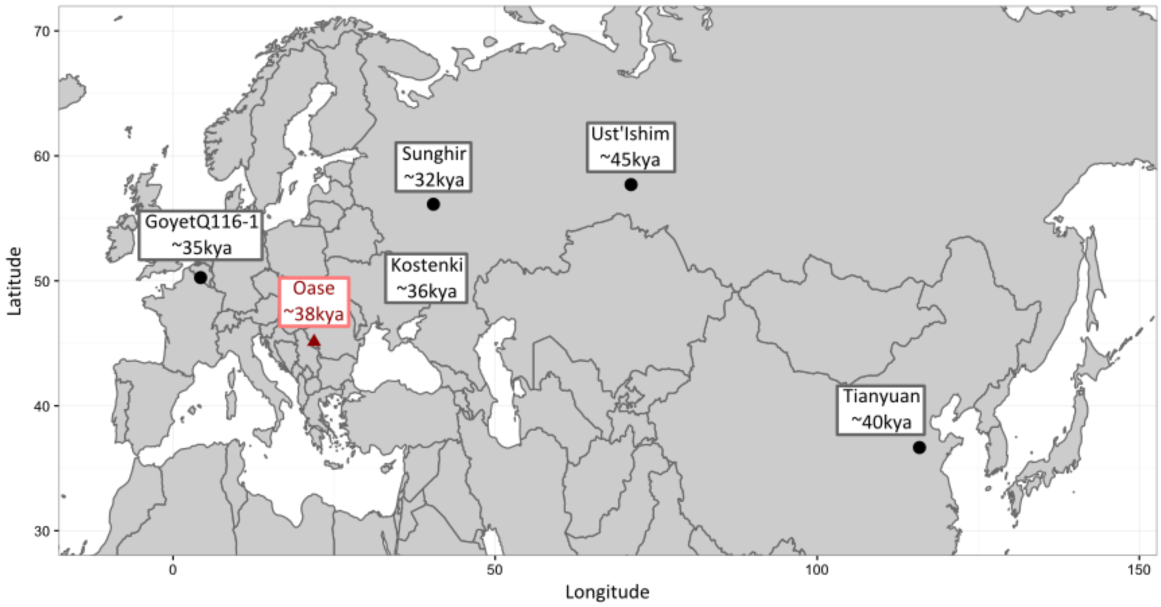

Figure 2.1 Location of Oase 2 and the key ancient samples mentioned in this study. GoyetQ116-1, Kostenki, Sunghir, Ust'Ishim and Tianyuan are shown, with their estimated ages displayed.

2.4 Results

2.4.1 DNA extraction, sequencing and authentification

DNA was extracted from a fragment of Oase 2's petrous bone. A total of eight extracts were obtained and one single stranded library was built from each of them. Seven of these libraries yielded percentages of endogenous DNA above 20% in a test run on the NextSeq500 Illumina platform (Supplementary Table A.1) and were selected for high through-put sequencing on a HiSeq2500. After mapping and filtering, the aligned reads of these libraries (with the exception of Oa2, see Methods section for details) were merged getting an average coverage of ~20x for the complete nuclear genome of Oase 2, as calculated by genomeCoverageBed from bedtools v2.25.0[23].

All libraries showed typical patterns of molecular damage, with deamination frequencies ranging from 5 to 15% in UDG-treated libraries and higher than 30% in a non-UDG treated library (Oa2, Figure 2.3 A and C). Treatment with UDG (Uracil-DNA glycosylase) is applied to repair damage in ancient DNA samples. The average read length was around 40 bp in all libraries, in agreement with expected DNA fragmentation in ancient remains[24,25] (Figure 2.3 B and D). The percentage of contaminating sequences was estimated to 1.29% based on the presence of non-consensus bases in the haploid mitochondrial genome. When only transversions were considered, which are invariant to damage patterns through deamination, the percentage of contamination decreased to 0.18%.

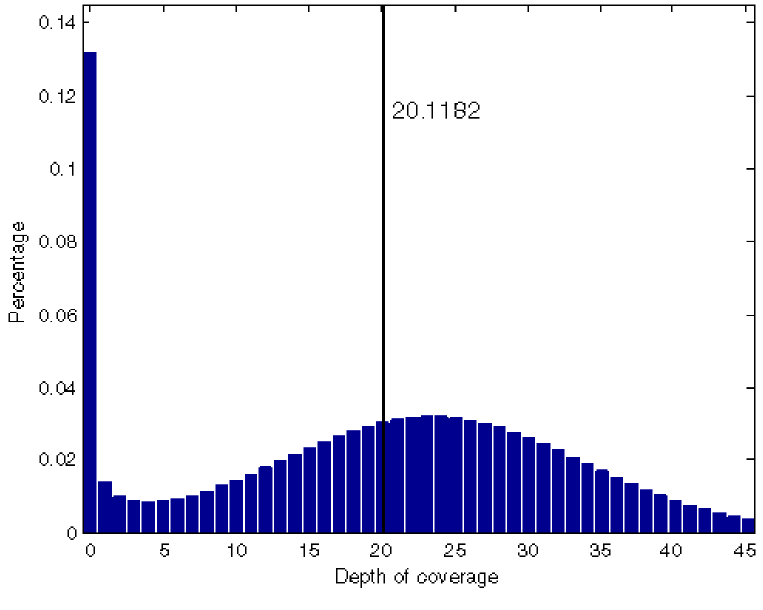

Figure 2.2 Depth of coverage for Oase 2, as calculated by genomeCoverageBed from bedtools v2.25.0[23]. The figure shows the percentage of reads in a given bin, with the black line marking the average coverage (~20.12X).

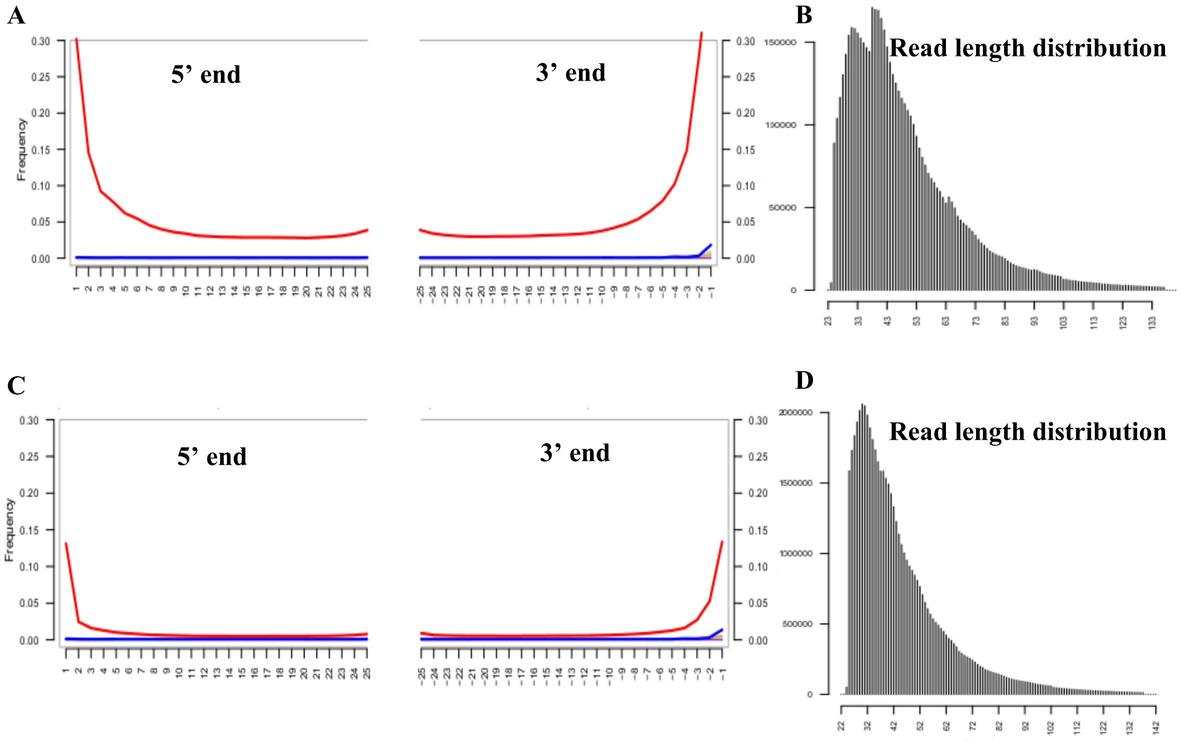

Figure 2.3 Patterns of damage in Oase's libraries. A. Percentages of deamination and B. read length distribution of mapped reads from a non-UDG treatment library (Oa2). C. Patterns of deamination and D. reads length distribution of the merged reads mapping to the reference in UDG treatment libraries (Oa1, Oa1b, Oa3, Oa4, Oa5 and Oa5b).

2.4.2 Mitochondrial haplogroup assignment

The mitochondrial genome of Oase 2 was sequenced to an average depth of coverage of 479.61x. Supplementary Table A.3 reports the polymorphic positions in Oase 2's consensus mitochondrial sequence with regards to the Revised Cambridge Reference Sequence (rCRS)[26]. Oase 2 carries the same defining positions already reported in Oase 1 for haplogroup N[15], but both individuals carry ancestral alleles at positions 8701 and 9540, where all present day lineages within the macrohaplogroup N carry the derived allele. This has been interpreted as the sign of an ancient mitochondrial haplogroup that is related to the macrohaplogroup N, which nowadays includes all Eurasian mitochondrial diversity, but diverged from its base[15]. The fact that Oase 1 and Oase 2 belong to the same, previously unobserved mtDNA haplogroup also implies a relatively close relationship between these samples on the maternal line.

2.4.3 Comparison of Oase 1 and Oase 2

Oase 1 and Oase 2 appear to be from related, but not identical populations. Their outgroup f_3 profiles are different: they are closest to each other, but Oase 1 shows a similarity to European Ice Age genomes that is absent from Oase 2, whereas the increased similarity to Asian populations is slightly more pronounced in Oase 2 than in Oase 1 (Figure 2.4 and Supplementary Figure A.1), even when only positions called in Oase 1 are considered (Supplementary Figure A.2 and Supplementary Figure A.3). A further peculiarity is the close relatedness between Muierii2 and Oase 1, which is missing in Oase 2. Muierii2 is a ~33ky old sample from Romania, not assigned to any lineage that contributed to later European hunter-gatherers. This also supports the differences between Oase 1 and Oase 2, and points to a complicated genetic landscape in Upper Palaeolithic Eurasia with multiple, differentially related populations, many of which did not contribute to modern-day diversity.

A formal test of whether the two samples from Pestera cu Oase form a clade, using D statistics[27] with an African outgroup of the form D(Oase 1, Oase 2; X, Yoruba), is also violated (absolute value of Z scores up to 4.2). However, this signal appears to be dominated by the unusually high Neanderthal proportion in Oase 1: Oase 1 is significantly closer to ancient hominids and Oase 2 to most modern populations; only deeply divergent populations from sub-Saharan Africa are neutral (Figure 2.5 and Figure 2.6). This suggests that the two samples are probably from related, but not identical populations, but we need to control for the difference in Neanderthal ancestry to be able to reach a firm conclusion.

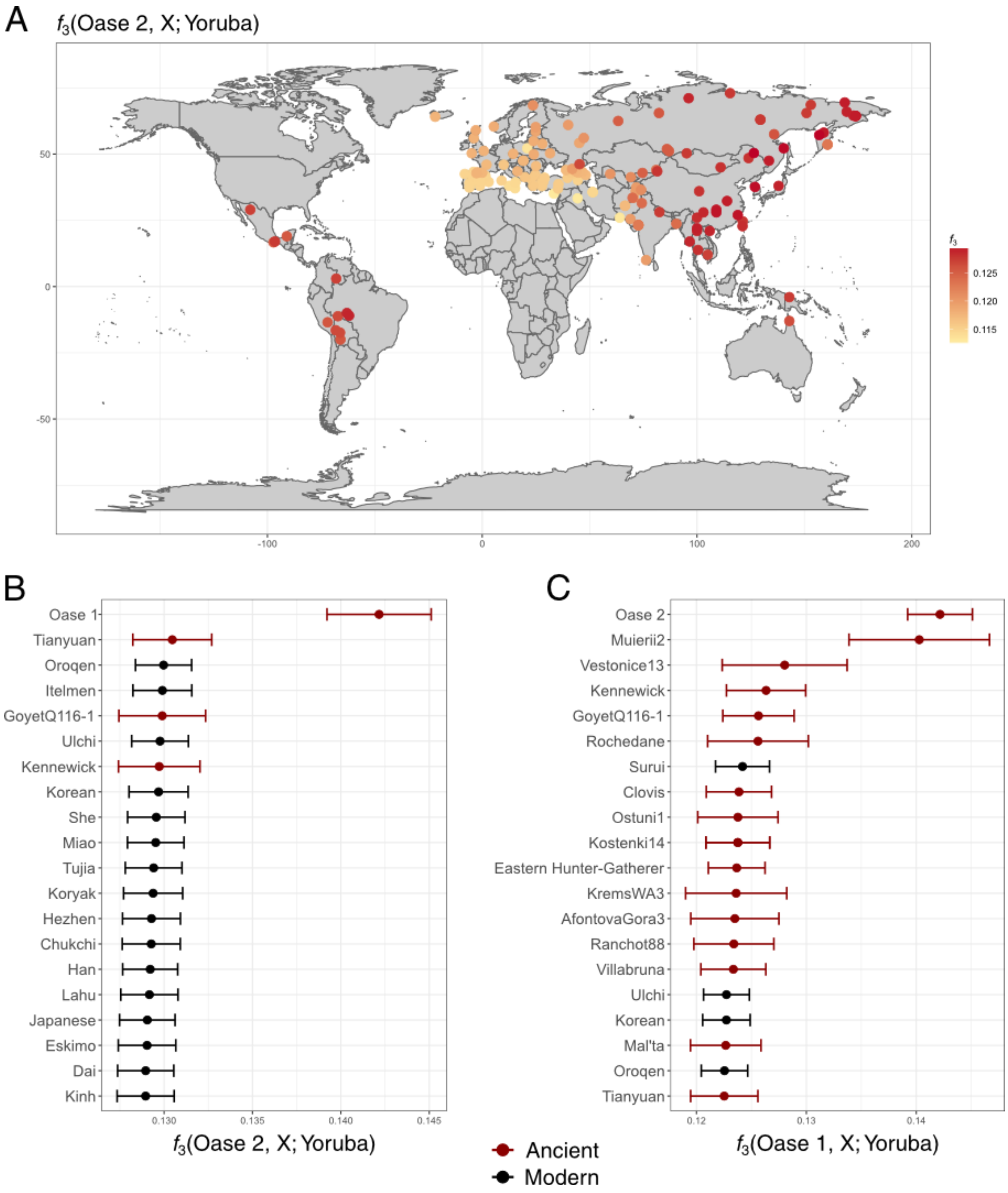

Figure 2.4 Outgroup f_3 statistics of the form f_3(Oase, X; Yoruba). A. 150 modern populations with the highest score for Oase 2. B. and C. 20 populations with the highest score for Oase 2 and Oase 1, respectively. Ancient populations displayed in red and moderns in black.

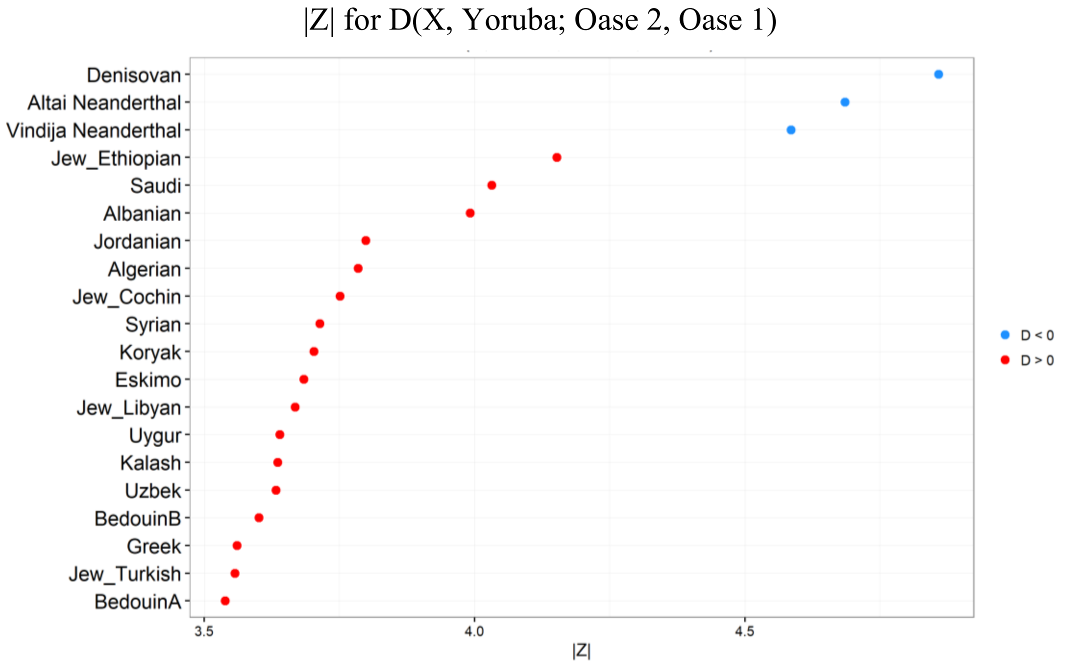

Figure 2.5 Absolute value of Z scores from the statistic D(X, Yoruba; Oase 2, Oase 1). Positive D statistics (X closer to Oase 2 than to Oase 1) are displayed in red and negative in red. The 20 populations with the highest absolute value of Z scores are displayed. More information on the samples is available in section 2.6.5.

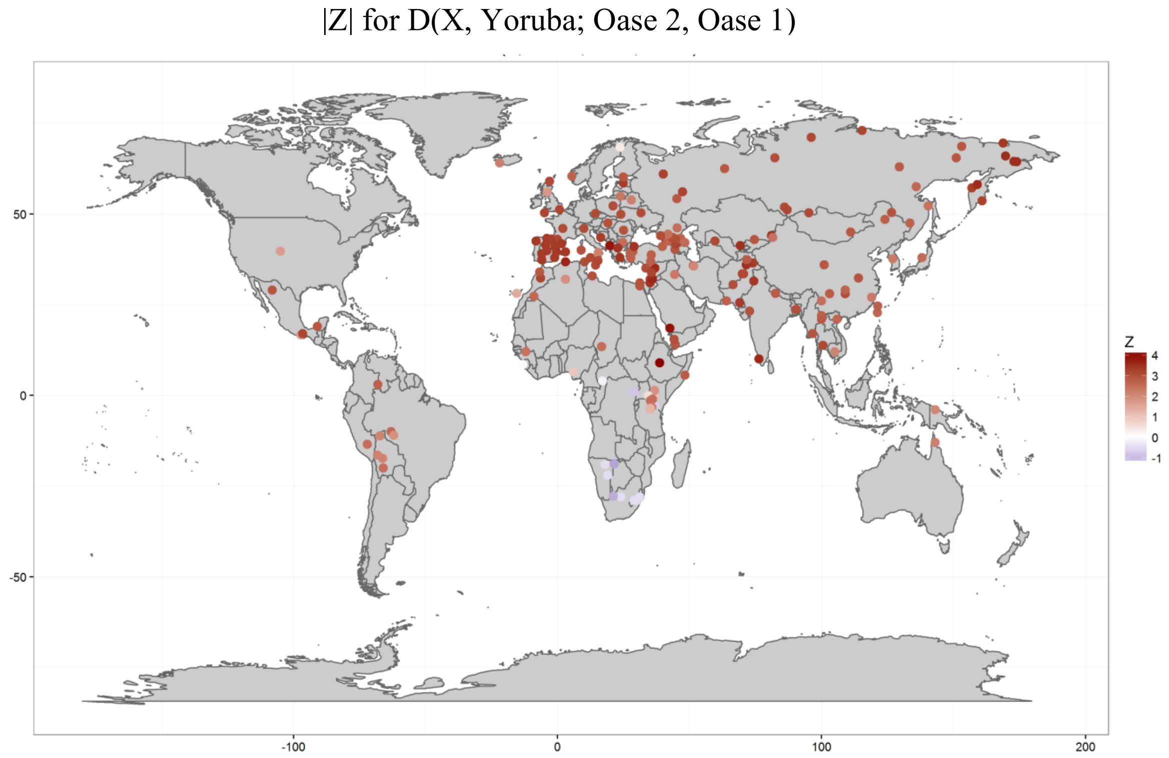

Figure 2.6 Z scores from the statistic D(Y, Yoruba; Oase 1, Oase 2). 150 highest scoring modern populations are displayed.

2.4.4 Neanderthal ancestry

Oase 1 harbours a high amount of Neanderthal-related ancestry[15] (6-9%), and it also has a morphology that is a mixture of anatomically modern and archaic features[20]. I found that although Oase 2 features a similar mosaic of morphological features[21], it has a lower Neanderthal proportion than Oase 1 (about 6.06% as measured by an f_4 ratio, Figure 2.7 and Table 2.1; for details see Methods). This is still significantly higher than what would be expected based on its age: the 95% confidence interval of an ordinary least squares linear fit on all samples but Oase1 and Oase 2 in Figure 2.7 is 4.23%-4.36%. This does not take the SNP-wise correlations between estimates from different samples into account, but even the more sophisticated method using a Weighted Block Jackknife method presented in Fu et al. 2016 puts the top of the 95% CI of Neanderthal ancestry at a time well before Oase 2, 50ky ago, at ~5.4%. However, Oase 2 is far from being such a pronounced outlier as Oase 1. My collaborators are currently investigating the pattern of haplotypes related to Neanderthals in Oase 2, which will give further information about the timing of admixture that gave rise these ancestry tracts and allow us to identify genes with alleles of a Neanderthal origin.

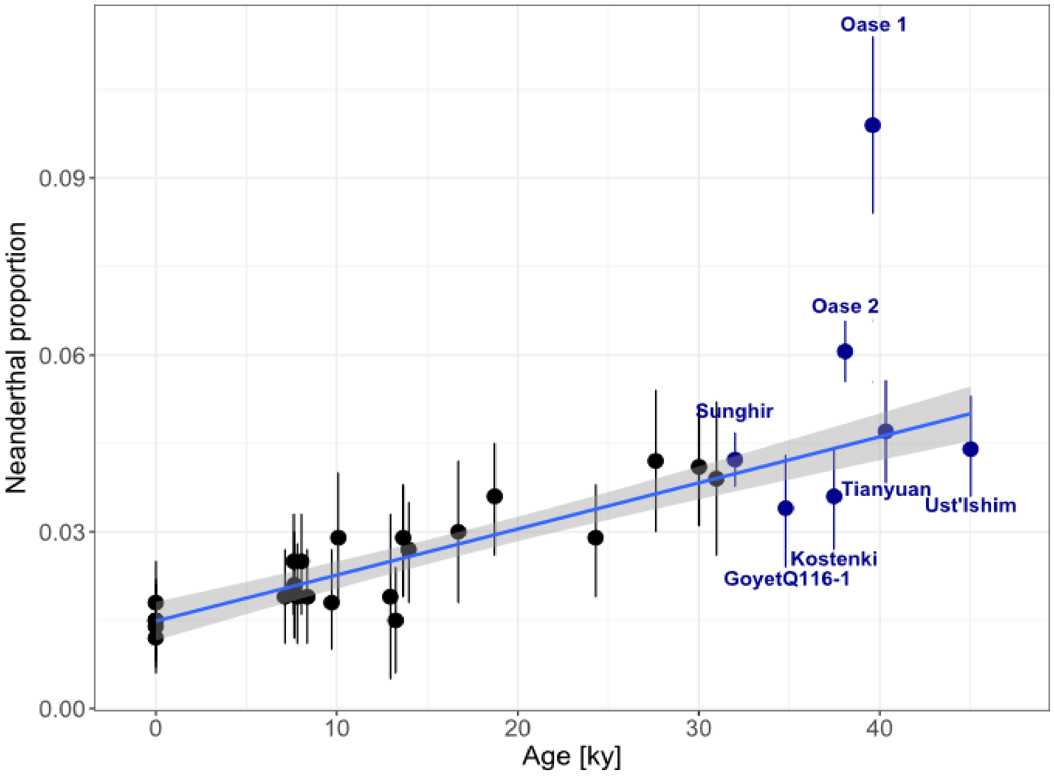

Figure 2.7 Estimated proportion of Neanderthal genetic material in Oase 2, Sunghir and genomes analysed in14. Data for Oase 2 and Sunghir were calculated and merged with the published proportions from14. Blue line marks the result of a linear fit on all genomes except Oase 1, with the 95% confidence interval (CI) marked in grey.

Table 2.1 Estimated proportion of Neanderthal genetic material in selected ancient genomes.

Population	Age [years]	No. of SNPs	f_4 estimate	95% CI minimum	95% CI maximum
Ust'Ishim	45,020	2,137,615	4.40%	3.60%	5.30%
Tianyuan	40,328	2,137,258	4.70%	3.83%	5.57%
Oase 1	39,610	285,076	9.90%	8.40%	11.40%
Oase 2	39,610	2,000,000	6.06%	5.54%	6.58%
Kostenki	37,470	1,774,156	3.60%	2.70%	4.40%
GoyetQ116-1	34,795	846,983	3.40%	2.40%	4.30%
Sunghir	32,000	2,000,000	4.40%	3.60%	5.30%

2.4.5 Comparison of Oase 2 and other modern and ancient samples

Oase 2 did not leave considerable ancestry in modern populations: it is not particularly close to any modern population as measured by outgroup f_3 statistics, similarly to Ust'Ishim[16] and Oase 1[15] (Figure 2.4A and Supplementary Figure A.1). It is slightly, but significantly closer to Asians and Native Americans than to Europeans, but this pattern is much weaker than that seen for East Asian ancient genomes, like Tianyuan[28] or the 7.7kya Devil's Gate[29], or even for European ancient genomes with a clear European affinity, like Kostenki[30] or Sunghir[31]. When ancient samples are also considered, Oase 1 stands out as the sample closest to Oase 2 (Figure 2.4B and C, Supplementary Figure A.1), implying that they at least come from related populations. Out of the rest of the ancient samples, Tianyuan is the closest to Oase 2, but its affinity is only as strong as that of modern East Asians. The fact that Oase 2 is closer to Tianyuan than to ancient European genomes implies that its Asian affinity seen in modern populations can not be attributed to the Near Eastern gene flow into Europe during the Neolithic. Taken together, these results suggest that Oase 2 is a representative of a group of out-of-Africa humans that was an outgroup to the direct ancestors of current populations, but, similarly to Ust'Ishim, was closer to the ancestors of Asian than to European populations.

2.4.6 African origins

I found that the relationships of these Late Pleistocene samples to ancient and modern Africans resemble that of modern Eurasians: they are closest to North Africans, followed by East Africans and then other sub-Saharan populations and without any population standing out (Figure 2.8, Supplementary Figure A.4 to Supplementary Figure A.10). One ancient East African sample from ~3.1ky ago (Tanzania_Luxmanda_3100BP) was close to Upper Palaeolithic Eurasians, but it was found to harbour ancestry related to early, pre-pottery farmers from the Levant[22]. This implies that the African groups directly ancestral to the first wave of Eurasians disappeared or got diluted, implying a lack of population continuity in Africa that mirrors what is seen in Eurasia.

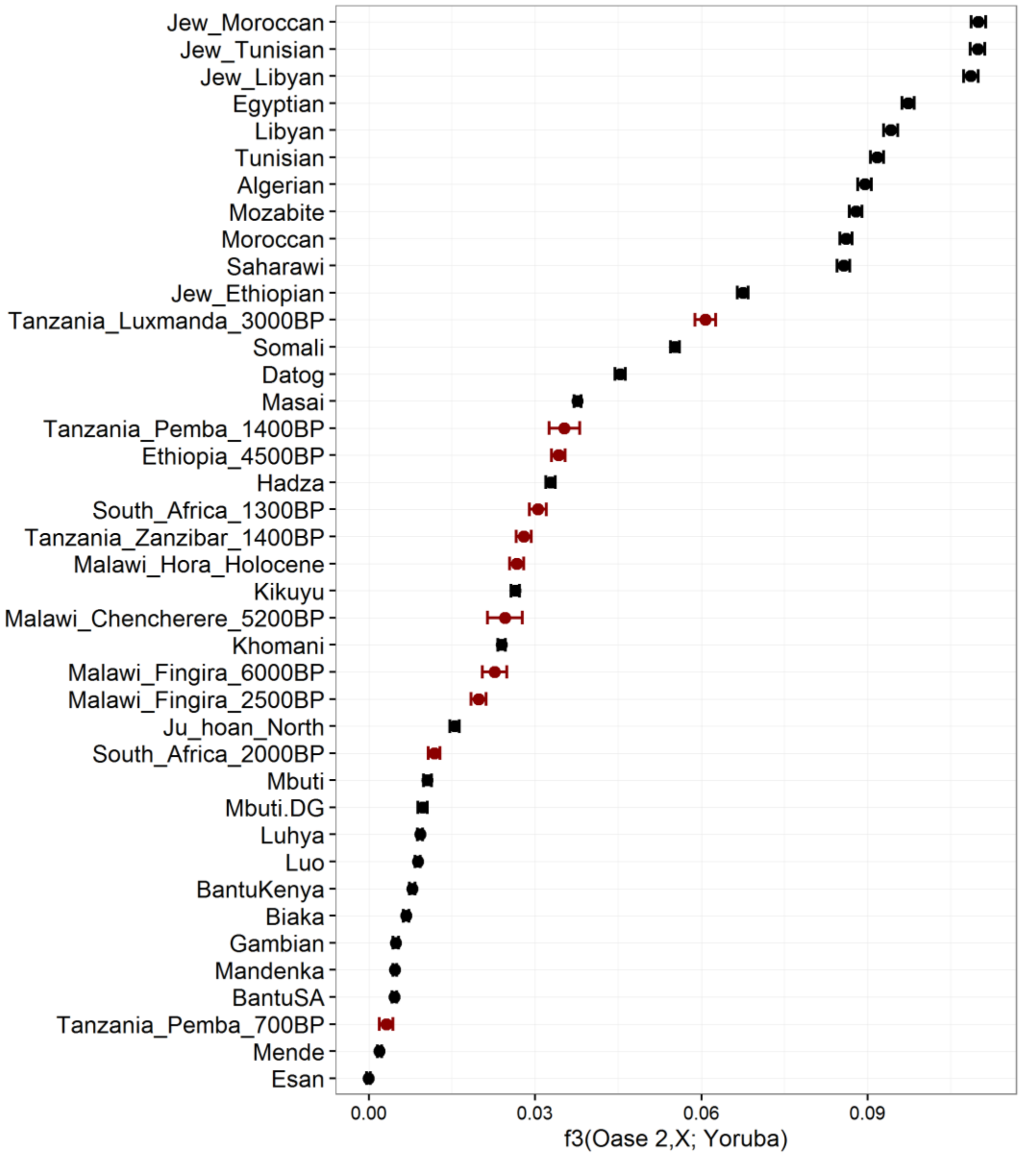

Figure 2.8 Outgroup f_3 statistics of the form f_3 (Oase 2, X; Yoruba) for modern and ancient African populations.

2.4.7 Demographic analysis on high-quality Upper Palaeolithic genomes

The high coverage of Oase 2 enables detailed coalescent modelling of how the three Upper Palaeolithic lineages with available high-coverage data, namely Sunghir, Oase 2 and Ust'Ishim, are related to each other. I used G-PhoCS[32] to estimate branch lengths, population sizes and migration rates upon a tree of the populations associated with these three Upper Palaeolithic genomes, the Neanderthal from the Altai Mountains[33] and an African outgroup, represented by a high coverage San genome[33] (see Figure 2.9 for the general topology). I first attempted to establish the topology of the tree using D-statistics of the form D(X, Y; Z, Yoruba), with X, Y and Z being a sample from the three modelled lineages: Sunghir and Kostenki for the "European" branch, Oase 1 and Oase 2 for inhabitants of Pestera cu Oase and Ust'Ishim separately, as it had no close relatives. Statistics were consistently non-significant only when Oase 1 or Oase 2 is population Z (Figure 2.10, Supplementary Table A.4 and A.5), implying that samples from Pestera cu Oase are the outgroup out of the three Upper Palaeolithic lineages. However, the signal was not strong and these statistics can be influenced by the differing levels of Neanderthal ancestry in the three genomes. I thus estimated split times between the Upper Palaeolithic populations in all possible topologies, accounting for the Neanderthal ancestry by explicitly modelling it in G-PhoCS[32].

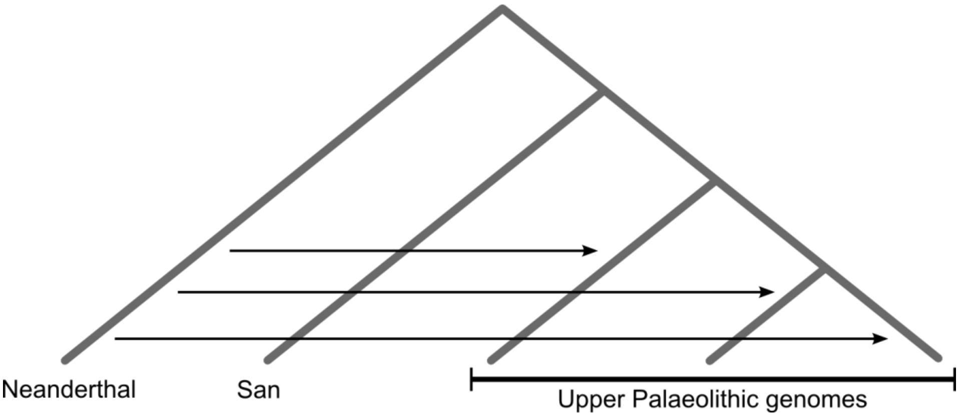

Figure 2.9 General topology of the tree used in the demographic analysis. Arrows mark migration bands and all possible permutations of Upper Palaeolithic genomes were explored.

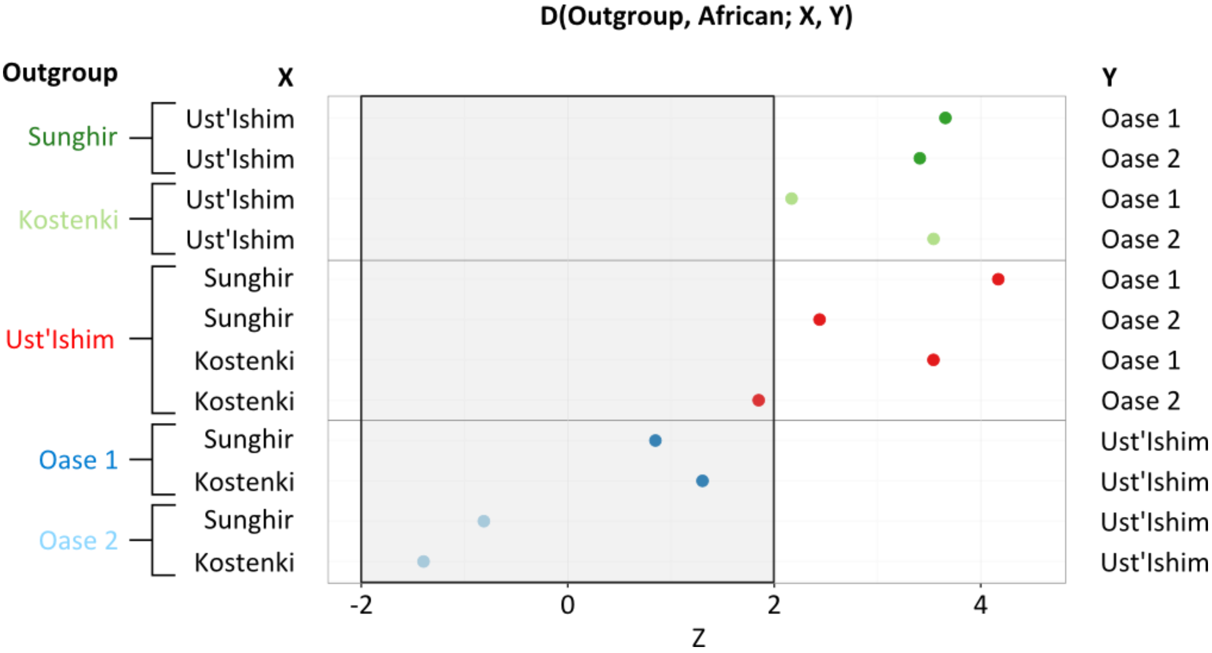

Figure 2.10 D statistics exploring the relationship between different Upper Palaeolithic lineages. Oase 1 and Oase 2 were explored as representatives of the population inhabiting Pestera cu Oase, Kostenki and Sunghir of the branch related to modern-day Europeans and Ust'Ishim was considered individually.

I first only included pairs of the Upper Palaeolithic genomes in addition to the San and the Neanderthal, which resulted in very similar split times between Oase 2 and Ust'Ishim (median 52.34 kya), Sunghir and Ust'Ishim (50.43 kya) and Sunghir and Oase 2 (52.86 kya). For detailed results and confidence intervals, see Supplementary Table A.6-6 to. This is in line with the lack of a close connection between any pairs of these genomes from our SNP-based analysis. I then estimated three-way split times, again investigating all three possible topologies, and obtained a near star-shaped split with median split times between the Upper Palaeolithic populations roughly 46-49kya for the first and 48-49 kya for the second level (range of medians; for full results and confidence intervals, see Supplementary Table A.6 to Supplementary Table A.11), depending on the topology (Figure 2.11).

The estimated Neanderthal proportions from this analysis for Oase 2 (range of medians 3.25%-3.70%), Ust'Ishim (1.59%-1.75%) and Sunghir (1.93%-2.13%) were lower than, but proportionally similar to the f_4 estimates (Table 2.1), depending on the topology. There was also a clear difference in estimated ancestral population sizes for our samples: the effective population size for Oase 2 (~2,300-4,300) was much lower than that of the San (~17,400-25,300), slightly lower than Ust'Ishim (~5,100-15,700), similar to the Altai Neanderthal (~3,800-3,900) and larger than Sunghir (~1,100-1,600). This is in agreement with previous reports of very small population sizes for the Neanderthals[33] and ancient hunter-gatherers from various regions (Western Europe[1,34,35], the Caucasus[1] or Siberia[31]) and the generally higher effective population sizes of African populations[32,36]; the order of the population sizes (smallest for Sunghir, followed by the Altai Neanderthal, Ust'Ishim and then Africans) is the same as that found by Sikora et al.[31].

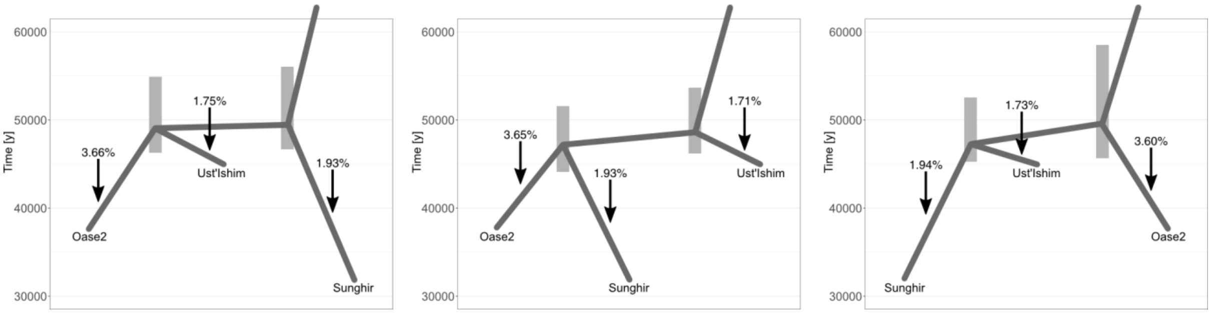

Figure 2.11 Estimated split times between the three high-quality Upper Palaeolithic genomes in all three possible topologies. Tree depicts the median estimate and grey bars mark the 95% confidence interval.

2.5 Conclusions

We sequenced to high coverage the genome of Oase 2, a sample from the same location where an anatomically modern human with a recent Neanderthal ancestor (Oase 1) was found. Compared to Oase 1, Oase 2 features a lower Neanderthal proportion, which is still significantly higher than what would be expected based on its age and what is seen in other Upper Palaeolithic genomes. The two samples from the cave probably originate from closely related, but not identical groups. However, for a formal statistical test, we would need to control for portions of the genome that originate from Neanderthals, which will be possible by identifying such haplotypes and excluding them from our analysis. This section of our analysis is performed by our collaborators and is still on-going.

Haplotype-based modelling implies a nearly simultaneous diversification event that led to various Upper Palaeolithic groups scattered across Eurasia. The timing of the event is in agreement with estimated exit times out of Africa roughly 50-60kya[32] and the estimated population sizes show the expected pattern from an out of Africa bottleneck. The simultaneity of the split implies that diversification started right after the exit out of Africa, but not necessarily meaning that these populations were fully separated into disjoint lineages. The timing of the split is consistent with a single exit out of Africa leading to all samples studied, but the reason why we do not see signs of an earlier exit in the form of an older split time, despite favourable climatic conditions, is not known. Competition with archaic hominins could have been a preventive factor, but the sparsity of ancient data does not yet allow for a formal test of such a hypothesis.

Oase 2 did not leave its ancestry in modern populations, similarly to some samples of a similar age, such as Oase 1[15], Ust'Ishim[16] and multiple early Upper Palaeolithic European samples[14], but unlike others that are related to modern populations from their respective regions (e.g. Tianyuan[28], Kostenki[30], Sunghir[31] and numerous other European samples[14]). The varying affinities of early Eurasian populations show a restructuring of genetic diversity between the Upper Palaeolithic and present day, including several extinction events. Numerous factors could play a role in such changes, such as climate affecting areas differentially (e.g. harsh conditions in Europe and Siberia only leaving few survivors, but not in East Asia), or geographic connectivity affecting how easily different areas can be repopulated. Furthermore, I did not find any particular pattern of similarity between Upper Palaeolithic samples and modern Africans, which could be a sign of similar extinction events in Africa and/or successive admixture within the continent. There is a wide range of evidence for the latter, for example through the admixed ancestry of most modern African populations[22].

The lineages leading to modern populations could originate from the surviving groups all over Eurasia, but could also be a result of large-scale movements from refugia with favourable conditions, such as the Near East or southern parts of Asia. Although genetic data from the period directly following the exit out of Africa is sparse, given that many of the observed Upper Paleolithic samples did not leave considerable ancestry, it is reasonable to suppose that this disappearance of an observable genetic trace (through extinction and/or admixture) was not a rare, special event. Consequentially, the signatures of events we can infer based on their signature in modern genomes (e.g. genes obtained via introgression, population bottlenecks) are probably only a subset of all such events and only give insight into the history of the fittest, or, more likely, the luckiest populations that contributed their genetic material to modern human diversity.

2.6 Methods

2.6.1 DNA extraction and library preparation

All decontamination steps and laboratory procedures before PCR amplification were carried out in ancient DNA dedicated facilities at the University of Potsdam. All tools used in these stages were decontaminated with bleach, DNA-ExitusPlus^{TM} and UV radiation.

DNA was extracted from a fragment of petrous bone sampled in Bucharest (Romania) in 2013. Before extraction, the bone fragment was exposed to UV radiation for 10 minutes on each side. Afterwards, the bone surface was physically removed using a dental drill attached to a dremel saw. A new drill was then used to remove all the porous parts until we got to the dense walls forming the inner ear channels. After cleaning, two fragments of compact bone, 172 mg and 212 mg respectively, were obtained. Both fragments were ground to fine bone powder using mortars and pestles.

Six DNA extracts were prepared from a starting amount of 50 mg of bone powder each (from now onwards we are referring to these extracts as: Oa1, Oa2, Oa3, Oa4, Oa5 and Oa6). We followed the DNA extraction protocol described in Dabney et al (2013)[37], which is specially optimized to recover short DNA fragments (from 30-40 bp length). In extracts Oa1 and Oa5, the bone powder was not completely digested after overnight incubation with proteinase K (PK), thus we add new digestion buffer with PK and performed a secondary extraction (Oa1b and Oa5b). Finally, we obtained eight DNA extracts, each in 25 µl of elution buffer.

One single stranded library was built from each extract following the protocol described by Gansauge and Meyer (2013)[38]. This protocol includes UDG treatment before library building in order to reduce the presence of uracils in aDNA molecules. We applied these treatments to all our extracts with the exception of Oa2, in order to accurately measure the deamination patterns in Oase's DNA molecules and thus support the authenticity of the sequences.

The number of cycles for the amplification of each library was estimated based on qPCR. We used Accuprime Pfx (Invitrogen^{TM}) for the amplification of the UDG treated libraries, while Oa2 was amplified using Accuprime SM (Invitrogen^{TM}), which is able to read over uracils. A different index sequence was incorporated during this amplification of each library, in order to be able to pool them for sequencing. Finally, each library was amplified in four parallel reactions with 4 µl of template and 16 µl of master mix each. PCR amplification conditions were as specified by the manufacture.

The amplified libraries were purified using a MinElute kit (Qiagen) and quantified using a 2200 TapeStation (Agilent Technologies). The libraries were pooled in equimolar quantities and sequenced on an Illumina NextSeq500 platform in 75PE mode. The output from this run (around 20 to 50 million reads per library) was used to estimate the percentage of endogenous DNA in each library. After this test, libraries Oa4 and Oa2a were discarded from further sequencing because of high duplication levels in Oa4 and the presence of uracils in Oa2a. All the other libraries showed percentages of endogenous DNA higher than 20% and low clonality, and they were selected for high through-put sequencing.

High throughput sequencing was carried out at TheragenEtex (Suwon, South Korea), using four whole flow cells of an Illumina HiSeq2500 platform. Two of the sequencing runs were set to 50 cycles in single end mode (50SE) and another two to 50 cycles in paired end mode (50PE). Libraries were selected for these runs based on their performance in the test NextSeq500 run, but also on the availability of enough library volume left to fill the flowcells.

2.6.2 Processing and mapping of NGS data

After sequencing, the raw BCL files were converted to fastq format following the Illumina base-calling pipeline (Illumina Pipeline v1.4). Raw reads were assigned to the corresponding libraries based on the barcode sequences, no mismatches were allowed in the first base of the barcode and a single mismatch was allowed at any other position. The software SeqPrep (https://github.com/jstjohn/SeqPrep) was used to trim and merge the forward (R1) and reverse (R2) reads from pair end (PE) runs, while cutadapt-1.3[39] was used to trim SE reads. In both cases, a minimum length of 25 bases was set as threshold after trimming.

The trimmed and merged reads were aligned to the human reference genome (GRCh37 build) using the software Burrows-Wheeler Aligner (BWA) version 0.7.5a-r405[40], with default parameters and seed option disabled (-l 1000). Prior to the alignment, the mitochondrial sequences in the GRCh37 reference were replaced by the Revised Cambridge Reference Sequence (NC_012920[26]).

After mapping, clonal sequences were removed from the alignment using the MarkDuplicates.jar tool in picards-1.98 (http://broadinstitute.github.io/picard/). Also, reads were realigned around indels using the RealignerTargetCreator and IndelRealigner tools in GATK-3.0-0[41]. The resulting bam files were filtered for mapping quality of 30 using Samtools-0.1.19[40]. Finally, we used Mapdamage[42] to downscale the quality score of bases at the end of the reads, in order to diminish possible errors when calling SNPs at likely damaged positions.

The mapped reads from the downscaled alignments were merged in a single bam file using picards-1.98. This merged file was used to estimate the whole genome coverage, as well as for SNP calling and downstream analysis described below.

2.6.3 Mitochondrial DNA

The mitochondrial genome of Oase 2 was reconstructed from the NGS output of the first run on the HiSeq2500 (Supplementary Table A.2). Seven libraries (Oa1a, Oa1b, Oa2, Oa3, Oa4, Oa5a, Oa5b and Oa6) were sequenced in 50PE mode and the output reads were processed as described in the previous section, with the only difference that the Revised Cambridge Reference Sequence (rCRS, NC_012920[26]) was used at the mapping stage.

Polymorphic positions with regards to the reference were called using the samtools-0.1.19 mpileup function[40]. Mapping and base quality scores equal to or higher than 30 were required for the base calling. The identified polymorphic positions were directly checked by visualizing the mitochondrial alignment in Tablet[43]. Finally, the confirmed polymorphisms were uploaded to Haplogrep[44], which bases the identification of the haplogroup on the updated mitochondrial phylogeny of PhyloTree (http://www.phylotree.org/). The resulting mitochondrial haplogroup was N, but in fact Oase 2 carried the ancestral allele at positions 7801 and 9540 instead of the defining derived alleles.

2.6.4 Authenticity of ancient DNA molecules

Negative controls were included during the extraction and library building procedures, and sequenced together with the libraries in the NextSeq500 run (Supplementary Table A.1). The percentage of reads mapping to the reference in these blanks ranged from 0.2 to 2.3%.

Also, we used MapDamage[42] to assess the patterns of molecular damage in Oase 2's libraries. Finally, the percentage of modern human contamination was estimated by measuring the frequency of non-consensus calls at haplogroup defining positions in Oase 2's mitochondrial DNA (mtDNA) sequences.

2.6.5 SNP calling and merging with reference panel

To compare our sample to modern and ancient human genetic variation, I called SNPs from the BAMfiles of Oase 2 and Sunghir using SAMtools 1.6[40] and the hg19 reference FASTA file. I only called positions overlapping with the ~600k SNPs from the Human Origins panel[45], also part of the 2.2M panel used in the study of Oase 1[15] and the genetic history of Ice Age Europe[14]. Bases were required to have a minimum mapping quality of 30 and base quality of 20. The resulting SNP data was then merged using Plink1.9[46] with the panels used in Fu et al. 2016[14] , Lazaridis et al. 2017[47] and Skoglund et al. 2017[22], as well as with a version of the Tianyuan genome[28] called on the same 2.2M SNP panel as in Fu et al. 2016[14], kindly sent by the authors(2423 individuals in total). SNPs were restricted to triallelic SNPs, which resulted in 587,247 SNPs (133,069 called in Oase 1).

2.6.6 Calculating statistics

2.6.6.1 D and outgroup f_3 statistics

D statistics[27] and f_3 statistics[48,49] were used to formally assess the relationships between the samples using the qpDstat (*D* statistics) and qp3PopTest (f_3 statistics) programs from the ADMIXTOOLS package[49]. Significance was assessed by these programs using a block jackknife over 5-centimorgan chunks of the genome, and statistics were considered significant if their Z score was of magnitude greater than 2, or, for admixture f_3 scores, if they were smaller than −2. These correspond approximately to P values of 0.046 and 0.023, respectively. Outgroup f_3 scores were filtered to include populations with at least 20,000 SNPs overlapping; 10,000 SNPs when the low coverage Oase 1 was the focal sample.

D statistics of the form D(X, Y; Z, Yoruba) were used first to formally assess the relationship between the three Upper Palaeolithic lineages that I later used in our demographic analysis:

Oase (Oase 1 or Oase 2), Ust'Ishim and Upper Palaeolithic Europeans (Kostenki14 or Sunghir).

2.6.6.2 Estimating the proportion of Neanderthal ancestry

f_4 ratios were used to estimate the proportion of Neanderthal ancestry in our samples, following [14]. I used the equation below:

$$Q(x) = 1 - \frac{f_4(West\ and\ Central\ Africans, Chimp; X, Archaic)}{f_4(West\ and\ Central\ Africans, Chimp; Dinka\ Archaic)}$$

I computed allele frequencies by pooling data from each of the following sets of samples:

- West and Central Africans: a pool of 9 samples from the Mbuti, Yoruba and Mende populations (S_Mbuti-1, S_Mbuti-2, S_Mbuti-3, B_Mbuti-4, S_Yoruba-1, S_Yoruba-2, S_Yoruba-3, S_Mende-1, S_Mende-2)
- Dinka: a pool of 3 samples (S_Dinka-1, S_Dinka-2, B_Dinka-3)
- Archaic: a pool of 2 samples (Altai Neanderthal and the Siberian Denisova)

This data was acquired from the Simons Genome Diversity Project (SGDP, https://www.simonsfoundation.org/simons-genome-diversity-project/)[9]. I downloaded v3 of the compressed SGDP-lite version and used Ctools to query the samples in question. I then merged these samples with Oase 2, Sunghir and ancient genomes used in [14], subsetting to the ~2.2 million SNPs used in [14] to stay directly comparable to those estimates. I finally merged the resulting proportions with those calculated using the same method from Fu et al. 2016[14]. For Oase 1, estimates using multiple methods and either using all SNPs or only transversions, were available from the original publication[15]. However, I decided to use the values recalculated in Fu et al. 2015[14] to be consistent in the method of estimating Neanderthal ancestry proportions.

2.6.7 G-PhoCS analysis for Oase

I used G-PhoCS 1.2.3[50] to reconstruct the joint demographic history of high-coverage Upper Palaeolithic samples from Europe. In addition to the three available high-coverage samples (Oase 2, Ust'Ishim and Sunghir), I also included the Altai Neanderthal[33] for information on Neanderthal admixture and a modern African as a reference sample largely free from the Neanderthal admixture[51]. I chose to use a high-quality San genome from the same publication as the Altai Neanderthal[33] (HGDP01037 from Panel B). This analysis estimates split times, population sizes and migration rates on a tree with a given topology, given sequence data from short, homologous windows from (some) samples at the leaves of the tree.

2.6.7.1 Topology of the tree

G-PhoCS represents the demographic history of a collection of samples by a binary tree in which each branch is a population, with each sample belonging to a different leaf branch and interior branches corresponding to (unsampled) ancestral populations. In addition, the sampling time of leaves and unidirectional migration bands between any two branches can be defined. I based the topology of our tree (Figure 2.9) on the literature and our previous analysis, the former showing that Neanderthals are an outgroup to anatomically modern humans and the San Pygmies are an outgroup to Eurasians. In order to establish the relationship between our three Upper Palaeolithic genomes, I first tried topologies with each pair of them, before running the final tree with all three genomes.

I set the sample ages to zero for the modern San Pygmy, to the age estimated using G-PhoCS for the Altai Neanderthal[50] and to the mean estimates from the radiocarbon dating of Sunghir[31]and Ust'Ishim[16] (Table 2.2). The radiocarbon dating for Oase 2 failed and since the human remains in Pestera cu Oase are a palaeo-surface find, stratigraphic dating is also not possible[19]. However, the morphological similarities point to contemporaneity between Oase 1 and Oase 2, so I decided to take the radiocarbon date for Oase 1 (~37.8 kya) as the estimated age of Oase 2.

Table 2.2 Sample ages used in the G-PhoCS analysis.

Sample	Age [years]
Altai Neanderthal	90,000
San Pygmy	0
Sunghir	32,000
Oase 2	37,800
Ust'Ishim	45,000

I only had migration bands from the Neanderthal to the Upper Palaeolithic tips of the tree, to estimate the proportion of their ancestry originating from Neanderthals. Migration to modern Africans was not allowed, as they are not thought to have a considerable Neanderthal component: the size of such a component was estimated to be only up to 0.7% using an ancient African reference[51] and the 95% confidence interval of the estimated migration rates overlapped with zero in a previous analysis using G-PhoCS[50].

2.6.7.2 Genome-wide windows of high sample coverage for demographic analysis

For each of our high-coverage samples, high-coverage, 1kb long windows were extracted. To find a good set of windows, I first generated all-sites coverage information for all chromosomes. I excluded problematic regions in the genome considered as: regions with poor alignment quality, recombination hotspots, regions of poor mapping quality, duplications, regions under selection (genes and conserved elements), repetitive regions and positions with systematic sequencing errors, using the following filters from Kuhlwilm et al. 2016[50], sent kindly by Ilan Gronau:

- filter_hotspot1000g: Recombination hotspots
- filter_Map20: Sites with poor mapping quality
- filter_rmsk20: Recent duplications
- filter_segDups: Recent segmental duplications
- filter_selection_10000_100: Gene exons together with the 1 kbp flanking regions in each direction and conserved non-coding sequences corresponding to PhastCons elements
- filter_simpleRepeat: Simple repeats
- filter_SysErrHCB and filter_SysErr: Positions with systematic sequencing errors

For more details, see Supplementary SI 8 in Kuhlwilm et al. 2016[50].

I then extracted the depth information using a custom code written in C, again filtering for sites with read depth between 10 and twice the average coverage of the sample:.

```
samtools-0.1.19 mpileup -C50 -uRID -f $FASTA  -r chr$CHR -l Beds/chr${CHR}.bed
$FILES $DINKA_DIR/chr$CHR.dedup.realign.recal.bam
$SAN_DIR/chr$CHR.dedup.realign.recal.bam $ALTAI_NEA.$CHR.dq.chr.bam
2>Genotypes/log.geno.chr$CHR.txt | bcftools-0.1.19 view -gc -
2>>Genotypes/log.geno.chr$CHR.txt | ./get_genotypes dpMin=10 maxDpProp=2.0
1>Genotypes/geno.chr$CHR.txt 2>>Genotypes/log.geno.chr$CHR.txt
```

Sites with very low and very high coverage were avoided because alignment and genotyping can be problematic[52] – for example, heterozygous calls are unreliable if coverage is too low, whereas a coverage unusually high given the average sample coverage can signal repetitive regions and spurious alignment.

I then scanned each chromosome for good windows, using a simple heuristic to maximise the sample coverage. I start by finding the first 1kb window with at least 80% coverage. I then search locally for a window within the next 10 kb for the 1kb window with the highest coverage. Finally, I jump 5 kb forward from the chosen location and repeat the process until I reach the end of the chromosome. For the whole genome, this yielded a total of 45759 windows. I then used SAMtools/BCFtools 0.1.19 [40](using flags as above) and custom programs written in C and MATLAB to extract genotypes or the windows and converted the genotypes into FASTA files for G-PhoCS. To deal with DNA damage in ancient samples, I "*in vitro*" deaminated all our sequences, as already done for previous analyses of aDNA[27].

2.6.7.3 G-PhoCS setup

Gamma distributed priors were used for all observables. The shape parameter was set to an intermediate value of 1 for both population sizes and split times, to obtain a mean to standard deviation ratio of unity and allow sufficient exploration of the parameter space without an overly long convergence time. The rate parameter was set to result in means in the correct range, based on previous knowledge on population sizes of hunter-gatherers and the split times between Neanderthals and modern humans, Africans and non-Africans and within Eurasia. I also ran initial exploratory runs with a variety of starting values, using a single MCMC chain with 200,000 iterations, out of which, the first 100,000 were discarded as burn-in. Furthermore, it was shown that the initial value for MCMC chains in G-PhoCS hardly affects the resulting means, it only slows down convergence[32]. The rate parameters used are shown in Table 2.3.

Table 2.3 Rate parameters used in the priors for the G-PhoCS analysis.

Parameter	Rate parameter	Mean
N (for all populations)	10,000	6,667 individuals
$\mathbf{t_{UP1\text{-}UP2}}$	100,000	66,667 years
$\mathbf{t_{UP1\text{-}UP2\text{-}UP3}}$	80,000	82,500 years
$\mathbf{t_{UP\ \text{-}San}}$	33,333	200,000 years
$\mathbf{t_{UP\text{-}San\text{-}Neanderthal}}$	11,111	600,000 years

For all our migration bands, I used a weak prior with a shape parameter of 0.002 and a mean of 200 to allow exploration of the whole space, as in previous publications[32,50].

I used G-PhoCS's automatic feature to set step sizes (finetune parameters) of the Markov chain for each parameter, which aims for intermediate acceptance ratios. During this procedure, the first 10,000 steps were used to find appropriate step sizes, by updating parameters every 100 MCMC steps and performing 100 updates. After step sizes were set, 250,000 MCMC steps were performed and the first 100,000 steps were discarded as burn-in. After observing traces of observables, I found that our demographic parameters of interest converged well before the end of the burn-in period (Supplementary Figure A.11 to Supplementary Figure A.17). I ran two independent chains for each setting to assess appropriate mixing of the chain, and observed no problems.

2.6.7.4 Converting dates

G-PhoCS reports mutation-scaled split times, which I converted back into calendar years based on the mutation rate calibrated on aDNA from the high quality Ust'Ishim[16] individual (0.5e-9 per site per year), which is also in line with estimates from high quality modern genomes[53]. I converted this mutation rate for our *in vitro* deaminated sequences by multiplying it with a factor of 0.3, based on the ratio of average levels of polymorphism before and after deamination on our modern genomes.

2.7 Bibliography

1. Jones, E. R. *et al.* Upper Palaeolithic genomes reveal deep roots of modern Eurasians. *Nat. Commun.* **6,** 8912 (2015).

2. Groucutt, H. S. *et al.* Rethinking the dispersal of Homo sapiens out of Africa. *Evol. Anthropol. Issues News Rev.* **24,** 149–164 (2015).

3. Soares, P. *et al.* Correcting for Purifying Selection: An Improved Human Mitochondrial Molecular Clock. *Am. J. Hum. Genet.* **84,** 740–759 (2009).

4. Liu, H., Prugnolle, F., Manica, A. & Balloux, F. A Geographically Explicit Genetic Model of Worldwide Human-Settlement History. *Am. J. Hum. Genet.* **79,** 230–237 (2006).

5. Eriksson, A. *et al.* Late Pleistocene climate change and the global expansion of anatomically modern humans. *Proc. Natl. Acad. Sci.* **109,** 16089–16094 (2012).

6. Foley, R. A. & Lewin, R. *Principles of Human Evolution*. (John Wiley & Sons, 2013).

7. Pagani, L. *et al.* Genomic analyses inform on migration events during the peopling of Eurasia. *Nature* **538,** 238–242 (2016).

8. Malaspinas, A.-S. *et al.* A genomic history of Aboriginal Australia. *Nature* **538,** nature18299 (2016).

9. Mallick, S. *et al.* The Simons Genome Diversity Project: 300 genomes from 142 diverse populations. *Nature* **538,** 201–206 (2016).

10. Mellars, P. Why did modern human populations disperse from Africa ca. 60,000 years ago? A new model. *Proc. Natl. Acad. Sci.* **103,** 9381 (2006).

11. Mellars, P. Going East: New Genetic and Archaeological Perspectives on the Modern Human Colonization of Eurasia. *Science* **313,** 796–800 (2006).

12. Barker, G. *et al.* The 'human revolution' in lowland tropical Southeast Asia: the antiquity and behavior of anatomically modern humans at Niah Cave (Sarawak, Borneo). *J. Hum. Evol.* **52,** 243–261 (2007).

13. Yang, M. A. *et al.* 40,000-Year-Old Individual from Asia Provides Insight into Early Population Structure in Eurasia. *Curr. Biol.* **27,** 3202–3208.e9 (2017).

14. Fu, Q. *et al.* The genetic history of Ice Age Europe. *Nature* **534,** 200–205 (2016).

15. Fu, Q. *et al.* An early modern human from Romania with a recent Neanderthal ancestor. *Nature* **524,** 216–219 (2015).

16. Fu, Q. *et al.* Genome sequence of a 45,000-year-old modern human from western Siberia. *Nature* **514,** 445–449 (2014).

17. Raghavan, M. *et al.* Upper Palaeolithic Siberian genome reveals dual ancestry of Native Americans. *Nature* **505,** 87–91 (2014).

18. Rosenberg, N. A. *et al.* Genetic Structure of Human Populations. *Science* **298,** 2381–2385 (2002).

19. Trinkaus, E., Milota, Ş., Rodrigo, R., Mircea, G. & Moldovan, O. Early modern human cranial remains from the Peştera cu Oase, Romania. *J. Hum. Evol.* **45,** 245–253 (2003).

20. Trinkaus, E. *et al.* An early modern human from the Peştera cu Oase, Romania. *Proc. Natl. Acad. Sci.* **100,** 11231–11236 (2003).

21. Rougier, H. *et al.* Peştera cu Oase 2 and the cranial morphology of early modern Europeans. *Proc. Natl. Acad. Sci.* **104,** 1165–1170 (2007).

22. Skoglund, P. *et al.* Reconstructing Prehistoric African Population Structure. *Cell* **171,** 59–71.e21 (2017).

23. Quinlan, A. R. & Hall, I. M. BEDTools: a flexible suite of utilities for comparing genomic features. *Bioinformatics* **26,** 841–842 (2010).

24. Green, R. E. *et al.* The Neandertal genome and ancient DNA authenticity. *EMBO J.* **28,** 2494–2502 (2009).

25. Ginolhac, A., Rasmussen, M., Gilbert, M. T. P., Willerslev, E. & Orlando, L. mapDamage: testing for damage patterns in ancient DNA sequences. *Bioinformatics* **27,** 2153–2155 (2011).

26. Andrews, R. M. *et al.* Reanalysis and revision of the Cambridge reference sequence for human mitochondrial DNA. *Nat. Genet.* **23,** 147 (1999).

27. Green, R. E. *et al.* A Draft Sequence of the Neandertal Genome. *Science* **328,** 710–722 (2010).

28. Fu, Q. *et al.* DNA analysis of an early modern human from Tianyuan Cave, China. *Proc. Natl. Acad. Sci.* **110,** 2223–2227 (2013).

29. Siska, V. *et al.* Genome-wide data from two early Neolithic East Asian individuals dating to 7700 years ago. *Sci. Adv.* **3,** e1601877 (2017).

30. Seguin-Orlando, A. *et al.* Paleogenomics. Genomic structure in Europeans dating back at least 36,200 years. *Science* **346,** 1113–1118 (2014).

31. Sikora, M. *et al.* Ancient genomes show social and reproductive behavior of early Upper Paleolithic foragers. *Science* (2017). doi:10.1126/science.aao1807

32. Gronau, I., Hubisz, M. J., Gulko, B., Danko, C. G. & Siepel, A. Bayesian inference of ancient human demography from individual genome sequences. *Nat Genet* **43,** 1031–1034 (2011).

33. Prüfer, K. *et al.* The complete genome sequence of a Neanderthal from the Altai Mountains. *Nature* **505,** 43–49 (2014).

34. Morin, E. Evidence for declines in human population densities during the early Upper Paleolithic in western Europe. *Proc Natl Acad Sci U A* **105,** 48–53 (2008).

35. Gamba, C. *et al.* Genome flux and stasis in a five millennium transect of European prehistory. *Nat. Commun.* **5,** 5257 (2014).

36. Li, H. & Durbin, R. Inference of human population history from individual whole-genome sequences. *Nature* **475,** 493–496 (2011).

37. Dabney, J. *et al.* Complete mitochondrial genome sequence of a Middle Pleistocene cave bear reconstructed from ultrashort DNA fragments. *Proc Natl Acad Sci U A* **110,** 15758–15763 (2013).

38. Gansauge, M.-T. & Meyer, M. Single-stranded DNA library preparation for the sequencing of ancient or damaged DNA. *Nat. Protoc.* **8,** 737–748 (2013).

39. Martin, M. Cutadapt removes adapter sequences from high-throughput sequencing reads. *EMBnet J* **17,** 10–12 (2011).

40. Li, H. *et al.* The Sequence Alignment/Map format and SAMtools. *Bioinformatics* **25,** 2078–2079 (2009).

41. McKenna, A. *et al.* The Genome Analysis Toolkit: a MapReduce framework for analyzing next-generation DNA sequencing data. *Genome Res* **20,** 1297–1303 (2010).

42. Jónsson, H., Ginolhac, A., Schubert, M., Johnson, P. L. F. & Orlando, L. mapDamage2.0: fast approximate Bayesian estimates of ancient DNA damage parameters. *Bioinformatics* **29,** 1682–1684 (2013).

43. Milne, I. *et al.* Using Tablet for visual exploration of second-generation sequencing data. *Brief. Bioinform.* **14,** 193–202 (2013).

44. Kloss-Brandstätter Anita *et al.* HaploGrep: a fast and reliable algorithm for automatic classification of mitochondrial DNA haplogroups. *Hum. Mutat.* **32,** 25–32 (2010).

45. Lazaridis, I. *et al.* Ancient human genomes suggest three ancestral populations for present-day Europeans. *ArXiv13126639 Q-Bio* (2013).

46. Purcell, S. *et al.* PLINK: a tool set for whole-genome association and population-based linkage analyses. *Am J Hum Genet* **81,** 559–575 (2007).

47. Lazaridis, I. *et al.* Genomic insights into the origin of farming in the ancient Near East. *Nature* **536,** 419–424 (2016).

48. Reich, D., Thangaraj, K., Patterson, N., Price, A. L. & Singh, L. Reconstructing Indian population history. *Nature* **461,** 489–494 (2009).

49. Patterson, N. *et al.* Ancient Admixture in Human History. *Genetics* **192,** 1065–1093 (2012).

50. Kuhlwilm, M. *et al.* Ancient gene flow from early modern humans into Eastern Neanderthals. *Nature* **530,** 429–433 (2016).

51. Llorente, M. G. *et al.* Ancient Ethiopian genome reveals extensive Eurasian admixture throughout the African continent. *Science* **350,** 820–822 (2015).

52. Rasmussen, M. *et al.* The genome of a Late Pleistocene human from a Clovis burial site in western Montana. *Nature* **506,** 225–229 (2014).

53. Kong, A. *et al.* Rate of de novo mutations and the importance of father's age to disease risk. *Nature* **488,** 471–475 (2012).

Chapter 3 Upper Palaeolithic genomes reveal deep roots of modern Eurasians

3.1 Abstract

We extend the scope of European palaeogenomics by sequencing the genomes of Late Upper Palaeolithic (13,300-year-old, 1.4-fold coverage) and Mesolithic (9,700-year-old, 15.4-fold) males from western Georgia in the Caucasus and a Late Upper Palaeolithic (13,700-year-old, 9.5-fold) male from Switzerland. While we detect genomic continuity from the Late Palaeolithic to the Mesolithic in both regions, we find that Caucasus hunter-gatherers (CHG) belong to a distinct ancient clade that split from western hunter-gatherers ~45 kya, shortly after the expansion of anatomically modern humans into Europe and from Neolithic farmers ~25 kya, around the Last Glacial Maximum. Relatives of the CHG genomes significantly contributed to the Yamnaya steppe herders who migrated into Europe ~3,000 BC, supporting a formative Caucasus influence on this important Early Bronze age culture. CHG-related populations also left their imprint on modern populations from the Caucasus and also central and south Asia, possibly marking the arrival of Indo-Aryan languages.

3.2 Contribution

This study was published as part of Jones et al., 2016[1]. I was responsible for performing the model-based clustering analysis and the coalescent-based modelling using the softwares ADMIXTURE and G-PhoCS, respectively.

3.3 Introduction

Ancient genomes from Eurasia have revealed three ancestral populations that contributed to contemporary Europeans in varying degrees[2]. Mesolithic individuals, sampled from Spain all the way to Hungary[2–4], belong to a relatively homogenous group, termed western hunter-gatherers (WHG). The expansion of early farmers (EF) out of South-West Asia during the Neolithic transition led to major changes in the European gene pool, with almost complete replacement in the south and increased mixing with local WHG further north and west[2–6]. Finally, a later wave represented by the Early Bronze Age Yamnaya from the Pontic steppe, carrying partial ancestry from ancient north Eurasians (ANE) and from a second, undetermined source, arrived from the east, profoundly changing populations and leaving a cline of admixture in Eastern and Central Europe[2,4,7]. This view, which was initially based on a handful of genomes, was recently confirmed by extensive surveys of Eurasian samples from the Holocene[6,8].

Since the publication that forms the basis of this chapter, additional data from the Near East and South-West Asia has become available, which expanded our views on the spread of farming in Western Eurasia. First, ancient genomes from the European and Asian sides of the Aegan uncovered a line of ancestry stretching from the Near East to early farmers from Europe[9]. Then, Early Neolithic genomes from Iran revealed an eastern group of farmers that was genetically different from their early European counterparts and was related more (although not directly descendant) to the samples from the Caucasus presented here[10,11].

Finally, data from the southern Caucasus (Armenia), northwestern Anatolia (Turkey), Iran, and the southern Levant (Israel and Jordan) including hunter-gatherers, early farmers and samples from later ages[12] confirmed that the first farmers were highly differentiated and related to local hunter-gatherers. This study also validated the link between early farmers from northwestern Anatolia and Europe and showed that relatives of Iranian farmers expanded north, towards the Eurasian steppe and contributed to the steppe herders. Together, these studies showed that pre-agricultural populations in the Near East were highly structured, and that the earliest farmers were related to local hunter-gatherers, thus preserving this structure. These distinct ancestries were then spread by the expansion of early farmers, but then mixed again through subsequent migrations, such as those during the Bronze Age. I will reflect on these results and on how they relate to the presented body of work in the discussion of this chapter.

In this study, we extended our view of the genetic makeup of early Europeans by both looking further back in time and sampling from the crossroads between the European and Asian continents. We sequenced a Late Upper Palaeolithic ('Satsurblia' from Satsurblia cave, 13,300-year-old, 1.4-fold coverage) and a Mesolithic genome ('Kotias' from Kotias Klde cave, 9,700-year-old, 15.4-fold) from western Georgia, at the very eastern boundary of Europe. We term these two individuals Caucasus hunter-gatherers (CHG). To extend our overview of WHG to a time depth similar to the one available for our samples from the Caucasus, we also sequenced a western European Late Upper Palaeolithic genome, 'Bichon' (13,700-year-old, 9.5-fold) from Grotte du Bichon, Switzerland. These new genomes, together with already published data, provide us with a much-improved geographic and temporal coverage of genetic diversity across Europe after the Last Glacial Maximum (LGM)[13]. We show that CHG belong to a new, distinct ancient clade that split from WHG ~45kya and from Neolithic farmers ~25kya. In our panel, this clade represents the best surrogate for the previously undetermined source of ancestry to the Yamnaya, and its relatives contributed to modern populations from the Caucasus all the way to Central Asia.

3.4 Results

3.4.1 Samples, sequencing and authenticity

Recent excavations of Satsurblia cave in western Georgia yielded a human right temporal bone, dated to the Late Upper Palaeolithic 13,132-13,380 cal. BP. Following the approach of Gamba *et al.*[4], extractions from the dense part of the petrous bone yielded sequencing libraries comprising 13.8% alignable human sequence which were used to generate 1.4-fold genome coverage. A molar tooth sampled from a later Mesolithic (9,529-9,895 cal. BP) burial in Kotias Klde, a rock shelter also in western Georgia showed excellent preservation, with endogenous human DNA content of 76.9%. This was sequenced to 15.4-fold genome coverage. Grotte du Bichon is a cave situated in the Swiss Jura Mountains where a skeleton of a young male of Cro-magnon type was found and dated to the late Upper Palaeolithic 13,560- 13,770 cal. BP. A petrous bone sample extraction from this also gave excellent endogenous content at 71.5% and was sequenced to 9.5-fold coverage. The sequence data from each genome showed sequence length and nucleotide misincorporation patterns which were indicative of post-mortem damage and contamination estimates, based on X chromosome and mitochondrial DNA tests (see methods), were less than 1%; comparable to those found in other ancient genomes [3,4,13].

3.4.2 Continuity across the Palaeolithic-Mesolithic boundary

Kotias and Satsurblia, the two Caucasus hunter gatherer genomes (CHG), are genetically different from all other early Holocene (*i.e.* Mesolithic and Neolithic) ancient genomes[2–7,13–15], while Bichon is similar to other younger WHG. The distinctness of CHG can be clearly seen on a principal component analysis (PCA) plot[16] where ancient samples were projected on contemporary Eurasian populations[2]. CHG genomes fall between modern Caucasian and South-Central Asian populations in a region of the graph separated from both other hunter gatherer and early farmer samples (Figure 3.1A). Clustering using ADMIXTURE software[17] confirms this pattern, with CHG forming their own homogenous cluster (Figure 3.1B). The close genetic proximity between Satsurblia and Kotias is also formally supported by *D*-statistics[18] , indicating the two CHG genomes form a clade to the exclusion of other pre-Bronze Age ancient genomes (Supplementary Table B.3), suggesting continuity across the Late Upper Palaeolithic and Mesolithic periods. This result is mirrored in western Europe as Bichon: i) is close to other WHG on the first two dimensions in the PCA space (Figure 3.1A) and outgroup f_3 analysis (Supplementary Figure B.1), ii) belongs to the same cluster as other WHG in ADMIXTURE analysis (Figure 3.1B) and iii) forms a clade with other WHG to the exclusion of other ancient genomes based on D-statistics (Supplementary Table B.4). Thus, these new data indicate genomic persistence between the Late Upper Palaeolithic and Mesolithic both within western Europe and, separately, within the Caucasus.

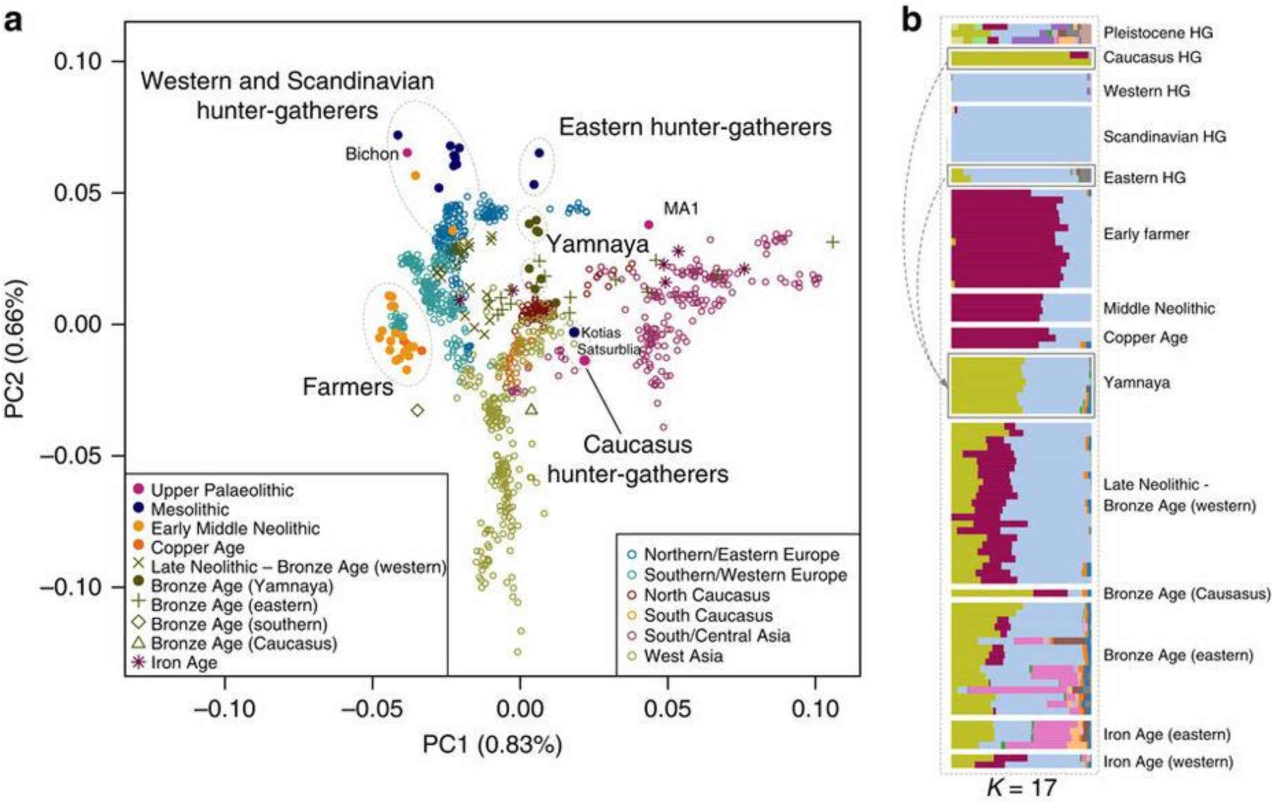

Figure 3.1 Genetic structure of ancient Europe. A. Principal component analysis. Ancient data from Bichon, Kotias and Satsurblia genomes were projected[11] onto the first two principal components defined by selected Eurasians from the Human Origins dataset[1]. The percentage of variance explained by each component accompanies the titles of the axes. For context we included data from published Eurasian ancient genomes sampled from the Late Pleistocene and Holocene where at least 200,000 SNPs were called[1–7,9] (Supplementary Table B.1). Among ancients, the early farmer and western hunter-gatherer (including Bichon) clusters are clearly identifiable, and the influence of ancient north Eurasians is discernible in the separation of eastern hunter-gatherers and the Upper Palaeolithic Siberian sample MA1. The two Caucasus hunter-gatherers occupy a distinct region of the plot suggesting a Eurasian lineage distinct from previously described ancestral components. The Yamnaya are located in an intermediate position between CHG and EHG. B. ADMIXTURE ancestry components[12] for ancient genomes (K=17) showing a CHG component (Kotias, Satsurblia) which also segregates in the Yamnaya and later European populations.

3.4.3 Deep coalescence of early Holocene lineages

The geographical proximity of the southern Caucasus to the Levant begs the question of whether CHG might be related to early Neolithic farmers with Near Eastern heritage. To formally address this question, we reconstructed the relationship among WHG, CHG and EF using available high quality ancient genomes[2–4]. Outgroup f_3-statistics[19] were used to compare the three possible topologies, with the correct relationship being characterised by the largest amount of shared drift between the two groups that form a clade with respect to the outgroup (Figure 3.2A; Supplementary Table B.5). A scenario in which the population ancestral to both CHG and EF split from WHG receives the highest support, implying that CHG and EF form a clade with respect to WHG. A scenario in which CHG and WHG form a distinct clade with respect to EF can be rejected. The known admixture of WHG with EF[2,4–6] (WHG component in our EF samples) implies that some shared drift is found between WHG and EF with respect to CHG, but this is much smaller than the shared drift between CHG and EF. Thus, WHG split first, with CHG and EF separating only at a later stage.

I next dated the splits among WHG, CHG and EF using a coalescent model implemented in G-PhoCS[20], based on the high coverage genomes in our dataset (Figure 3.2B for a model using the German farmer Stuttgart[2] to represent EF; Supplementary Table B.6 for models using the Hungarian farmer NE1[4]) and taking advantage of the mutation rate recently derived from Ust'-Ishim[15]. G-PhoCS dates the split between WHG and the population ancestral to CHG and EF at ~40-50 kya (range of best estimates depending on which genomes are used; see Supplementary Table B.6 for details), implying that they diverged early on during the colonisation of Europe[21], and well before the LGM. On the WHG branch, the split between Bichon and Loschbour[2] is dated to ~16-18 kya (just older than the age of Bichon), implying continuity in western Europe, which supports the conclusions from our previous analyses. The split between CHG and EF is dated at ~20-30 kya, emerging from a common basal Eurasian lineage[2] (Supplementary Figure B.2) and suggesting a possible link with the LGM, although the broad confidence intervals require some caution with this interpretation. Overall, the sharp genomic distinctions between these post-LGM populations contrasts with the comparative lack of differentiation between the earlier Eurasian genomes, *e.g.* as visualised in the ADMIXTURE analysis (Figure 3.1A), and it seems likely that this structure could have emerged as a result of ice age habitat restriction. WHG and CHG also carry different markers with known links to their phenotypes. For example, like EF, but in contrast to WHG, CHG carry a variant of the *SLC24A5* gene[22] associated with light skin pigmentation (rs1426654, see Supplementary Information). This trait, which is believed to have risen to high frequency during the Neolithic expansion[23], may thus have a relatively long history in Eurasia, with its origin probably predating the LGM, if the variant in EF and CHG has a common origin.

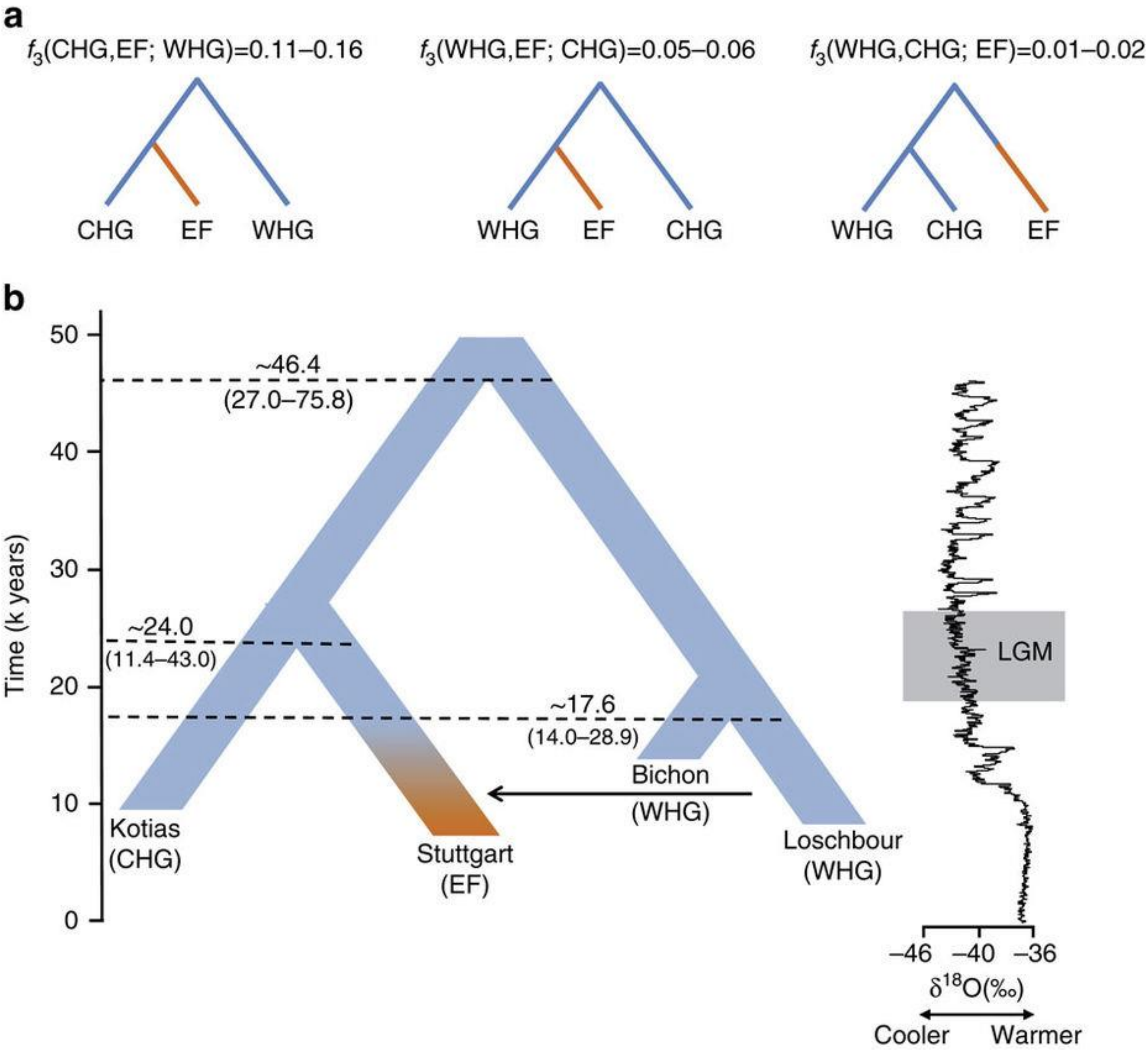

Figure 3.2 The relationship between Caucasus hunter-gatherers, western hunter-gatherers and early farmers. A. Alternative phylogenies relating western hunter-gatherers (WHG), Caucasus hunter-gatherers (CHG), and early farmers (EF, highlighted in orange), with the appropriate outgroup f_3-statistics. B. The best supported relationship among CHG (Kotias), WHG (Bichon, Loschbour), and EF (Stuttgart), with split times estimates using G-Phocs[20]. Oxygen 18 values (per mile) from the NGRIP core provide the climatic context; the grey box shows the extent of the Last Glacial Maximum (LGM).

We also investigated the relationship between a partial genome from a 24,000 year old individual (MA1) from Mal'ta, Siberia[7] and CHG. MA1 had been shown to be divergent from other ancient samples and to have more shared alleles with nearly all modern Europeans than with an EF genome by Lazaridis et al.[2]. This allowed inference of an ancient north Eurasian (ANE) component in European ancestry, which was subsequently shown to have an influence in later eastern hunter gatherers and to have spread into Europe via incoming Steppe herders beginning ~4,500 years ago[6,8]. Several analyses indicate that CHG genomes are not a subset of this ANE lineage. First, MA1 and CHG fall in distinct regions of the PCA plot and also have very different profiles in the ADMIXTURE analysis (Figure 3.1). Second, when we test if CHG shows any evidence of excess allele sharing with MA1 or with EHG relative to western hunter gatherers using tests of the form *D*(Yoruba, *CHG*; MA1, *WHG*), no combinations were significantly positive (Supplementary Table B.7). Although such a test loses power when the number of overlapping SNPs is low, in this case, we had a high number of markers for the comparison (over 200,000 for MA1 and over 100,000 for EHG). Last, we also tested whether the ancestral component inferred in modern Europeans from MA1 was distinct from any that may have been donated from CHG using tests of the form *D*(Yoruba, MA1; CHG, *modern north European population*) (Supplementary Table B.8). All northern Europeans showed a significant amount of shared alleles with MA1 separate to any they shared with CHG.

We have shown that WHG and CHG are the descendants of two ancient populations that appear to have persisted in Europe since the mid Upper Palaeolithic and survived the LGM separately. We looked at runs of homozygosity (ROH: Figure 3.3) which inform on past population size or inbreeding[4,24,25]. Both WHG and CHG have a high frequency of ROH and in particular, the older CHG, Satsurblia, shows signs of recent consanguinity, with a high frequency of longer (>4Mb) ROH. In contrast, EF are characterised by lower frequency of ROH of all sizes, suggesting a less constricted population history with larger population sizes and/or less inbreeding[25,26], perhaps associated with a more benign passage through the LGM than the more northern populations.

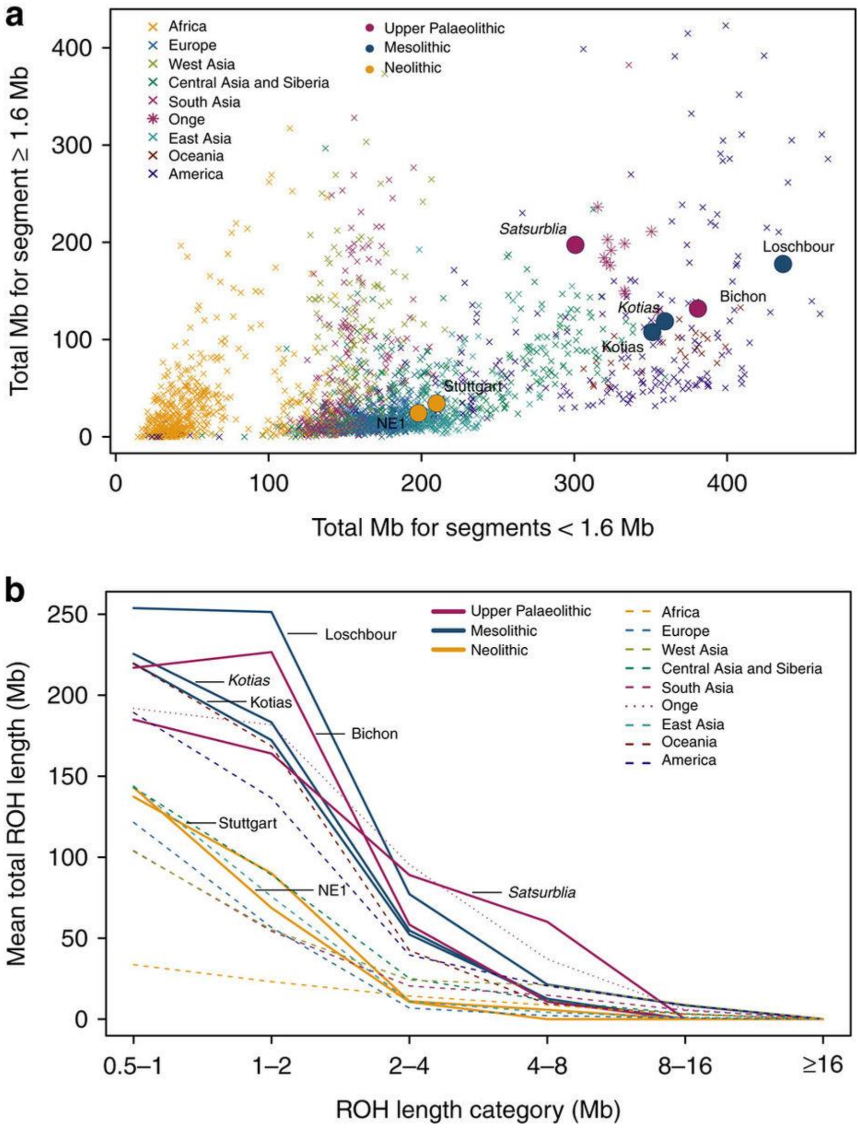

Figure 3.3 Distribution of ROH. A. The total length of short ROH (<1.6Mb) plotted against the total length of long ROH (≥1.6 Mb) and B. mean total ROH length for a range of length categories. ROH were calculated using a panel of 199,868 autosomal SNPs. For Kotias we analysed both high-coverage genotypes and genotypes imputed from down-sampled data (marked in italics; see Supplementary Information). Diploid genotypes imputed from low-coverage variant calls were used for Satsurblia and high coverage genotypes were used for all other samples. A clear distinction is visible between both WHG and CHG who display an excess of shorter ROH, akin to modern Oceanic and Onge populations, and EF who resemble other populations with sustained larger ancestral population sizes.

3.4.4 Caucasus hunter-gatherer contribution to subsequent populations

We next explored the extent to which Bichon and CHG contributed to contemporary populations using outgroup f_3(African; *modern*, *ancient*) statistics, which measure the shared genetic history between an ancient genome and a modern population since they diverged from an African outgroup. Bichon, like younger WHG, shows strongest affinity to northern Europeans (Supplementary Figure B.3), whilst contemporary southern Caucasus populations are the closest to CHG (Figure 3.4A & Supplementary Figure B.3), thus implying a degree of continuity in both regions stretching back at least 13,000 years to the late Upper Palaeolithic. Continuity in the Caucasus is also supported by the mitochondrial and Y-chromosomal haplogroups of Kotias (H13c and J2a respectively) and Satsurblia (K3 and J), which are all found at high frequencies in Georgia today[27–29] (see Supplementary Information for further details).

EF share greater genetic affinity to populations from southern Europe than to those from northern Europe with an inverted pattern for WHG[2–6]. Surprisingly, we find that CHG influence is stronger in northern than southern Europe (Figure 3.4A & Supplementary Figure B.3) despite the closer relationship between CHG and EF compared to WHG, suggesting an increase of CHG ancestry in western Europeans subsequent to the early Neolithic period. We investigated this further using *D*-statistics of the form *D*(Yoruba, Kotias; EF, *modern western European population*), which confirmed a significant introgression from CHG into modern northern European genomes after the early Neolithic period (Supplementary Figure B.4).

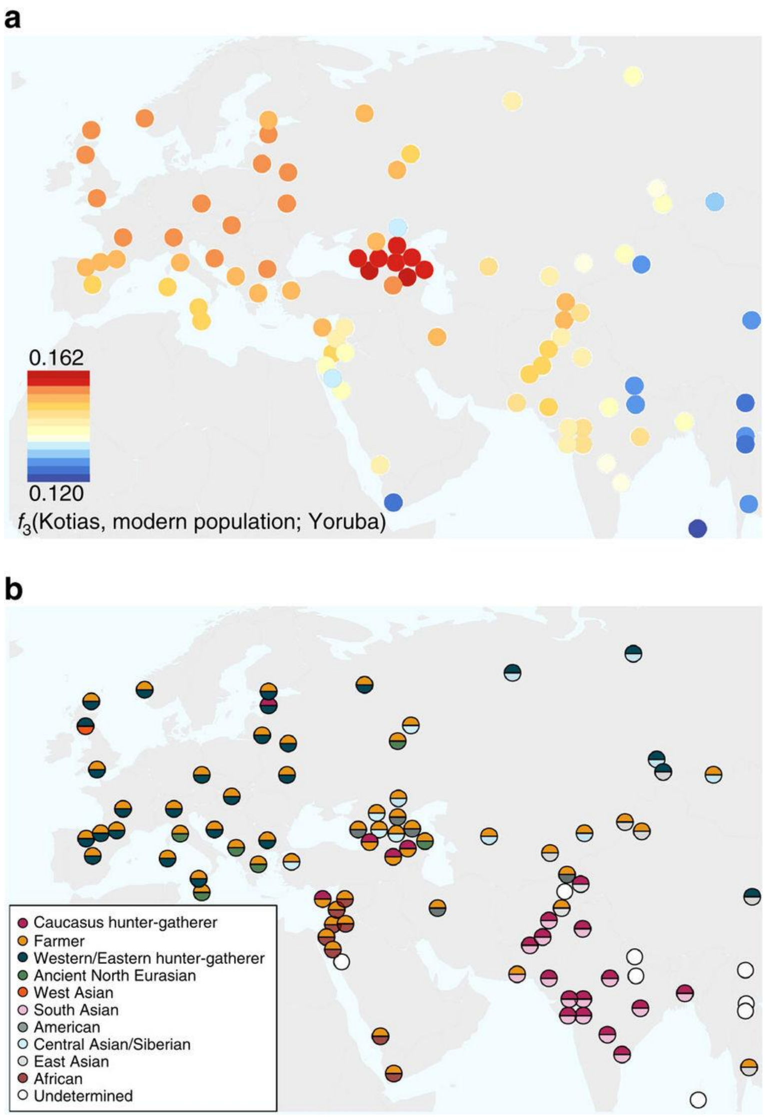

Figure 3.4 The relationship of Caucasus hunter-gatherers to modern populations. A. Genomic affinity of modern populations[2] to Kotias, quantified by the outgroup f_3-statistics of the form f_3(Kotias, modern population; Yoruba). Kotias shares the most genetic drift with populations from the Caucasus with high values also found for northern Europe and central Asia. B. Sources of admixture into modern populations: semicircles indicate those that provide the most negative outgroup f_3 statistic for that population. Populations for which a significantly negative statistic could not be determined are marked in white. Populations for which the ancient Caucasus genomes are best ancestral approximations include those of the southern Caucasus and interestingly, south and central Asia. Western Europe tends to be a mix of early farmers and western/eastern hunter-gatherers while Middle Eastern genomes are described as a mix of early farmers and Africans.

3.4.5 CHG origins of migrating Early Bronze Age herders

We investigated the temporal stratigraphy of CHG influence by comparing these data to previously published ancient genomes. We find that CHG, or a population close to them, contributed to the genetic make-up of individuals from the Yamnaya culture, which have been implicated as vectors for the profound influx of Pontic steppe ancestry that spread westwards into Europe and east into central Asia with metallurgy, horse-riding and possibly Indo-European languages in the third millenium BC[6,8]. CHG ancestry in these groups is supported by ADMIXTURE analysis (Figure 3.1B) and admixture f_3-statistics[19,30] (Figure 3.5), which best describe the Yamnaya as a mix of CHG and Eastern European hunter-gatherers.

The Yamnaya were semi-nomadic pastoralists, mainly dependent on stock-keeping but with some evidence for agriculture, including incorporation of a plow into one burial[31]. As such, it is interesting that they lack an ancestral component of the EF genome (Figure 3.1B), which permeates through western European Neolithic and subsequent agricultural populations. During the Early Bronze Age, the Caucasus was in communication with the steppe, particularly via the Maikop culture[32], which emerged in the first half of the fourth millennium BC. The Maikop culture predated and, possibly with earlier southern influences, contributed to the formation of the adjacent Yamnaya culture that emerged further to the north and may be a candidate for the transmission of CHG ancestry. In the ADMIXTURE analysis of later ancient genomes (Figure 3.1B) the Caucasus component gives a marker for the extension of Yamnaya admixture, with substantial contribution to both western and eastern Bronze Age samples. However, this is not completely coincident with metallurgy; Copper Age genomes from Northern Italy and Hungary show no contribution and neither does the earlier of two Hungarian Bronze Age individuals.

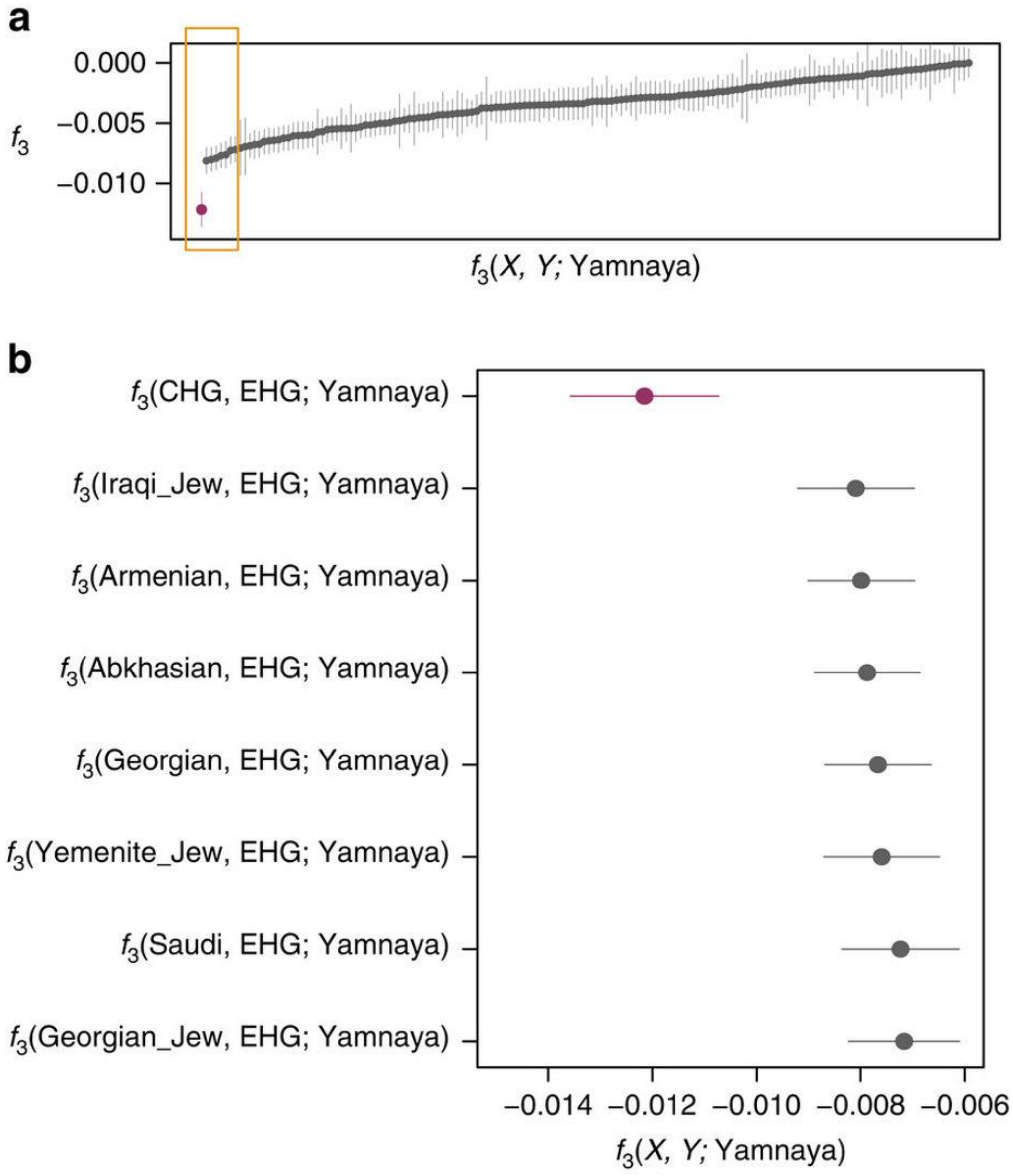

Figure 3.5 Lowest admixture f_3-statistics of the form f_3 (X, Y; Yamnaya). These statistics represent the Yamnaya as a mix of two populations with a more negative result signifying the more likely admixture event. A. All negative statistics found for the test f_3(X, Y; Yamnaya) with the most negative result f_3(CHG, EHG; Yamnaya) highlighted in purple. Lines bisecting the points show the standard error. B. The most significantly negative statistics which are highlighted by the yellow box in A. Greatest support is found for Yamnaya being a mix of Caucasus hunter gatherers (CHG) and Russian hunter gatherers who belong to the eastern extension of the WHG clade (EHG).

3.4.6 Modern impact of CHG ancestry

In modern populations, the impact of CHG also stretches beyond Europe to the east. Central and south Asian populations received genetic input from CHG (or a population close to them), as indicated by a prominent CHG component in ADMIXTURE (Supplementary Figure B.5) and admixture f_3-statistics, which represent many samples as a mix of CHG and another south Asian population (Figure 3.4B; Supplementary Table B.10). It has been proposed that modern Indians are a mixture of two ancestral components, an Ancestral North Indian (ANI) component related to modern west Eurasians and an Ancestral South Indian component related more distantly to the Onge[30]. Kotias provides the majority best surrogate for the former[33,34] (Supplementary Table B.11): it has the highest D(Yoruba,ANI; Onge, Indian population) score for 5 out of the 9 Indian populations in our panel. However, samples from the Afanasievo culture, relatives of the Early Bronze Age Yamnaya, are also a good proxy: they score highest for 3 populations, with Z scores higher than that for Kotias. A third population, the South Indian Mala is the best ANI proxy for the Kharia, but the Kharia tends to differ from other Indian populations on genetic analysis (e.g. ADMIXTURE). It is estimated that this admixture in the ancestors of Indian populations occurred relatively recently, 1,900-4,200 years BP, and is possibly linked with migrations introducing Indo-European languages and Vedic religion to the region[33].

3.5 Conclusions

Given their geographic origin, it seems likely that CHG and EF are the descendants of early colonists from Africa who stopped south of the Caucasus, in an area stretching south to the Levant and possibly east towards central and south Asia. WHG, on the other hand, are likely the descendants of a wave that expanded further into Europe. The separation of these populations is one that stretches back before the Holocene as indicated by local continuity through the Late Palaeolithic/Mesolithic boundary and deep coalescence estimates which date to around the LGM and earlier. Several analyses indicate that CHG are distinct from another inferred minority ancestor, ANE, making them a divergent fourth strand of Eurasian ancestry that expands the model of human colonisation of Europe.

The separation between CHG and both EF and WHG ended during the Early Bronze Age when a major ancestral component linked to CHG was carried west by migrating herders from the Eurasian Steppe. The foundation group for this seismic change was the Yamnaya, who we estimate to owe half of their ancestry to CHG-linked sources. These sources may be linked to the Maikop culture, which predated the Yamnaya and was located further south, closer to the Southern Caucasus. Through the Yamanya, the CHG-related ancestral strand contributed to most modern European populations, especially in the northern part of the continent. The link we found between CHG and the Yamnaya also agrees with Broushaki et al.[10] and Lazaridis et al.[12], where the the Yamnaya is modelled as a mixture of two sources, one of which is related to EHG and the other to a population from the western Near East. Although Broushaki et al. [10] found that the CHG was a better proxy than early Iranian farmers for this second component, additional, younger Iranian samples from the Chalcolithic, published by Lazaridis et al. [12] were an even better surrogate than the CHG.

Finally, we found that CHG-related ancestry was also carried east to become a major contributor to the Ancestral North Indian component found in the Indian subcontinent. The additional genomes from the Near East also failed to pinpoint the direct source of the ANI component, but found that it was related to both Iranian farmers and to populations from the Eurasian steppe[10,12]. Given that these two populations are both also related to the CHG, the similarity we found between CHG and ANI was not surprising. Exactly when the eastwards movement related to the ANI component occurred is unknown, but it likely included migration around the same time as their contribution to the western European gene pool and may be linked with the spread of Indo-European languages. However, earlier movements associated with other advancements, such as cereal farming and herding, are also plausible.

The discovery of CHG as a fourth ancestral component of the European gene pool underscores the importance of a dense geographical sampling of human palaeogenomes, especially among diverse geographical regions. Its separation from other European ancestral strands ended dramatically with the extensive population, linguistic and technological upheavals of the Early Bronze Age resulting in a wide impact of this ancestral strand on contemporary populations, stretching from the Atlantic to Central and South Asia.

3.6 Methods

3.6.1 Sample preparation and DNA sequencing

DNA was extracted from three samples: two from Georgia (Kotias and Satsurblia) and one from Switzerland (Bichon; Supplementary Figure B.6). Sample preparation, DNA extraction and library construction were carried out in dedicated ancient DNA facilities at Trinity College Dublin (Kotias and Satsurblia) and at the University of York, England (Bichon). DNA was extracted from Kotias and Satsurblia following a silica column based protocol[3] based on Yang et al.[35] and libraries were prepared and amplified with AccuPrime^{TM} Pfx Supermix (Life Technology), using a modified version of [36] as outlined in [3]. For the ancient Swiss sample Bichon, DNA was extracted following [37] and libraries were built as described above with the exception that enzymatic end-repair was arrested using heat inactivation rather than a silica-column purification step[38,39]. Libraries were first screened to assess their human DNA content on an Illumina MiSeq platform at TrinSeq, Dublin using 50 base pair (bp) single-end sequencing (Supplementary Table B.12). Selected libraries were further sequenced on a HiSeq 2000 platform using 100 bp single-end sequencing (Supplementary Table B.13).

3.6.2 Sequence processing and alignment

To reduce the effects of post-indexing contamination, raw reads were retained if the Hamming distance for the observed index was within 1 base of the expected index. Adapter sequences were trimmed from the 3' ends of reads using cutadapt version 1.3[40], requiring an overlap of 1 bp between the adapter and the read. As ancient DNA damage is more apparent at the ends of sequences[41,42], the first and last two base pairs of all reads from the deep sequencing phase of analysis (Supplementary Table B.13) were removed using SeqTK (https://github.com/lh3/seqtk). A minimum read length of 30 bp was also imposed.

Sequences were aligned using Burrows-Wheeler Aligner (BWA) version 0.7[43], with the seed region disabled, to the GRCh37 build of the human genome with the mitochondrial sequence replaced by the revised Cambridge reference sequence (NCBI accession number NC_012920.1). Sequences from the same sample were merged using Picard MergeSamFiles (http://picard.sourceforge.net/) and duplicate reads were removed using SAMtools version 0.1.19[44]. Average depth of coverage was calculated using genome analysis toolkit (GATK) Depth of Coverage and indels were realigned using RealignerTargetCreator and IndelRealigner from the same suite of tools[45]. Reads with a mapping quality of at least 30 were retained using SAMtools[39], and mapDamage 2.0[46] was used with default parameters to downscale the quality scores of likely damaged bases, reducing the influence of nucleotide misincorporation on results. Only data from the deep sequencing phase of the project (100 bp single-end sequencing on a HiSeq 2,000) were used in the subsequent analyses.

Alignment data are available through the Sequence Read Archive (SRA) under the project accession number PRJNA284219.

3.6.3 Authenticity of results

Rigorous measures were taken during laboratory work in an effort to minimize DNA contamination[4] and negative controls were processed in parallel with samples. The authenticity of the data was further assessed *in silico* in a number of ways. The data were examined for the presence of short average sequence length and nucleotide misincorporation patterns which are characteristic of aDNA[41,42] (Supplementary Figure B.7 and Supplementary

Figure B.8). The degree of mitochondrial DNA contamination[4,47] (Supplementary Table B.14) and X chromosome contamination in male samples[3] (Supplementary Table B.15 to 16) was also assessed.

3.6.3.1 Estimation of molecular damage and sequence length

Ancient DNA molecules are subject to post-mortem degradation typified by short sequence length and an over-representation of nucleotide misincorporation sites at the ends of reads[41,42]. Using a subsample of 500,000 reads per sample, which had been processed as described in the methods section with the SeqTK step omitted, we examined the sequence length distribution of our reads (Supplementary Figure B.7) and patterns of molecular damage using mapDamage 2.0[46] (Supplementary Figure B.8). Only bases with a minimum quality of 30 were considered when running mapDamage.

Endogenous DNA sequences from ancient samples tend to have an average sequence length of less than 100 bp[48] and for Kotias and Satsurblia a peak in DNA sequence length was observed at 47 bp and 48 bp respectively, with a second peak at 100bp (Supplementary Figure B.7A&B). As 100 bp sequencing was performed, all sequences greater than this length are truncated, inflating the count of 100 bp reads. The peaks at < 50 bp are more likely an accurate reflection of the modal sequence length of the molecules. Bichon shows a large peak at 100 bp with a longer, flatter distribution of reads than that from the Georgian samples (Supplementary Fig. 7C). A different extraction protocol was used for Bichon[37] compared to Satsurblia and Kotias[4]. Different extraction protocols can result in distinctive sequence length distributions for ancient next-generation sequencing data[49] and this, along with variation in DNA preservation, may have contributed to the observed differences in the length of sequences between the Caucasus hunter-gatherers (CHG) samples and Bichon.

For each sample a clear increase in C to T and G to A transitions can be seen at the 5' and 3' ends of molecules respectively (Supplementary Figure B.8), a typical hallmark of aDNA[41,42].

Misincorporation frequencies at the start and end of reads (>20% for the Georgian samples and >7% for Bichon) are consistent with levels present in other similarly aged specimens[2–4,6]. Bichon may have less damage at the 5' ends of molecules (the 3' ends were not always completely sequenced) than CHG because DNA fragments retrieved from Bichon tended to be longer (Supplementary Figure B.7) and thus better preserved.

3.6.3.2 Mitochondrial DNA contamination

Mitochondrial DNA contamination was evaluated by assessing the proportion of secondary (non-consensus) bases at haplogroup defining positions in our ancient samples[4,50]. Haplogroup defining positions determined using HAPLOFIND[51] were called in our samples using GATK Pileup[45] and filtered to remove bases with a quality < 30. The contamination rate ("C + MD") was determined by calculating the secondary base count as a fraction of the total base count at all haplogroup-defining positions[4,47]. Because of the possible influence of residual molecular damage on estimates, this was also repeated omitting sites where the secondary base could be explained by deamination ("C") [4,47]. We found low contamination rates of ≤ 0.62% for all samples (Supplementary Table B.14).

3.6.3.3 X-chromosomal contamination estimates

As all our samples were male (Supplementary Table B.18), we were able to assess the level of X chromosome contamination in our samples as described in [4] which was based on[52]. The X chromosome is found in single copy in males and therefore two or more different alleles found at a given site along this chromosome may be due to contamination, damage, sequence error or mismapping. Assuming a similar background site error rate, it is expected that contamination will be more conspicuous at polymorphic sites than at neighbouring monomorphic sites due to the increased propensity for allelic diversity at these sites in contaminating populations. We examined discordance in the rate of heterozygous calls between known polymorphic sites on the non-pseudoautosomal region of the X chromosome reported in the 1,000 Genomes Project[53] and their adjacent sites. Genotypes in the 1,000 Genomes dataset and ancient samples were called and filtered according to [4] with a minimum sequence depth of 5 required for genotypes called in Kotias and Bichon and 3 for loci called in Satsurblia (a lower threshold was used for Satsurblia due to its comparatively lower coverage). Two tests, which employ a maximum likelihood based approach, were performed to evaluate the rate of contamination. "Test 1" uses all high quality reads provided per sample while "test 2" removes the assumption of independent error rates by only sampling a single read per site (Supplementary Table B.15 & 16)[52]. A very low contamination rate of 0.99% (p-value $< 2.2 \times 10^{-16}$) was found for Kotias with similarly low levels of 0.56-0.58% (p-value = 0.001) for Satsurblia and 0.45-0.54% (p-value $< 2.2 \times 10^{-16}$) for Bichon (Supplementary Table B.17).

3.6.4 Molecular sex and uniparental haplogroups

Genetic sex was determined by examining the ratio of Y chromosome reads to reads aligning to both sex chromosomes[54] (Supplementary Table B.18). Mitochondrial haplogroups were assigned following [5] with coverage determined using GATK Depth of Coverage[45] (Supplementary Table B.19). YFitter[55], which employs a maximum likelihood based approach, was used to determine Y-chromosomal haplogroups for our ancient male samples (Supplementary Table B.20).

3.6.4.1 Mitochondrial haplogroups

Kotias (425x-fold coverage of the mitochondria) was assigned to haplogroup H13c. Mitochondrial haplogroup H, the most prevalent and diverse haplogroup found in west Eurasia, peaks in frequency in western Europe, accounting for more than 40% of total mtDNA diversity with a decreasing yet still appreciable frequency towards the Near East, the Caucasus and Central Asia (10-30%)[50]. Coalescence age estimates are considerably older for H in the Near East (23-28 kya) than in Europe (19-21 kya) and it has been proposed that H may have evolved in the southern Caucasus and northern part of the Near East where the most ancient clades of H are present[28,50,56]. Sub-haplogroup H13 is most common in the Near East and Caucasus reaching highest frequencies in Georgia and Daghestan[28]. Interestingly this sub-haplogroup has been found in individuals from the Late Neolithic Bell Beaker culture in Germany and the Early Bronze Age Yamnaya culture from the Pontic Steppe[6]. Individuals from these cultures are proposed to have a component of Near Eastern ancestry distinct from that of Early European farmers[6]. H13 has an estimated coalescence time of 20-24 kya (17-24 kya for H13c) thus placing the origin of this subclade during the LGM or even before[28].

Satsurblia (144x -fold coverage) was assigned to haplogroup K3. Satsurblia lacked 5 of the 11 mutations associated with the K3 haplogroup (Supplementary Table B.19)[51,57]. These "missing" mutations (all sites had a minimum of 119x coverage) are all on the branch leading from K to K3 suggesting that the haplotype of Satsurblia could represent an early manifestation of the K3 haplogroup. Haplogroup K is found at about 11% frequency in Georgia today with similarly high level found in the Near East[58]. Its average European frequency is 5.6%[58] however it has been a found at higher frequencies in Early European Neolithic farmers and its diffusion in Europe has been associated with the Neolithic transition[59]. Haplogroup K was found to be the predominant haplogroup among samples from Pre-Pottery Neolithic B sites in Syria[60]. This culture is thought to represent one of the original Near Eastern Neolithic communities.

Bichon (314x) belongs to haplogroup U5b1h. The U branch, especially haplogroup U5, has been found to be a dominant mitochondrial haplogroup among European hunter-gatherer communities[2,3,5,6,38,47,61].

3.6.4.2 Y-chromosomal haplogroups

Both Georgian hunter-gatherer samples were assigned to haplogroup J with Kotias belonging to the subhaplogroup J2a. Haplogroup J is estimated to have arisen 31.7 kya in the Middle East and is widely distributed in Eurasia, the Middle East and North Africa[27,29]. Patterns of haplogroup frequency are consistent with an expansion from the Middle East towards Europe which has been suggested to have accompanied the Neolithic transition in Europe[27,62,63]. In a study exploring J haplogroups in 445 individuals from Eurasia, J2a was found at highest frequency in Georgia and Iraq[27]. It is intriguing that the mitochondrial haplogroup of Satsurblia and the Y-chromosomal haplogroups of both our ancient Georgian samples have been associated with the Neolithization of Europe. This tentatively suggests a genetic link between Georgian hunter-gatherers and early European migrants from the Near East. Bichon belongs to Y haplogroup I2a (see methods). Haplogroup I has been found at high frequencies in Europe but is virtually absent elsewhere[64]. This haplogroup is suggested to have a European pre-LGM origin[65] and has been found in ancient samples with hunter-gatherer backgrounds from central and northern Europe[2,4–6].

3.6.5 Merging ancient data with published data

3.6.5.1 Modern reference dataset

Genotype calls from Kotias, Satsurblia, Bichon and selected Eurasian samples (Supplementary Table B.1) were merged with modern genotype calls from the Human Origins dataset[2] using PLINK[66]. This dataset was first filtered to exclude genotypes which had a minor allele frequency of zero in the modern populations, non-autosomal sites and modern populations with less than 4 individuals. Genotypes where neither allele was consistent with the GRCh37 orientation of the human genome were also removed.

3.6.5.2 Ancient reference dataset

3.6.5.2.1 Data sources and pre-processing

Hungarian ancient data: MapDamage 2.0[46] was used to rescale selected high coverage BAM files (Supplementary Table B.1) from Hungary[4] using default parameters.

Swedish Samples, Loschbour and Stuttgart: BAM files with genome-level coverage (Supplementary Table B.1) from [5] and [2] were realigned to the human genome as outlined before. MapDamage rescaling[46] was not performed on data from [2] as these samples had been molecularly treated to remove deaminated cytosines, reducing DNA damage associated errors.

Mal'ta (MA1) and La Braña: FASTQ files from [7] and [3] were aligned to the GRCh37 build of the human genome with the mitochondrial sequence removed. For MA1, mapDamage rescaling[46] was omitted due to the low deamination rates found in this sample[7].

Ust'-Ishim: A BAM file containing sequences from the Ust'-Ishim genome[15] was filtered to remove reads with mapping quality of less than 30. This sample had been molecularly treated to remove deaminated cytosines so mapDamage rescaling[46] was not performed.

Kostenki: A BAM file containing sequences from the Kostenki genome was downloaded from [13] and duplicate reads were removed. Sequences had already been filtered to have mapping quality > 30 and the first and last 5 bp of all reads had been soft-clipped to a base quality of zero. As terminal bases had been soft-clipped and the sample had been molecularly treated to remove deaminated cytosines, mapDamage rescaling[46] was not carried out.

Otzi the Tyrolean Iceman: Forward FASTQ files were downloaded from [14] and realigned to the GRCh37 build of the human genome with the mitochondrial sequence removed. Reads were not rescaled using mapDamage as the substitution frequencies were outside the bounds of the posterior predictive distribution intervals set by the mapDamage model[46].

Haak ancient data: Genotypes for Eurasian ancient samples (Supplementary Table B.1) which overlapped the Human Origins array[2] were downloaded from[6]. Only samples with at least 200,000 called genotypes were used, in-keeping with the level of data from other samples used in analyses. Genotypes had not been called in the first and last two bases of sequence reads and all samples had been UDG-treated (molecularly treated to remove deaminated cytosines) to reduce the influence of deaminated cytosines on analyses[6].

Allentoft ancient data: Genotypes for Bronze and Iron Age ancient samples published in [8] were kindly provided by GeoGenetics, Copenhagen. Only samples with at least 200,000 called genotypes were used (Supplementary Table B.1).

3.6.5.2.2 Genotype calling

For ancient samples with > 8x genome-wide coverage (namely Kotias, Bichon, Ust'-Ishim, Loschbour, Stuttgart, NE1 and BR2 (Supplementary Table B.1)) genotypes were determined using GATK Unified Genotyper[45]. Genotypes were called at SNP positions observed in the Human Origins dataset using sequencing data with a base quality ≥ 30, depth ≥ 8 and genotype quality ≥ 20. The resulting VCF files were converted to PLINK format using VCFtools[67].

For lower coverage samples genotypes were called at positions that overlapped with the Human Origins dataset using GATK Pileup[45]. Bases were required to have a minimum quality of 30 and all triallelic SNPs were discarded. For SNP positions with more than one base call, one allele was randomly chosen with a probability equal to the frequency of the base at that position. This allele was duplicated to form a homozygous diploid genotype which was used to represent the individual at that SNP position[68]. This merged dataset was used for PCA, ADMIXTURE, f_3-statistics, D-statistics and ROH analysis. This number of SNPs per sample for those ancient samples that were recalled is shown in Supplementary Table B.2.

3.6.5.2.3 Soft-clipping ancient data

Due to the SeqTK step carried out prior to alignment (see methods), Kotias, Satsurblia, and Bichon had the first and last two bases of all reads removed. To mirror this step in published ancient data which had not been trimmed in this way, the first and last 2 bp of all sequences were soft-clipped to a base quality of two before genotypes were called (with the exception of data from [6] and [8] for which genotypes were already called).

3.6.6 Population genetic analyses

PCA was performed by projecting selected ancient Eurasian data onto the first two principal components defined by a subset of the filtered Human Origins dataset (Fig. 1A). This analysis was carried out using EIGENSOFT 5.0.1 smartpca[16] with the lsqproject option on and the outlier removal option off. One SNP from each pair in linkage disequilibrium with $r^2 > 0.2$ was removed[68].

A clustering analysis was performed using ADMIXTURE version 1.23[17]. Genotypes were restricted to those that overlapped with the SNP capture panel described in [6]. SNPs in linkage disequilibrium were thinned using PLINK (v1.07)[66] with parameters --indep-pairwise 200 25 0.5[6] resulting in a set of 229,695 SNPs for analysis. 2 to 20 clusters (*K*) were explored using 10 runs with 5-fold cross validation at each *K* with different random seeds (Supplementary Figure B.5). The minimal cross-validation error was found at *K*=17, but the error already starts plateauing from roughly *K*=10, implying little improvement from this point onwards. (Supplementary Figure B.9).

D-statistics[18] and f_3-statistics[19,30] were used to formally assess the relationships between samples. Statistics were computed using the qpDstat (*D*-statistics) and 3PopTest (f_3-statistics) programs from the ADMIXTOOLS package[19]. Significance was assessed using a block jackknife over 5cM chunks of the genome[19] and statistics were considered significant if their

Z-score was of magnitude greater than 3[30] corresponding approximately to a p-value of less than 0.001. For f_3-statistics where the test population was ancient the inbreed:YES option was used.

3.6.6.1 ADMIXTURE analysis

The admixture proportions are shown on Supplementary Figure B.5 for all samples and in Figure 3.1 for ancient individuals at *K*=17 (the minimal cross validation error;Supplementary Figure B.9). In Supplementary Figure B.5, samples are hierarchically clustered by region (as on the PCA plot) and population. For better visibility, ancient samples are positioned on the left side of the figure and represented as bars with a width corresponding to five individuals. There are no clear outliers in any population, suggesting that they were well-defined and that the number of SNPs was sufficient to correctly define the clusters, even after LD-based pruning.

The cluster membership of published modern and ancient samples is similar to previous analyses[6]. Modern individuals harbour components as expected from their location and history, and ancient samples have components similar to those seen in [7] and other studies. European hunter-gatherers from the Mesolithic form a distinct component (“light blue”), which is also present in most Europeans and many populations from Western Asia. Early European farmers as well as modern European and West Asian groups additionally harbour a component dominant in the Middle East (“magenta”), appearing at *K*=9, in agreement with a Middle Eastern source of early Neolithic farmers. European groups from the late Neolithic onwards and many West Asian groups also possess a component prevalent in South Asia, as soon as this appears at *K*=7. This component is at first the same one that is prevalent in India (“dark purple”), but is later replaced by the Caucasus-related component (“lime green”).

Bichon, our Upper Palaeolithic hunter-gatherer from Switzerland, harbours mainly the European Mesolithic hunter-gatherer component, in agreement with our PCA analysis while the Caucasus hunter-gatherers look unlike any other modern or ancient group. From *K*=9 to

K=14, when both the South Asian "dark purple" and the Near Eastern "magenta" are present, they mainly consist of those two components, with a small fraction of Western hunter-gatherer related ancestry. Modern populations from the Caucasus and West Asia harbour the same components, but with an increased fraction of the Near Eastern "magenta" component. From *K*=15 onwards, a new cluster nearly completely describing CHG ("lime green") appears. Out of the two CHG samples, the older Satsurblia is fully assigned to the "lime green" cluster, whereas the later sample Kotias also features minor (<10%) Near Eastern ancestry. This new CHG-related component also appears in modern populations in west Eurasia, but no modern population belongs purely to this cluster. Even modern populations from the Caucasus continue to harbour a large amount (close to 50%) of the Near Eastern "magenta" component.

Both Kotias and Satsurblia show a certain similarity to the early European Farmers (EF) and the Yamnaya, in that they feature both the Middle Eastern component of the EF and the South Asian of the Yamnaya. However, in contrast to EF and the Yamnaya and in agreement with a deep CHG-WHG split, they only harbour a minor proportion (<10%) of the European hunter-gatherer ancestry. Also from *K*=15 onwards, the new CHG-related component replaces the South Asian "dark purple" and reduces the Near Eastern "magenta" component in the Yamnaya and all Neolithic and later European populations.

The components characteristic of Native American populations ("dark green", "light brown", "dark grey" and "dark blue") are also worth noting. These components are present in MA1 and eastern hunter-gatherers, in agreement with previous studies[6,7], but are at very low levels in the Yamnaya and virtually absent from our samples from the Caucasus. These components may point to the presence of the Ancient North Eurasian ancestry of both Native Americans and eastern hunter-gatherers. Their absence in Caucasus hunter-gatherers is in agreement with their southern geographical position and their separation from northern Eurasia by the Caucasus mountain range.

3.6.6.2 Relationship of Satsurblia, Kotias and Bichon to other samples

D-statistics of the form *D*(Yoruba, *OA*; Satsurblia, Kotias) and *D*(Yoruba, *OA*; Bichon, *WHG*) were used to assess whether the pairs of samples (Kotias, Satsurblia) and (Bichon, *WHG*) are compatible with forming a clade in an unrooted tree with respect to an African outgroup and other ancient samples (OA). For the test *D*(Yoruba, *OA*; Satsurblia, Kotias) we found most statistics to have non-significant (zero) values (Supplementary Table B.3) which support Kotias and Satsurblia forming a clade to the exclusion of other branches of ancient ancestry. The only population for which a positive value was observed was the Sintasha Bronze Age culture. These Uralic people are genetically similar to Corded Ware populations[8] and this result could be explained by the temporally closer Kotias representing a better donor for CHG ancestry than the older Satsurblia for this population. These *D*-statistics confirm inferences from PCA and ADMIXTURE that Kotias and Satsurblia are genetically distinct from other broadly contemporaneous ancient genomes. When we performed the tests *D*(Yoruba, Satsurblia; *OA*, Kotias) and *D*(Yoruba, Kotias; *OA*, Satsurblia) we found positive values of 0.07 to0.16 with associated Z-scores of 9.66 to 24.18, depending on the CHG sample and the other ancient (OA) population. This shows that there is enough power to detect signals of admixture using this dataset and that the zero values found above are not due to paucity of data.

The test *D*(Yoruba, OA; Bichon, WHG) (where WHG were represented by the highest coverage WHG genomes, Loschbour[2] and La Braña[4]) resulted in non-significant values for 95% of tests consistent with Bichon having more recent shared ancestry with WHG than with most other ancient lineages (Supplementary Table B.4). We consistently found zero-values when the OA involved was an eastern hunter-gatherer (EHG), a CHG or a Pleistocene hunter-gatherer showing that Bichon forms a clade with WHG to the exclusion of these other hunter-gatherer groups. However, we did not always find zero-values when we let OA be a Scandinavian hunter-gatherer (SHG; Supplementary Table B.4). WHG are proposed to be part of a hunter-gatherer metapopulation, which also encompasses SHG and EHG and ranges over northern Europe from as far west as Spain to as far east as Russia[7]. These three hunter-gatherer groups cannot be related by a simple tree as there are signals of admixture between these groups[7]. This explains why Bichon does not always form a clade with other WHG to the exclusion of SHG.

When we inverted the statistics and evaluated *D*(Yoruba, Bichon; *OA*, WHG) and *D*(Yoruba, WHG; *OA*, Bichon) we consistently found statistically significant values (Z >3). This shows that admixture can be detected for the genotype coverage found in this dataset. We also found similar results when we let the Hungarian sample KO1[4] represent WHG. It is interesting to note that Bichon, as well as other WHG, form a clade with both MA1 and EHG to the exclusion of CHG (Supplementary Table B.7). This suggests the Ancient North Eurasian (ANE) ancestry and WHG ancestry may have shallower roots and diverged subsequent to splitting from CHG (Supplementary Figure B.2). This is consistent with ADMIXTURE analysis and the geographic range of these groups - CHG were separated from these North Eurasian hunter-gatherers by the Caucasus mountain range.

We also explored the relationships between ancient samples by performing outgroup f_3-statistics of the form f_3(*X*, *OA*; Yoruba) where we let X be Kotias, Satsurblia and Bichon in turn and OA be all other ancient groups in the dataset (Supplementary Fig. 1). These statistics are informative as their magnitude is proportional to the amount of shared genetic history between the ancient individuals (X and OA) since they diverged from an African (in this case Yoruba) outgroup.

We found that CHG share the most drift with each other and the least drift with the Pleistocene sample Ust'-Ishim (Supplementary Figure B.1A&B). Other ancient samples share an intermediate amount of drift with no obvious pattern to the distribution of allele sharing. Bichon shares the most genetic drift with other western hunter-gatherers, followed by Scandinavian and eastern hunter-gatherers (Supplementary Figure B.1C). The fact that Bichon is closest to other WHG, and not equally close to SHG and EHG, suggests that there may have already been sub-structure between these hunter-gatherer groups 13,700 years ago when Bichon was alive.

3.6.7 Dating split times using G-PhoCS.

A coalescent model implemented with G-PhoCS[20] was used to reconstruct the joint demographic history of western and Caucasus hunter -gatherers (WHG and CHG respectively) and early farmers (EF). This analysis requires (1) the topology of the underlying population tree; (2) sequence data from short, homologous windows; and (3) specified directional gene flow between branches (migration bands).

3.6.7.1 Topology of population tree

G-PhoCS represents the demographic history of a collection of samples by a (binary) tree in which each branch is a population, with each sample belonging to a different leaf branch and interior branches corresponding to ancestral populations. To find the most likely topology of this tree, we used f_3 analysis to determine the most likely ordering of the population splits (see Figure 3.2B for a graphical representation). For the G-PhoCS analyses, we considered both a tree with only the ancient genomes, and a tree with an African San Pygmy[69] as the outgroup.

To explore the topology between CHG, WHG and early farmers (EF) we used available high coverage data and performed f_3-statistics (see methods), attempting all possible triplet combinations for these three groups (Figure 3.2A; Supplementary Table B.5). When we did this we presumed that two samples form a clade and the other sample is the outgroup to this clade. For the correct topology we would expect $f_3 > 0$, as the two correctly grouped samples will have shared drift since they diverged from the outgroup. For incorrect topologies we would expect $f_3 = 0$ as the incorrectly grouped samples will not have shared drift exclusive to themselves. We found that $f_3(WHG, CHG; EF)$ tended to equal zero, depending on the representing samples used and gave the smallest values of all our tests. This makes it unlikely that WHG and CHG are sister groups to the exclusion of EF. The largest values were found for f_3(*CHG, EF*; *WHG*) (Z > 14.4) suggesting that CHG and EF form a clade to the exclusion of WHG. However, we did also find positive statistics for the test f_3(*WHG, EF*; *CHG*) (Z > 8.5) but these were not as significant as for the former topology. WHG introgression into EF has been previously proposed[2,4,7,13] and positive statistics for f_3(*WHG, EF; CHG*) could be a function of this admixture (admixture is also suggested by *D*-statistics of the form *D*(Yoruba, WHG; CHG, EF) (Supplementary Table B.9) and ADMIXTURE analysis (Figure 3.1B)). As the signal for EF and CHG forming a clade is much stronger than for the other two topologies we consider the most parsimonious scenario to be that farmers and CHG are sister groups that diverged from each other after splitting from WHG.

Unfortunately we did not have a high coverage diploid sample representing ANE to include in this approach. Analyses using *D*-statistics (Supplementary Table B.7) revealed however that ANE and WHG group together to the exclusion of CHG. It therefore seems likely that an ancient south (Neolithic farmers and CHG) divergence from the ancient North (WHG and ANE) was the earliest split for these groups. This is shown in Supplementary Figure B.2 which extends the model proposed in [2] to include CHG. To fit this proposed model, CHG and EF should form a clade to the exclusion of Eastern non-Africans which is indeed supported by zero values for *D*(Yoruba, *eastern non-African*, *CHG*, *EF*) (Supplementary Table B.9). CHG and EF also form a clade to the exclusion of ANE as represented by MA1 (Supplementary Table B.9).

3.6.7.2 Genome-wide windows of high sample coverage for demographic analyses

Since this analysis requires sequence data from all genomes in short (1 kilobase (kb)) homologous windows, we chose high-coverage genomes to represent each group: Bichon and Loschbour to represent WHG, Kotias to represent CHG, and either Stuttgart or NE1 to represent EF. In addition, we used a high-quality San Pygmy genome[69] as an outgroup. To find the best set of windows, we first generated all-sites coverage information from chromosomes 1 to 22, restricted to regions classified as "neutral" according to the filters in[20] (using UCSC liftOver tool to translate coordinates from hg18 to hg19), and extracted the depth information using a program written in C, again filtering for sites with read depth between 10 and 35 (we avoid sites with very low and very high coverage because alignment and genotyping is problematic (for more details see[70]):

```
samtools mpileup -C50 -uDI -f <reference.fa>  -r <chromosome> \
-l <bedfile with accepted regions> <bamfiles> | bcftools view -gc – \
| get_depth_intervals minCover=10 maxCover=35
interval_file=<chromosome>
```

We then scanned each chromosome for windows satisfying the previous criteria, using a simple heuristic approach to maximise the sample coverage. We start by finding the first 1 kb window with at least 80% coverage. We then search within the next 10 kb to find the 1 kb window with the highest coverage. Finally, we jump 5 kb forward from the chosen location and repeat the process until we reach the end of the chromosome. For the whole genome, this search yielded a total of 152,883 high-quality windows. We then used SAMtools/BCFtools[44] (using flags as above) and custom programs written in C and MATLAB to extract genotypes for the windows and converted the genotypes into fasta files for G-PhoCS. To deal with DNA damage in ancient samples, we "in vitro" deaminated all our sequences, as already done for previous studies[18].

3.6.7.3 Directional gene flow between branches

Because our WHG samples predate the arrival of farming to central and northern Europe[21], any gene flow creating shared drift between EF and WHG must be from WHG to EF. Ideally, we would like our model to only allow gene flow between WHG and EF after the arrival of farming to the WHG locations. However, G-PhoCS requires migration to start or stop at time where populations split. Fortunately, our analysis puts the split between the two WHG, Bichon and Loschbour, at around 14k years ago, just a few thousand years prior to farming. We therefore allow gene flow between WHG and EF only after this split. Because Loschbour is temporally and geographically closer than Bichon to the EF, we allow only gene flow from Loschbour to the EF.

3.6.7.4 G-PhoCS set up

Gamma distributed priors were used for all observables (split times, population sizes and migration rates). The shape parameter α was set to an intermediate value of 1 for both population sizes and split times, to obtain a mean to standard deviation ratio of unity and allow sufficient exploration of the parameter space without an overly long convergence time. The rate parameter β was set to result in means in the correct range, based on initial exploratory runs with a variety of starting values (running two MCMC chains of 1,000,000 steps for each set of starting values, which is enough to get an order of magnitude estimate of variables of interest; see below for details of how chains were set up). For θ, the effective population sizes, we set β=2,500 for the San (i.e. for θ_{San}), and β=10,000 for all other populations, corresponding to mean effective population sizes of 26,667 and 6,667, respectively. The rate parameters were β=1,000,000 (mean split time of 6,667 years) for the Bichon-Loschbour and Stuttgart-Kotias splits, β=250,000 (mean split time of 26,667 years) for the (Bichon-Loschbour)-(Stuttgart-Kotias split) and β=30,000 (mean split time of 222,222 years) for the San and ancient genomes.

With regards to migration from Loschbour to Stuttgart, we explored three different settings: no migration and migrations bands with either a strong or a weak prior. In the case of a weak prior, the shape parameter was set to 0.002 and the mean to 200, to allow exploration of the whole space. With such a broad distribution, the value of the mean hardly influenced our results, based on exploratory runs. As for the strong prior, the shape parameter was set to 1 and the mean to 20,000, corresponding to ~18% of the genealogies sampled as Stuttgart actually originating from Loschbour, with a Loschbour-Bichon split time of 6,666 years (the prior mean). Migration had a negligible effect on split times. The only exception was the split between EF and Caucasus Hunter Gatherers, which was approximately 4-10 thousand year younger without migration; however, the confidence interval for this split was similar, and very broad, for levels of migration, suggesting that this split is difficult to date with the current data. In this supplementary, we present the results with the strong prior, since previous studies[1,7,46] have pointed to mixing between hunter-gatherers and early farmers. We also explored models with migration going in the opposite direction or bidirectional, but this did not affect the results (as already noted in the original paper describing G-Phocs[54], the direction of migration tends not to be captured by this method).

We used G-PhoCS's automatic feature to set step sizes (finetune parameters) of the Markov chain for each parameter, which aims for intermediate acceptance ratios. During this procedure, the first 10,000 steps were used to find appropriate step sizes, by updating the parameters every 100 MCMC steps and performing 100 updates. After the step sizes were set, 3,000,000 MCMC steps were performed, with the first 100,000 steps discarded as burn-in. After observing traces of observables, we found that our demographic parameters of interest converged well before the end of the burn-in period. We started two independent chains for each setting in order to assess appropriate mixing of the chain, and observed no problems in any setting.

3.6.7.5 Converting dates from ancient genomes

The available version of G-PhoCS assumed samples to be contemporaneous. The ages of our ancient genomes all fell within a range of about 6 thousand years (about 7 thousand years for the youngest, EF, to about 13 thousand years for the oldest, Bichon). This discrepancy is relatively small compared to the ages of the splits of interest, and will not affect estimates in a qualitative way (especially given the size of the confidence interval of this type of analysis). To convert split times for a given node as computed by G-PhoCS into calendar dates, we added the mean of the ages of the samples that defined that node. The only modern genome is the San, which is only used as an outgroup; as such, the age of that split between the San and the ancient genomes is not of interest (and given how old that split is, a difference of 10k years in age of the genomes has negligible consequences on the estimates).

Split times estimates from G-PhoCS have to be converted into calendar years based on a mutation rate. Recent work on the high quality genome from Ust'Ishim[3] provides a mutation rate calibrated on ancient DNA, (0.5×10^{-9} per site per year) which is also in line with estimates from high quality modern genomes[71]. We converted this mutation rate into an appropriate substitution rate for our *in vitro* deaminated sequences.

3.6.7.6 G-PhoCS Results

If we consider the model with Stuttgart to represent EF, and San as an outgroup, we find that the split between WHG and the population ancestral to CHG and EF is dated at around ~46 kya, implying an early divergence at the time of, or shortly after, the colonisation of Europe. On the WHG branch, the split between Bichon and Loschbour is dated to ~18 kya (just older than the age of Bichon), implying continuity in western Europe. The split between CHG and EF is dated at ~24 kya, thus suggesting a possible link with the LGM, although the broad confidence intervals require some caution with this interpretation.

Our conclusions are qualitatively similar for other models, irrespective of which genome (Stuttgart or NE1) was used to represent EF, nor whether we used an outgroup (San) or not. In the main text and in Figure 3.2B, we report the dates from the model including Stuttgart and San, but details of the other models are available in Supplementary Table B.6.

3.6.8 Runs of homozygosity

To gain an insight into past population structure we examined runs of homozygosity (ROH) in our ancient samples. ROH occur when identical extended regions of the genome are inherited from both parents and their distribution can be informative about past population demography[4,25,26,72]. Long homozygous genomic stretches provide evidence for recent endogamy because recombination has not acted to break down these long tracts which are identical by descent. In contrast short runs can be indicative of an ancient population bottleneck. After such a constrictive event a population will experience a period of increased inbreeding creating long homozygous haplotypes but these segments can be broken up by recombination over time as the population expands, creating short homozygous runs.

Examination of ROH requires dense diploid genotypes. We used imputation to maximise the information content of our most ancient sample, Satsurblia, which was sequenced to 1.44x, following the procedure described in[15]. Imputation allows the inference of missing genotypes by comparing surrounding haplotypes in the sample to those found in a phased reference panel and has been shown to be a valid method for leveraging palaeogenomic data[4]. We were concerned that the haplotypes present in Satsurblia may not be well represented by haplogroups in our modern dataset. To test if CHG genotypes could be accurately imputed we down-sampled our high coverage genome Kotias to ~1x and compared 546,625 imputed genotypes which overlapped with our confidently called high coverage genotypes for the filtered Human Origins dataset (Supplementary Figure B.10). When we imposed a genotype probability of 0.99 we found that 85% of loci were retained and of those 99.41% (97.91% of heterozygotes) matched our high coverage calls (Supplementary Figure B.8). This high concordance rate supports the use of imputed CHG data in our analyses.

Imputed data for Satsurblia and downsampled-Kotias, implementing a genotype probability threshold of 0.99 (Supplementary Figure B.10), was merged with high confidence diploid calls for selected ancient samples (namely Bichon, Loschbour, NE1, Stuttgart and Kotias) as well as with SNP data from modern samples using PLINK[66]. This resulted in 199,868 overlapping high-quality diploid loci for ROH analysis which was carried out using PLINK[66] as described in[15]. When we plotted short ROH (<1.6 Mb) against long ROH (≥ 1.6 Mb) (Figure 3.3A)[4,26] we found that our three hunter-gatherer samples, Satsurblia, Kotias and Bichon locate with other hunter-gatherer samples in a region of the plot with a relative excess of both short and long ROH compared to Neolithic farmers. These short runs suggest an ancestrally restricted population size for CHG as well as WHG which could reflect the effect of a reduced population size in glacial refugia. This contrasts with the relatively low frequency ROH found for Neolithic samples, perhaps because the ancestors of these people resided in a location further south with a more moderate climate during the LGM, permissive of a larger effective population size. Longer runs of ROH found in hunter-gatherer samples are compatible with more recent consanguinity in their family lines than that experienced by Neolithic farmers.

Kotias, Bichon and Loschbour all overlap with individuals from America with the former two samples also overlapping Oceanic individuals. Both American and Oceanic populations have experienced a population bottleneck during their histories[25]. Of all the ancient samples Satsurblia has the most long ROH and lies closest to the Onge, indigenous people from the Andaman islands. This island population has experienced long term isolation resulting in a small ancestral population size[30] and recent population reduction after colonisation by the British in 1858[73].

We also placed our ROH into size bins[25] (Figure 3.2B) and found Neolithic farmers to have a ROH distribution that follows a similar pattern to modern Eurasian groups. In contrast hunter-gatherers had a relative excess of ROH <4 Mb in size, a signature of a small ancestral population size. Compared to other hunter-gatherer samples, Satsurblia has an excess of long ROH 4-16 Mb in size suggestive of a more recent interbreeding event in the family history of this individual.

3.6.9 Phenotypes of interest

We called genotypes in Bichon, Kotias and Satsurblia using GATK Unified Genotyper[45]. For each position under investigation we only called alleles which were present in the 1,000 Genomes dataset[53], using bases with a quality ≥ 30 in positions with a depth ≥ 4. Due to the low average coverage of Satsurblia (1.44x) we also used imputed genotypes for this sample (see above) imposing a genotype probability cut-off of 0.85[4]. We used the 8-plex[74] and Hirisplex[75] prediction models to predict hair, eye and skin colour for our samples. Other loci investigated are discussed in the Supplementary Information.

To get a picture of the phenotypic characteristics of our samples, we examined genes which have been associated with particular phenotypes in modern populations, including some loci which have been subject to selection in European populations. To investigate skin tone in our samples we began by using the 8-plex prediction model[74], a tool developed for forensic applications. We found the skin colour results for Kotias, Satsurblia and Bichon to be inconclusive (Supplementary Table B.21). To explore further we looked at genotypes in two pigmentation genes proposed to have been strongly selected in the ancestors of modern Europeans, namely *SLC45A2* and *SLC24A5*[22,76,77,77–79]. Skin colour tends to get progressively paler with increasing distance from the equator[80] and this pattern is thought be the result of natural selection. In higher latitudes, with restricted ultraviolet radiation exposure, lighter skin colour confers a selective advantage as it allows increased dermal vitamin D synthesis[81,82]. Selected SNPs in the *SLC45A2* and *SLC24A5* genes (rs16891982 and rs1426654 respectively) contribute to lightening of skin and are almost fixed in modern Europeans[22,76,77,77–79]. We found that Kotias and Satsurblia have the ancestral version of the *SLC45A2* (rs16891982) variant but both CHG have the selected version of the *SLC24A5* (rs1426654) gene (Supplementary Table B.22) encompassed by the most commonly associated haplotype (C11) found in modern populations[76]. Bichon on the other hand has the ancestral version of both genes suggesting that our Caucasus hunter-gatherers may have had lighter skin than our western hunter-gatherer, Bichon (Supplementary Table 20).

We used the Hirisplex online tool to predict hair and eye colour for our samples[75]. We found it most likely that Bichon, Kotias and Satsurblia had dark/black hair and brown eyes (

Supplementary Table B.23 & 24). It is unlikely that any of our samples was able to drink milk into adulthood as all samples had the ancestral genotype at two positions (rs4988235 and rs182549) upstream of the *LCT* locus where the derived genotype is associated in Europeans with the ability to process lactose. The ability to digest milk is thought to have been driven to high frequencies in Europe subsequent to the introduction of farming[4,83].

3.7 Bibliography

1. Jones, E. R. *et al.* Upper Palaeolithic genomes reveal deep roots of modern Eurasians. *Nat. Commun.* **6,** 8912 (2015).

2. Lazaridis, I. *et al.* Ancient human genomes suggest three ancestral populations for present-day Europeans. *Nature* **513,** 409–413 (2014).

3. Olalde, I. *et al.* Derived immune and ancestral pigmentation alleles in a 7,000-year-old Mesolithic European. *Nature* **507,** 225–228 (2014).

4. Gamba, C. *et al.* Genome flux and stasis in a five millennium transect of European prehistory. *Nat. Commun.* **5,** 5257 (2014).

5. Skoglund, P. *et al.* Genomic Diversity and Admixture Differs for Stone-Age Scandinavian Foragers and Farmers. *Science* **344,** 747–750 (2014).

6. Haak, W. *et al.* Massive migration from the steppe was a source for Indo-European languages in Europe. *Nature* **522,** 207–211 (2015).

7. Raghavan, M. *et al.* Upper Palaeolithic Siberian genome reveals dual ancestry of Native Americans. *Nature* **505,** 87–91 (2014).

8. Allentoft, M. E. *et al.* Population genomics of Bronze Age Eurasia. *Nature* **522,** 167–172 (2015).

9. Hofmanová, Z. *et al.* Early farmers from across Europe directly descended from Neolithic Aegeans. *Proc. Natl. Acad. Sci.* **113,** 6886–6891 (2016).

10. Broushaki, F. *et al.* Early Neolithic genomes from the eastern Fertile Crescent. *Science* aaf7943 (2016). doi:10.1126/science.aaf7943

11. Gallego-Llorente, M. *et al.* The genetics of an early Neolithic pastoralist from the Zagros, Iran. *Sci. Rep.* **6,** (2016).

12. Lazaridis, I. *et al.* Genomic insights into the origin of farming in the ancient Near East. *Nature* **536,** 419–424 (2016).

13. Seguin-Orlando, A. *et al.* Paleogenomics. Genomic structure in Europeans dating back at least 36,200 years. *Science* **346,** 1113–1118 (2014).

14. Keller, A. *et al.* New insights into the Tyrolean Iceman's origin and phenotype as inferred by whole-genome sequencing. *Nat Commun* **3,** 698 (2012).

15. Fu, Q. *et al.* Genome sequence of a 45,000-year-old modern human from western Siberia. *Nature* **514,** 445–449 (2014).

16. Patterson, N., Price, A. L. & Reich, D. Population Structure and Eigenanalysis. *PLOS Genet* **2,** e190 (2006).

17. Alexander, D. H., Novembre, J. & Lange, K. Fast model-based estimation of ancestry in unrelated individuals. *Genome Res.* (2009). doi:10.1101/gr.094052.109

18. Green, R. E. *et al.* A Draft Sequence of the Neandertal Genome. *Science* **328,** 710–722 (2010).

19. Patterson, N. *et al.* Ancient Admixture in Human History. *Genetics* **192,** 1065–1093 (2012).

20. Gronau, I., Hubisz, M. J., Gulko, B., Danko, C. G. & Siepel, A. Bayesian inference of ancient human demography from individual genome sequences. *Nat Genet* **43,** 1031–1034 (2011).

21. Pinhasi, R., Thomas, M. G., Hofreiter, M., Currat, M. & Burger, J. The genetic history of Europeans. *Trends Genet* **28,** 496–505 (2012).

22. Lamason, R. L. *et al.* SLC24A5, a putative cation exchanger, affects pigmentation in zebrafish and humans. *Science* **310,** 1782–1786 (2005).

23. Mathieson, I. *et al.* Eight thousand years of natural selection in Europe. *bioRxiv* (2015).

24. Morin, E. Evidence for declines in human population densities during the early Upper Paleolithic in western Europe. *Proc Natl Acad Sci U A* **105,** 48–53 (2008).

25. Kirin, M. *et al.* Genomic runs of homozygosity record population history and consanguinity. *PLoS One* **5,** e13996 (2010).

26. Pemberton, T. J. *et al.* Genomic patterns of homozygosity in worldwide human populations. *Am J Hum Genet* **91,** 275–292 (2012).

27. Semino, O. *et al.* Origin, diffusion, and differentiation of Y-chromosome haplogroups E and J: inferences on the neolithization of Europe and later migratory events in the Mediterranean area. *Am J Hum Genet* **74,** 1023–1034 (2004).

28. Derenko, M. *et al.* Complete mitochondrial DNA diversity in Iranians. *PLoS One* **8,** e80673 (2013).

29. Balanovsky, O. *et al.* Parallel evolution of genes and languages in the Caucasus region. *Mol Biol Evol* **28,** 2905–2920 (2011).

30. Reich, D., Thangaraj, K., Patterson, N., Price, A. L. & Singh, L. Reconstructing Indian population history. *Nature* **461,** 489–494 (2009).

31. Mallory, J. P. Yamna Culture. *Encycl. Indo-Eur. Cult.* (1997).

32. Kohl, P. L. *The Making of Bronze Age Eurasia*. (Cambridge University Press, 2007).

33. Moorjani, P. *et al.* Genetic evidence for recent population mixture in India. *Am J Hum Genet* **93,** 422–438 (2013).

34. Metspalu, M. *et al.* Shared and Unique Components of Human Population Structure and Genome-Wide Signals of Positive Selection in South Asia. *Am. J. Hum. Genet.* **89,** 731–744 (2011).

35. Yang, D. Y., Eng, B., Waye, J. S., Dudar, J. C. & Saunders, S. R. Technical note: improved DNA extraction from ancient bones using silica-based spin columns. *Am J Phys Anthr.* **105,** 539–543 (1998).

36. Meyer, M. & Kircher, M. Illumina sequencing library preparation for highly multiplexed target capture and sequencing. *Cold Spring Harb Protoc* **2010,** db.prot5448 (2010).

37. Rohland, N., Siedel, H. & Hofreiter, M. A rapid column-based ancient DNA extraction method for increased sample throughput. *Mol Ecol Resour* **10,** 677–683 (2010).

38. Bollongino, R. *et al.* 2000 Years of Parallel Societies in Stone Age Central Europe. *Science* **342,** 479–481 (2013).

39. Fortes, G. G. & Paijmans, J. L. A. Analysis of whole mitogenomes from ancient samples. (2015).

40. Martin, M. Cutadapt removes adapter sequences from high-throughput sequencing reads. *EMBnet J* **17,** 10–12 (2011).

41. Briggs, A. W. *et al.* Patterns of damage in genomic DNA sequences from a Neandertal. *Proc Natl Acad Sci U A* **104,** 14616–14621 (2007).

42. Brotherton, P. *et al.* Novel high-resolution characterization of ancient DNA reveals C > U-type base modification events as the sole cause of post mortem miscoding lesions. *Nucleic Acids Res* **35,** 5717–5728 (2007).

43. Li, H. & Durbin, R. Fast and accurate short read alignment with Burrows-Wheeler transform. *Bioinformatics* **25,** 1754–1760 (2009).

44. Li, H. *et al.* The Sequence Alignment/Map format and SAMtools. *Bioinformatics* **25,** 2078–2079 (2009).

45. McKenna, A. *et al.* The Genome Analysis Toolkit: a MapReduce framework for analyzing next-generation DNA sequencing data. *Genome Res* **20,** 1297–1303 (2010).

46. Jónsson, H., Ginolhac, A., Schubert, M., Johnson, P. L. F. & Orlando, L. mapDamage2.0: fast approximate Bayesian estimates of ancient DNA damage parameters. *Bioinformatics* **29,** 1682–1684 (2013).

47. Sánchez-Quinto, F. *et al.* Genomic Affinities of Two 7,000-Year-Old Iberian Hunter-Gatherers. *Curr. Biol.* **22,** 1494–1499 (2012).

48. Shapiro, B. & Hofreiter, M. Analysis of ancient human genomes. *Bioessays* **32,** 388–391 (2010).

49. Dabney, J. *et al.* Complete mitochondrial genome sequence of a Middle Pleistocene cave bear reconstructed from ultrashort DNA fragments. *Proc Natl Acad Sci U A* **110,** 15758–15763 (2013).

50. Roostalu, U. *et al.* Origin and Expansion of Haplogroup H, the Dominant Human Mitochondrial DNA Lineage in West Eurasia: The Near Eastern and Caucasian Perspective. *Mol Biol Evol* **24,** 436–448 (2007).

51. Vianello, D. *et al.* HAPLOFIND: a new method for high-throughput mtDNA haplogroup assignment. *Hum Mutat* **34,** 1189–1194 (2013).

52. Rasmussen, M. *et al.* An Aboriginal Australian genome reveals separate human dispersals into Asia. *Science* **334,** 94–98 (2011).

53. 1000 Genomes Project Consortium *et al.* An integrated map of genetic variation from 1,092 human genomes. *Nature* **491,** 56–65 (2012).

54. Skoglund, P., Stor\a a, J., Götherström, A. & Jakobsson, M. Accurate sex identification of ancient human remains using DNA shotgun sequencing. *J Archaeol Sci* **40,** 4477–4482 (2013).

55. Jostins, L. *et al.* YFitter: Maximum likelihood assignment of Y chromosome haplogroups from low-coverage sequence data. (2014).

56. Richards, M. *et al.* Tracing European founder lineages in the Near Eastern mtDNA pool. *Am J Hum Genet* **67,** 1251–1276 (2000).

57. Van Oven, M. & Kayser, M. Updated comprehensive phylogenetic tree of global human mitochondrial DNA variation. *Hum Mutat* **30,** E386–94 (2009).

58. Simoni, L., Calafell, F., Pettener, D., Bertranpetit, J. & Barbujani, G. Geographic patterns of mtDNA diversity in Europe. *Am J Hum Genet* **66,** 262–278 (2000).

59. Brandt, G. *et al.* Ancient DNA reveals key stages in the formation of central European mitochondrial genetic diversity. *Science* **342,** 257–261 (2013).

60. Fernández, E. *et al.* Ancient DNA analysis of 8000 B.C. near eastern farmers supports an early neolithic pioneer maritime colonization of Mainland Europe through Cyprus and the Aegean Islands. *PLoS Genet* **10,** e1004401 (2014).

61. Bramanti, B. *et al.* Genetic discontinuity between local hunter-gatherers and central Europe's first farmers. *Science* **326,** 137–140 (2009).

62. Cinnioğlu, C. *et al.* Excavating Y-chromosome haplotype strata in Anatolia. *Hum Genet* **114,** 127–148 (2004).

63. Jobling, M. A. & Tyler-Smith, C. The human Y chromosome: an evolutionary marker comes of age. *Nat Rev Genet* **4,** 598–612 (2003).

64. Rootsi, S. *et al.* Phylogeography of Y-chromosome haplogroup I reveals distinct domains of prehistoric gene flow in europe. *Am J Hum Genet* **75,** 128–137 (2004).

65. Semino, O. *et al.* The genetic legacy of Paleolithic Homo sapiens sapiens in extant Europeans: a Y chromosome perspective. *Science* **290,** 1155–1159 (2000).

66. Purcell, S. *et al.* PLINK: a tool set for whole-genome association and population-based linkage analyses. *Am J Hum Genet* **81,** 559–575 (2007).

67. Danecek, P. *et al.* The variant call format and VCFtools. *Bioinformatics* **27,** 2156–2158 (2011).

68. Skoglund, P. *et al.* Origins and Genetic Legacy of Neolithic Farmers and Hunter-Gatherers in Europe. *Science* **336,** 466–469 (2012).

69. Prüfer, K. *et al.* The complete genome sequence of a Neanderthal from the Altai Mountains. *Nature* **505,** 43–49 (2014).

70. Rasmussen, M. *et al.* The genome of a Late Pleistocene human from a Clovis burial site in western Montana. *Nature* **506,** 225–229 (2014).

71. Kong, A. *et al.* Rate of de novo mutations and the importance of father's age to disease risk. *Nature* **488,** 471–475 (2012).

72. McQuillan, R. *et al.* Runs of homozygosity in European populations. *Am J Hum Genet* **83,** 359–372 (2008).

73. Sharma, A. N. *Tribal Development in Andaman Islands*. (Sarup & Sons, 2003).

74. Hart, K. L. *et al.* Improved eye- and skin-color prediction based on 8 SNPs. *Croat Med J* **54,** 248–256 (2013).

75. Walsh, S. *et al.* The HIrisPlex system for simultaneous prediction of hair and eye colour from DNA. *Forensic Sci Int Genet* **7,** 98–115 (2013).

76. Canfield, V. A. *et al.* Molecular phylogeography of a human autosomal skin color locus under natural selection. *G3* **3,** 2059–2067 (2013).

77. Sturm, R. A. & Duffy, D. L. Human pigmentation genes under environmental selection. *Genome Biol.* **13,** 248 (2012).

78. Basu Mallick, C. *et al.* The Light Skin Allele of SLC24A5 in South Asians and Europeans Shares Identity by Descent. *PLoS Genet* **9,** e1003912 (2013).

79. Wilde, S. *et al.* Direct evidence for positive selection of skin, hair, and eye pigmentation in Europeans during the last 5,000 y. *Proc. Natl. Acad. Sci.* **111,** 4832–4837 (2014).

80. Relethford, J. H. Hemispheric difference in human skin color. *Am J Phys Anthr.* **104,** 449–457 (1997).

81. Loomis, W. F. Skin-pigment regulation of vitamin-D biosynthesis in man. *Science* **157,** 501–506 (1967).

82. Jablonski, N. G. & Chaplin, G. The evolution of human skin coloration. *J Hum Evol* **39,** 57–106 (2000).

83. Itan, Y., Powell, A., Beaumont, M. A., Burger, J. & Thomas, M. G. The Origins of Lactase Persistence in Europe. *PLoS Comput Biol* **5,** e1000491 (2009).

84. Meshveliani, T. *et al.* Anthromorphic Figurine from Kotias Klde Cave Bulletin of the Georgian National Museum. *Bull. Georgian Natl. Mus.* **IV (49-B):11-17,** (2013).

85. Liubin, V. Pervye svedeija o mezolite gornogo Kavkaza (Osetija) (First evidence concerning the Mesolithic of the Caucasus Highlands (Ossetia)). . In: Gurnia N, editor. U istokov drevnikh kul’tur: epokha mezolita (At the Dawn of the Ancient Cultures: The

Mesolithic Period). *Mosc. LeningradNakua Mater. Issled. Po Arkheologii SSSR* 155–163 (1966).

86. Grigolia, G. K. Centraluri Kolhetis neoliti Paluri [The Neolithic of Central Colchis: Paluri]. Tbilisi. *Metsniereba* (1977).

87. Arimura, M., Chataigner, C. & Gasparyan, B. Kmlo 2. An Early Holocene site in Armenia. *Neo-Lithics* **2/2009:17-19.,** (2009).

88. Nebieridze, L. Darkvetis mravalpeniani ekhi. (The Darkveti Multilayer Rockshelter). **Tbilisi: Metsniereba,** (1978).

89. Meshveliani, T. *et al.* Mesolithic Hunters at Kotias Klde, Western Georgia: Preliminary Results. *paleo* **33,** 47–58 (2007).

90. Kalandadze, A. N. & Kalandadze. Archaeological Research of Karstic Caves in Tskaltubo region (in Georgian, with Russian summary). *Caves Ga.* 116–136 (1978).

91. Kalandadze, K. S., Bugianishvili, T., Ioseliani, N., Jikia, M. & Kalandadze, N. Tskaltubo Expedition. The short reports of the archaeological expedition of 1989-1992. (in Georgian with Russian summary). *Tbil Math J* (2004).

92. Pinhasi, R. *et al.* Satsurblia: new insights of human response and survival across the Last Glacial Maximum in the southern Caucasus. *PLoS One* **9,** e111271 (2014).

93. Morel, P. Une chasse à l’ours brun il y a 12’000 ans: nouvelle découverte à la grotte du Bichon (La Chaux-de-Fonds). *Archéologie Suisse* **16,** 110–117 (1993).

94. Chauviere, F. *La grotte du Bichon : un site préhistorique des montagnes neuchâteloises*.

95. Simon, C. & Formicola, V. Anatomie générale de l’homme du Bichon. In: Chauvière F-X, editor. La grotte du Bichon: un site préhistorique des montagnes neuchâteloises: Archéologie neuchâteloise, 42. (2008).

96. Holt, B. & Churchill, S. Anatomie fonctionnelle du squelette post-crânien de l'homme du Bichon. *Chauvière F-X Dir Grotte Bichon Un Site Préhistorique Mont. Neuchâtel. Archéologie Neuchâtel. 42* (2008).

97. Iacumin, P. Étude des isotopes stables : détermination du régime alimentaire de l'homme du Bichon. In: Chauvière F-X, editor. La grotte du Bichon: un site préhistorique des montagnes neuchâteloises: Archéologie neuchâteloise, 42. (2008).

98. Behar, D. M. *et al.* A 'Copernican' reassessment of the human mitochondrial DNA tree from its root. *Am J Hum Genet* **90,** 675–684 (2012).

Chapter 4 Genome-wide data from two early Neolithic East Asian individuals dating to 7,700 years ago

4.1 Abstract

Ancient genomes have revolutionized our understanding of Holocene prehistory and, particularly, the Neolithic transition in western Eurasia. In contrast, East Asia has so far received little attention, despite representing a core region at which the Neolithic transition took place independently ~3 millennia after its onset in the Near East. I report genome-wide data from two hunter-gatherers from Devil's Gate, an early Neolithic cave site (dated to ~7.7 thousand years ago) located in East Asia, on the border between Russia and Korea. Both of these individuals are genetically most similar to geographically close modern populations from the Amur Basin, all speaking Tungusic languages, and in particular to the Ulchi. The similarity to nearby modern populations and the low levels of additional genetic material in the Ulchi imply a high level of genetic continuity in this region during the Holocene, a pattern that markedly contrasts with that reported for Europe.

4.2 Contribution

This study was published in Siska et al. 2017[1]. I was responsible for the computational population genetics analysis of the nuclear genome, for coordinating the project and for writing the manuscript. Sequencing, the analysis of uniparental markers, and predicting phenotypes were conducted by my collaborators. All co-authors gave their input on the manuscript.

4.3 Introduction

Ancient genomes from western Asia have revealed a degree of genetic continuity between preagricultural hunter-gatherers and early farmers 12 to 8 thousand years ago (ka)[2,3]. In contrast, studies on southeast and central Europe indicate a major population replacement of Mesolithic hunter-gatherers by Neolithic farmers of a Near Eastern origin during the period 8.5 to 7 ka[4]. This is then followed by a progressive “resurgence” of local hunter-gatherer lineages in some regions during the Middle/Late Neolithic and Eneolithic periods and a major contribution from the Asian Steppe later, ~5.5 ka, coinciding with the advent of the Bronze Age[4–6].

Compared to western Eurasia, for which hundreds of partial ancient genomes have already been sequenced, East Asia has been largely neglected by ancient DNA studies to date. The only exceptions are the Siberian Arctic belt, which has received attention in the context of the colonization of the Americas[7,8] and a 40,000 year-old Chinese sample (Tianyuan) which was more similar to modern Asians and South Americans than to ancient or modern Europeans[9,10]. However, East Asia represents an extremely interesting region as the shift to reliance on agriculture appears to have taken a different course from that in western Eurasia. In the latter region, pottery, farming, and animal husbandry were closely associated. In contrast, Early Neolithic societies in the Russian Far East, Japan, and Korea started to manufacture and use pottery and basketry 10.5 to 15 ka, but domesticated crops and livestock arrived several millennia later[11,12]. Because of the current lack of ancient genomes from East Asia, we do not know the extent to which this gradual Neolithic transition, which is generally considered to have happened independently from the one taking place in western Eurasia, reflected actual migrations, as found in Europe, or cultural diffusion associated with a higher level of population continuity.

4.4 Results

4.4.1 Samples, sequencing and authenticity

To fill this gap in our knowledge about the Neolithic in East Asia, we sequenced to low coverage five genomes (DevilsGate1, 0.059-fold coverage; DevilsGate2, 0.023-fold coverage; and DevilsGate3, DevilsGate4 and DevilsGate5 under 0.001-fold coverage) of five early Neolithic burials from a single occupational phase at Devil's Gate (Chertovy Vorota) Cave in the Russian Far East, close to the border with China and North Korea (see Suppl. Mat.). This site dates back to 9.4-7.2 kya, with the human remains dating to ~7.7 kya, and includes some of the world's earliest evidence of ancient textiles[13]. The people inhabiting Devil's Gate were hunter-fisher-gatherers with no evidence of farming, and even the main raw material for textile production were fibres of wild plants[13].

I focus the analysis on the two samples with the highest coverage, DevilsGate1 and DevilsGate2, both of which were female. DevilsGate1's sex is in accordance with that inferred from archaeology, but DevilsGate2 was thought to be male based on its skull. DevilsGate1 was directly radiocarbon dated to 6756±37 uncalibrated bp (OxA 27678) and DevilsGate2 to 6765±40 uncalibrated before present (OxA 27677). The calibrated range of both dates is 5726-5622 cal BC (2 SD. 95.4% confidence interval range, Supplementary Figure C.1).

The mitochondrial DNA (mtDNA) of the individual with higher coverage (DevilsGate1, coverage of the mtDNA ~9.76-fold) could be assigned to haplogroup D4. DevilsGate1 has one of the two mutations which define haplogroup D (T16362C, 13-fold coverage; the other position had no spanning sequence data) and all three mutations which are associated with haplogroup D4 (G3010A, 2-fold coverage; C8414T, 3-fold coverage; C14668T, 6-fold coverage). Haplogroup D4 is found in present day populations in East Asia[14], and has also been found in Jomon skeletons in northern Japan[15,16]. The other individual with lower coverage (DevilsGate2, coverage of the mtDNA ~2.75-fold), had three of the four mutations which define haplogroup M (T489C, 7-fold coverage; C10400T, 3-fold coverage; T14783C, 2 -fold coverage), to which D4 belongs. DevilsGate2 was assigned with equal likelihood to subhaplogroups M9 and M13’46’61; suggesting that this sample may not be accurately assigned to a subhaplogroup due to low sequence coverage.

Contamination, estimated from the number of discordant calls in the mtDNA on non-consensus bases at haplogroup-defining positions, was low: 0.87% [95% confidence interval (CI), 0.28 to 2.37%] and 0.59% [95% CI, 0.03 to 3.753%] for DevilsGate1 and DevilsGate2, respectively. These were reduced to 0% for both samples when non-consensus base calls which could be explained by deamination were omitted from the analysis. Using schmutzi[17] on the higher-coverage genome, DevilsGate1, also gives low contamination levels (1% [95% CI, 0 to 2%]). As a further check against the possible confounding effect of contamination, we made sure that our most important analyses, outgroup f_3 scores and principal components analysis (PCA), were qualitatively replicated using only reads showing evidence of postmortem damage[18] (see Supplementary Figure C.4, Supplementary Figure C.5 and Supplementary Figure C.7), although these latter results had a high level of noise due to the low coverage (0.005X for DevilsGate1 and 0.001X for DevilsGate2).

4.4.2 Relation to modern populations

I compared the individuals from Devil's Gate to a large panel of modern-day Eurasians and examined their genetic relationships to published ancient genomes[5,6,19–22] (Figure 4.1) using Principal Component Analysis (PCA)[23], an unsupervised clustering approach, ADMIXTURE[24], and outgroup f_3 statistics[25]. I investigated two different reference panels for both PCA and ADMIXTURE, the first consisting of all modern individuals in our worldwide set of populations and the second of a regional panel.

On the PCA analysis using the worldwide panel, samples from Devil's Gate clearly clustered with northern Asian populations, in particular with those from East Asia, Central Asia and Siberia (see Supplementary Figure C.5 and Supplementary Figure C.6 for the full analysis on all SNPs or only transversion SNPs, respectively). We then restricted our panel to these populations, to which we refer as the regional panel from now on. Here, both Devil's Gate individuals were close to populations from the Amur Basin, particularly to the Ulchi, Oroqen, and Hezhen (see Figure 4.1 for the first two components and Supplementary Figure C.7 and Supplementary Figure C.8 for the full analysis on all SNPs or only transversion SNPs, respectively). This is also the geographic region where Devil's Gate is located (Figure 4.1), which contrasts with observations in Western Eurasia, where, due to a number of major intervening migration waves, hunter-gatherers of a similar age fall outside modern genetic variation[4,26].

For ADMIXTURE on both panels, the main clusters reported in previous analyses were found[4–6] (see Figure 4.1 for K=5 and K=8 number of clusters and Supplementary Figure C.11 to Supplementary Figure C.14 for K up to 20 panels, using all SNPs or transversions only). Except for higher K-s (all K-s for the global and up to K=7 for the regional panel), Devil's Gate consisted of two components in roughly equal proportions. The first is an "East Asian" component, prevalent in the Han Chinese, Koreans and Japanese, among others, and the second is a “Siberian” component, typical for the Nganasan. Other populations from the Amur Basin, but also the Koreans and the Japanese, had the same components, but with a higher proportion of “East Asian” ancestry, and, for the Koreans and Japanese, also a small amount from a different component which is common in South-East Asia. On the regional panel from K=8 onwards, a new component corresponding to Devil’s Gate appeared. It also contributed to various other East Asian populations, including those from the Amur Basin (especially the Ulchi), and from modern-day China, Japan and Korea.

I further confirmed the affinity between Devil’s Gate and modern-day Amur Basin populations by using outgroup f_3 statistics in the form, f_3(African; DevilsGate, X), which measures the amount of shared genetic drift between a Devil’s Gate individual and X, a modern or ancient population, since they diverged from an African outgroup. Modern populations that live in the same geographic region as Devil’s Gate have the highest genetic affinity to our ancient genome (Figure 4.2), with a progressive decline in affinity with increasing geographic distance ($R^2 = 0.756$, $F_{1,96}=301$, $p < 0.001$,Figure 4.3), in agreement with neutral drift leading to a simple isolation-by-distance pattern. The Ulchi, traditionally fishermen who live geographically very close to Devil’s Gate, are the genetically most similar samples in our panel. Other populations that show high affinity to Devil’s Gate are Oroqen and Hezhen, also from the Amur Basin, as well as Koreans and Japanese. Given their geographic distance from Devil’s Gate (Figure 4.3), Amerindian populations are unusually genetically close to samples from this site; in agreement with their previously reported relationship to Siberian and other north Asian populations.

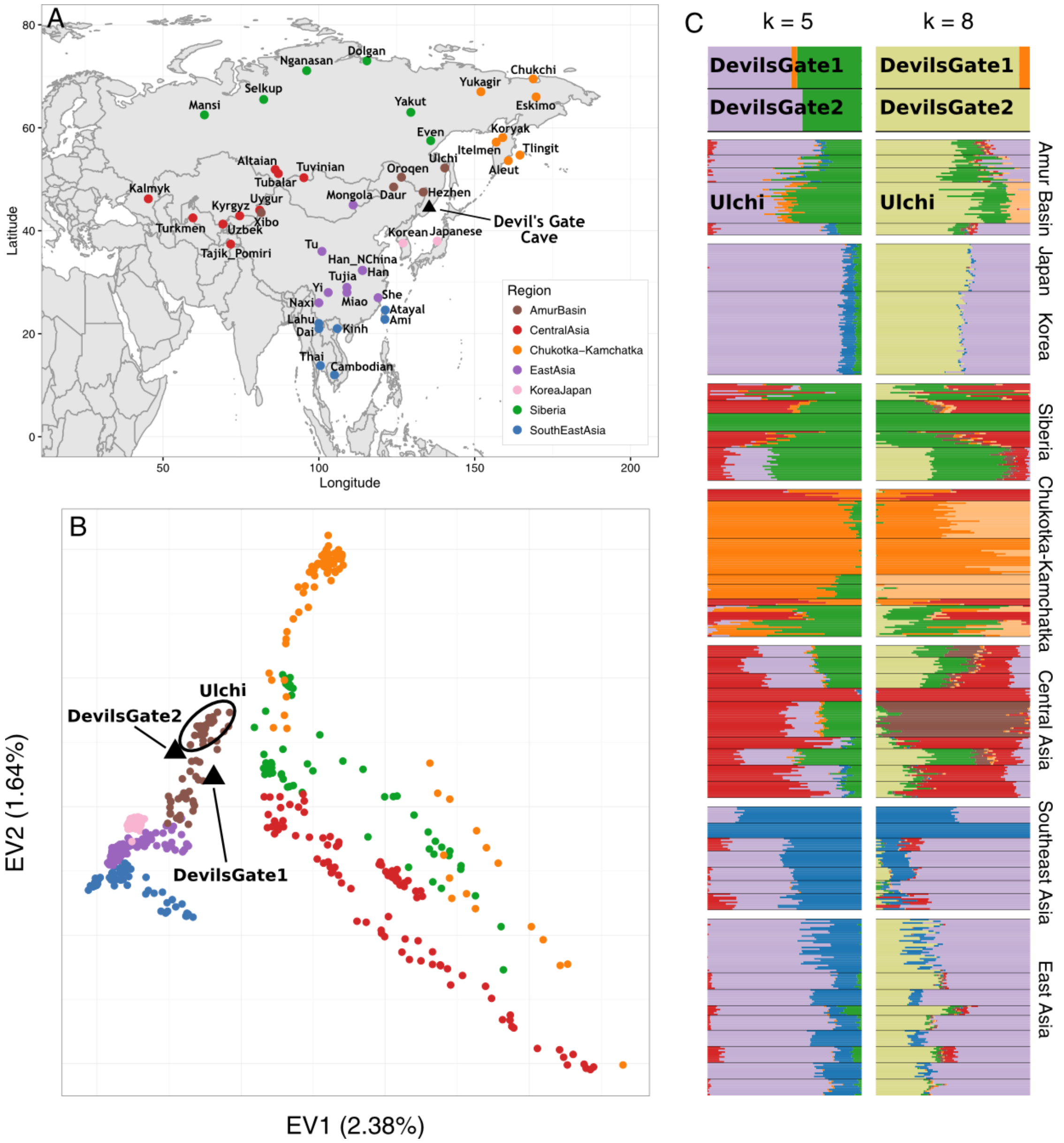

Figure 4.1 Regional reference panel, Principal Component analysis and ADMIXTURE analysis. (A) Map of Asia showing the location of Devil’s Gate (black triangle) and of modern populations forming the regional panel of our analysis. (B) Plot of the first two Principal Component Analysis as defined by our regional panel of modern populations from East and Central Asia shown on panel (A), with the two samples from Devil’s Gate (black triangles) projected upon them23. (C) ADMIXTURE analysis24 performed on Devil’s Gate and our regional panel, for k=5 (lowest cross-validation error) and k=8 (appearance of Devil’s Gate-specific cluster).

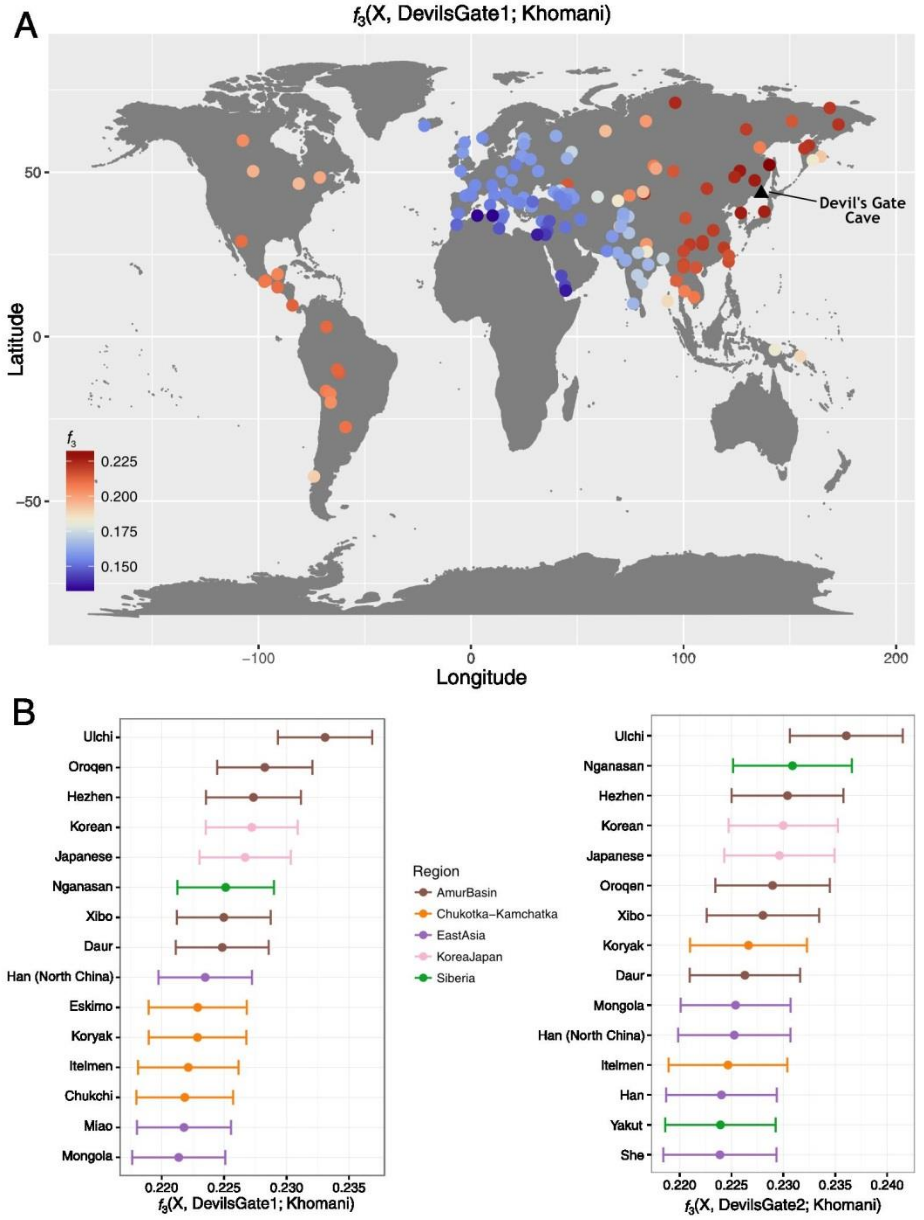

Figure 4.2 Outgroup f_3 statistics. Outgroup f_3 measuring shared drift between Devil's Gate (black triangle shows sampling location) and modern populations with respect to an African outgroup (Khomani). (A) Map of the whole world. (B) 15 populations with the highest shared drift with Devil's Gate, color-coded by regions as on Figure PCA. Error bars represent one standard error.

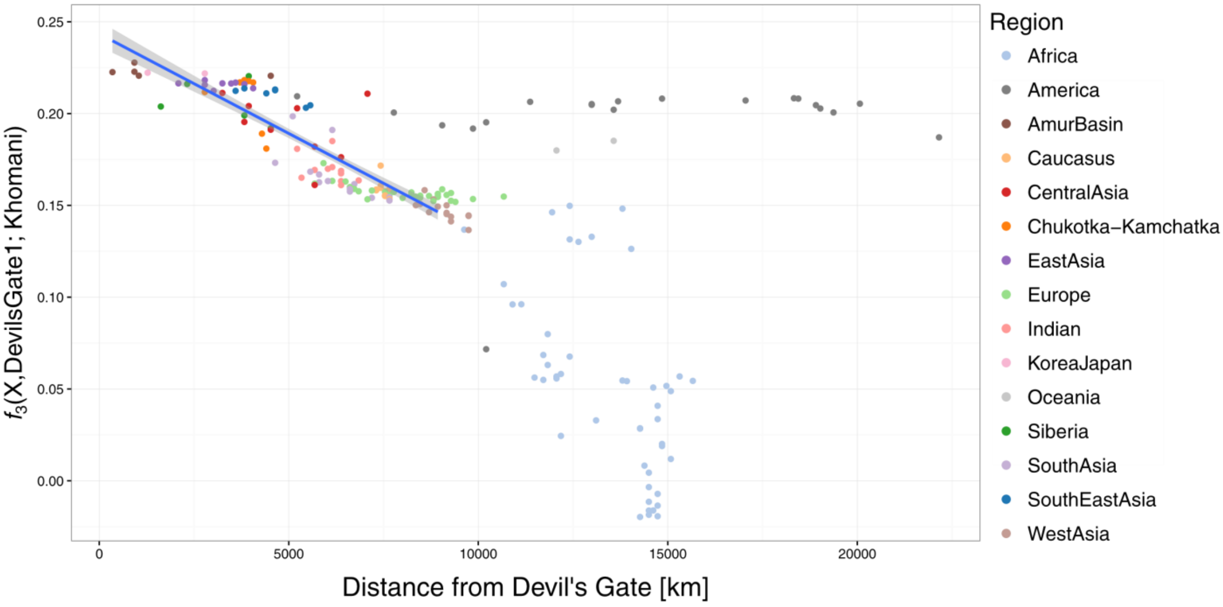

Figure 4.3 Spatial pattern of outgroup f3 statistics. Relationship between outgroup f3(X,Devil's Gate; Khomani) and distance on land from Devil's Gate, using DevilsGate1 and all SNPs. Populations up to 9000 km-s away from Devil's Gate were considered when computing correlation. The highest distance considered was chosen to acquire the highest Pearson correlation in steps of 500 km-s. Best linear fit (R2 = 0.772, F1,108=368.4, p < 0.001) is shown as blue line, with 95% confidence interval indicated by the shaded area.

The languages spoken by the Ulchi and by other populations from the Amur Basin all belong to the Tungusic language family, and the Ulchi are the only Tungusic-speaking population from the Amur Basin sampled in Russia. The rest were sampled in China, which is in agreement with their higher similarity to East Asian populations living south of the Amur Basin. Although some scholars consider the Tungusic languages as part of the Altaic language family, together with the Mongolic and Turkic groups and sometimes even including Koreanic and Japonic, this theory is not widely accepted[27]. The isolated nature of the Tungusic language family and the close connection between its speakers and our ancient samples point to the deep roots of these populations.

4.4.3 Relation to ancient genomes from Asia

No previously published ancient genome shows marked genetic affinity to Devil's Gate: the top 50 populations in our outgroup f_3 statistic were all modern, an unsurprising result given that all other ancient genomes are either geographically or temporally very distant from Devil's Gate. Amongst these ancient genomes, the closest to Devil's Gate are from Steppe populations dating from the Bronze onwards and mesolithic European hunter-gatherers, but they are at most as close as modern populations from the same regions (e.g. Tuvinian, Kalmyk, Russian, Finnish). The two ancient genomes geographically closest to Devil's Gate, Mal'ta (MA1) and Ust'-Ishim, also do not show high genetic affinity, probably due to them both dating to a much earlier time period. MA1 is genetically closer to Devil's Gate, but it is equally distant from Devil's Gate and from other East Asians (Supplementary Figure C.15-17). A similar pattern is found for Ust'Ishim, which is basal to all Eurasians, including Devil's Gate (Supplementary Figure C.18-20).

At the time of this work, only a very limited amount of data (chromosome 21 and an additional ~3000 polymorphic sites) was available from the single sequenced ancient genome with clear affinities to East Asians, Tianyuan[9]; which did not allow a direct comparison with the Devil's Gate samples. In 2017, the whole genome of this individual was published[10], but it revealed no particular similarities with the samples from Devil's Gate, or even with modern populations close to them (Ulchi and the other Amur Basin populations).

4.4.4 Continuity between Devil's Gate and the Ulchi

As Devil's Gate falls within the range of modern variability in a number of analyses and shows a high genetic affinity to the Ulchi, I investigated the extent of genetic continuity within this region. I modelled the Ulchi as a mixture of Devil's Gate and other modern populations, using admixture f_3 statistics. Despite a large panel of possible modern sources, the Ulchi are best represented by Devil's Gate alone without any further contribution (no admixture *f_3* gave a significant negative result, Supplementary Table C.20-21). In contrast, European populations gave significantly negative *f_3* statistics with numerous pairs of populations even on our smallest SNP panel consisting of those called in DevilsGate2. (e.g. Lithuanians, the population with the highest hunter-gatherer-related component: Supplementary Table C.23 and Sardinians, harbouring the highest early farmer-related component: Supplementary Table C.22).

Since admixture *f_3* can be affected by demographic events such as bottlenecks, I also tested whether Devil's Gate formed a clade with the Ulchi using a *D* statistic in the form *D*(African outgroup, *X*; Ulchi, Devil's Gate). A number of primarily modern populations worldwide gave significantly non-zero results ($|Z| > 2$), which, together with the additional components for the Ulchi in the ADMIXTURE analysis implies that the continuity is not perfect. Populations from Central Asia scored highest, but for DevilsGate1 on the total SNP panel (the case with the highest power), a very wide range of populations from all over the world also gave smaller, but still significantly non-zero scores, in the direction indicating that they are closer to the Ulchi than to Devil's Gate. The high-scoring Central Asian populations are in agreement with the Central Asian-related ADMIXTURE ancestry components in the Ulchi, but the wide variety of the rest of the populations is difficult to explain. Possible contributors to this result could be the large uncertainty in SNP calling due to our very low coverage (even data from SNPs covered only originate from a single read in most cases), and errors from DNA degradation, which can also decrease the inferred level of continuity.

To compare the inferred level of continuity between the Ulchi and inhabitants of Devil's Gate to that between modern Europeans and European hunter-gatherers, I compared the sizes of ancestry proportions as inferred by ADMIXTURE. I found that the proportion of Devil's Gate-related ancestry in the Ulchi was significantly higher than that for the local hunter-gatherer related ancestry in any European population (t=3.10, df=27.23, p=0.002 using all SNPs for modern Lithuanians who have the largest European hunter-gatherer component and

$p < 0.001$ for all other populations, Supplementary Table C.6-11). Even when not only the hunter-gatherer-related components were considered, the difference was significant for every comparison except for the early European farmer-related component in the Sardinians (Supplementary Table C.7 and Supplementary Table C.10), a pair where a high level of continuity was observed in other analysis already.

These results suggest a relatively high degree of population continuity in this region; the Ulchi are likely descendants of Devil's Gate or a population genetically very close to it, but connectivity among populations in the region means that this modern population also shows increased association with related modern populations. Compared to Europe, these results suggest a higher level of genetic continuity in this region of northern East Asia over the last ~7.7 ky, without any major population turnover since the early Neolithic.

4.4.5 Southern and Northern genetic material in the Japanese and the Korean

The high genetic affinity between Devil's Gate and modern Japanese and Koreans, who live further south, is also of interest. Japanese have been argued, based on archaeology[28] and genetic analyses[29–32], to have a dual origin, descending from an admixture event between hunter-gatherers of the Jomon culture (16 kya – 3 kya) and migrants of the Yayoi culture (3 kya – 1.7 kya), who brought wet rice agriculture from the Yangtze estuary in southern China through Korea. The few ancient mtDNA samples available from Jomon sites on the northern Hokkaido island show an enrichment of particular haplotypes (N9b and M7a, with D1, D4, and G1 also detected) present in modern Japanese populations, particularly the Ainu and Ryukyuans, and also in southern Siberians (for example, Udegey and Ulchi)[15,16]. Recently, nuclear genetic data from two Jomon samples also confirmed the dual origin hypothesis and implied that the Jomon diverged before the diversification of present-day East Asians[33]. The mtDNA haplogroups of our samples from Devil's Gate (D4 and M) are also present in Jomon samples, although they are not the most common ones (N9b and M7a). Unfortunately the low coverage of both our and the Jomon samples did not allow for a direct comparison of nuclear genetic data.

I investigated whether it was possible to recover these two components by modelling modern Japanese as a mixture of all possible pairs of sources, including modern Asian populations and Devil's Gate, using admixture f_3 statistics. The clearest signal was given by a combination of Devil's Gate and aboriginal populations from Taiwan, southern China and Vietnam (Figure 4.4), which could represent hunter-gatherer and agriculturalist components, respectively. However, it is important to note that these scores were just about significant ($-3 < Z < -2$) and that some modern pairs also gave negative scores, even if not reaching our significance threshold (Z scores as low as -1.9, see Supplementary Table C.28-31). The origin of Koreans has received less attention, and, because of their location on the mainland, they likely experienced a greater degree of contact with neighbouring populations through history. However, they show similar characteristics to the Japanese on genome-wide SNP data[34] (Supplementary Table C.24-27) and are also shown to harbour mtDNA[35] and Y chromosomal haplogroups[35,36] common in both northern and southern Asian populations. Unfortunately our coverage and sample size from Devil's Gate was not enough to reliably estimate mixture coefficients or to use linkage disequilibrium-based methods to investigate whether the components originate from secondary contact (admixture) or continuous differentiation, and if the former is the case, to date the admixture event.

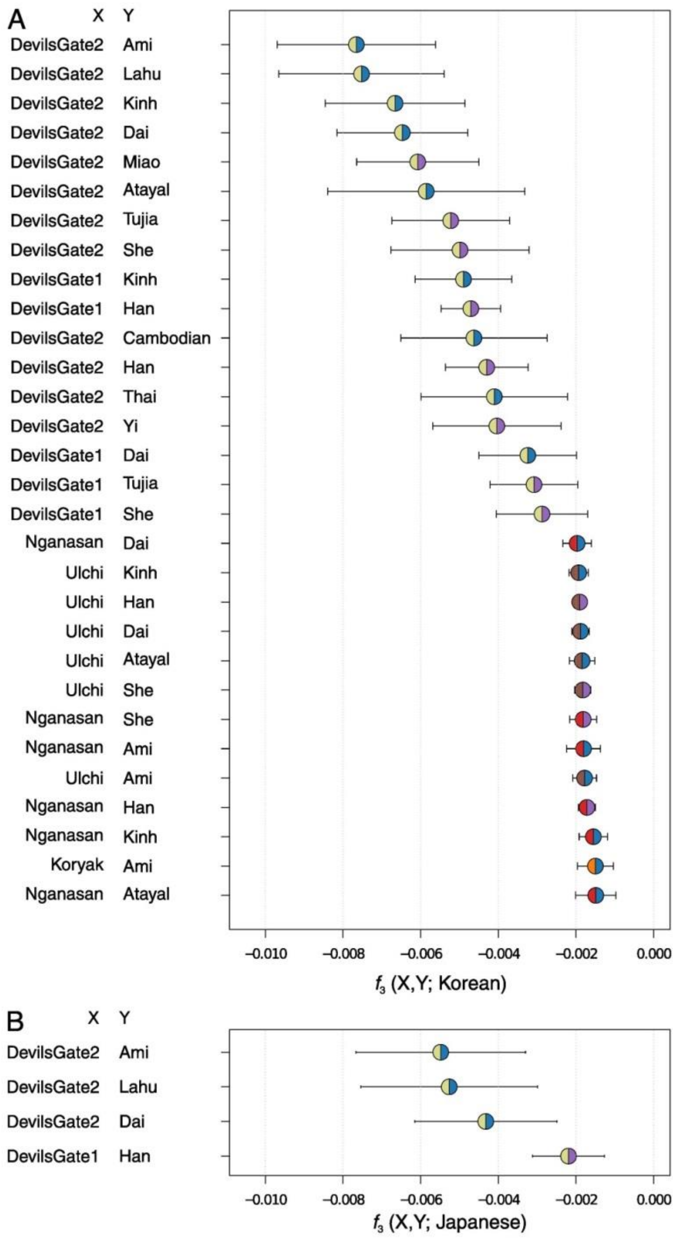

Figure 4.4 Admixture f3 statistics. Admixture f3 representing modern Koreans and Japanese as a mixture of two populations, X and Y, colour coded by regions as on Figure 4.1. (A) 30 pairs with the lowest f3 score for the Koreans as the target, out of those giving a significantly (Z < -2) value. (B) All 4 pairs giving a significantly (Z < -2) negative score for the Japanese as the target. Error bars represent one standard error.

4.4.6 Phenotypic prediction

The low coverage of our sample does not allow for direct observation of most SNPs linked to phenotypic traits of interest, but imputation based on modern-day populations can provide some information (although locations under selection can still be problematic). I focussed on the genome with the highest coverage, DevilsGate1, using the same imputation approach that has previously been used to estimate genotype probabilities (GP) for ancient European samples[6,21,22]. For the detailed results, see Supplementary Table C.32. DevilsGate1 likely had brown eyes (rs12913832 on HERC2; GP=0.905) and, where it could be determined, had pigmentation-associated variants which are common in East Asia[37]. She appears to have had at least one copy of the derived EDAR allele (rs3827760, GP = 0.865) common in East Asia, which gives increased odds of straight, thick hair[38,39] as well as shovel-shaped incisors [40]. She almost certainly lacked the most common Eurasian allele for lactase persistance[41] (rs4988235, LCT gene, GP>0.999), and was unlikely to have suffered from alcohol flush[42] (rs671, ALDH2 gene; GP=0.847). Thus, at least with regard to those phenotypic traits for which the genetic basis is known, there also seems to have been some degree of phenotypic continuity.

4.5 Conclusions

By sequencing two ancient East Asians who lived at the beginning of the Neolithic period in this region, I was able to demonstrate a high level of genetic continuity over the last ~7.7 ky in the northern part of this region, both demographically and phenotypically. The cold climate experienced in this area, where modern populations still rely on a number of hunter-gatherer-fishing practices, likely played a role in preventing major settlements of migrating Neolithic food-producers. Thus, it seems plausible that the local hunter-gatherers progressively added food-producing practices to their original lifestyle. However, it is interesting to note that in Europe, even at very high latitudes where hunter-gathering practices were still similarly important until very recent times, the Neolithic expansion left a significant genetic signature in modern populations, albeit attenuated when compared to the southern part of the continent. Our ancient genomes thus provide evidence for a qualitatively different population prehistory during the Neolithic transition in this part of East Asia compared to Western Eurasia, suggesting stronger genetic continuity in the former region. These results encourage further study of the East Asian Neolithic, which would greatly benefit from genetic data from early agriculturalists (ideally from areas near the origin of wet rice cultivation and other types of agriculture in southern East Asia), as well as higher coverage hunter-gatherer samples from different regions in order to quantify population structure before intensive agriculture.

4.6 Methods

4.6.1 Experimental Design

4.6.1.1 Radiocarbon dates

Direct AMS radiocarbon dates were obtained at the Oxford AMS Radiocarbon Laboratory for the two highest-coverage individuals, DevilsGate1 and DevilsGate2.

4.6.1.2 Sample preparation and sequencing

Molecular analyses were carried out in dedicated ancient DNA facilities at Trinity College Dublin, Ireland. Samples were prepared and DNA extracted using a silica column based protocol following Gamba et al.[22] which was based on Yang et al.[43]. DNA extracted from both the first and second lysis buffers[22] were used for library preparation which was carried out using a modified version of Meyer & Kircher[44] as described in Gamba et al.[22]. Libraries were sequenced on either an Illumina MiSeq or HiSeq platform (for further details and sequencing statistics see Supplementary Table C.1).

4.6.1.3 Data processing and alignment

For single-end sequencing data (Supplementary Table C.1), adapter sequences were trimmed from the ends of reads using cutadapt[45] allowing an overlap of only 1 base pair (bp) between the adapter and the read. For paired end data (Supplementary Table C.1), adapters were trimmed using leeHom[46]. This was run using the --ancientdna option and paired end reads which overlapped were merged. For paired end reads that could not be overlapped only data from read 1 were used in downstream analyses. Reads were aligned using BWA[47], with the seed region disabled, to the GRCh37 build of the human genome with the mitochondrial sequence replaced by the revised Cambridge reference sequence (National Centre for Biotechnology Information (NCBI) accession number NC_012920.1). Reads from different sequencing experiments were merged using Picard MergeSamFiles (http://picard.sourceforge.net/) and clonal reads were removed using SAMtools[48]. A minimum read length of 30 bp was imposed and for the higher coverage (above 0.01X) samples, DevilsGate1 and DevilsGate2, indels were realigned using RealignerTargetCreator and IndelRealigner from the Genome Analysis Toolkit (GATK[49]). SAMtools[48] was used to filter out reads with a mapping quality of less than 30 and reads were rescaled using mapDamage 2.0[50] to reduce the qualities of likely damaged bases, therefore lessening the effects of ancient DNA damage associated errors on analysis[50]. Average genomic depth of coverage was calculated using the genomecov function of bedtools[51].

4.6.1.4 Authenticity of results

Patterns of molecular damage and the length distribution of reads were assessed using all reads for DevilsGate3, DevilsGate4, and DevilsGate5. As a portion of the reads from

DevilsGate1 and DevilsGate2 derived from 50 bp single end sequencing, only reads sequenced with 150 bp paired end sequencing were considered in the following analyses in order to avoid using truncated reads (library ID MOS5A.E1 for DevilsGate1 and MOS4A.E1 for DevilsGate2). MapDamage 2.0[50] was used to assess patterns of molecular damage which are typical of ancient DNA. Only reads with mapping quality ⩾ 20 were considered. An increased rate (up to 11%) of C to T misincorporations was found at the 5' ends of reads with reciprocal patterns of G to A misincorporations at the 3' read termini (Supplementary Figure C.2). The sequence length distribution was analysed as in [52]. For all samples a peak in DNA sequence length is visible at <70 bp, consistent with the short fragment length expected for ancient molecules[53] (Supplementary Figure C.3).

Low coverage data like ours often does not provide sufficient information to distinguish the C to T mutations on the sample relative to the reference sequence, which appear close to the 5' terminus, from damage. Thus, such positions can be downscaled in quality and dropped, which can lead to a bias pulling the ancient sample closer to the human reference genome. On the other hand, not applying MapDamage can lead to the opposite bias due to damage. Thus, I also replicated our analysis on versions of Devil's Gate samples without MapDamage rescaling, to confirm that neither of these biases affect our conclusions.

4.6.1.5 Contamination estimates

The rate of mitochondrial contamination was assessed for our highest coverage samples, DevilsGate1 and DevilsGate2. This was calculated by evaluating the percentage of non-consensus bases at haplogroup-defining positions (haplogroup D4 for DevilsGate1 and M for DevilsGate2) using bases with quality ⩾ 20[22,26].

Schmutzi, a tool which employs a Bayesian maximum a posteriori algorithm[17], was also used to estimate the mitochondrial contamination for DevilsGate1 (the contamination rate for DevilsGate2 was not estimated using this tool, as it estimates a contamination prior using deamination frequencies at read termini and as 99% of reads from DevilsGate2 derive from 50 bp sequencing, its read termini are likely truncated). For DevilsGate1 only reads from >=100bp sequencing were used in the analysis. The contDeam.pl script was run using the --library double option followed by the schmutzi.pl script with default parameters, using a dataset of putative contaminants provided with the schmutzi package. It should be noted that this program will underestimate the contamination rate if the contaminating molecules are deaminated or if there are multiple contaminating sources.

Since other ways of estimating contamination were not possible (e.g. based on the X-chromosome), I also attempted to replicate our main results using only reads with evidence of postmortem damage. I applied PMDtools (9), a framework assigning likelihood scores to degraded sequences that are unlikely to originate from modern contamination. In this part of the analysis, I restricted our reads to those with a PMD score of at least 3. This greatly decreased our coverage, to 0.0050X for DevilsGate1 and 0.0012X for DevilsGate2, but it was still enough to perform two of our most robust analysis: the outgroup f_3 statistics (Supplementary Figure C.4) and a Principal Component Analysis (Supplementary Figure C.5 and Supplementary Figure C.7 using the world-wide or the reginal panel, respectively).

4.6.2 Statistical Analysis

4.6.2.1 Mitochondrial Haplogroup Determination

Mitochondrial consensus sequences were generated for DevilsGate1 and DevilsGate2 using ANGSD[54]. Called positions were required to have a depth of coverage ⩾ 3 and only bases with quality ⩾ 20 were considered. The resulting FASTA files were uploaded to HAPLOFIND[55] for haplogroup determination. Mutations defining the assigned haplogroup were also manually checked. Coverage was calculated using GATK DepthOfCoverage[49].

4.6.2.2 Sex determination

Sex was assigned using the script described by Skoglund et al.[56]. The observed fraction of Y chromosome alignments compared to the total number of alignments to the X and Y chromosome and it's estimated 95% confidence interval was $R_Y = 0.0057$ (0.0053-0.0061) and $R_Y = 0.0059$ (0.0054-0.0064) for DevilsGate1 and DevilsGate2, respectively, implying that both of them were females.

4.6.2.3 SNP calling and merging with reference panel

In order to compare our sample to modern and ancient human genetic variation, we called SNPs using the hg19 reference FASTA file at positions overlapping with the Human Origins (HO) reference panel (591,356 positions)[25], using Samtools 1.2[48]. Bases were required to have a minimum mapping quality of 30, base quality of 20, and all triallelic SNPs were discarded. Then, a read was chosen uniformly at random, since our low coverage does not provide sufficient information to infer diploid genotypes. This allele was duplicated to form a homozygous diploid genotype which was used to represent the individual at that SNP position[56]. This method of SNP calling, referred to as the proportional method from now on, will artificially increase the appearance of drift on the lineage leading to the ancient individual; however, this drift is not expected to be in any particular direction and therefore should not bias inferences about population relationships [4]. A total of 35,903 positions in DevilsGate1 and 14,739 in DevilsGate2 were covered by at least one high-quality read.

The resulting SNP data for Devil's Gate 1 and 2 were then merged with a reference panel containing modern genomes from the HO panel and selected ancient genomes (this dataset was described in [6]) as well as an additional 45 Korean genomes from the Personal Genome Project Korea (http://opengenome.net/) using PLINK 1.07[57]. Additional sample information is available in Supplementary Table C.2 to Supplementary Table C.5, including sample ID-s, populations and groupings used throughout the manuscript. Finally, a transversion-only version of all the above data was created, by converting all T-s to C-s and G-s to A-s and keeping only SNPs still polymorphic. This alternative dataset was used to confirm that biases originating from ancient DNA damage do not influence our conclusions.

In the later analyses (outgroup and admixture f_3 statistics, Principal Component Analysis and ADMIXTURE analysis), results from the two different calling methods were qualitatively equivalent. Results using all mutations or only transversions were also qualitatively similar, apart from increased noise in the transversion-only data due to the reduced information content. Thus, in the main text, I will only report results using all mutations and the default calling method, referred to as the proportional method (choosing a read uniformly at random from the reads covering any given position). I present results using the Khomani San as our African outgroup for outgroup f_3 and D statistics, but other populations (the Yoruba, the Mbuti and the Dinka) gave equivalent results.

4.6.2.4 Affinities of the samples from Devil's Gate

a. Principal Component Analysis

In order to explore where our samples from Devil's Gate are placed in the context of the main axes defining modern genetic variation, I performed a Principal Component Analysis (PCA) with two different reference panels, both subset of the worldwide panel of contemporary and ancient individuals from [6]. The analysis was carried out using EIGENSOFT 6.0.1 smartpca[23] with the lsqproject and normalisation options on, the outlier removal option off and one SNP from each pair in linkage disequilibrium with r^2>0.2 removed. Ancient samples were projected onto the Principal Components defined by modern populations.

b. ADMIXTURE analysis

A clustering analysis was performed using ADMIXTURE version 1.23[24] SNPs in linkage disequilibrium were thinned using PLINK 1.07 with parameters –indep-pairwise 200 25 0.5 resulting in a set of 334,359 SNPs for analysis (91,379 transversions). K=2-20 clusters were explored for the global panel and K=1-10 for the regional panel, using 10 independent runs with fivefold cross-validation at each K with different random seeds. The minimal cross-validation error was found at K=17 for the global panel (Supplementary Figure C.9) and K=5 for the regional (East & Central Asian) panel (Supplementary Figure C.10), but the error already started plateauing around K=9 for the global, suggesting little improvement.

I further used the ADMIXTURE results to compare the levels of Devil's Gate-related ancestry in the Ulchi to hunter-gatherer, Early European Farmer and Bronze Age steppe-related ancestries in modern Europeans. Supplementary Table C.6-11 shows the p-values from T-tests for each European population in our panel. I investigated both K=8, where the Devil's Gate-specific cluster first. For the Europeans, I used k=18, where cross-validation error is the lowest (although the proportions hardly change once the three main European clusters corresponding to hunter-gatherers, Neolithic farmers and steppe ancestry are all present).

The proportion of Devil's Gate-related ancestry depends on the choice of K for the ADMIXTURE analysis. However, K=8, which was chosen (lowest k with a defined Devil's Gate cluster on both all SNPs and transversion only SNPs) results in the lowest Devil's Gate-related ancestry components in the Ulchi. Therefore, higher K-s would only increase the significance in the difference from European proportions.

c. Outgroup f$_3$ statistics

I used outgroup *f*$_3$-statistics to estimate the amount of shared drift between inhabitants of Devil's Gate and a range of modern-day and ancient populations. I computed *f*$_3$(*X*, DevilsGate; Khomani), where *X* was a population from our panel, and the Khomani (Khoisan) acted as our outgroup. *f*$_3$ statistics were calculated with the 3PopTest tool from the AdmixTools[25]. Figure 2 shows results using all SNP-s and MapDamage treatment, Supplementary Figure C.4 those using PMD-filtered data and all other results are shown on Supplementary Table C.12-15.

4.6.2.5 Relation to MA1 and Ust'Ishim

d. Outgroup *f*$_3$

Outgroup f3 with MA1

First, I used the outgroup *f*$_3$-statistics to investigate if the inhabitants of Devil's Gate were related to the ancient lineages represented by MA1 and Ust'Ishim. I considered all modern-day and ancient populations in our panel, including the two new samples from Devil's Gate. I computed *f*$_3$(*X*, MA1; Khomani), where *X* was a population from our panel, and the Khomani (Khoisan) acted as outgroup. *f*$_3$ statistics were calculated with the 3PopTest tool from the AdmixTools package[25].

e. D statistics

Next, I used D statistics to investigate how MA1 and Ust'Ishim and Devil's Gate are related to modern populations. I considered all modern-day and ancient populations in our panel, including the two new samples from Devil's Gate. I computed D(X, Khomani; MA1, DevilsGate1), where X was a population from our panel, and the Khomani (Khoisan) acted as outgroup. D-statistics were calculated with the qpDstat tool from the AdmixTools package[25].

4.6.2.6 Searching for signals of admixture in the Ulchi

f. Admixture f3 shows no signal of admixture

In order to search for signals of admixture in the Ulchi, I first used the admixture f_3-statistics in the form $f_3(X, Y;$ Ulchi), using the pq3Pop tools from the AdmixTools package[25]. I scanned every possible pair of populations X and Y, taken from our global panel of modern and ancient populations and Devil's Gate. Only considered pairs with at least 1000 SNPs in common were considered. This statistic can be significantly negative if the target population (in this case, the Ulchi) has genetic material from both populations X and Y.

In order to test for signals of admixture in the Ulchi, I tested the statistics of the form $f_3(X, Y;$ Ulchi), scanning every possible pair of populations X and Y in our global panel (including Devil's Gate). Pairs of populations with Z<-1 and at least 1000 SNPs covered are Supplementary Table C.20 and Supplementary Table C.21, using all SNPs or transversions only. As a comparison, I conducted the same analysis for the Lithuanians (Supplementary Table C.23), who harbour the highest hunter-gatherer component on ADMIXTURE and the Sardinians (Supplementary Table C.22) who are closest to Early European Farmers on numerous analysis.

g. D statistics can't reject a breach of continuity

I then tested if the samples from Devil's Gate and the Ulchi form a clade against other populations by examining D statistics of the form D(Khomani, X; Ulchi, Devil's Gate). This statistic deviates from zero if the Ulchi or Devil's Gate are not symmetrically related to population X when compared to an outgroup population (I used the African Khomani San).

For both DevilsGate1 and DevilsGate2, populations with a significantly non-zero score (|Z| > 2) are shown on Supplementary Table C.16-19).

4.6.2.7 Dual origin of the Koreans and the Japanese

In order to search for signals of multiple components in the Koreans and the Japanese, I again used the admixture f_3-statistics in the form f_3(X, Y; Target) for the Japanese and the Koreans as target populations, using the pq3Pop tools from the AdmixTools package[25]. I scanned every possible pair of populations *X* and *Y*, taken from our global panel of modern and ancient populations and Devil's Gate. Only pairs with at least 1000 SNPs in common were considered. This statistic can be significantly negative if the target population has genetic material from both populations X and Y (this does not exclude additional populations also contributing to the target population). In order to investigate the origin of the northern component and whether it is related to the occupants of Devil's Gate, I calculated admixture f_3 statistics of the form f_3 (X, Y; Korean) and f_3 (X, Y; Japanese). Pairs giving significantly negative admixture f_3 statistics at a significance level of Z<-2 and at least 1000 SNPs are included on Supplementary Table C.24-31.

4.6.2.8 Phenotypic prediction

Phenotypes of interest were investigated in our highest coverage sample, DevilsGate1, including some loci known to have been under selection in Eurasian populations. Due to the low quality of our samples, BEAGLE[58] was used to impute genotypes using a reference panel containing phased genomes from the 1,000 Genomes Project (26 different populations). Following [22], GATK Unified genotyper[49] was used to call genotype likelihoods at SNP sites in Phase 3 of the 1,000 Genomes Project. Equal likelihoods were set for positions with no spanning sequence data as well as positions where the observed genotype could be explained by deamination[22]. At least 1Mb upstream and downstream from the loci of interest was imputed, using 10 iterations to estimate genotypes at ungenotyped markers. The only position covered by a read was rs74653330 SNP on the OCA2 gene. It had 1x coverage of a C allele (the allele predicted using imputation). The summary of our results is shown in Supplementary Table C.32.

4.7 Bibliography

1. Siska, V. *et al.* Genome-wide data from two early Neolithic East Asian individuals dating to 7700 years ago. *Sci. Adv.* **3,** e1601877 (2017).

2. Lazaridis, I. *et al.* Genomic insights into the origin of farming in the ancient Near East. *Nature* **536,** 419–424 (2016).

3. Gallego-Llorente, M. *et al.* The genetics of an early Neolithic pastoralist from the Zagros, Iran. *Sci. Rep.* **6,** (2016).

4. Lazaridis, I. *et al.* Ancient human genomes suggest three ancestral populations for present-day Europeans. *Nature* **513,** 409–413 (2014).

5. Haak, W. *et al.* Massive migration from the steppe was a source for Indo-European languages in Europe. *Nature* **522,** 207–211 (2015).

6. Jones, E. R. *et al.* Upper Palaeolithic genomes reveal deep roots of modern Eurasians. *Nat. Commun.* **6,** 8912 (2015).

7. Raghavan, M. *et al.* The genetic prehistory of the New World Arctic. *Science* **345,** 1255832 (2014).

8. Raghavan, M. *et al.* Genomic evidence for the Pleistocene and recent population history of Native Americans. *Science* **349,** aab3884 (2015).

9. Fu, Q. *et al.* DNA analysis of an early modern human from Tianyuan Cave, China. *Proc. Natl. Acad. Sci.* **110,** 2223–2227 (2013).

10. Yang, M. A. *et al.* 40,000-Year-Old Individual from Asia Provides Insight into Early Population Structure in Eurasia. *Curr. Biol.* **27,** 3202–3208.e9 (2017).

11. Kuzmin, Y. The Paleolithic-to-Neolithic transition and the origin of pottery production in the Russian Far East: a geoarchaeological approach. *Archaeol. Ethnol. Anthropol. Eurasia* **4,** 16–26 (2003).

12. Chi, Z. & Hsiao-chun, H. 26 Eastern Asia: archaeology. in *The Encyclopedia of Global Human Migration* (Blackwell Publishing Ltd, 2013).

13. Kuzmin, Y. V., Keally, C. T., Jull, A. J. T., Burr, G. S. & Klyuev, N. A. The earliest surviving textiles in East Asia from Chertovy Vorota Cave, Primorye Province, Russian Far East. *Antiquity* **86,** 325–337 (2012).

14. Tanaka, M. *et al.* Mitochondrial Genome Variation in Eastern Asia and the Peopling of Japan. *Genome Res.* **14,** 1832–1850 (2004).

15. Adachi, N., Shinoda, K., Umetsu, K. & Matsumura, H. Mitochondrial DNA analysis of Jomon skeletons from the Funadomari site, Hokkaido, and its implication for the origins of Native American. *Am. J. Phys. Anthropol.* **138,** 255–265 (2009).

16. Adachi, N. *et al.* Mitochondrial DNA analysis of Hokkaido Jomon skeletons: Remnants of archaic maternal lineages at the southwestern edge of former Beringia. *Am. J. Phys. Anthropol.* **146,** 346–360 (2011).

17. Renaud, G., Slon, V., Duggan, A. T. & Kelso, J. Schmutzi: estimation of contamination and endogenous mitochondrial consensus calling for ancient DNA. *Genome Biol.* **16,** 224 (2015).

18. Skoglund, P. *et al.* Separating endogenous ancient DNA from modern day contamination in a Siberian Neandertal. *Proc. Natl. Acad. Sci.* **111,** 2229–2234 (2014).

19. Fu, Q. *et al.* Genome sequence of a 45,000-year-old modern human from western Siberia. *Nature* **514,** 445–449 (2014).

20. Raghavan, M. *et al.* Upper Palaeolithic Siberian genome reveals dual ancestry of Native Americans. *Nature* **505,** 87–91 (2014).

21. Allentoft, M. E. *et al.* Population genomics of Bronze Age Eurasia. *Nature* **522,** 167–172 (2015).

22. Gamba, C. *et al.* Genome flux and stasis in a five millennium transect of European prehistory. *Nat. Commun.* **5,** 5257 (2014).

23. Patterson, N., Price, A. L. & Reich, D. Population Structure and Eigenanalysis. *PLOS Genet* **2,** e190 (2006).

24. Alexander, D. H., Novembre, J. & Lange, K. Fast model-based estimation of ancestry in unrelated individuals. *Genome Res.* (2009). doi:10.1101/gr.094052.109

25. Patterson, N. *et al.* Ancient Admixture in Human History. *Genetics* **192,** 1065–1093 (2012).

26. Sánchez-Quinto, F. *et al.* Genomic Affinities of Two 7,000-Year-Old Iberian Hunter-Gatherers. *Curr. Biol.* **22,** 1494–1499 (2012).

27. Pereltsvaig, A. in *Languages of the world: An introduction* 211–216 (Cambridge University Press, 2017).

28. Imamura, K. *Prehistoric Japan: New Perspectives on Insular East Asia*. (University of Hawaii Press, 1996).

29. Jinam, T. A., Kanzawa-Kiriyama, H. & Saitou, N. Human genetic diversity in the Japanese Archipelago: dual structure and beyond. *Genes Genet. Syst.* **90,** 147–152 (2015).

30. Rasteiro, R. & Chikhi, L. Revisiting the peopling of Japan: an admixture perspective. *J. Hum. Genet.* **54,** 349–354 (2009).

31. He, Y., Wang, W. R., Xu, S., Jin, L. & Consortium, P.-A. S. Paleolithic Contingent in Modern Japanese: Estimation and Inference using Genome-wide Data. *Sci. Rep.* **2,** 355 (2012).

32. Jinam, T. A. *et al.* Unique characteristics of the Ainu population in Northern Japan. *J. Hum. Genet.* **60,** 565–571 (2015).

33. Kanzawa-Kiriyama, H. *et al.* A partial nuclear genome of the Jomons who lived 3000 years ago in Fukushima, Japan. *J. Hum. Genet.* (2016). doi:10.1038/jhg.2016.110

34. Consortium, T. H. P.-A. S. Mapping Human Genetic Diversity in Asia. *Science* **326,** 1541–1545 (2009).

35. Jin, H.-J., Tyler-Smith, C. & Kim, W. The Peopling of Korea Revealed by Analyses of Mitochondrial DNA and Y-Chromosomal Markers. *PLoS ONE* **4,** (2009).

36. Jin, H.-J. *et al.* Y-chromosomal DNA haplogroups and their implications for the dual origins of the Koreans. *Hum. Genet.* **114,** 27–35 (2003).

37. Sturm, R. A. & Duffy, D. L. Human pigmentation genes under environmental selection. *Genome Biol.* **13,** 248 (2012).

38. Fujimoto, A. *et al.* A scan for genetic determinants of human hair morphology: EDAR is associated with Asian hair thickness. *Hum. Mol. Genet.* **17,** 835–843 (2008).

39. Fujimoto, A. *et al.* A replication study confirmed the EDAR gene to be a major contributor to population differentiation regarding head hair thickness in Asia. *Hum. Genet.* **124,** 179–185 (2008).

40. Park, J.-H. *et al.* Effects of an Asian-specific nonsynonymous EDAR variant on multiple dental traits. *J. Hum. Genet.* **57,** 508–514 (2012).

41. Itan, Y., Powell, A., Beaumont, M. A., Burger, J. & Thomas, M. G. The Origins of Lactase Persistence in Europe. *PLoS Comput Biol* **5,** e1000491 (2009).

42. Crabb, D. W., Edenberg, H. J., Bosron, W. F. & Li, T. K. Genotypes for aldehyde dehydrogenase deficiency and alcohol sensitivity. The inactive ALDH2(2) allele is dominant. *J. Clin. Invest.* **83,** 314–316 (1989).

43. Yang, D. Y., Eng, B., Waye, J. S., Dudar, J. C. & Saunders, S. R. Technical note: improved DNA extraction from ancient bones using silica-based spin columns. *Am. J. Phys. Anthropol.* **105,** 539–543 (1998).

44. Meyer, M. & Kircher, M. Illumina Sequencing Library Preparation for Highly Multiplexed Target Capture and Sequencing. *Cold Spring Harb. Protoc.* **2010,** pdb.prot5448 (2010).

45. Martin, M. Cutadapt removes adapter sequences from high-throughput sequencing reads. *EMBnet.journal* **17,** pp. 10–12 (2011).

46. Renaud, G., Stenzel, U. & Kelso, J. leeHom: adaptor trimming and merging for Illumina sequencing reads. *Nucleic Acids Res.* **42,** e141 (2014).

47. Li, H. & Durbin, R. Fast and accurate short read alignment with Burrows-Wheeler transform. *Bioinforma. Oxf. Engl.* **25,** 1754–1760 (2009).

48. Li, H. *et al.* The Sequence Alignment/Map format and SAMtools. *Bioinforma. Oxf. Engl.* **25,** 2078–2079 (2009).

49. McKenna, A. *et al.* The Genome Analysis Toolkit: a MapReduce framework for analyzing next-generation DNA sequencing data. *Genome Res.* **20,** 1297–1303 (2010).

50. Jónsson, H., Ginolhac, A., Schubert, M., Johnson, P. L. F. & Orlando, L. mapDamage2.0: fast approximate Bayesian estimates of ancient DNA damage parameters. *Bioinforma. Oxf. Engl.* **29,** 1682–1684 (2013).

51. Quinlan, A. R. & Hall, I. M. BEDTools: a flexible suite of utilities for comparing genomic features. *Bioinforma. Oxf. Engl.* **26,** 841–842 (2010).

52. Llorente, M. G. *et al.* Ancient Ethiopian genome reveals extensive Eurasian admixture throughout the African continent. *Science* **350,** 820–822 (2015).

53. Shapiro, B. & Hofreiter, M. A Paleogenomic Perspective on Evolution and Gene Function: New Insights from Ancient DNA. *Science* **343,** 1236573 (2014).

54. Korneliussen, T. S., Albrechtsen, A. & Nielsen, R. ANGSD: Analysis of Next Generation Sequencing Data. *BMC Bioinformatics* **15,** 356 (2014).

55. Vianello, D. *et al.* HAPLOFIND: a new method for high-throughput mtDNA haplogroup assignment. *Hum. Mutat.* **34,** 1189–1194 (2013).

56. Skoglund, P. *et al.* Genomic Diversity and Admixture Differs for Stone-Age Scandinavian Foragers and Farmers. *Science* **344,** 747–750 (2014).

57. Purcell, S. *et al.* PLINK: a tool set for whole-genome association and population-based linkage analyses. *Am. J. Hum. Genet.* **81,** 559–575 (2007).

58. Browning, B. L. & Browning, S. R. Genotype Imputation with Millions of Reference Samples. *Am. J. Hum. Genet.* **98,** 116–126 (2016).

59. Balueva, T. S. . Kraniologicheskij material neoliticheskogo sloya peshchery «Chertovy Vorota» (Primor'e) (Cranial samples from a Neolithic layer from Devil's Gate Cave, Primorye). *Vopr. Antropol.* **58,** 184–187 (1978).

60. Andreeva, Z. V. & Tatarnikov, V. Peshera «Chertovy Vorota» v Primor'e. *Arheol. Otkrytiya 1973 Goda Cave Devils Gate Primorye 1973 Excav. Seas. Mosc.* 180–181 (1974).

61. Zhushchikhovskaya, IS. Neolithic of the Primorye. in *.), Archaeology of the Russian Far East: essays in Stone Age prehistory* (eds. S.M. Nelson, A.P. Derevianko, Y.V. Kuzmin & R.L. Bland) 101–122 (Archaeopress, 2006).

62. Kuznecov, A. Drevnee poselenie v peshchere Chertovy Vorota i nekotorye problemy neolita Primor'ya (The ancient settlement in a cave Devil's Gate and some problems of the Neolithic of Primorye). *Ross. Arheol.* **2,** 17–19 (2002).

63. Lamason, R. L. *et al.* SLC24A5, a Putative Cation Exchanger, Affects Pigmentation in Zebrafish and Humans. *Science* **310,** 1782–1786 (2005).

64. Sturm, R. A. Molecular genetics of human pigmentation diversity. *Hum. Mol. Genet.* **18,** R9–R17 (2009).

65. Canfield, V. A. *et al.* Molecular Phylogeography of a Human Autosomal Skin Color Locus Under Natural Selection. *G3 GenesGenomesGenetics* **3,** 2059–2067 (2013).

66. Basu Mallick, C. *et al.* The Light Skin Allele of SLC24A5 in South Asians and Europeans Shares Identity by Descent. *PLoS Genet* **9,** e1003912 (2013).

67. Wilde, S. *et al.* Direct evidence for positive selection of skin, hair, and eye pigmentation in Europeans during the last 5,000 y. *Proc. Natl. Acad. Sci.* **111,** 4832–4837 (2014).

68. Norton, H. L. *et al.* Genetic Evidence for the Convergent Evolution of Light Skin in Europeans and East Asians. *Mol. Biol. Evol.* **24,** 710–722 (2007).

69. Donnelly, M. P. *et al.* A global view of the OCA2-HERC2 region and pigmentation. *Hum. Genet.* **131,** 683–696 (2011).

70. Hider, J. L. *et al.* Exploring signatures of positive selection in pigmentation candidate genes in populations of East Asian ancestry. *BMC Evol. Biol.* **13,** 150 (2013).

71. Yuasa, I. *et al.* Distribution of Two Asian-Related Coding SNPs in the MC1R and OCA2 Genes. *Biochem. Genet.* **45,** 535–542 (2007).

72. Yuasa, I. *et al.* OCA2*481Thr, a hypofunctional allele in pigmentation, is characteristic of northeastern Asian populations. *J. Hum. Genet.* **52,** 690–693 (2007).

73. Yuasa, I. *et al.* Distribution of OCA2∗481Thr and OCA2∗615Arg, associated with hypopigmentation, in several additional populations. *Leg. Med.* **13,** 215–217 (2011).

74. Ramos, E. M. *et al.* Phenotype–Genotype Integrator (PheGenI): synthesizing genome-wide association study (GWAS) data with existing genomic resources. *Eur. J. Hum. Genet.* **22,** 144–147 (2014).

75. Kamberov, Y. G. *et al.* Modeling Recent Human Evolution in Mice by Expression of a Selected EDAR Variant. *Cell* **152,** 691–702 (2013).

76. Goedde, H. W. *et al.* Distribution of ADH2 and ALDH2 genotypes in different populations. *Hum. Genet.* **88,** 344–346 (1992).

77. Li, H. *et al.* Refined Geographic Distribution of the Oriental ALDH2*504Lys (nee 487Lys) Variant. *Ann. Hum. Genet.* **73,** 335–345 (2009).

78. Matsuo, K. *et al.* Gene–environment interaction between an aldehyde dehydrogenase-2 (ALDH2) polymorphism and alcohol consumption for the risk of esophageal cancer. *Carcinogenesis* **22,** 913–916 (2001).

79. Cusi, D. *et al.* Polymorphisms of α-adducin and salt sensitivity in patients with essential hypertension. *The Lancet* **349,** 1353–1357 (1997).

80. Van den Wildenberg, E. *et al.* A functional polymorphism of the mu-opioid receptor gene (OPRM1) influences cue-induced craving for alcohol in male heavy drinkers. *Alcohol. Clin. Exp. Res.* **31,** 1–10 (2007).

81. Haerian, B. S. & Haerian, M. S. OPRM1 rs1799971 polymorphism and opioid dependence: evidence from a meta-analysis. *Pharmacogenomics* **14,** 813–824 (2013).

82. Rodriguez, S., Steer, C. D., Farrow, A., Golding, J. & Day, I. N. M. Dependence of Deodorant Usage on ABCC11 Genotype: Scope for Personalized Genetics in Personal Hygiene. *J. Invest. Dermatol.* **133,** 1760–1767 (2013).

83. Yoshiura, K. *et al.* A SNP in the ABCC11 gene is the determinant of human earwax type. *Nat. Genet.* **38,** 324–330 (2006).

84. Cho, Y. S. *et al.* Meta-analysis of genome-wide association studies identifies eight new loci for type 2 diabetes in east Asians. *Nat. Genet.* **44,** 67–72 (2012).

Chapter 5 Behaviour of selection statistics in a spatially explicit, neutral demographic model

5.1 Abstract

Natural selection is the main driving process behind adaptive evolution. Detecting signals of selection in the genome is not only useful for medical genetics, but can also uncover key processes in the dynamics of speciation and the population histories of species. However, complex demographic processes can confound signals and are one of the likely causes of the commonly observed contradicting results between different studies. Here I made use of a paleoclimate-informed, spatially explicit demographic model to explore the behaviour of commonly used selection statistics. I investigated how different statistics behave when the confounding effects of space and population history are taken into account. I focused on three statistics: allele frequency spectrum-based Tajima's D, population differentiation-based F_{ST} and linkage disequilibrium-based iHS. To investigate which statistics are linked to similar processes and to what extent purely demographic signals in different populations are correlated, I measured the amount of overlap between signals from different statistics or different populations and compared them to those from the 1000 Genomes Phase 3 dataset. I found that different statistics overlap to a smaller extent in the neutral simulations than in observed data, but the relationships between signals from different populations were better captured by our model.

5.2 Contribution

The base demographic model that generated recombining and non-recombining genealogies and TMRCA-s was created by Anders Eriksson. The non-recombining version was used in publications concerning the spread of anatomically modern humans[1] and the population history of the Americas[2], but this chapter is the first use case for the model including recombination. I implemented modules in this existing C++ modelling framework for sequence generation upon both non-recombining (tree-like) and recombining (network-like) genealogies, as well as to calculate Tajima's D. I also performed the complete analysis outside the modelling framework: processed the observed data, calculated selection statistics on both observed and simulated data, compared them to each other and created this manuscript.

5.3 Introduction

The availability of high-resolution genetic datasets made it possible to detect signals of natural selection in observed data. For humans, most efforts have been dedicated to the indirect method of looking for signals of past selection in present-day genomes by scanning the whole genomes for outlier segments on the basis of different statistics. Such outliers can arise from a scenario where a single, new allele has a beneficial effect (positive selection) and rapidly spreads to high frequencies or fixation in a population (a hard sweep). As a consequence, diversity in the region surrounding the beneficial allele's locus is reduced, until mutation and recombination together restore it to values typical of neutral variation. Additionally, in the case of localised selection pressures, the target population becomes unusually differentiated from others around the selected locus. There are three basic families of methods to detect signals of positive selection that exploit these signatures: allele frequency spectrum-, population differentiation- and linkage disequilibrium-based methods[3].

The first family, based on the allele frequency spectrum, uses the distribution of alleles in a population to detect deviations from neutral expectation. For instance, Tajima's D[4] looks for a departure from neutrality as reflected by the difference between low-frequency and intermediate frequency variants, and Fay and Wu's H[5] focuses on differences between high and intermediate frequency variants whilst also using ancestral state information.

The second family, based on population differentiation, focuses on population-specific selection pressures and looks for loci where allele frequencies differ between populations to a greater extent than expected. As a result, population differentiation-based statistics have the highest power to detect selection in variants that are fixed in a given population – in contrast to the previous measures comparing different variants at a given locus and thus suitable only for incomplete sweeps. Typical examples of this family are statistical tests based on Wright's fixation index (F_{ST})[6]. This index measures the proportion of genetic variance contained in a subpopulation, relative to the total population: $F_{ST} = \frac{\sigma_S^2}{\sigma_T^2}$, where σ_S^2 is the variance in the frequency of an allele between different subpopulations, weighted by the sizes of the subpopulations and σ_T^2 is the variance of the allelic state in the total population.

The third family, based on linkage disequilibrium (LD), looks for regions of strong LD surrounding the beneficial allele; in other words, it focuses on the low diversity around a given allele at a specific location (long linked regions, also called haplotypes). Two common examples of such tests are the integrated Haplotype Score[7] (iHS) and the number of Segregating sites by Length[8] ($\mathrm{nS_L}$), with the only difference being in the distance measure they use. Both statistics begin by calculating the probability that any two haplotypes carrying a chosen allele at a chosen, focal SNP are identical up to a certain distance away from the focal SNP. This probability is then integrated over all possible distances and compared to the integral from other variants at the same locus as a baseline. iHS, the most commonly used LD-based selection test, measures distance in the metric $4Nr$, where N is the effective population size and r is the recombination rate per generation. $\mathrm{nS_L}$ is a more recent statistic; it uses the number of alleles in the remaining haplotypes in the data set in the same region as a distance measure. Therefore, nS_L does not require a fine estimation of recombination rates and was shown to be more robust to recombination rate variation[8]. A third LD-based statistic is the cross-population extended haplotype homozygosity[9] (XP-EHH), which is similar to iHS but compares integrated haplotype homozygosities between variants in different populations instead of different variants in the same set of individuals. Therefore, XP-EHH does not require the presence of alternative alleles at the focal locus and can work also for fixed variants, similarly to population differentiation-based statistics.

A strong warning that using different methods together is not without problems comes from the low congruence in the loci they detect as under selection. Some researchers combine multiple metrics to look for regions that consistently score highly, either through composite measures (e.g. composite likelihood ratio[10]), or by applying the methods separately, and focusing on shared outlier windows[3,11,12]. Both of these approaches are based on the assumption that false signals would be correlated to a lesser extent than those arising from selection, and thus false positives would be excluded from shared signals. However, the extent to which signals become more correlated under different cases of selection is not well known, and different statistics are sensitive for different kinds of selection and/or selection acting on different timescales. Furthermore, a complete lack of correlation would not be expected even in genomic regions that are completely neutral. In fact, multiple populations are likely to be influenced by the same confounding demographic processes and, from the signal side, different statistics can be sensitive to similar confounding effects. In order to disentangle signals of selection from false positives caused by demographic events and assess significance, we need a realistic demographic model to explore the null distributions of these quantities.

5.4 Methods

5.4.1 Spatially explicit demographic model

Here I applied an individual-based, climate-driven, spatially explicit demographic model (Figure 5.1) created in C++, which was previously used to investigate the effect of climate on human dispersal[1] (using data from microsatellite markers) and the peopling of the Americas[2] (based on SNP-data).

In the model, the Earth was divided into hexagons that could be inhabited by separate populations (Figure 5.1A). Each hexagon was roughly 100km wide and was characterised by the maximum number of individuals it could sustain (carrying capacity), with local population growth following a simple logistic growth model. Palaeoclimate reconstructions based on the Hadley Centre model HadCM3 were used to determine sea level (defining which hexagons were above water at any point in time), ice coverage (which made some land hexagons uninhabitable), and vegetation. Vegetation was quantified in terms of Net Primary Productivity (NPP), which was used as a measure of available resources. The local carrying capacities were then scaled by a saturating function (Figure 5.1B) of the local NPP. The relationship between carrying capacity and NPP was a continuous, piecewise linear function: zero below a lower habitability threshold, the maximal carrying capacity above an upper NPP threshold and linearly increasing in-between.

Migration was allowed between neighbouring hexagons, with empty hexagons potentially colonised from inhabited neighbours if the neighbours' carrying capacity was reached (Figure 5.1C). The simulation was initiated with a population in a single hexagon in East Africa, spreading by the successive colonisation of neighbouring.

The parameters determining the conversion between NPP and carrying capacity (threshold NPP values for inhabitability and for reaching maximal carrying capacity), as well as unknown demographic parameters (growth, migration and colonisation rates), the length of the simulation and the global maximal carrying capacity were fitted based on genetic data (see section 5.4.2). The resulting demography was simulated in a stochastic, individual-based framework.

While running the demography forward, reconstructing the last 120k years of human demographic history and the major expansion out of Africa, time-series of population sizes and migration events were recorded. Using these time-series, genealogies were simulated backwards based on the Fisher-Wright coalescent model, with or without recombination. Non-recombining sequences were used to fit the model and recombining ones to calculate the amount of overlap between statistics/populations. Finally, sequences of fixed length were generated by distributing mutations along the genealogies with a constant rate and inferring the resulting alleles at the tips of the genealogies.

The whole simulation framework was coded in C++. The modules for sequence generation upon both non-recombining (tree-like) and recombining (network-like) genealogies were developed as part of the work for this chapter, while the upstream part of the framework (demographic simulation and genealogy generation) were developed by Anders Eriksson for previous projects[1,2].

Chapter 5 Behaviour of selection statistics in a spatially explicit, neutral demographic model

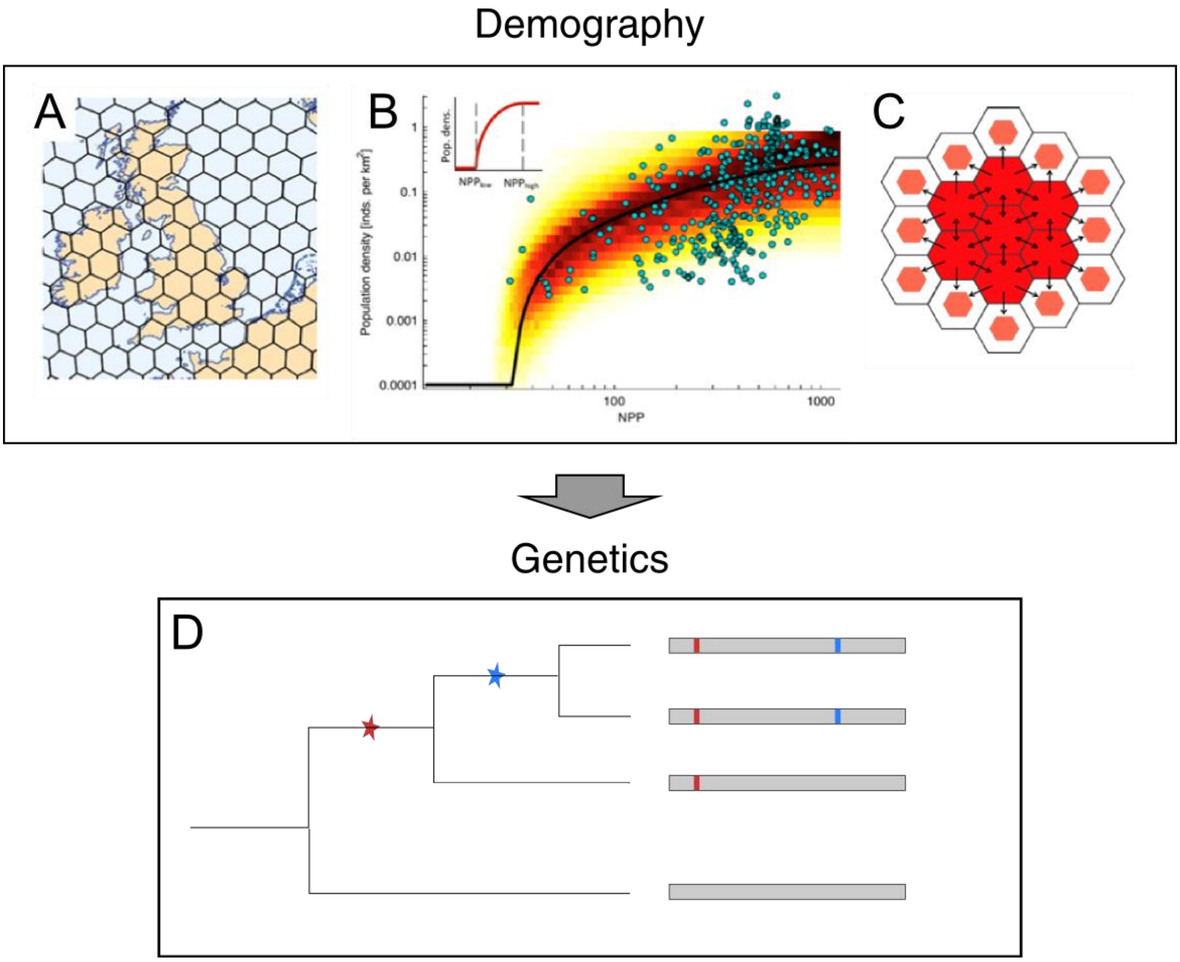

Figure 5.1 Illustration of the spatial demographic model. A. Carrying capacities are a saturating function of NPP. B. The Earth is divided into equally-sized, roughly 100km wide hexagons. C. Neighbouring cells are connected through migration and colonisation. D. Genealogies are simulated given the number of individuals per cell and generation and the number of migrants per pairs of cells and generation. Mutations are generated on these genealogies and their effects on the sequences of each simulated sample is inferred.

5.4.2 Refitting the model

5.4.2.1 Rationale and comparison to previous versions

To make the existing model suitable for the study of selection, a few adjustments had to be made to the original framework[1,2]: we had to use a different dataset and an additional summary statistic during the fitting procedure. Given these changes, I needed to refit our model to acquire realistic demographic parameter sets.

Selection scans are generally based on a large number of whole genomes. However, in the previous model versions, only microsatellite[1] and SNP-based[2] panels were used, mostly with small sample sizes per population (down to a single representative diploid sample). To enable direct comparison between data and model output, I chose to use the 1000 Genomes Phase 3 dataset[13,14] instead, which includes whole-genome data from a high number of samples per population. Furthermore, this dataset has previously been used to study selection[15–17], and consists of populations covering most large geographic areas (with the exception of Oceania and Australia).

Furthermore, our initial investigations showed that although I acquired well-fitting values for F_{ST} and iHS using demographic parameters fitted through TMRCA values only[1,2], in that the model output was within the variation seen in data, I generally did not get realistic Tajima's D values. Although the general trend of increasing mean *D* values with distance from Africa was present to a similar extent in both observed data and our simulations, the mean values were higher in the former, with the exception of a subset of parameter values associated with stronger bottlenecks. Therefore, I supplemented the TMRCA-based summary statistics previously used to fit the model[1,2] with continental-level means of Tajima's D.

5.4.2.2 Statistics from the spatial simulation

The following summary statistics were calculated on the simulated data: average times to the most recent common ancestor (TMRCA) within and between populations, as well as Tajima's D for each population. To save computational time, TMRCA was calculated directly from the simulated genealogies, but it was also verified using the π-based estimator from section 1.4.1.2, applied on the generated sequences. The results from the π-based estimator were more noisy than those directly from genealogies, but converged to the same results given enough (more than ~1000) generated genealogies. All statistics were calculated in modules within the modelling framework coded in C++.

Average nucleotide diversity (π) and Tajima's D were calculated according to definition:

$$\langle\pi\rangle_{ab} = \frac{1}{2N_a(2N_b - \delta_{ab})} \sum_{i=1}^{2N_a} \sum_{j=1}^{2N_b} \pi_{ij}\,,$$

$$D_a = \frac{\langle\pi\rangle_{aa} - \frac{S_a}{a_1}}{\sqrt{e_1 S_a + e_2 S_a(S_a - 1)}},$$

Where $\langle\pi\rangle_{ab}$ is the average nucleotide difference between populations a and b, $2N_a$ and $2N_b$ are the number of haploid sequences in populations a and b, π_{ij} is the number of nucleotide differences between sequences i and j, S_a is the total number of polymorphisms in population a, and a_1, e_1 and e_2 are normalising factors calculated as follows:

$$e_1 = \frac{c_1}{a_1} \qquad e_2 = \frac{c_2}{a_1^2 + a_2}$$

$$c_1 = b_1 - \frac{1}{a_1} \quad c_2 = b_2 - \frac{n+2}{a_1 n} + \frac{a_2}{a_1^2}$$

$$b_1 = \frac{n+1}{3(n-1)} \quad b_2 = \frac{2(n^2 + n + 3)}{9n(n-1)}$$

$$a_1 = \sum_{i=1}^{n-1} \frac{1}{i} \qquad a_2 = \sum_{i=1}^{n-1} \frac{1}{i^2}$$

I then scaled π values by the mutation rate to obtain an estimate of TMRCA, as follows:

$$T_{ab} = \frac{\langle \pi \rangle_{ab}}{2\mu L},$$

where T_{ab} is the estimated TMRCA between populations *a* and *b*, μ is the mutation rate per nucleotide and time unit, *L* is the number of loci and $\langle \pi \rangle_{ab}$ is the average nucleotide difference between populations *a* and *b*.

I used a mutation rate of 1.276x10^{-8} per nucleotide per generation, which was calculated by counting the number of mutations in one generation in our 10k windows from [18]. This mutation rate was similar to the mean mutation rate over the whole genome (1.202 x10^{-8} per nucleotide per generation), as calculated in the same publication[18].

5.4.2.3 Statistics from the 1000 Genomes data

I estimated the summary statistics, Tajima's D and TMRCA, from the 1000 Genomes Phase 3 dataset[13,14]. I first downloaded vcf files of genotype data from all populations from the 1000 genomes data portal (ftp://ftp.1000genomes.ebi.ac.uk/vol1/ftp/release/20130502/) and then filtered both genetic positions and populations before extracting windows from which to calculate the statistics.

○ Filtering samples

I excluded populations of African origin that were sampled in the Americas (ASW and ACB), due to their mixed origin within Africa and the presence of European admixture in their genomes[13]. I also excluded the Finnish samples because they had an unusually high Tajima's D value compared to other European populations, likely because they are genetically isolated with severe bottlenecks in their history, experienced an unusually low amount of admixture and could have less internal structure than other, larger populations[19]. I also excluded highly admixed Native American populations (CLM, PUR and MXL), as seen on the ADMIXTURE analysis[13]. I kept the least admixed Native American population in the dataset, the Peruvians (PEL), but I only considered data with Native American ancestry on both chromosomes. Ancestry was inferred using RFMix in Martin et al. 2017[20], and the data was provided by Alicia Martin. I selected the 10,000 windows (for details, see "Filtering positions") in regions with the highest amount of Peruvian samples with purely Native American ancestry available, which increased the number of such samples available at all of our windows to 45. The selected populations, their size and their assignment to continental-level groupings are shown in Table 5.1.

Chapter 5 Behaviour of selection statistics in a spatially explicit, neutral demographic model

Table 5.1 Populations from the from the 1000 Genomes Phase 3 dataset[13,14] that were used to fit the model.

Population code	Population name	Superpopulation name	Number of samples	Longitude	Latitude
PEL	Peruvian	American	45*	-12.06	-77.02
GWD	Gambian	African	113	13.38	-16.33
MSL	Mende	African	85	8.52	-11.84
ESN	Esan	African	99	9.06	7.35
YRI	Yoruba	African	108	7.52	3.9
LWK	Luhya	African	99	0.6	34.78
TSI	Tuscan	European	107	43.52	11.33
IBS	Spanish	European	107	40.39	-3.7
GBR	British	European	91	51.61	0.1
CEU	CEPH	European	99	46.74	2.48
PJL	Punjabi	South Asian	96	31.54	74.35
ITU	Indian	South Asian	102	17.47	78.69
BEB	Bengali	South Asian	86	23.68	90.22
STU	Sri Lankan	South Asian	102	7.19	80.61
GIH	Gujarati	South Asian	103	23.26	71.06
CHS	Southern Han Chinese	East Asian	105	22.65	113.99
KHV	Kinh Vietnamese	East Asian	99	10.81	106.65
CDX	Dai Chinese	East Asian	93	22.01	100.81
CHB	Han Chinese	East Asian	103	40.09	116.24

*Restricted to samples with purely Native American ancestry in the selected 10,000 windows. The windows could come from a different set of Peruvian individuals for different windows.

○ Filtering positions

I excluded the following regions in the genome considered as problematic: regions with poor alignment quality, recombination hotspots, regions of poor mapping quality, duplications, regions under selection (genes and conserved elements), repetitive regions and positions with systematic sequencing errors. I applied the following filters from Kuhlwilm et al. 2016[21], provided by Ilan Gronau:

- filter_hotspot1000g: Recombination hotspots
- filter_Map20: Sites with poor mapping quality
- filter_rmsk20: Recent duplications
- filter_segDups: Recent segmental duplications
- filter_selection_10000_100: Gene exons together with the 1 kbp flanking regions in each direction and conserved non-coding sequences corresponding to PhastCons elements
- filter_simpleRepeat: Simple repeats
- filter_SysErrHCB and filter_SysErr: Positions with systematic sequencing errors

For more details, see Supplementary SI 8 in Kuhlwilm et al. 2016[21].

I then considered windows containing 10kb unfiltered sites with at most 30% of the sites missing. I did not impose a minimal separation between the windows, but my previous investigation on 1kb windows with/without 10kb separation showed no change in the resulting statistics. This procedure yielded in 12,662 windows.

Last, I pruned our windows to increase the number of available Peruvian individuals with purely Native American diploid ancestry tracts at all of our windows. At keeping the 10,000 windows with the highest number of available such tracts, I could acquire data from 45 individuals (down from the original 85 diploid samples). For each window, I choose 45 individuals at random out of those with Native American ancestry on both chromosomes, thus potentially using different sets of individuals for different windows. This procedure generated diploid individuals that were a mosaic of Native American tracts from different samples. I then treated these generated diploid individuals in the same way as the rest of our samples.

I also attempted to keep Mexican individuals, but I only managed to keep 18 of them out of the original 64, even with a strong pruning down to 5000 windows. Such a low number of windows resulted in an unequal distribution of windows across chromosomes, and reduced the number of available Peruvians down to 37. I thus decided to keep only the Peruvians in the final dataset. I also attempted to allow a mix of individuals within a single window, but the Native American ancestry tracts were long enough in comparison to our window size so that this would not have increased the number of retained samples.

○ Calculating statistics

I extracted the chosen 10,000 windows from the filtered population set, applied the above mentioned filters and considered only biallelic sites; using vcftools 0.1.15[22]. I then calculated counts of the two alleles per population and chromosome, also using vcftools 0.1.15[22]. For the Peruvians, I first created per-individual filters, including only those windows where that particular individual was chosen. I then used these allele counts to calculate average pairwise π within and between populations, as well as Tajima's D within populations, using custom scripts in Python based on their definitions (for the formulas, see Section 5.4.2.2).

In the final step, I calculated mean TMRCA-s and Tajima's D for our continental groups: Africa, Europe, Asia and America. I pooled South Asian and East Asian population, since their corresponding summary statistics were linearly dependent on each other. I chose a subset of the summary statistics for fitting the model, to exclude statistics linearly dependent on each other (Supplementary Figure D.1-7 in Appendix D.1). In particular, TMRCA within

Africa was determined by TMRCA between African and Europe and TMRCA-s between non-neighbouring continental groups were determined by neighbouring ones (Africa – Asia by Africa – Europe, Africa – America by Asia – America, etc.). Finally, the statistics I used were mean Tajima's D from all four continental groups, mean TMRCA from all groups except Africa and mean between-population TMRCA between neighbouring groups (Africa – Europe, Europe – Asia and Asia – America). The observed summary statistics are shown in Table 5.2.

Table 5.2 Observed summary statistics from the 1000 genomes data.

Summary statistic	Acronym	Value
Tajima's D within Africa	D_AF	-0.6195
Tajima's D within Europe	D_EU	-0.0974
Tajima's D within Asia	D_AS	-0.1433
Tajima's D within America	D_AM	0.5654
TMRCA between Africa and Europe	T_AF_EU [years]	57791.69
TMRCA within Europe	T_EU_EU [years]	43545.74
TMRCA between Europe and Asia	T_EU_AS [years]	51362.65
TMRCA within Asia	T_AS_AS [years]	44450.85
TMRCA between Asia and America	T_AS_AM [years]	48151.22
TMRCA within America	T_AM_AM [years]	34784.69

5.4.2.4 Fitting procedure

To fit the model, I sampled 100,000 input parameter sets, performed a single demographic run and simulated 200x10kb sequences along independent (non-recombining) genealogies for each. I first sampled the input parameters from wide prior distributions (Table 5.3) for the demographic input parameters and recorded TMRCA-s and Tajima's D at the population-level for all simulations. Due to problems with the resulting posterior distribution of parameters, I also sampled parameter sets from the central 99% of the posterior distributions of each parameter from Raghavan et al.[2] (Table 5.4), which was obtained through fitting to a panel of genomes more densely and homogeneously distributed across the globe but with a lower sample size per population, up to only 2 diploid genomes per population. This latter, narrow posterior is what I used for further investigations.

Table 5.3 Wide parameter ranges for ABC sampling. Generation time is assumed to be 25 years[1].

Parameter	Acronym	Low limit	High limit	Sampling
Simulation time [generation]	tSim	1000	8000	Linear
Migration rate [1/generation]	m	0.0001	0.166666	Logarithmic
Colonisation number	c	10.0	5000.0	Logarithmic
Growth rate [1/generation]	r	0.3	1.00	Logarithmic
Maximal carrying capacity	K	1000	100000	Logarithmic
Low NPP offset	npp_offs_low	0.001	0.1	Linear
High NPP offset	npp_offs_high	0.001	0.5	Linear
Ancestral carrying capacity	Ka	1000	100000	Logarithmic
Initial carrying capacity	K0	22000	30000	Logarithmic

Table 5.4 Narrow parameter ranges for ABC sampling. Generation time is assumed to be 25 years [1].

Parameter	Acronym	Low limit	High limit	Sampling
Simulation time [generation]	tSim	4677	8172	Linear
Migration rate [1/generation]	m	0.0000575	0.16666	Logarithmic
Colonisation number	c	33.60	1817.61	Logarithmic
Growth rate [1/generation]	r	0.370	1.000	Logarithmic
Maximal carrying capacity	K	872.57	14269.21	Logarithmic
Low NPP offset	npp_offs_low	0.0191	0.0388	Linear
High NPP offset	npp_offs_high	0.0134	0.0872	Linear
Ancestral carrying capacity	Ka	88.49	14167.72	Logarithmic
Initial carrying capacity	K0	17290.02	29737.19	Logarithmic

I filtered out simulations where any cell with a sampled population was empty. For these runs, I first calculated TMRCA-s directly from the genealogies and Tajima's D from the generated sequences and then used a custom Matlab script to aggregate population-level means into continental-level quantities, used as summary statistics. Finally, I used ABCestimator from ABC toolbox[23] to estimate posterior distributions for all inputs. I used the standard ABC-GLM estimator in the toolbox, standardizing all statistics prior to the estimation, retaining 200 simulations for the posterior estimation, using Dirac peaks with a width of 0.01 for smoothing the marginal posterior distribution and calculating the marginal posterior density on 200 points.

5.4.3 Overlap between different statistics

I used the neutral demographic model to investigate how different statistics behave when the confounding effects of space and population history are taken into account. I focused on a commonly used statistic from each group: allele frequency spectrum-based Tajima's D, population differentiation-based F_{ST} and linkage disequilibrium-based iHS. I measured the amount of overlap between different statistics and different populations and compared our estimates to the relevant quantities computed for neutral genomic windows from the 1000 Genomes Phase 3 dataset[13,14], in order to investigate which statistics suggest similar processes and to what extent purely demographic signals in different populations are correlated.

5.4.3.1 1000 Genomes data

For the 1000 genomes data, I used the same windows as used for fitting TMRCAs and Tajima's D. I estimated F_{ST} using vcftools 0.1.15[22], implementing Weir and Cockerham's estimator[24] and used Tajima's D as calculated when fitting the model.

To calculate iHS[7], I first estimated genetic distances in these windows. To acquire data for all our SNP-s, I linearly interpolated the genetic map generated by the HapMap 2 Project[25]. This map, which is an average over recombination rates in the CEU, YRI, and ASN populations, was lifted over to hg19 by Adam Auton and is available at ftp://ftp-trace.ncbi.nih.gov/1000genomes/ftp/technical/working/20110106_recombination_hotspots/. I then calculated iHS scores on the vcf-formatted data from the chosen populations and windows using selscan[26], a multi-threaded program capable of calculating linkage-based selection statistics efficiently. I finally calculated the proportion of significant ($|Z| > 2$) iHS scores in each 10kb-long window, as suggested by Voight et al.[7] and following Clemente et al.[11].

5.4.3.2 Simulation

I used our spatial model to generate data equivalent to the windows from the 1000 genomes data. To simulate recombining sequences needed for linkage disequilibrium-based statistics like iHS, I used a modified version of our spatial framework, which generated a network of recombining genealogies instead of separate trees. I generated sequences upon these networks, which could then be analysed in the same way as for the 1000 Genomes data. Generating such sequences is computationally expensive, therefore I used only the 5 best-fitting demographic parameter sets (Table 5.5). For each parameter set, I simulated five 4Mbp-long recombining sequences either with a constant or a variable recombination rate. In order to set recombination rates, I estimated the mean recombination rate in each 10kb window by summing the genetic distances within that window from the HapMap 2 Project[25], linearly interpolating the distance at the border of the windows, and scaled genetic distances back to recombination rates. I used the mean recombination rate over all 10kb windows, 0.7961 cM/Mbp, as our constant recombination rate.

Since a study found that the effect of a varying recombination rate was necessary to reach realistic levels of signal-sharing[27], I also generated equivalent data with a non-uniform recombination rate in our model. For this investigation, I chose a recombination rate uniformly at random for each simulated window from the 10,000 mean recombination rates from the windows used for fitting the model, calculated as detailed before.

Table 5.5 Parameters for the five best-fitting simulations

Parameter	1	2	3	4	5
Simulation time [generation]	5821	5533	7634	4840	6309
Migration rate [1/generation]	0.000160	0.000401	0.000104	0.001138	0.000162
Colonisation number	0.0267	0.0355	0.0254	0.0935	0.0851
Growth rate [1/generation]	0.3975	0.4976	0.5851	0.9964	0.3838
Maximal carrying capacity	13696.6	6747.3	14245.6	5348.1	12719.6
Low NPP offset	0.0252	0.0245	0.0293	0.0245	0.0253
High NPP offset	0.0290	0.0256	0.0351	0.0344	0.0399
Ancestral carrying capacity	1114.2	565.9	1318.7	174.3	457.5
Initial carrying capacity	26370.5	27397.3	26383.7	26731.6	26726.2

5.4.3.3 Calculating overlaps

Finally, I calculated the amount of overlap between pairs of statistics and populations focusing on one population per continental group: the Yoruba (YRI) for Africa, Utah residents (CEPH) with Northern and Western European ancestry (CEU) for Europe, the Han Chinese (CHB) for Asia and the Peruvians (PEL) for the Americas. In each case, I ordered the windows according to their significance and calculated the proportion of windows in the top X percent on one statistic which is included in the top Y percent of the other statistic; keeping Y fixed and varying X.

To compare the closeness of populations and the overlap between different populations using the same statistics, I calculated the mean F_{ST} values. For each pair out of the four chosen populations, I averaged F_{ST} values over all 10,000 windows. The resulting values are shown in Table 5.6.

Table 5.6 Average F_{ST}

	YRI	CEU	CHB	PEL
YRI		0.1322	0.1539	0.1765
CEU	0.1322		0.0971	0.1283
CHB	0.1539	0.0971		0.0974
PEL	0.1765	0.1283	0.0974	

5.5 Results

5.5.1 Refitting the model

First, I refitted our model to a curated version of the 1000 Genomes Phase 3 dataset[13,14]. When I fitted the simulated data to the observed quantities from the 1000 Genomes using a wide prior distribution (Table 5.3), I found that a proportion of the best fits came from unusually short simulations (Figure 5.2). These resulted in a rapid dispersal all across the globe, unrealistically uniform arrival times and hardly any effect of climate: even very low lower npp thresholds (npp_offs_low) were possible, meaning that areas with unfavourable climate were still habitable. This was not only contrary to the current consensus view of human evolution, but had also not been found in previous applications of the framework[1,2]. A possible reason to this discrepancy could be the sparse spatial distribution of the populations in the 1000 Genomes dataset, not providing enough information to distinguish between alternative dynamics on a fine geographic and temporal scale.

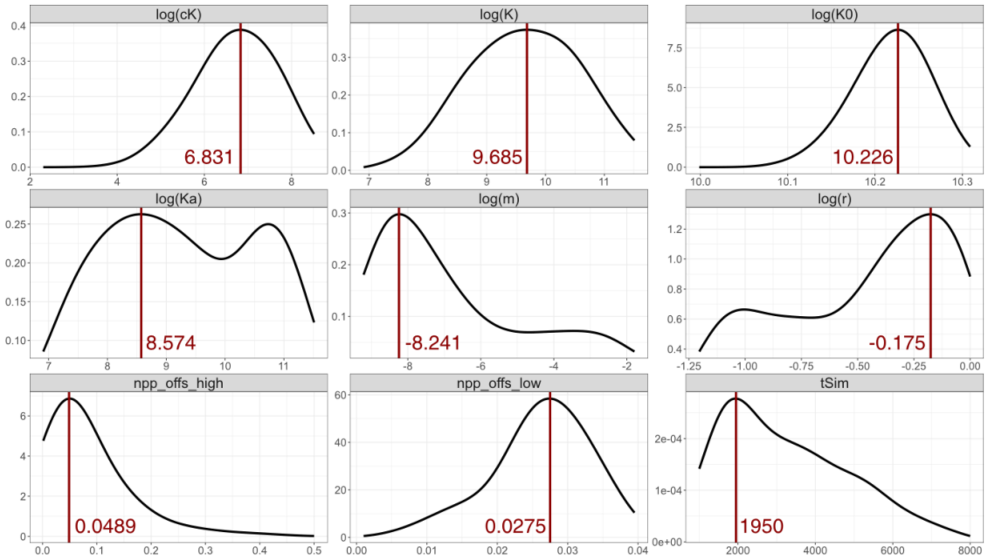

Figure 5.2 Posterior distributions of each parameter after fitting the model the original, wide priors (Table 5.3). Each panel shows the estimated posterior density as a function of parameter value for different demographic parameters. The x axis is on a log-scale for parameters with a logarithmic prior. The red vertical bars represent the median, with its value displayed..

When I used the narrow ranges for the prior distribution (Table 5.4), the posterior distributions of fitted demographic parameters were similar to those seen in previous applications of this modelling framework[1,2] (Figure 5.3). These parameters highlighted the effect of climate on population history by requiring a high lower npp threshold (npp_offs_low), which prevents humans from inhabiting areas with an unfavourable climate. Furthermore, I obtained values of TMRCA and Tajima’s D with these priors which were equally well-fitting to the data, but derived from globally feasible scenarios and only used realistic areas of the parameter space. Therefore, I used the parameter sets obtained from this second fit for the rest of my results.

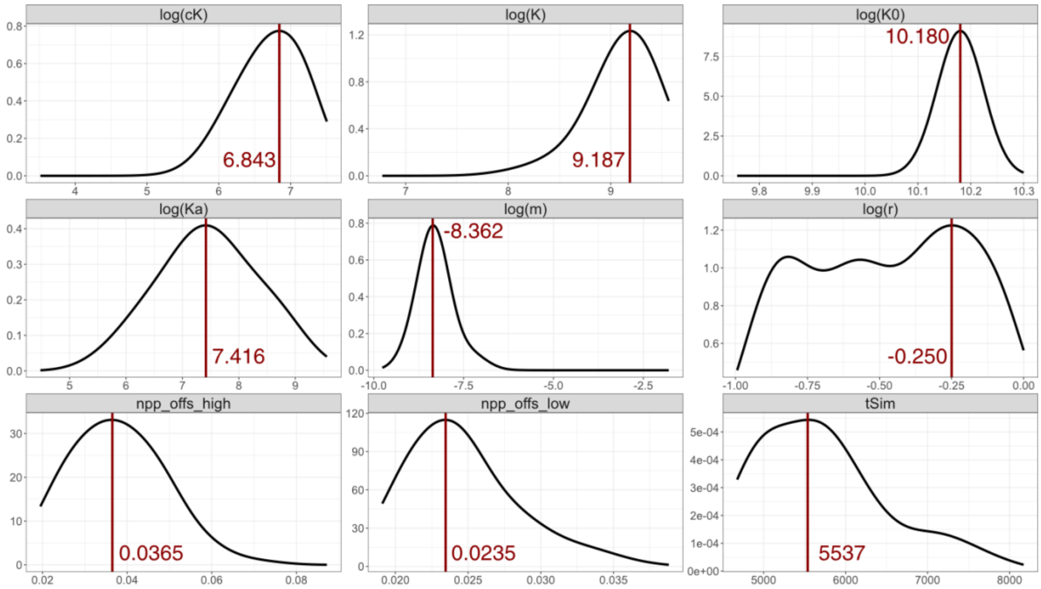

Figure 5.3 Posterior distributions of each parameter after fitting the model on priors in the central 95% interval of posteriors from Raghavan et al[2] (Table 5.4). Each panel shows the estimated posterior density as a function of parameter value for different demographic parameters. The x axis is on a log-scale for parameters with a logarithmic prior. The red vertical bars represent the median, with its value displayed..

5.5.2 Overlap between different statistics and populations

I then compared neutral windows from the 1000 Genomes Phase 3 dataset[13,14] with simulated recombining windows from our neutral model, with a constant or a varying recombination rate. The amount of overlap between different statistics was generally higher in the 1000 Genomes data than what our model produced, regardless of whether the recombination rate was fixed or variable (Figure 5.4 to Figure 5.7). This is in contrast with Pagani et al.[27], who obtained similar levels of between-statistic overlap from a simple demographic model to what was seen in the data, as long as recombination rate was not fixed. Potential causes for this difference are that our model struggles to capture severe bottlenecks and extinction-recolonisation events, or the effect of selection in the human genome even in regions flagged as “neutral”.

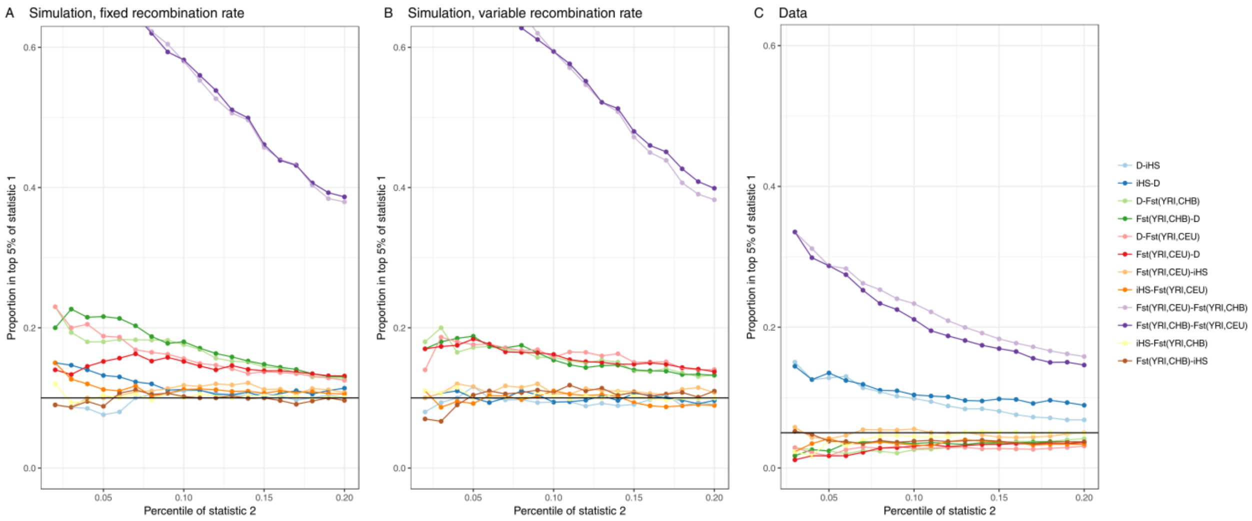

Figure 5.4 Overlap between different statistics for the Yoruba (YRI). First 5% of the windows that scored highest on statistic 1 were chosen. Then, a fixed percentile (x axis) of the windows that scored highest on statistic 2 was recorded. Finally, the amount of overlap was measured as the proportion of high-scoring windows from statistic 2 that were also in the top 5% windows on statistic 1. The legend displays the names of statistics 1 and 2, in that order. Black line marks 0.05, which is the expectation from purely random, independent statistics. A. Simulation with a fixed recombination rate. B. Simulation with a variable recombination rate. C. 10,000 selected neutral windows from the 1000 Genomes data.

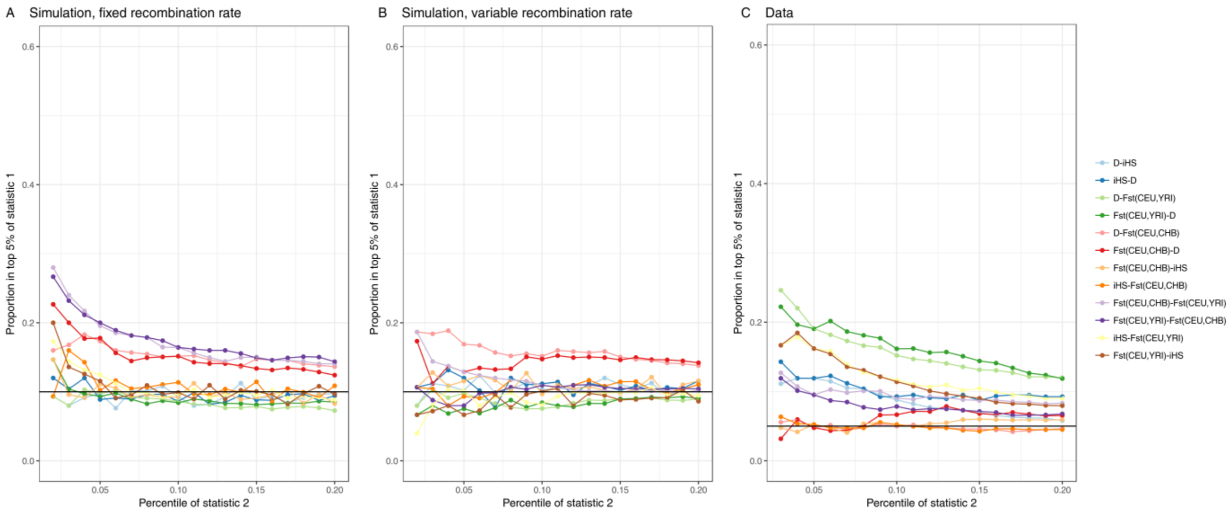

Figure 5.5 Overlap between different statistics for Utah residents of European ancestry (CEU). First 5% of the windows that scored highest on statistic 1 were chosen. Then, a fixed percentile (x axis) of the windows that scored highest on statistic 2 was recorded. Finally, the amount of overlap was measured as the proportion of high-scoring windows from statistic 2 that were also in the top 5% windows on statistic 1. The legend displays the names of statistics 1 and 2, in that order. Black line marks 0.05, which is the expectation from purely random, independent statistics. A. Simulation with a fixed recombination rate. B. Simulation with a variable recombination rate. C. 10,000 selected neutral windows in the 1000 genomes data.

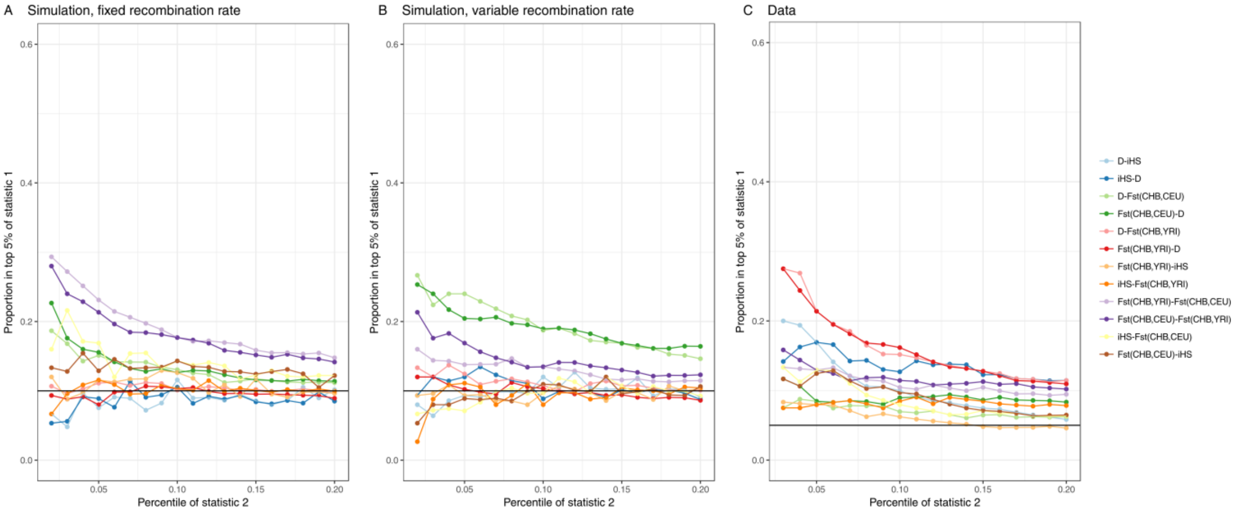

Figure 5.6 Overlap between different statistics for the Han Chinese (CHB). First 5% of the windows that scored highest on statistic 1 were chosen. Then, a fixed percentile (x axis) of the windows that scored highest on statistic 2 was recorded. Finally, the amount of overlap was measured as the proportion of high-scoring windows from statistic 2 that were also in the top 5% windows on statistic 1. The legend displays the names of statistics 1 and 2, in that order. A. Simulation with a fixed recombination rate. B. Simulation with a variable recombination rate. C. 10,000 selected neutral windows in the 1000 genomes data.

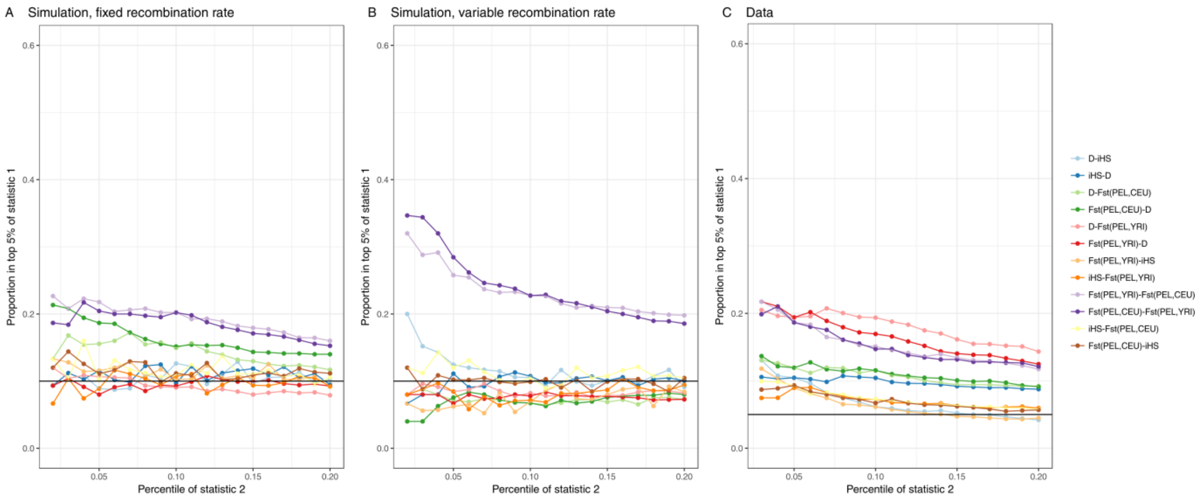

Figure 5.7 Overlap between different statistics for the Native American segments in Peruvians (PEL). First 5% of the windows that scored highest on statistic 1 were chosen. Then, a fixed percentile (x axis) of the windows that scored highest on statistic 2 was recorded. Finally, the amount of overlap was measured as the proportion of high-scoring windows from statistic 2 that were also in the top 5% windows on statistic 1. The legend displays the names of statistics 1 and 2, in that order. Black line marks 0.05, which is the expectation from purely random, independent statistics. A. Simulation with a fixed recombination rate. B. Simulation with a variable recombination rate. C. 10,000 selected neutral windows in the 1000 genomes data.

Regarding the amount of signal-sharing between different populations, the model could reproduce what is seen in the data for populations from the same continent on Tajima's D (Figure 5.8). The amount of overlaps from populations in different continents was slightly lower in the simulation than in the data. This could be because our model does not facilitate high levels of mixing between populations: it is based on hunter-gatherers and cannot capture the increase in mobility that started after the Neolithic transition and accelerated in modern times. An alternative explanation would be, if the parts of the human genome not flagged as under selection are still affected by natural selection (particularly background selection), for example through linkage to loci under selection[28] or due to their regulatory functions[29]. In this case, populations living far away from each other could be subject to different selection pressures, such as through background selection acting against continuously arising new alleles, which would decrease the amount of signals they share. For iHS, on the other hand, the amount of signal sharing was grossly underestimated in our model (Figure 5.9). I suspect that the unusual behaviour of iHS on the neutral windows could be due to the gaps between the windows: iHS is not suited for the study of short segments, but there are not enough long neutral segments in observed genomes to allow a realistic comparison with our simulations.

As expected, the amount of signal sharing was highly correlated to how close the populations were to each other genetically (Figure 5.10 and Figure 5.11): the highest amount of overlap was observed between Eurasian populations, followed by comparisons between neighbouring continents (Africa-Eurasia, America-Eurasia) and the lowest concordance was between populations from Africa and America.

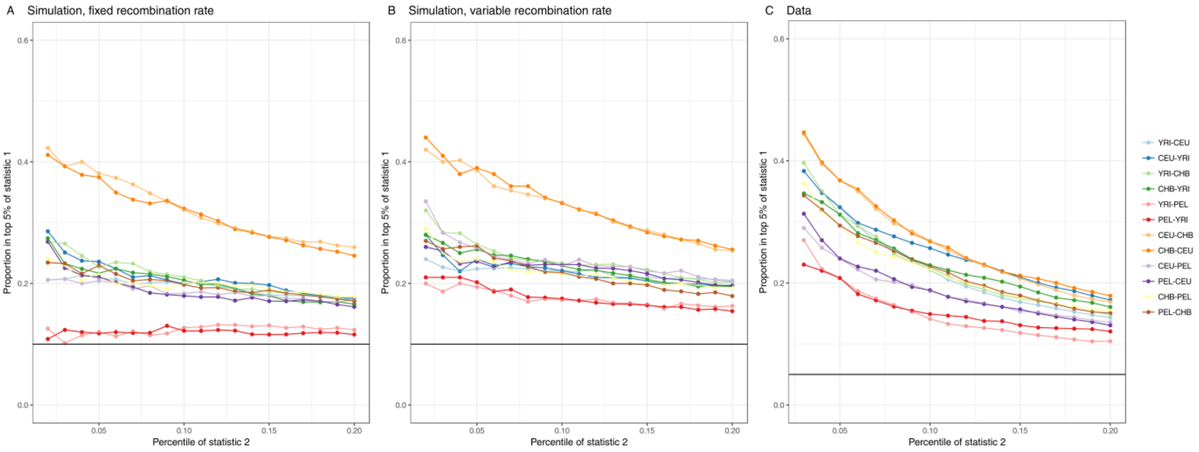

Figure 5.8 Overlap between pairs of populations in Tajima's D. First 5% of the windows that scored highest on Tajima's D from population 1 (statistic 1) were chosen. Then, a fixed percentile (x axis) of the windows that scored highest on Tajima's D from population 3 (statistic 3) was recorded. Finally, the amount of overlap was measured as the proportion of high-scoring windows from statistic 2 that were also in the top 5% windows on statistic 1. The legend displays the names of populations 1 and 2, in that order. Black line marks 0.05, which is the expectation from purely random, independent statistics. A. Simulation with a fixed recombination rate. B. Simulation with a variable recombination rate. C. 10,000 selected neutral windows in the 1000 genomes data.

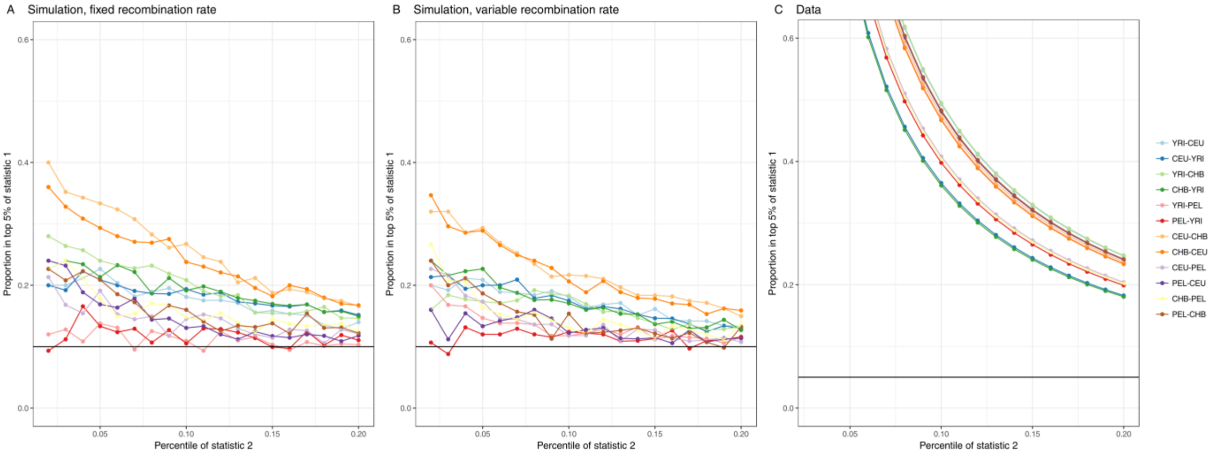

Figure 5.9 Overlap between pairs of populations in iHS. First 5% of the windows that scored highest on iHS from population 1 (statistic 1) were chosen. Then, a fixed percentile (x axis) of the windows that scored highest on iHS from population 3 (statistic 3) was recorded. Finally, the amount of overlap was measured as the proportion of high-scoring windows from statistic 2 that were also in the top 5% windows on statistic 1.The legend displays the names of populations 1 and 2, in that order. Black line marks 0.05, which is the expectation from purely random, independent statistics. A. Simulation with a fixed recombination rate. B. Simulation with a variable recombination rate. C. 10,000 selected neutral windows from the 1000 Genomes data.

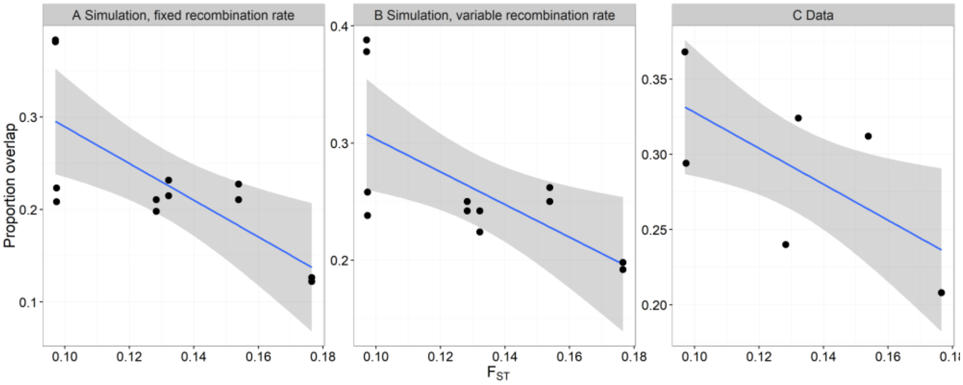

Figure 5.10 Relationship between population differentiation as measured by F_{ST} and the amount of overlap of Tajima’s D between different populations. The amount of overlap is measured by the proportion of windows in the top 5% for both populations, relative to the number of windows in the top 5% on one population. Each dot represents a pair out of the four modelled populations (YRI, CEU, CHB and PEL) and the blue line marks the result of a linear fit with the shaded area marking its 95% confidence interval, using the ggplot2 package in R[30]. A. Simulation with a fixed recombination rate. B. Simulation with a variable recombination rate. C. 10,000 selected neutral windows from the 1000 Genomes data.

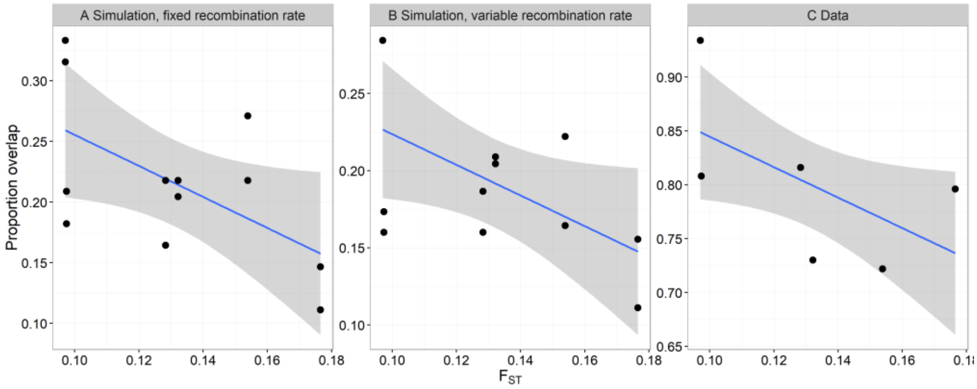

Figure 5.11 Relationship between population differentiation as measured by F_{ST} and the amount of overlap of iHS between different populations. The amount of overlap is measured by the proportion of windows in the top 5% for both populations, relative to the number of windows in the top 5% on one population. Each dot represents a pair out of the four modelled populations (YRI, CEU, CHB and PEL) and the blue line marks the result of a linear fit with the shaded area marking its 95% confidence interval, using the ggplot2 package in R[30]. A. Simulation with a fixed recombination rate. B. Simulation with a variable recombination rate. C. 10,000 selected neutral windows from the 1000 Genomes data

5.6 Discussion

We used a uniquely realistic, neutral demographic model and showed that it could produce selection statistics similar to what is seen in neutral parts of the genome. The advantages of this model derive from its mechanistic nature: assumptions are only made regarding the underlying demographic processes, such as isotropic migration and colonisation and linear population growth up to the carrying capacity. Furthermore, the resulting spatial reconstruction of human population history can be used to simulate genetic data for any chosen population. However, in addition to sufficient computational capacity, the model requires detailed geographical and climate data to infer the ecology and therefore the local carrying capacities. Furthermore, it only captures the effect of climate, but might miss other factors such as cultural or linguistic differences that could also influence population demography. Therefore, this model works best for events occurring during the early parts of the out-of-Africa expansion, rather than for recent processes such as the Neolithic expansion.

Even though our model could produce realistic selection statistics, we first had to adjust it to the statistics we aimed to reproduce. Some statistics, such as Tajima's D, were very sensitive to demographic parameters: without fitting the model accordingly, we could not obtain values similar to those observed. It was also difficult to capture fine-scale geographic patterns: using the only dataset available with large enough population sizes, the 1000 Genomes dataset, the signal was still not strong enough to distinguish populations from the same continent.

The quality of our fit could have been improved by using a larger dataset, or by combining multiple sources. Unfortunately the latter is particularly problematic, due to incompatibilities in the bioinformatics pipeline between different commonly used datasets. For example, the 1000 Genomes data was treated with a custom pipeline that does not allow for integration with other datasets. In the future, such datasets should be reanalysed using a standard pipeline and combined with different datasets that provide more spatial breadth in sampling, to compile a reference set with both a high spatial resolution and high enough samples sizes that allow scans for natural selection.

Finally, we found that the amount of signal sharing between different populations within the same continent was closely matched between observed and simulated data. However, the level of overlap between high-scoring regions for populations from different continents was lower in the data than in the simulation, which could be due to the high level of mixing in historical times. Signals from different statistics were shared to a lower extent in the simulation than in the data, which could point to either our model not capturing certain demographic events or that regions of the human genomes that are flagged as "neutral" are still affected by natural selection. The latter is also not unreasonable given that signals of purifying selection have been detected even in non-coding regions[31]. In this case, populations in different continents would be subject to different selection pressures, decreasing signal sharing, whereas different selection statistics in the same populations could pick up the same signal, thus increasing overlaps.

5.7 Bibliography

1. Eriksson, A. *et al.* Late Pleistocene climate change and the global expansion of anatomically modern humans. *Proc. Natl. Acad. Sci.* **109,** 16089–16094 (2012).

2. Raghavan, M. *et al.* Genomic evidence for the Pleistocene and recent population history of Native Americans. *Science* **349,** aab3884 (2015).

3. Vitti, J. J., Grossman, S. R. & Sabeti, P. C. Detecting Natural Selection in Genomic Data. *Annu. Rev. Genet.* **47,** 97–120 (2013).

4. Tajima, F. Statistical method for testing the neutral mutation hypothesis by DNA polymorphism. *Genetics* **123,** 585–595 (1989).

5. Fay, J. C. & Wu, C.-I. Hitchhiking Under Positive Darwinian Selection. *Genetics* **155,** 1405–1413 (2000).

6. Holsinger, K. E. & Weir, B. S. Genetics in geographically structured populations: defining, estimating and interpreting FST. *Nat. Rev. Genet.* **10,** 639–650 (2009).

7. Voight, B. F., Kudaravalli, S., Wen, X. & Pritchard, J. K. A Map of Recent Positive Selection in the Human Genome. *PLoS Biol* **4,** e72 (2006).

8. Ferrer-Admetlla, A., Liang, M., Korneliussen, T. & Nielsen, R. On Detecting Incomplete Soft or Hard Selective Sweeps Using Haplotype Structure. *Mol. Biol. Evol.* **31,** 1275–1291 (2014).

9. Sabeti, P. C. *et al.* Detecting recent positive selection in the human genome from haplotype structure. *Nature* **419,** 832–837 (2002).

10. Kim, Y. & Nielsen, R. Linkage Disequilibrium as a Signature of Selective Sweeps. *Genetics* **167,** 1513–1524 (2004).

11. Clemente, F. J. *et al.* A Selective Sweep on a Deleterious Mutation in CPT1A in Arctic Populations. *Am. J. Hum. Genet.* (2014). doi:10.1016/j.ajhg.2014.09.016

12. Sabeti, P. C. *et al.* Genome-wide detection and characterization of positive selection in human populations. *Nature* **449,** 913–918 (2007).

13. 1000 Genomes Project Consortium *et al.* A global reference for human genetic variation. *Nature* **526,** 68–74 (2015).

14. Sudmant, P. H. *et al.* An integrated map of structural variation in 2,504 human genomes. *Nature* **526,** 75–81 (2015).

15. Hider, J. L. *et al.* Exploring signatures of positive selection in pigmentation candidate genes in populations of East Asian ancestry. *BMC Evol. Biol.* **13,** 150 (2013).

16. Pybus, M. *et al.* 1000 Genomes Selection Browser 1.0: a genome browser dedicated to signatures of natural selection in modern humans. *Nucleic Acids Res.* **42,** D903–D909 (2014).

17. Nédélec, Y. *et al.* Genetic Ancestry and Natural Selection Drive Population Differences in Immune Responses to Pathogens. *Cell* **167,** 657–669.e21 (2016).

18. Kong, A. *et al.* Rate of de novo mutations and the importance of father's age to disease risk. *Nature* **488,** 471–475 (2012).

19. Arcos-Burgos, M. & Muenke, M. Genetics of population isolates. *Clin. Genet.* **61,** 233–247 (2002).

20. Martin, A. R. *et al.* Human Demographic History Impacts Genetic Risk Prediction across Diverse Populations. *Am. J. Hum. Genet.* **100,** 635–649 (2017).

21. Kuhlwilm, M. *et al.* Ancient gene flow from early modern humans into Eastern Neanderthals. *Nature* **530,** 429–433 (2016).

22. Danecek, P. *et al.* The variant call format and VCFtools. *Bioinformatics* **27,** 2156–2158 (2011).

23. Wegmann, D., Leuenberger, C., Neuenschwander, S. & Excoffier, L. ABCtoolbox: a versatile toolkit for approximate Bayesian computations. *BMC Bioinformatics* **11,** 116 (2010).

24. Weir B. S. & Cockerham C. Clark. Estimating f-statistics for the analysis of population structure. *Evolution* **38,** 1358–1370 (2017).

25. The International HapMap Consortium. A second generation human haplotype map of over 3.1 million SNPs. *Nature* **449,** 851 (2007).

26. Szpiech, Z. A. & Hernandez, R. D. selscan: An Efficient Multithreaded Program to Perform EHH-Based Scans for Positive Selection. *Mol. Biol. Evol.* **31,** 2824–2827 (2014).

27. Pagani, L. *et al.* Genomic analyses inform on migration events during the peopling of Eurasia. *Nature* **538,** 238–242 (2016).

28. Lohmueller, K. E. *et al.* Natural Selection Affects Multiple Aspects of Genetic Variation at Putatively Neutral Sites across the Human Genome. *PLOS Genet.* **7,** e1002326 (2011).

29. Dermitzakis, E. T., Reymond, A. & Antonarakis, S. E. Conserved non-genic sequences — an unexpected feature of mammalian genomes. *Nat. Rev. Genet.* **6,** 151–157 (2005).

30. Wickham, H. *ggplot2: Elegant Graphics for Data Analysis*. (Springer-Verlag New York, 2009).

31. Miller, W., Makova, K. D., Nekrutenko, A. & Hardison, R. C. Comparative Genomics. *Annu. Rev. Genomics Hum. Genet.* **5,** 15–56 (2004).

Chapter 6 Explaining spatial patterns of adaptation against malaria

6.1 Abstract

Malaria is a widespread disease that placed one of the highest selective pressures on the human genome over the last 5-10 ky. Numerous alleles provide a level of genetic resistance, most of which are associated with blood disorders and thus lead to an evolutionary trade-off. These alleles have different spatial distributions, some global and some present only in certain populations, with disjoint or overlapping distributions between different variants of the same genetic disorder, and the reason for these dissimilarities is not well understood. I use a spatially explicit, climate-conditioned demographic framework and an empirical map of malaria presence to study the dynamics of variants offering genetic resistance against the disease. I aim to infer the likely origins of the different variants and to determine which factors are necessary to explain the main characteristics of their spatial distribution. I find that our framework is incompatible with a single origin for sickle-cell disease and that it can reproduce the spatial distribution of variants for sickle-cell disease (disjoint ranges) but not for β^0 thalassemia (overlapping pattern). The ability to recover the observed distribution for sickle-cell variants show the power of a spatially explicit framework, but the incompatibilities with thalassemia highlight the importance of additional mechanisms not represented in our model, such as long-distance and/or large-scale migrations and differences in the time of appearance of different variants and selection pressures.

6.2 Contribution

I conducted the analysis and wrote the manuscript for this chapter, with the exception of the following two points. The map for the spatial distribution of malaria endemicity was digitalised by Michela Leonardi and the base of the demographic model was created by Anders Eriksson (for the description and contributions to the model, see Chapter 5).

6.3 Introduction

6.3.1 Malaria and protective genetic disorders

Malaria is linked to one of the strongest selection pressures in the population history of anatomically modern humans and multiple alleles are associated with a protective effect against it. Due to this strong environmental connection, malaria also lead to one of the earliest hypothesis about the relationship between an infection and a genetic disease, proposed by Haldane in 1948[1,2]. Protective alleles most commonly affect the hemoglobin or other molecules that are essential for red blood cell function and are associated with a negative effect on fitness in malaria-free regions through the corresponding blood disorders. Balancing selection maintains these alleles despite their deleterious effect and they appear at high frequencies in regions where malaria is endemic[3]. The selection pressure associated with malaria is thought to be recent (last 5-10k years or less)[3,4] and linked to the lifestyle changes and increased population density following the Neolithic transition.

Sickle cell disease (β^S) and the severe form of β·thalassemia, β^0 thalassemia, are two particularly well-studied, classical examples of genetic disorders that increase resistance to malaria. In the heterozygous form, these alleles offer a protective effect against malaria with hardly any negative effects, whereas homozygote mutants suffer from the associated severe blood disorders. In the absence of early diagnosis and treatment, these disorders generally lead to death within the first few years of life. Both sickle cell disease and β^0 thalassemia are inherited through a set of different haplotypes, i.e. a set of genetic alleles, including the variant under selection, that are located on the same chromosome within close proximity and are inherited together. Sickle-cell disease is caused by a single mutation (HBB c. 20 A → T; p. Glu6-Val) and is associated with five "classical" restriction fragment length polymorphism haplotypes[5,6] named Bantu, Benin, Arab-Indian, Senegal and Cameroon haplotypes after the areas where they were first discovered. β^0 thalassemia, on the other hand, can be caused by any mutation that completely eliminates protein production from the β-globin gene. As a result, there are many more β^0 thalassemia variants than sickle-cell disease variants: 163 different mutations are reported (as queried from http://globin.bx.psu.edu/cgi-bin/hbvar/query_vars3 on 22 April 2018), and many of them can appear on multiple haplotypes.

6.3.2 Variants of protective disorders

The origins of the different variants are still not well-understood, even though this is a crucial piece of information for modelling studies. Most variants offering resistance to malaria are thought to be the result of recent mutations that arose at most 5-10k years ago[3]. For sickle-cell disease, the five "classical" haplotypes were traditionally thought to be the result of independent mutations[5]. However, a recent study by Shriner & Rotimi[7], based on the analysis of whole-genome sequence data and a systematic identification of haplotypes, points to a single origin roughly 259 generations ago (~6,5ky ago using a generation time of 25 years). This would then be followed by a spatial expansion and diversification and finally an increase in frequency due to the appearance of the strong malaria-related selection pressure. The authors inferred that the single original mutation arose in West or Central Africa 395-123 generations ago, possibly linked to the last Green Sahara phase in the middle of the Holocene Wet Phase that lasted from 9,500-9,000 years ago until 5,500-5,000 years ago.

Different causal mutations for the β^0 haplotypes, on the other hand, are clearly independent, but different haplotypes with the same causal mutation are thought to be the result of gene conversion[8]. Since gene conversion is not represented in our framework, we modelled haplotypes as variants for sickle-cell disease, but different causal mutations, regardless of the haplotype background, as variants for β^0 thalassemia.

The spatial distributions of different variants for these two disorders are remarkably different. Neither of them is present globally, but both have a wide distribution: sickle-cell disease is prevalent all over Africa, the Near East and in India, and β^0 thalassemia is found throughout Eurasia[9]. The five "classical" sickle-cell haplotypes have largely disjoint spatial distributions[10] (Table 6.2 and Figure 6.1), but β^0 thalassemia shows an overlapping distribution, with multiple variants present in any studied region[10] (Table 6.4, Table 6.5 and Figure 6.2). Previous modelling work using a homogeneous metapopulation model inferred that the prerequisites of a disjoint, sickle cell-like pattern were high population subdivision, low migration rate and the absence of long-distance migration, whereas the opposite was true for overlapping, thalassemia-like patterns.

6.3.3 Aim of this study

In this chapter, I explore whether a discrete-time, spatially explicit model can explain these two contrasting patterns. I aim to answer three questions: where different variants of the same disorder originated from, whether our model can produce realistic variant distributions (both disjoint sickle-cell-like and overlapping thalassemia-like patterns) and if a single origin for sickle-cell disease is plausible even in the absence of long-distance migrations.

6.4 Methods

6.4.1 Model

6.4.1.1 Base model

The model in this chapter is based on the climate-informed, spatially explicit framework introduced in Chapter 5. Only its demographic module was used, but with multiple layers of populations to represent the different genetic variants. In the original model, the demographic processes were fitted using genetic data (SNP-data) to produce a realistic structure of genetic diversity[11,12], and thus population subdivision and migration rates were constant. The spatial structure of populations was explicitly taken into account, but long-distance migrations were not included.

For the main results, I used the best-fitting parameter set from Raghavan et al[12] (Table 6.1). These parameters were fitted using world-wide genetic data and represent the demographic parameters suitable to describe human populations in general. The hexagon where the whole human population originated from was still the same as in Chapter 5, located at -9.23° latitude and 33.25° longitude. For a sensitivity analysis on parameters that were pre-defined using previous results (selection coefficient, demographic parameters and the starting time of selection), see Appendix E.2.

Table 6.1 Three best-fitting parameter sets from Raghavan et al[12], used for the main results.

Parameter	**1**	**2**	**3**
Simulation time [generation]	6263	6978	5121
Migration rate [1/generation]	0.00512	0. 001628	0.00144
Colonisation number	0.00973	0.02820	0.0254
Growth rate [1/generation]	0.82870	0.60289	0.81939
Maximal carrying capacity	8952.78	4300.57	6557.33
Low NPP offset	0.02305	0.02442	0.03144
High NPP offset	0.02456	0.02504	0.03338
Ancestral carrying capacity	2587.71	1666.55	1782.3

6.4.1.2 Selection in the framework

In the new version of the model, each cell could potentially be the home to individuals from multiple layers, representing different alleles. Migration was possible between neighbouring populations in the same layer, or between different layers in the same cell. For the purpose of this study, migration was only modelled within layers: conversion (mutation) between different, pre-defined genetic variants was not allowed. The population was initially monomorphic for the ancestral allele and the malaria-related alleles all appeared at the same, pre-defined time and were characterised by the same selection-related parameters.

I implemented selection in the framework as a Moran process, with the overall population dynamics (growth, migration and colonisation) independent of selection. These processes followed the same rules as in the original model described in Chapter 5, but the number of individuals affected was calculated based on the total number of individuals in the cell, and then re-distributed between variants to represent natural selection. Homozygote mutants were modelled as deleterious, while heterozygotes had an advantage in malarious regions (selection coefficient, $s \approx 0.152$[3]) and were neutral otherwise.

The implemented steps in each generation were therefore as follows, in order of execution:

1. Count the total number of individuals per cell.
2. Apply the same rules as in the original model (Chapter 5) to the total number of individuals per cell to determine the new population sizes and the number of colonists and exchanged migrants.
3. Re-distribute the number of individuals per layer (including colonists) to represent the effect of diploid natural selection with deleterious homozygote mutants:

$$p_i' = \frac{p_i\left(1 - \sum_j p_j\right) w_i}{\left(1 - \sum_j p_j\right)^2 w_0 + \ 2 \sum_j p_j \left(1 - \sum_k p_k\right) w_j},$$

   where p_i is the frequency of variant *i* at the previous generation, p_i' is the frequency of variant *i* at the current (new) generation, w_i is the fitness of variant *i* and the ancestral variant is indexed 0.

4. Distribute the number of migrants such that the ratio of the different variants is the same as that in the source node at the current (new) generation.

The selection coefficient w_i was the same for all variants (ancestral and derived) in areas where malaria is not present and 0.868 for the ancestral allele and 1.0 for all derived alleles in malarious areas[3]. However, our model was not sensitive to its exact value (see Appendix E.2.1 for sensitivity analysis).

I modelled the variants only after the "turn-on" of malaria-related selection pressure when I studied the dynamics of multiple sickle-cell haplotypes and thalassemia variants, which means that their origin represented the centre of their area of presence at that time. Therefore, variants were modelled in the same way regardless of whether they were the result of diversification after a common origin (sickle-cell trait) or independent mutations (β^0

thalassemia). For sickle-cell disease, this corresponds to a soft sweep, where the alleles on different haplotype backgrounds are part of standing variation. For all of our analysis on multiple variants, a selection turn-on time of 200 generations (5000 years) ago was imposed, roughly coinciding with the beginning of the migrations of Bantu-speaking populations[3] (for a sensitivity analysis, see Appendix E.2.3).

6.4.2 Data

6.4.2.1 Malaria distribution

To represent the range of malaria, we used a pre-control map of malaria endemicity that was previously used to confirm the malaria hypothesis for the sickle-cell trait[13]. This map is based on a review from the 1960s by a team of Russian researchers who synthesised historical records, documents and maps of several malariometric indices used to record malaria endemicity[14]. Combined with expert opinion and data on temperature and rainfall, a unique global map of the pre-control distribution of malaria could then be reconstructed at the peak of its hypothesized distribution[15]. This map was digitalised using Figure 1C in Piel et al.[13] by Michela Leonardi, which was then converted to a Boolean presence-absence mask for the cells of our model, based on the hypoendemic regions of the map.

6.4.2.2 Variant distributions

To examine the distribution of variants, I used country-level data assembled from multiple sources by Hockham et al[10]. For countries with multiple data sources available, I used the mean of the proportions from all sources. The data for sickle-cell disease in Saudi Arabia showed a conflicting picture, one study showing an overwhelming majority of the Benin haplotype, and the other the same for the Arab-Indian haplotype. The cause of this inconsistency in Saudi Arabia is probably due to its large spatial extent that allows different modal (most common) sickle-cell haplotypes in different areas[16,17]: Benin in the west and Arab-Indian in the east. However, there was no available data on the exact boundary between these regions or on the spatial origin of the ancestors of the individuals from these studies and we also had data available from another country on the Arabian Peninsula (Kuwait), so we did not use Saudi Arabia for our error estimates. Furthermore, we pooled all Italian studies (two from Sardinia and one from Sicily), since our coarse spatial resolution is not capable of representing such small scales accurately.

Due to computational limitations, I only considered the ancestral variant and those that reached a frequency of at least 25% in at least one country in the assembled country-level frequency data in Hockham et al.[10]. This resulted in four haplotypes for sickle-cell disease (Bantu, Benin, Arab-Indian and Senegal) and three mutations for β^0 thalassemia (Cd39, IVS-I-1 and FSC-6). I then scaled the proportions of these variants to amount to unity.

The original data for all variants is shown in Table 6.2 and Figure 6.1 (sickle-cell disease) and Table 6.4, Table 6.5 and Figure 6.2 (β^0 thalassemia), while the resulting proportions of modelled variants are in Table 6.3 (sickle-cell disease) and Table 6.6 (β^0 thalassemia).

Table 6.2 Distribution of sickle-cell haplotypes in different geographical regions. Adapted from Table 1 in Hockham et al[10].

Country	Arab-Indian	Benin	Cameroon	Bantu	Senegal	Other	Reference
Angola	-	12.00%	-	88.00%	-	-	Flint et al., 1998[18]
Benin	-	100.00%	-	-	-	-	Gabriel and Przybylski, 2010[19]
Burkina Faso	-	100.00%	-	-	-	-	Gabriel and Przybylski, 2010[19]
Cameroon	-	83.70%	16.30%	-	-	-	Flint et al., 1998[18]
Central African Republic	-	6.90%	3.40%	82.80%	3.40%	3.50%	Flint et al., 1998[18]
Kenya	-	1.30%	-	98.20%	0.00%	0.50%	Flint et al., 1998[18]
Nigeria	-	92.90%	3.40%	0.70%	0.90%	2.10%	Flint et al., 1998[18]
Senegal	-	14.00%	-	1.80%	80.70%	3.50%	Flint et al., 1998[18]
Tanzania, United Republic of	-	-	-	100.00%	-	-	Flint et al., 1998[18]
Togo	-	100.00%	-	-	-	-	Gabriel and Przybylski, 2010[19]
Algeria	-	100.00%	-	-	-	-	Flint et al., 1998[18]
Egypt	-	100.00%	-	-	-	-	Gabriel and Przybylski, 2010[19]
Morocco	-	100.00%	-	-	-	-	Flint et al., 1998[18]
Saudi Arabia	1.50%	98.50%	-	-	-	-	el-Hazmi et al., 1999[17]
Saudi Arabia	94.00%	0.00%	-	4.00%	-	2.00%	Kulozik et al., 1986[16]
Kuwait	77.80%	16.70%	-	-	-	5.50%	Adekile et al., 1994[20]
Syrian Arab Republic	-	100.00%	-	-	-	0.00%	Flint et al., 1998[18]
Tunisia	-	94.80%	-	-	-	5.20%	Flint et al., 1998[18]
Turkey	0.40%	96.30%	-	-	-	3.30%	Flint et al., 1998[18]
Turkey	-	100.00%	-	-	-	-	Gabriel and Przybylski, 2010[19]
India	100.00%	-	-	-	-	-	Gabriel and Przybylski, 2010[19]
India	90.70%	-	-	-	-	9.30%	Labie et al., 1989[21]
India	98.45%	-	1.55%	-	-	-	Oner et al., 1992[22]
India	91.67%	-	2.78%	1.39%	-	4.17%	Niranjan et al., 1999[23]

Table 6.3 Proportion of variants used for fitting sickle-cell disease from Hockham et al. [10]. The proportion of modelled variants is the ratio of derived mutants in the original data source that came from a modelled variant, while the rest of the percentages refer to the ratio of samples in a variant relative to the number in modelled variants.

Country	Proportion in modelled variants	Saudi	Benin	Bantu	Senegal
Angola	100.0%	0.0%	12.0%	88.0%	0.0%
Benin	100.0%	0.0%	100.0%	0.0%	0.0%
Burkina Faso	100.0%	0.0%	100.0%	0.0%	0.0%
Cameroon	83.7%	0.0%	100.0%	0.0%	0.0%
Central African Republic	93.1%	0.0%	7.4%	88.9%	3.7%
Kenya	99.5%	0.0%	1.3%	98.7%	0.0%
Nigeria	94.5%	0.0%	98.3%	0.7%	1.0%
Senegal	96.5%	0.0%	14.5%	1.9%	83.6%
Tanzania	100.0%	0.0%	0.0%	100.0%	0.0%
Togo	100.0%	0.0%	100.0%	0.0%	0.0%
Algeria	100.0%	0.0%	100.0%	0.0%	0.0%
Egypt	100.0%	0.0%	100.0%	0.0%	0.0%
Morocco	100.0%	0.0%	100.0%	0.0%	0.0%
Kuwait	94.5%	82.3%	17.7%	0.0%	0.0%
Bahrain	97.5%	92.3%	2.6%	5.1%	0.0%
Syria	100.0%	0.0%	100.0%	0.0%	0.0%
Tunisia	94.8%	0.0%	100.0%	0.0%	0.0%
Turkey	98.4%	0.2%	99.8%	0.0%	0.0%
India	95.6%	99.6%	0.0%	0.4%	0.0%

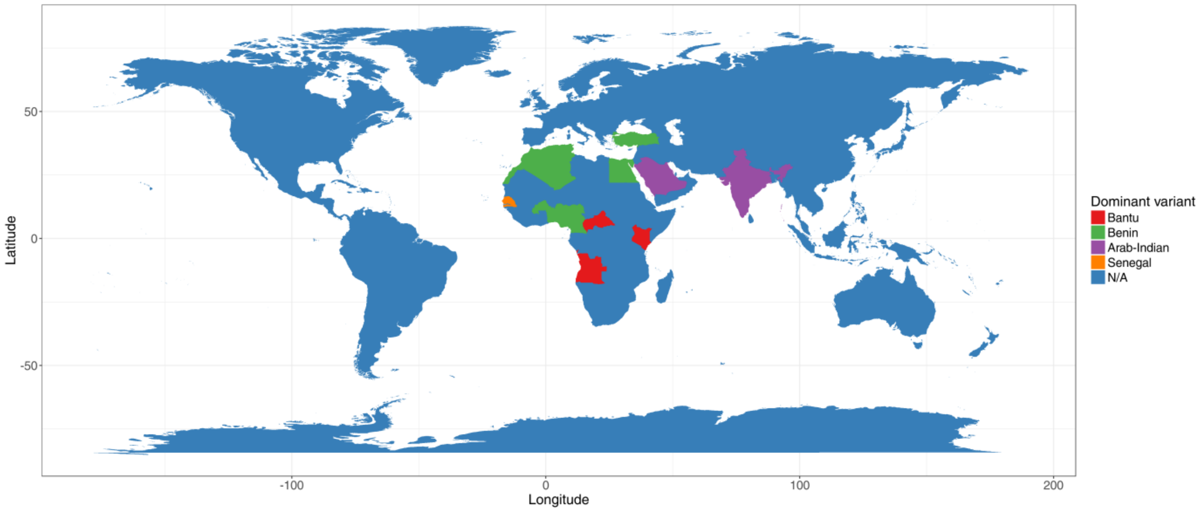

Figure 6.1 Most common sickle-cell variant out of modelled variants in countries with data available, as collected by Hockham et al[10]. For numerical data, see Table 6.3.

Table 6.4 Distribution of β^0 thalassemia variants in North Africa and the Middle East. Adapted from Table 2 in Hockham et al. Haplotype definitions are given in Antonarakis et al[24].

	Cd37 (G->A)	Cd39 (C->T)	IVS-I-1 (G->A)	IVS-I-2 (T->C)	IVS2-1 (G->A)	FSC-8 (-AA)	FSC-6 (-A)	IVS-I-2 (T->G)	Other	Reference
Algeria	-	44.59%	18.91%	5.40%	-	-	27.70%	-	3.37%	Bennani et al., 1994[25]
Algeria	-	50.00%	11.90%	19.05%	-	-	16.67%	-	2.38%	Bouhass et al., 1994[26]
Morocco	4.67%	39.26%	7.48%	7.48%	3.74%	20.56%	8.41%	4.67%	3.74%	Agouti et al., 2008[27]
Morocco	3.51%	24.56%	21.05%	5.26%	1.75%	24.56%	15.79%	0.78%	3.51%	Lemsaddek et al., 2003[28]
Morocco	1.55%	37.98%	12.40%	3.10%	-	13.95%	19.38%	3.45%	10.85%	Lemsaddek et al., 2004[29]
Tunisia	-	62.07%	-	-	-	3.45%	3.45%	3.45%	27.59%	Fattoum et al., 1991[30]

Table 6.5 Distribution of β^0 thalassemia in Europe. Adapted from Table 2 in Hockham et al. Haplotype definitions are given in Antonarakis et al[24].

	Cd39 (C->T)	IVS-I-1 (G->A)	IVS-I-2 (T->C)	IVS2-1 (G->A)	Cd6 (-A)	Other	Reference
Albania	65.00%	15.00%	-	5.00%	-	15.00%	Boletini et al., 1994[31]
Greece	50.86%	39.66%	-	6.03%	-	3.45%	Boletini et al., 1994[31]
Macedonia	21.43%	59.52%	-	7.14%	-	11.90%	Boletini et al., 1994[31]
Sardinia	97.80%	0.04%	-	0.04%	2.13%	-	Cao et al., 1991[32]
Sicily	79.35%	20.65%	-	-	-	-	Schiliro et al., 1997[33]
Sicily	71.92%	18.72%	3.45%	3.94%	1.23%	0.74%	Schiliro et al., 1995[34]

Table 6.6 Proportion of variants used for fitting thalassemia from Hockham et al.[10]. The proportion of modelled variants is the ratio of derived mutants in the original data source that came from a modelled variant, while the rest of the percentages refer to the ratio of samples in a variant relative to the number in modelled variants

Country	Proportion in modelled variants	Cd39_C_T	IVS-I-1_G_A	FSC-6_-A
Algeria	62.7%	75.5%	24.5%	35.3%
Morocco	67.3%	50.8%	20.1%	21.7%
Tunisia	65.5%	94.7%	0.0%	5.3%
Albania	80.0%	81.3%	18.8%	0.0%
Greece	90.5%	56.2%	43.8%	0.0%
Macedonia	81.0%	26.5%	73.5%	0.0%
Italy	97.3%	85.2%	13.7%	0.0%

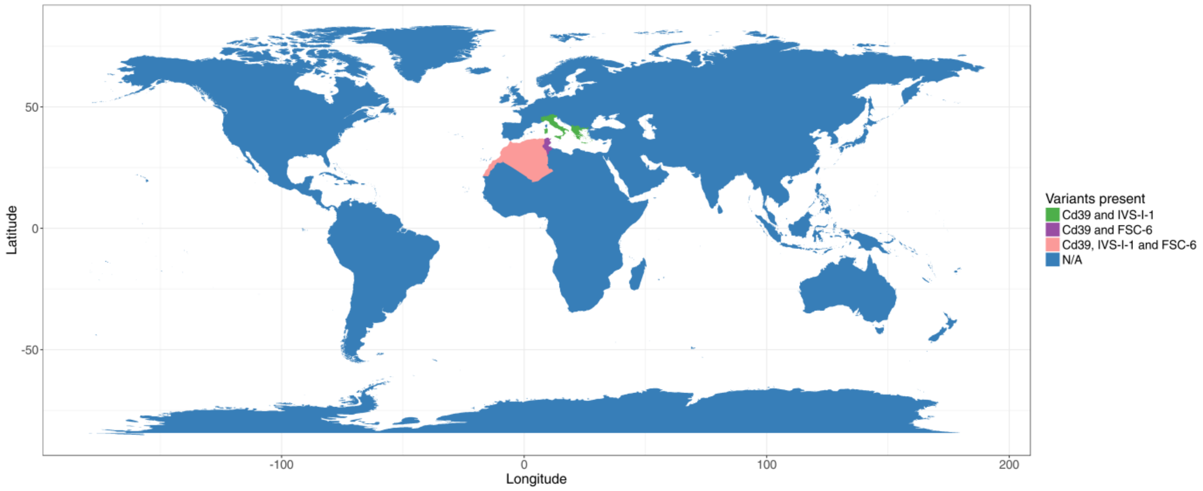

Figure 6.2 Thalassemia variants present out of those modelled in countries with data available, as collected by Hockham et al[10]. For numerical data, see Table 6.6.

6.4.3 Inferring haplotype origins

6.4.3.1 Sampling origins

To find the most likely geographic origin of variants, I ran the model with five layers for sickle-cell disease (ancestral allele and Bantu, Benin, Senegal and India-Arab haplotypes) and with four layers for thalassemia (ancestral allele and Cd39, IVS-I-1 and FSC-6 variants). I sampled 2500 sets of random origins for sickle-cell disease and 3500 for thalassemia, chosen uniformly at random out of those possible for each variant (the choice of possible origins is detailed below). After running the simulation, I recorded the count of each variant at the final time-step for all countries present in our data and calculated error terms as detailed in Section 6.4.3.3.

6.4.3.2 Possible origins

For sickle-cell disease, I chose the possible origins per variant according to the following procedure:

1. Determine the cells belonging to countries where the variant is the most common one.
2. Add a 10-cell buffer around this region
3. Assign cells between -25 and 110 in longitude and -40 and 55 in latitude that are not yet in the set of possible origins to the haplotype with the closest already assigned cell

The only country with available data where the Senegal haplotype was most common was Senegal, but initial runs pointed to areas north of Senegal to also be plausible origins. We therefore included Western Sahara as an additional core country for the Senegal haplotype.

Since the dominance of haplotypes for thalassemia was not well-defined, we adapted a different procedure, considering all cells lying between -25 and 60 in longitude and 15 and 60 in latitude and choosing the three origins for the derived haplotypes independently and uniformly at random out of these. This sampling region contained most of Europe, North

Africa and the Middle East and therefore also all countries with data that we considered. We focused only on Europe and North Africa, because of the large spatial gap to the other available regions (India and the Maldives). When calculating the error function, all possible permutations of the assignment of modelled variants to the three observed variants were considered.

6.4.3.3 Error function

For sickle-cell disease, a mean squared error-based error function was used. I first calculated the mean of squared errors between the proportion of different haplotypes from the simulation and the data over all countries per haplotype and then calculated the mean of the haplotype-specific errors, which served as my error term for that particular simulation.

For thalassemia, this error function generally lead to a very good fit to the two common variants, Cd39 and IVS-I-1, at the cost of the complete absence of the rare FSC-6 (Appendix E.1), probably because its absence was not penalised enough due to its low frequencies in the observed data. However, the characteristic of the distribution that we aimed to capture was the presence of multiple variants. I therefore decided to use a different error function, commonly used for multi-class classification: the count of the number of variants with mismatching presence-absence values between the data and simulation.

6.4.4 Single-origin hypothesis of sickle-cell disease

I only modelled the ancestral variant and a single derived allele in the study of the single-origin hypothesis of sickle-cell disease. I considered three appearance times: the estimated age by Shriner & Rotimi[7] (259 generations), as well as the bottom and the top of its 95% confidence interval (123 and 395 generations). They deem starting points in East to Central Africa possible, and mention the Green Sahara as their primary hypothesis and the equatorial rainforest as an alternative. Therefore, I also examined two starting points: one in the eastern part of this region, in the Green Sahara (longitude 2°, latitude 20°) and one in Central Africa in the equatorial rainforest (longitude 22°, latitude 12°), as close to the centre of the present-day range as possible.

For the main results, I present two settings: the primary hypothesis with our best-fitting demographic parameter set and a second setting that maximises the range reached by sickle-cell disease in the simulation. The latter corresponds to the earliest possible appearance time, the origin in Central Africa and the demographic parameter set with the quickest spread out of those we examined (Table 6.1), namely parameter set 2 (see sensitivity analysis in Appendix E.2.2).

6.5 Results

6.5.1 Inferring haplotype origins

6.5.1.1 Sickle cell

In the data, the Bantu haplotype is wide-spread all over sub-Saharan Africa and the Benin haplotype in North Africa and the Middle East. The Arab-Indian and Senegal haplotypes have narrower distributions: in our dataset, the former is modal only on the Arabian Peninsula and in India, and the latter in Senegal (Table 6.4, Table 6.5 and Figure 6.2). The inferred distribution of most likely origins for sickle-cell disease looked realistic for each haplotype (Figure 6.3 to Figure 6.6). The Benin haplotype had its origin near Benin, the Arab-Indian haplotype in India and the Senegal haplotype somewhat north of Senegal, close to the coast. The Bantu haplotype had a wide range of plausible origins: most cells in Sub-Saharan Africa were good candidates, as long as they were not too close to the Benin haplotype.

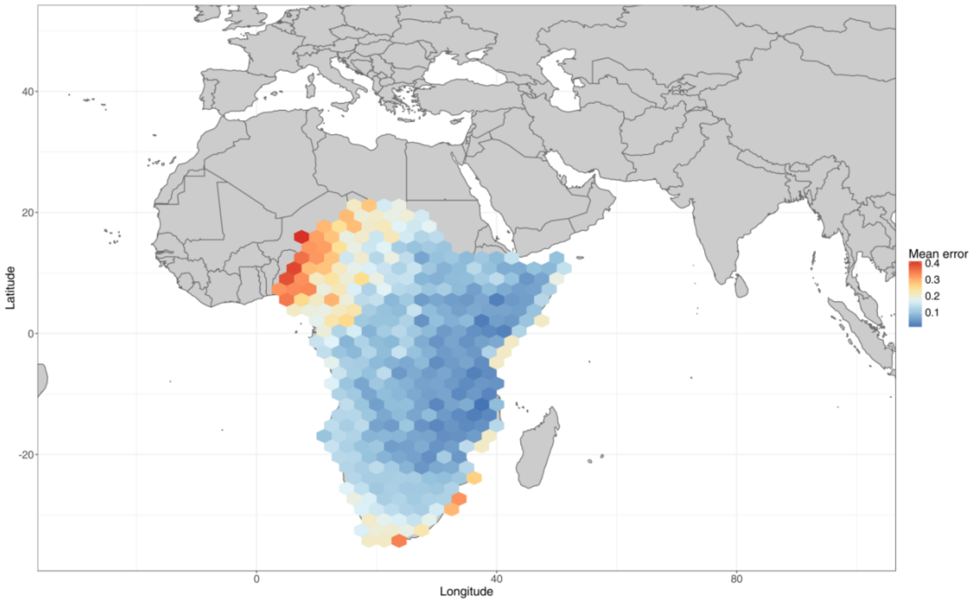

Figure 6.3 Most likely origins for the Bantu haplotype. The figure shows the mean sum of squared errors for the haplotype from simulations where it originated from that cell, averaged over 2.5° bins in both latitude and longitude.

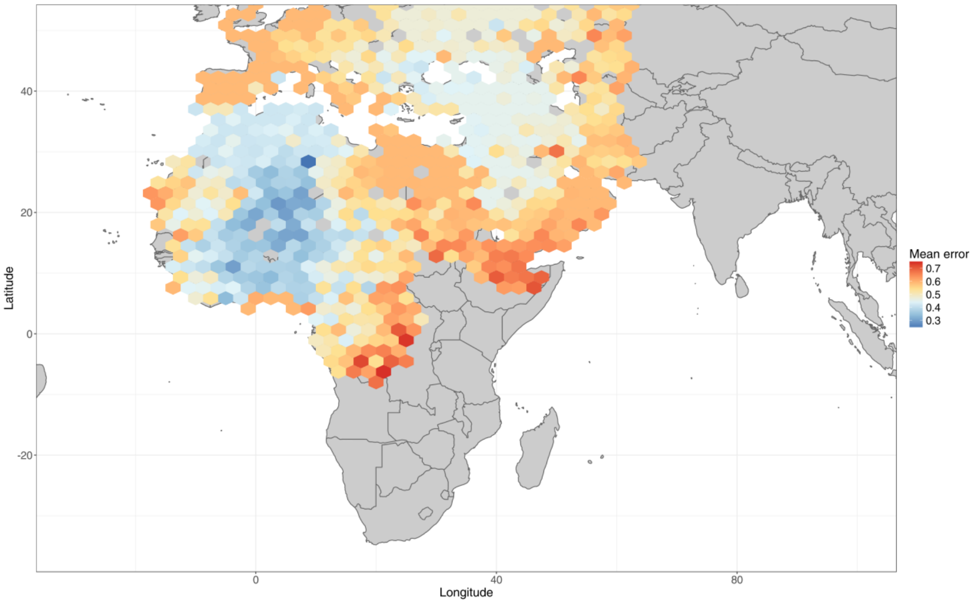

Figure 6.4 Most likely origins for the Benin haplotype. The figure shows the mean sum of squared errors for the haplotype from simulations where it originated from that cell, averaged over 2.5° bins in both latitude and longitude.

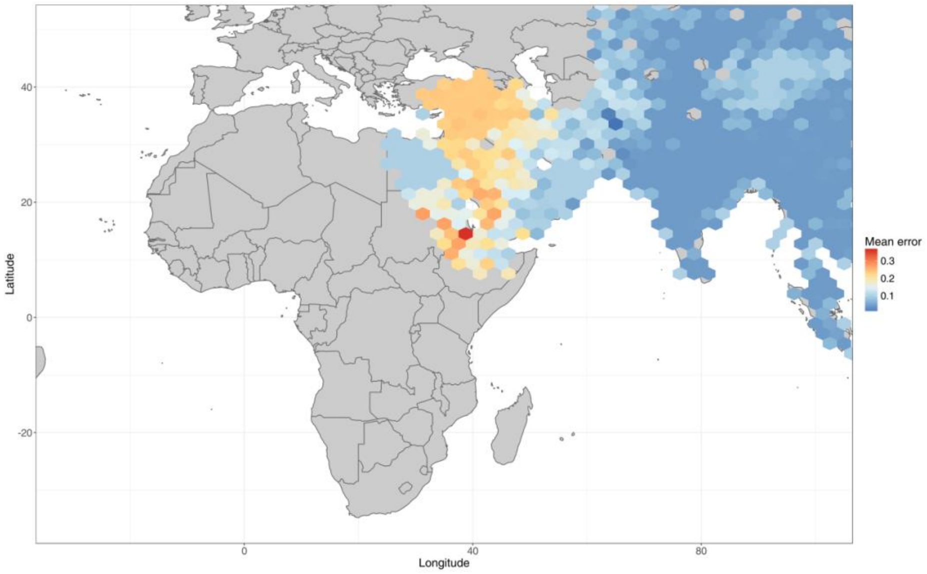

Figure 6.5 Most likely origins for the Arab-Indian haplotype. The figure shows the mean sum of squared errors for the haplotype from simulations where it originated from that cell, averaged over 2.5° bins in both latitude and longitude.

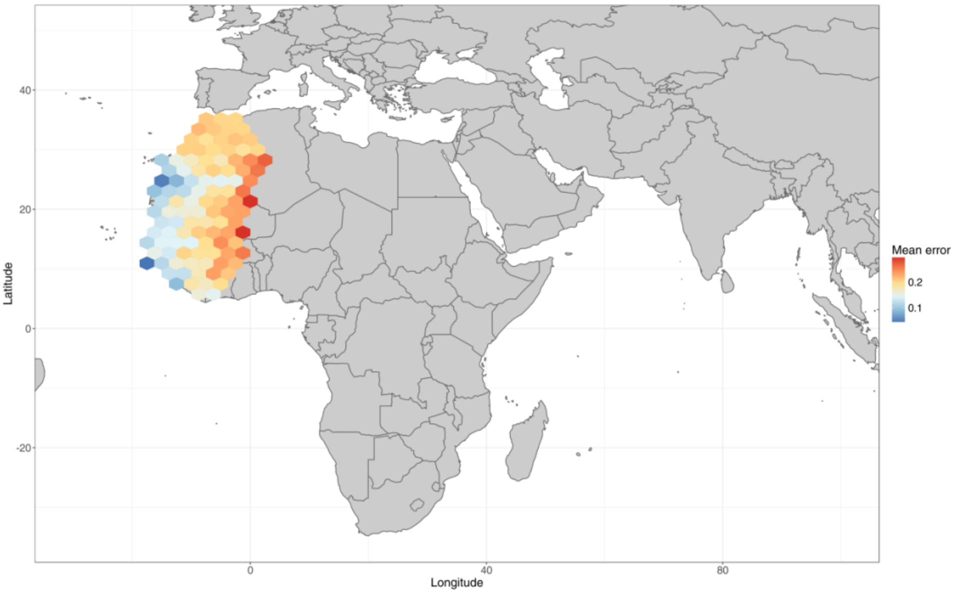

Figure 6.6 Most likely origins for the Senegal haplotype. The figure shows the mean sum of squared errors for the haplotype from simulations where it originated from that cell, averaged over 2.5° bins in both latitude and longitude.

6.5.1.2 Thalassemia

Thalassemia variants have highly overlapping distributions: Cd39 is present in all sampled countries, IVS-I-1 mainly appears in Europe but is also in North Africa at smaller proportions and FSC-6 is only reported in North Africa and at low proportions (Table 6.4, Table 6.5 and Table 6.6). Correspondingly, the inferred origins in our model were also less well-defined. Cd39 could have originated either in eastern Europe or western North Africa (

Figure 6.7), FSC-6 in western North Africa (Figure 6.8) and IVS-I-1 in eastern Europe (Figure 6.9). These patterns are reasonable given the data, since IVS-I-1 is indeed mainly present in Europe and FSC-6 only identified in North Africa. The bimodal nature of the possible origins for Cd39 can also be explained. In our model, overlapping distributions are produced when variants start close enough to each other so that they invade each other's ranges. Therefore, a higher amount of overlap and thus a classification closer to that observed was obtained when Cd39 could infiltrate the range of at least one other variant.

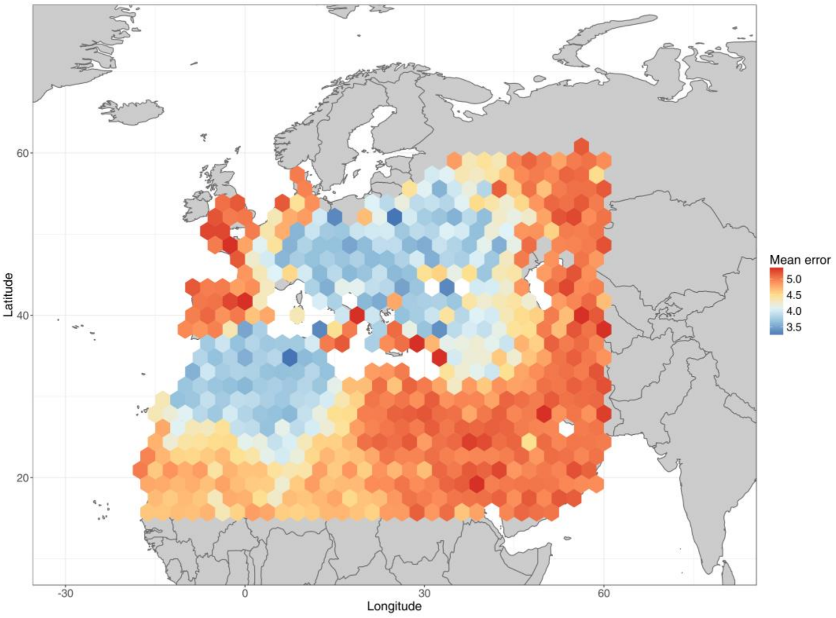

Figure 6.7 Most likely origins for the Cd39 variant. The figure shows the mean classification error (sum of misclassified variants per country) for simulations where the variant originated from that cell, averaged over 2.5° bins in both latitude and longitude.

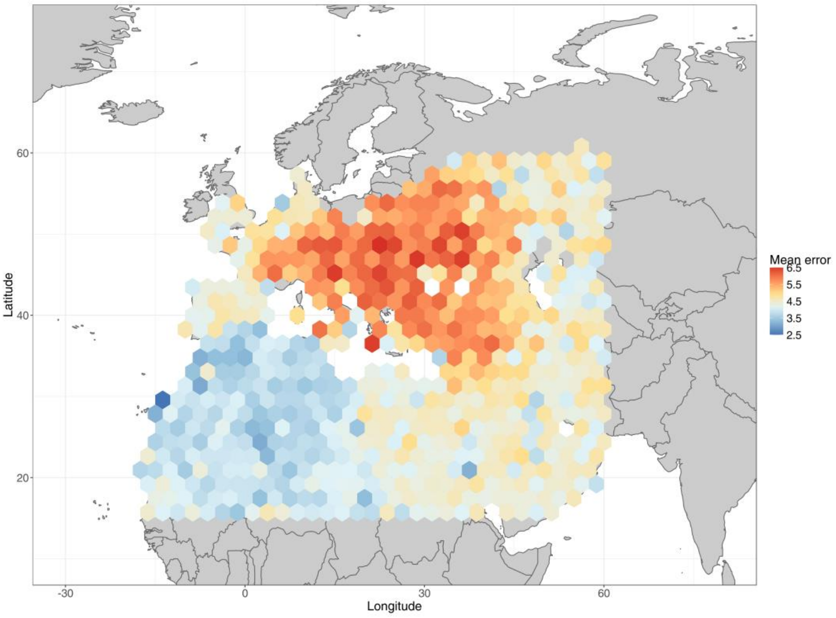

Figure 6.8 Most likely origins for the FSC-6 variant. The figure shows the mean classification error (sum of misclassified variants per country) for simulations where the variant originated from that cell, averaged over 2.5° bins in both latitude and longitude.

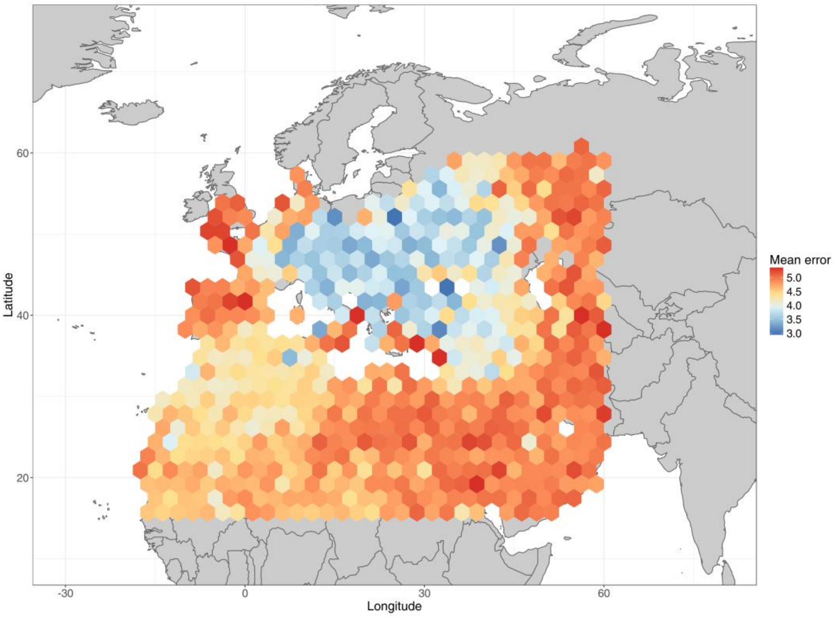

Figure 6.9 Most likely origins for the IVS-I-1 variant. The figure shows the mean classification error (sum of misclassified variants per country) for simulations where the variant originated from that cell, averaged over 2.5° bins in both latitude and longitude.

6.5.2 Qualitative spatial patterns

Once plausible origins for the different sickle-cell and thalassemia variants were established, I proceeded by examining the distributions of variants. The disjoint pattern of sickle-cell variants was closely matched using the best-fitting origins (Figure 6.10). However, for thalassemia, we could not produce a high amount of overlap between variants and instead obtained sickle cell-like, mostly disjoint distributions (Figure 6.11). The best simulations for thalassemia included some amount of overlap between two variants, but there was no single variant prevalent in all sampled regions, unlike what is observed for Cd39. There were also no countries with more than two variants present, even though that was observed in two out of the three sampled countries in North Africa (Algeria and Tunisia). To sum up, our model could produce spatial patterns similar to what was observed for sickle-cell disease, but those for thalassemia could not be matched.

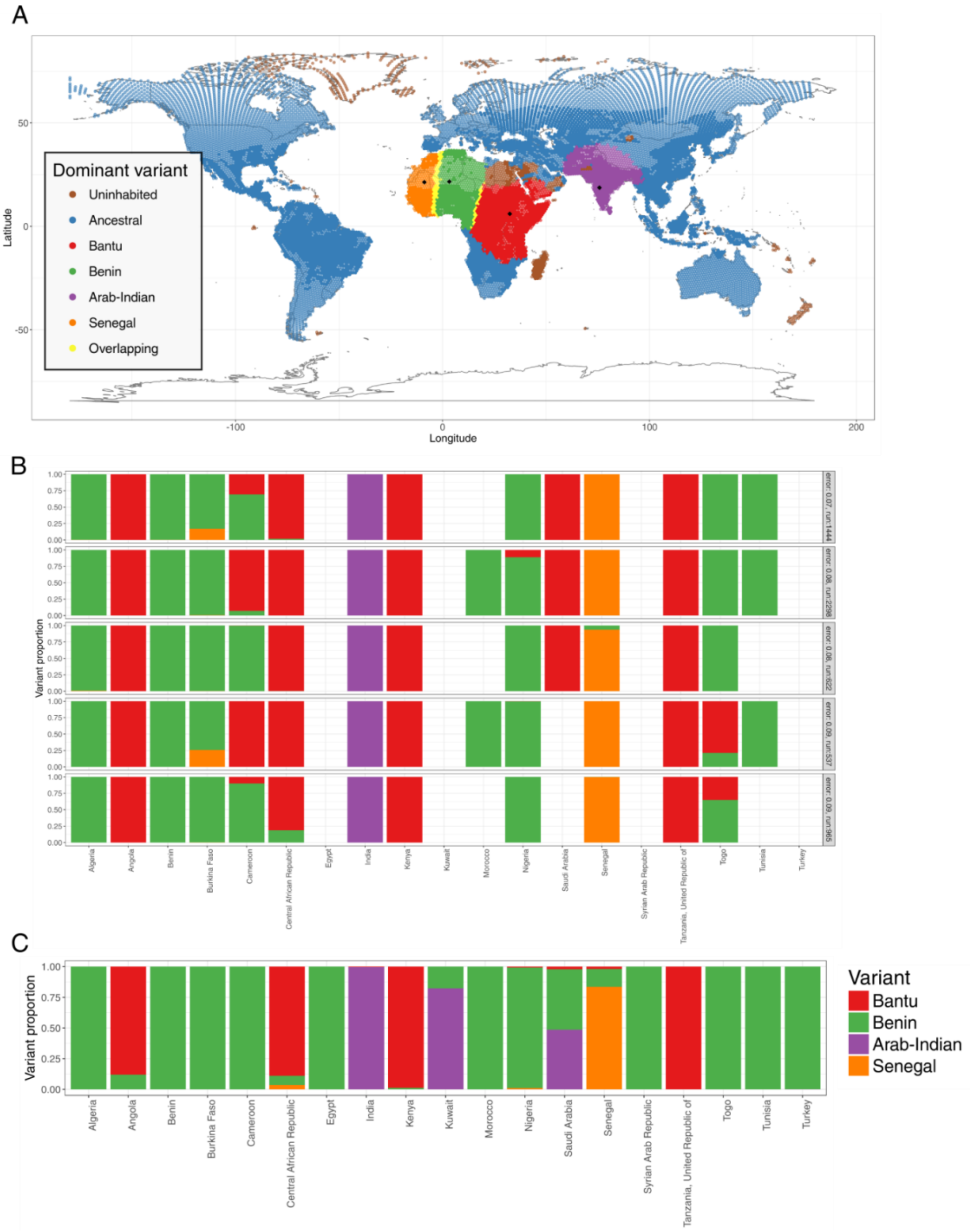

Figure 6.10 Distribution of sickle-cell haplotypes from our model. A. Spatial distribution of modal variants from the best-fitting set of origins. Areas with no single variant with a frequency above 80% are marked as "Overlapping" and black symbols show the origin of each haplotype. B. Distribution of variants in monitored countries from the five best-fitting sets of origins. In countries not reached by any variant, no data is shown. C. Distribution of modelled variants from simulated countries (bar chart representation of Table 6.3).

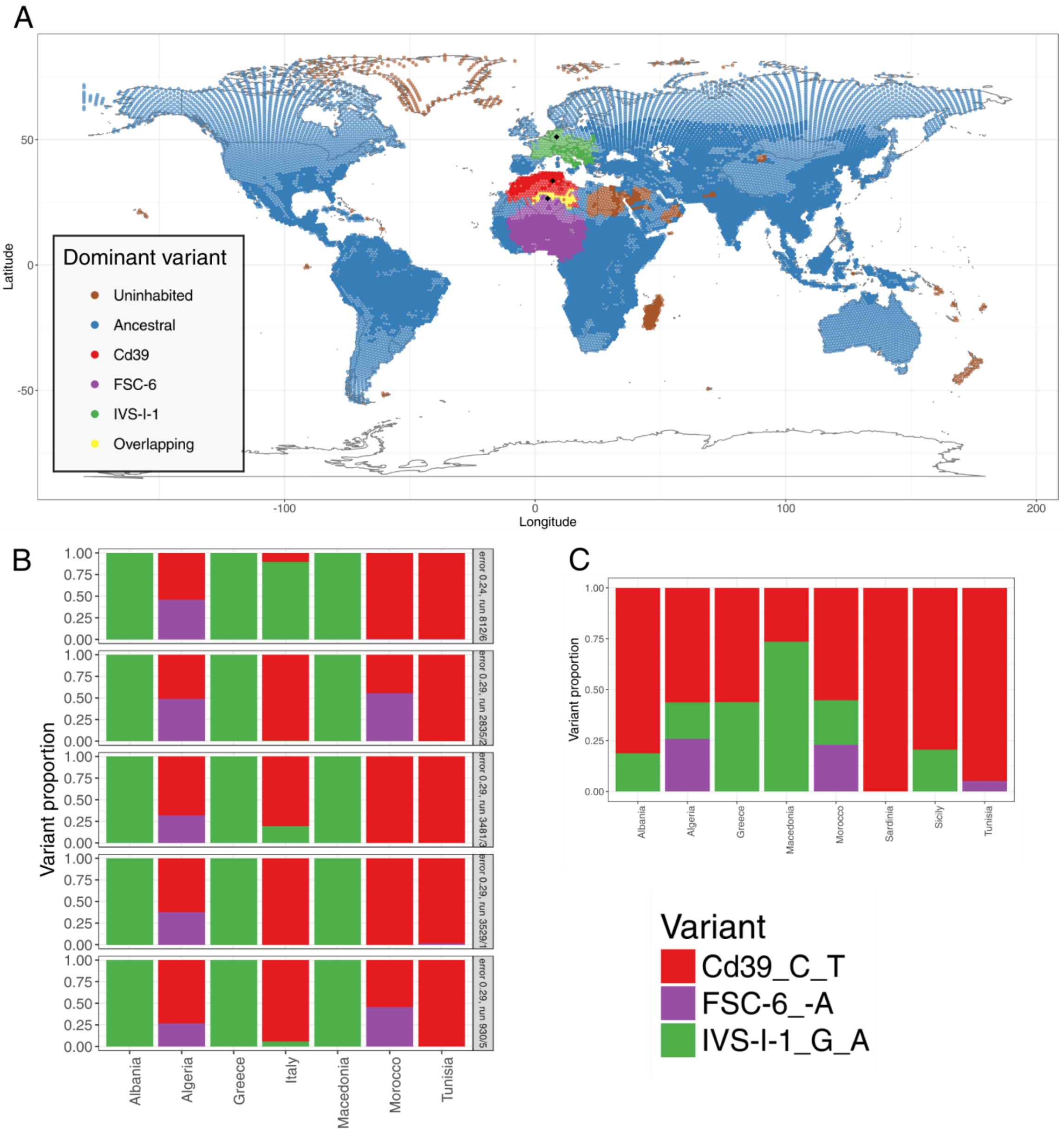

Figure 6.11 Distribution of thalassemia variants from our model. A. Spatial distribution of modal variants from the best-fitting set of origins. Areas with no single variant with a frequency above 80% are marked as “Overlapping” and black symbols show the origin of each haplotype. B. Distribution of variants in monitored countries from the five best-fitting origins. In countries not reached by any variant, no data is shown. C. Distribution of modelled variants from simulated countries (bar chart representation of Table 6.6).

6.5.3 Single-origin hypothesis of sickle-cell anaemia

After studying the spatial distribution of separate variants, I focused on the single-origin hypothesis by Shriner and Rotimi[7]. We first considered parameters resembling their primary scenario: an origin 259 generations ago in the western part of what is now the Sahara. In this case, the sickle-cell trait would not have expanded to its current range by today in our model (Figure 6.12). More strikingly, it would not even have reached all malarious areas in Africa with only such short-scale, gradual migrations. I also examined the parameters that are still considered plausible when following Shriner and Rotimi[7] and that result in the widest spread in the present-day range of sickle-cell disease. However, even in this case, we do not obtain the full present-day range: the allele spreads outside of Africa, but still does not reach India (Figure 6.13). Taken together, these results show that our model largely agrees with the single-origin hypothesis in that it could produce nearly the full present-day range of the disorder with extreme, but still plausible parameters. However, additional mechanisms are necessary for the observed presence of sickle-cell disease in India.

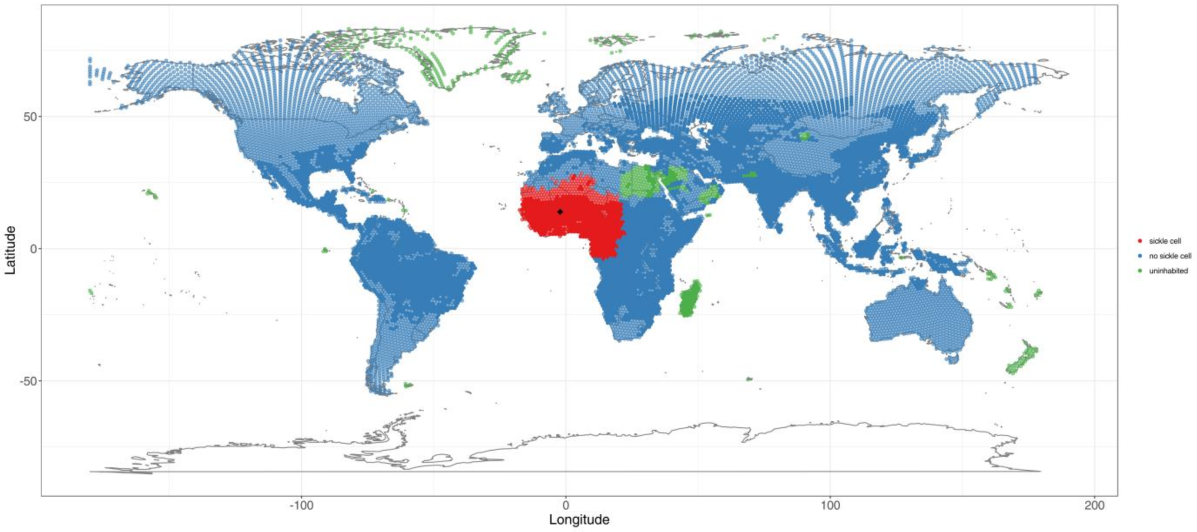

Figure 6.12 Spread of a single sickle-cell haplotype starting 259 generations ago in West Africa, using demographic parameter set 1 (Table 6.1). Black diamond marks the origin of the sickle-cell allele.

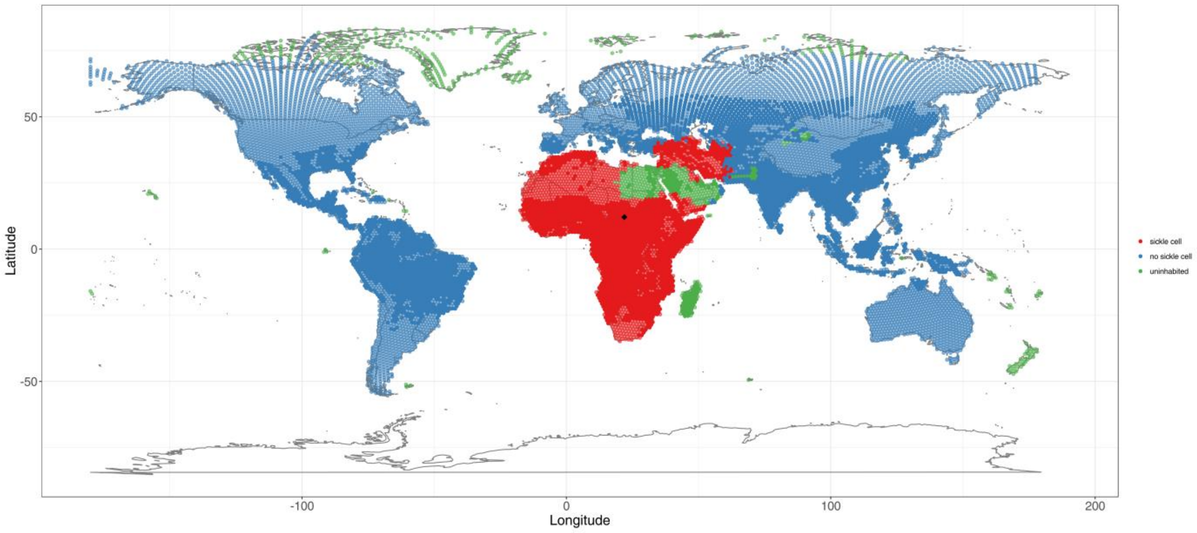

Figure 6.13 Spread of a single sickle-cell haplotype starting 395 generations ago in Central Africa, using demographic parameter set 2 (Table 6.1). Black diamond marks the origin of the sickle-cell allele.

6.6 Discussion

6.6.1 Results

Our mechanistic, spatially explicit model with only short-distance migrations could reproduce the spatial distribution of variants for sickle-cell disease, but not for β^0 thalassemia: overlapping, β^0 thalassemia-like patterns were not possible given the processes and parameters considered. Furthermore, the model was also not completely in agreement with the single-origin hypothesis for sickle-cell disease. In both cases, the short-distance migrations explored were insufficient to produce enough mixing: the single, original sickle-cell allele was not carried far enough and the different thalassemia variants could not invade each other’s ranges.

It should be noted that the migration rates in the three demographic parameter sets explored (~0.005 per generation and individual) are relatively low compared to the high end of the

95% credible interval of possible migration rates (~0.167 per generation and individual) from Raghavan et al.[12] It would be interesting to explore such higher migration rates, as they might be sufficient to produce the overlapping patterns of β^0 thalassemia and be compatible with the expansion of a single haplotype of sickle cell anaemia. Furthermore, it is possible that migration rates might have increased in recent time, as reported for Europe[35], but the model currently does not allow for such time-dependent changes in migration rate.

Long distance movements are another possible mechanism that could produce a higher amount of mixing. There is ample evidence for long-distance, large-scale migrations in the time range considered here, from about 10,000 years ago until today. For example, the Neolithic transition[36] and the Bronze Age migrations[37] both left their signatures in European genetic diversity, evidence of an expansion wave into India has also been described on the basis of genetic data[38] and high levels of mixed genetic ancestry amongst Africans also point to a high level of admixture in that continent[39]. Furthermore, these dynamics have previously been suggested to facilitate the spread of sickle-cell haplotypes: the migrations of Bantu-speaking people have been postulated as a cause for the wide distribution within Africa[7] and long-distance overseas connections for the presence of the same haplotype in India and the Near East[40].

6.6.2 Limitations

There are multiple limitations to this approach. First, the simultaneous appearance of malaria-related selection pressure and the identity of haplotypes regarding selection strength and the level of deleteriousness is an oversimplification. Estimates for the ages of the different haplotypes differ[3,41] and there are also signs for a diversity in clinical effects between different sickle-cell haplotypes[42], but the model outcomes were reasonably robust to the corresponding parameters. I also did not account for variability in selection pressure and only used a binary representation of the presence of malaria. However, our results were also not sensitive to changes in selection coefficient and I therefore do not expect a non-binary profile of the strength of selection to make a substantial difference.

This model also represented a simplified view of the origin of variants by starting in just a single deme. If the alleles were already part of standing variation at the start of selection, as it likely was the case for at least the sickle-cell trait, they could have been present over a wider range. This would accelerate the spread of both the overall trait and the different variants and our range estimates can thus only be considered as lower boundaries. Furthermore, standing variation could also influence our incapability of producing the highly overlapping patterns characteristic of thalassemia: if the variants were already present in a wide range, they could have spread further and had more time to invade each other's ranges. In particular, if alleles with a wider geographic distribution (e.g. Cd39) were already present when the other variants (e.g. IVS-I-1, FSC-6 and the less common, not modelled variants) appeared, the observed overlapping distribution would have been more likely. Since β^0 thalassemia can be caused by any mutation that completely eliminates protein production from the β -globin gene and as many such mutations have already been reported, it is likely that new mutations continuously occur. In the future, our model could easily be adapted to account for such a scenario.

An additional limitation of our model is the lack of epistatic interactions. These can lead to a diminishing advantage offered by one variant where another is already present[13], or even to negative epistasis. For example, both the sickle-cell trait and α thalassemia offer some level of protection, but individuals heterozygous for both are just as vulnerable to malaria as the controls[43]. The boundaries between the current distributions of different disorders, such as the relatively low incidence of sickle-cell disease in the Mediterranean[44], has been attributed to epistatic interaction between different genetic disorders[13]. Since these effects were not represented in our model, it is no surprise that the overall extent of the simulated range of all variants is only bounded by malaria endemicity. For example, if the system is simulated long enough, the sickle-cell trait would become common also outside of Africa.

Lastly, but perhaps most importantly, our model did not include migration waves or long-distance connections, despite their likely effect in the spread of protective variants. In the current framework, such events would have to have been pre-defined using other, non-genetic lines of evidence. However, this made it possible to test the importance of such events and showed that they indeed could be necessary to explain the present-day extent of sickle-cell anaemia and possibly also the overlapping distribution of β^0 thalassemia.

6.6.3 Perspectives

A considerable advantage of this layer-based modelling framework is that it is very easy to generalise to other cases of selection and beyond. Different protective variants and their interactions, or other types of selection (e.g. haploid and diploid selection; additive, dominant and recessive traits; epistatic interactions) can all be modelled by simply changing the corresponding term in the population growth step. The spatial aspect also provides a convenient way to represent space- and time-dependent selection pressures, or even a link to climatic variables. Last, the layer-based framework can even be used for arbitrary types of interacting individuals, such as hunter-gatherers and farmers over the Neolithic transition or anatomically modern humans and Neanderthals in Europe.

6.6.4 Summary

This chapter presented a spatially explicit model for selection and its application to sickle-cell disease and β^0 thalassemia, two well-studied traits with a protective effect against malaria. It showed the importance of modelling spatial effects and the limitations of such a framework when applied to recent events when long-distance migrations were probably already common for humans. The exact cause of our model's inability to capture the quick spread of malaria-resistant traits and the contrast between the spatial distributions of variants of these traits remains to be determined, but this application highlighted the power of a spatially explicit model and paved the way for its future applications.

6.7 Bibliography

1. Bengtsson, B. O. & Tunlid, A. The 1948 International Congress of Genetics in Sweden: People and Politics. *Genetics* **185,** 709–715 (2010).

2. Haldane J. B. S. The rate of mutation of human genes. *Hereditas* **35,** 267–273 (2010).

3. Hedrick, P. W. Population genetics of malaria resistance in humans. *Heredity* **107,** 283 (2011).

4. Carter, R. & Mendis, K. N. Evolutionary and Historical Aspects of the Burden of Malaria. *Clin. Microbiol. Rev.* **15,** 564–594 (2002).

5. Pagnier, J. *et al.* Evidence for the multicentric origin of the sickle cell hemoglobin gene in Africa. *Proc. Natl. Acad. Sci.* **81,** 1771–1773 (1984).

6. Lapouniéroulie, C. *et al.* A novel sickle cell mutation of yet another origin in Africa: the Cameroon type. *Hum. Genet.* **89,** 333–337 (1992).

7. Shriner, D. & Rotimi, C. N. Whole-Genome-Sequence-Based Haplotypes Reveal Single Origin of the Sickle Allele during the Holocene Wet Phase. *Am. J. Hum. Genet.* **102,** 547–556 (2018).

8. Chen, J.-M., Cooper, D. N., Chuzhanova, N., Férec, C. & Patrinos, G. P. Gene conversion: mechanisms, evolution and human disease. *Nat. Rev. Genet.* **8,** 762–775 (2007).

9. Cao, A. & Galanello, R. Beta-thalassemia. *Genet. Med.* **12,** 61–76 (2010).

10. Hockham, C., Piel, F. B., Gupta, S. & Penman, B. S. Understanding the contrasting spatial haplotype patterns of malaria-protective β-globin polymorphisms. *Infect. Genet. Evol.* **36,** 174–183 (2015).

11. Eriksson, A. *et al.* Late Pleistocene climate change and the global expansion of anatomically modern humans. *Proc. Natl. Acad. Sci.* **109,** 16089–16094 (2012).

12. Raghavan, M. *et al.* Genomic evidence for the Pleistocene and recent population history of Native Americans. *Science* **349,** aab3884 (2015).

13. Piel, F. B. *et al.* Global distribution of the sickle cell gene and geographical confirmation of the malaria hypothesis. *Nat. Commun.* **1,** 104 (2010).

14. Lysenko, A. & Semashko, I. Geography of malaria. A medico-geographic profile of an ancient disease. *Itogi Nauki Med. Geogr.* 25–146 (1968).

15. Hay, S. I., Guerra, C. A., Tatem, A. J., Noor, A. M. & Snow, R. W. The global distribution and population at risk of malaria: past, present, and future. *Lancet Infect. Dis.* **4,** 327–336 (2004).

16. Kulozik, A. E. *et al.* Geographical survey of βS-globin gene haplotypes: Evidence for an independent Asian origin of the sickle-cell mutation. *Am. J. Hum. Genet.* **39,** 239–244 (1986).

17. El Hazmi, M. A. *et al.* Haplotypes of the beta-globin gene as prognostic factors in sickle-cell disease. (1999).

18. Flint, J., Harding, R. M., Boyce, A. J. & Clegg, J. B. 1 The population genetics of the haemoglobinopathies. *Baillières Clin. Haematol.* **11,** 1–51 (1998).

19. Gabriel, A. & Przybylski, J. Sickle-cell anemia: a look at global haplotype distribution. (2010).

20. Adekile, A. D. *et al.* Molecular Characterization of α-Thalassemia Determinants, β-Thalassemia Alleles, and βs Haplotypes among Kuwaiti Arabs. *Acta Haematol.* **92,** 176–181 (1994).

21. LABIE, D. *et al.* Haplotypes in Tribal Indians Bearing the Sickle Gene: Evidence for the Unicentric Origin of the β s Mutation and the Unicentric Origin of the Tribal Populations of India. *Hum. Biol.* **61,** 479–491 (1989).

22. Öner, C. *et al.* β<Superscript>s</Superscript> Haplotypes in various world populations. *Hum. Genet.* **89,** 99–104 (1992).

23. NIRANJAN, Y., CHANDAK, G. R., VEERRAJU, P. & SINGH, L. Some Atypical and Rare Sickle Cell Gene Haplotypes in Populations of Andhra Pradesh, India. *Hum. Biol.* **71,** 333–340 (1999).

24. Antonarakis, S. E., Kazazian, H. H. & Orkin, S. H. DNA polymorphism and molecular pathology of the human globin gene clusters. *Hum. Genet.* **69,** 1–14 (1985).

25. BENNANI, C. *et al.* Anthropological Approach to the Heterogeneity of ß-Thalassemia Mutations in Northern Africa. *Hum. Biol.* **66,** 369–382 (1994).

26. Bouhass, R., Perrin, P. & Trabuchet, G. The spectrum of β-thalassemia mutations in the oran region of algeria. *Hemoglobin* **18,** 211–219 (1994).

27. Agouti, I., Badens, C., Abouyoub, A., Levy, N. & Bennani, M. Molecular Basis of β-Thalassemia in Morocco: Possible Origins of the Molecular Heterogeneity. *Genet. Test.* **12,** 563–568 (2008).

28. Lemsaddek, W. *et al.* Spectrum of β thalassemia mutations and HbF levels in the heterozygous Moroccan population. *Am. J. Hematol.* **73,** 161–168 (2003).

29. Lemsaddek, W. *et al.* The β-Thalassemia Mutation/Haplotype Distribution in the Moroccan Population. *Hemoglobin* **28,** 25–37 (2004).

30. Fattoum, S. *et al.* β-Thalassemia, HB S-β-Thalassemia and Sickle Cell Anemia Among Tunisians. *Hemoglobin* **15,** 11–21 (1991).

31. Boletini, E. *et al.* Sickle cell anemia, sickle cell β-thalassemia, and thalassemia major in Albania: characterization of mutations. *Hum. Genet.* **93,** 182–187 (1994).

32. Cao, A., Rosatelli, C., Pirastu, M. & Galanello, R. Thalassemias in Sardinia: molecular pathology, phenotype-genotype correlation, and prevention. *Am. J. Pediatr. Hematol. Oncol.* **13,** 179–188 (1991).

33. Schilirò, G., Mirabile, E., Testa, R., Russo-Mancuso, G. & Dibenedetto, S. P. Presence of hemoglobinopathies in Sicily: A historic perspective. *Am. J. Med. Genet.* **69,** 200–206 (1997).

34. Schilirò, G. *et al.* Genetic heterogeneity of β-thalassemia in southeast sicily. *Am. J. Hematol.* **48,** 5–11 (1995).

35. Loog, L. *et al.* Estimating mobility using sparse data: Application to human genetic variation. *Proc. Natl. Acad. Sci.* 201703642 (2017). doi:10.1073/pnas.1703642114

36. Lazaridis, I. *et al.* Ancient human genomes suggest three ancestral populations for present-day Europeans. *ArXiv13126639 Q-Bio* (2013).

37. Haak, W. *et al.* Massive migration from the steppe was a source for Indo-European languages in Europe. *Nature* **522,** 207–211 (2015).

38. Reich, D., Thangaraj, K., Patterson, N., Price, A. L. & Singh, L. Reconstructing Indian population history. *Nature* **461,** 489–494 (2009).

39. Tishkoff, S. A. *et al.* The Genetic Structure and History of Africans and African Americans. *Science* **324,** 1035–1044 (2009).

40. Stuart, M. J. & Nagel, R. L. Sickle-cell disease. *Lancet Lond. Engl.* **364,** 1343–1360 (2004).

41. Modiano, D. *et al.* Haemoglobin S and haemoglobin C: 'quick but costly' versus 'slow but gratis' genetic adaptations to Plasmodium falciparum malaria. *Hum. Mol. Genet.* **17,** 789–799 (2008).

42. Loggetto, S. R. Sickle cell anemia: clinical diversity and beta S-globin haplotypes. *Rev. Bras. Hematol. E Hemoter.* **35,** 155–157 (2013).

43. Williams, T. N. *et al.* Negative epistasis between the malaria-protective effects of α^+-thalassemia and the sickle cell trait. *Nat. Genet.* **37,** 1253–1257 (2005).

44. Penman, B. S., Pybus, O. G., Weatherall, D. J. & Gupta, S. Epistatic interactions between genetic disorders of hemoglobin can explain why the sickle-cell gene is uncommon in the Mediterranean. *Proc. Natl. Acad. Sci.* **106,** 21242–21246 (2009).

Chapter 7 Epilogue

7.1 Introduction

In this thesis, I explored human evolutionary history and its interplay with natural selection on the basis of ancient DNA and spatially explicit modelling. Chapters 2, 3 and 4 studied important episodes in the history of anatomically modern humans through the analysis of novel ancient genetic data. Chapter 2 focussed on early anatomically modern humans in Europe and highlights their diversification shortly after their exit out of Africa, but also that many of the resulting populations did not manage to contribute significantly to modern genetic diversity. Chapter 3 introduced a separate, divergent lineage of hunter-gatherers in the Caucasus, and Chapter 4 pointed to a high level of continuity in northern East Asia throughout the Neolithic transition. Chapters 5 and 6 used a climate-driven, spatially explicit modelling framework: the former explored the effect of space on selection statistics in a neutral model, and the latter focussed on selection for variants providing resistance against malaria.

In this last chapter, I first discuss the use of ancient DNA in uncovering demographic processes. I compare two main data acquisition strategies: broad sampling of many genomes and deep sampling, focussing on a few, high-quality genomes. I also touch on the teething problems and future directions in the field, as well as on the issue of compatibility of datasets from different sources. I then continue with the discussion of continuity and extinction in human evolution, particularly the signals of these processes in ancient and modern genetic data and the different definitions of continuity. I then finish this epilogue with a few remarks on complex spatial models, including advantages, disadvantages, and technical challenges.

7.2 aDNA and its use in uncovering demographic processes

7.2.1 Introduction

Genetic data from ancient samples is a relatively new source in the study of human evolution. Not only does it give access to individual ancient samples, giving a chance to examine extinct species (e.g. the quagga[1]), subspecies (e.g. Neanderthals[2]) or populations (e.g. the ancestors of early European farmers[3]), but it also broadens our sampling domain in time and space. The additional time dimension enables a direct estimation of the mutation rate[4] and the direct study of temporal processes, such as changes in allele frequencies (e.g. alleles influencing skin pigmentation[5]) or the appearance of alleles (e.g. lactase persistence in the Bronze Age instead of the Neolithic[3,6,7]). However, the imputation of unobserved alleles can be problematic, especially if the locus in focus has risen rapidly in allele frequency, as is the case for many variants under selection. Furthermore, we can pinpoint the location of events in evolutionary history by observing changes through samples from a known location and time. Common examples are the study of the origin and extent of expansion waves (e.g. Bronze Age migrations in Europe[6] or the spread of eskimo cultures in North America[8]) or admixture events (e.g. sources of European genetic diversity[9] or back-migration to North Africa[10]). However, aDNA is still a developing field and has a number of limitations. Protocols in data generation and analysis are still under development, and although the amount of available data has drastically increased, jointly using these datasets is very problematic. Furthermore, projects are sometimes driven by the availability of data instead of a scientific question or hypothesis, and the quality of analysis sometimes suffers from the time-pressure for high-profile publications that are based on the novelty of the data.

7.2.2 Broad and deep sampling

There are two main strategies in the use of ancient genetic data. First, one can focus on a few high-quality samples and sequence those to high coverage, which I will refer to as deep sampling. Alternatively, a large number of individuals can be studied in parallel, but are then usually sequenced to only low coverage and/or at selected genetic loci. I will refer to this latter strategy as broad sampling. The high-quality samples presented in Chapters 2 and 3 are cases of deep sampling, while Chapter 4 belongs to neither of these strategies: it is based on only a few low-coverage samples as sample availability was limited and the samples were not well preserved.

The ancient DNA community seems to move more towards broad sampling, but certain characteristics of samples and processes can only be studied through deep sampling. A broad sample is more suited to study large-scale changes in evolution that affect multiple populations, such as the space- and time-dependent, complex details of the Bronze Age migrations in Eurasia[6] or the definition of and the interplay between different genetic groups in Ice Age Europe[11]. However high-quality samples are necessary to study haplotype patterns or diploid genotypes[12–14]. Detailed demographic inference through the assignment of sections of the genomes to different ancestries is only possible in the knowledge of diploid haplotypes; for example, the distribution of the length of such ancestries can give information about changes in past population size or the timing of admixture events. Haplotypes can also be analysed to extract genetic data from the source populations of admixture, such as Neanderthal and Denisovan ancestry in Melanesians[15] or Native American segments in the 1000 Genomes populations[16] (Chapter 5). Furthermore, high-confidence diploid genotype calls are necessary to reliably study particular locations in the genome[17], such as those associated with phenotypic changes – although broad sampling is still needed for population-level information[18]. Last, a practical consideration regarding these two sampling strategies is that a large number of samples is not always within reach. Therefore, we are often restricted to extract as much information as possible from those few sample(s) that are available and sufficiently preserved.

7.2.3 Increase in data volume and issues of compatibility

Although the ancient DNA field is still new, a large amount of data has already been generated. Technological advances enable us to sequence samples in a worse preservation state and using a smaller quantity of the ancient material than ever before. In addition, the increasing credibility of the field after the initial lack of confidence facilitates the acquisition of samples: archaeologists and anthropologists are naturally more willing to give up a piece of their sample when they can expect to receive reliable information in exchange. Furthermore, ethical issues are now more carefully considered. For example, clear guidelines along with personal connections help build long-term relations with indigenous people and gain their support to conduct analysis on the remains of their ancestors[19].

The increase in data quantity also highlights problems around the compatibility of different datasets, where samples that went through different processing pipelines share similarities independent from their actual genetic relationship. Researchers are still exploring best practices and protocols for sequencing and bioinformatics pipelines and each lab has its own standards. Such differences are difficult to take into account after the processing has been done, although some considerations are generally taken, such as the reproduction of results on a reduced set of markers which are highly invariant to the differences (e.g. transversions only for differences in how damaged bases are handled). However, such checks do not guarantee an unbiased analysis and also usually lead to a reduction in data quantity. Ideally, all samples should be processed in exactly the same way from the very beginning, but given that that is rarely feasible, the sequenced data should at least be reprocessed using a standardised bioinformatics pipeline if different datasets are merged.

7.2.4 Data-driven projects

Even with the increase in availability, many ancient DNA studies are still purely data-driven and the directed collection of samples to study a hypothesis is rare. In addition, the main determinant of the success of a publication can often be the novelty of the data and not the quality of the research. The resulting rush for the first publication in an area or time period creates a time pressure that can increase the chances of errors. However, there are promising signs to address this concern: the push for open data enables such errors to be discovered by the scientific community[10], leading to high-quality, reproducible ancient DNA studies. Furthermore, as the field matures and low-hanging fruits disappear, high-quality analysis with a well-defined goal will become more important and simply possessing novel data is no longer sufficient for a high-profile paper.

7.3 Continuity and extinctions in human evolution

7.3.1 Introduction

The notions of continuity and extinction are strongly linked in human evolution. Current knowledge points to a series of expansion events, followed by continuous diversification[20]. In contrast, we often see lineages in genetic data, but what processes generated these deep splits is still unclear. A further complication is coming from the unclear and arbitrary definitions of continuity, especially considering human populations which are characterised by a high level of contact and a lack of reproductive isolation.

7.3.2 Extinctions and lineages

The division between lineages in ancient genetic diversity is often unclear and/or does not correspond to modern genetic diversity. Chapter 2 showcases such a situation in Europe, but there are also cases in other regions, like the affinities of the Siberian Mal'ta boy to both Native Americans and North Europeans[21] or the lack of continuity on the Eurasian steppes[18]. The notion of lineages can also become obscured as more data is analysed, especially for ancient data. For example, the initial view of Neanderthals mixing into anatomically modern humans (AMHs)[22] became increasingly complex. Additional Neanderthal samples indicated structure within their population and identified the Neanderthal group closest to that which contributed to modern humans[23]; the discovery of Denisovans added a sister group of Neanderthals to the picture[24], and further modelling even showed signals of gene flow into Neanderthals from a different archaic hominin and from an early AMH group[25]. This is just one simple example, but it illustrates the general trend of tree-like models becoming increasingly complex as new data is incorporated, implying that many apparent ancient "lineages" could just be artifacts due to limited sampling.

However, for modern populations in large reference datasets, a lack of spatial sampling is less of a problem. Therefore, the presence of well-supported lineages in modern genetic data, such as deeply divergent populations in Africa (e.g. the San or the Mbuti) or the clearly separated European and East Asian continental groups, need a different explanation. The extinction of the original intermediate populations, such as what was found in Upper Palaeolithic Europe (as discussed in Chapter 2 using novel and published[4,11,26] data), seems like a good candidate.

7.3.3 Definition of continuity

The other point that needs discussing with regards to the notion of lineages is population continuity. In its purest definition, continuity means that a population evolves in complete isolation, without any genetic exchange with other populations. In this case, samples from different times that originate from the same, continuous population only differ due to genetic drift[27]. However, for a species where migration and admixture are as common as in humans, such perfect continuity is highly improbable. For uniparental markers, haplogroup membership has been used to infer continuity and admixture[28,29], but such analysis, based on a single locus, is sensitive to stochastic effects. For nuclear genetic data, formal tests can be used to detect admixture (as in multiple papers investigating, for example, the origins of Europeans[3,6,9,18] or South Asians[3,30,31], but also Chapters 3[12] and 4[32]), but since a complete lack of such signal cannot be expected, the threshold level for "continuity" must be chosen carefully. The level of continuity can also be compared to that between other pairs of populations on the basis of inferred admixture proportions, such as in the analysis performed in Chapter 4. However, just like for any hypothesis test, the lack of a clear signal of admixture does not necessarily imply continuity, as it might simply be due to the lack of power[33].

7.4 Importance of space in modelling

7.4.1 Advantages

Spatial models have multiple advantages and disadvantages, as mentioned in Chapter 1. They are capable of representing gradual changes and complex population structure without the constraints of lineages for tree-like models. Continuous processes are natural in such models: admixture and expansion are the consequence of mechanistic processes and do not need to be pre-defined. Spatial models are also capable of providing a different view on continuity: we can consider a population continuous if it is in contact with its geographic neighbours at a level typical for the model and is not affected by any major expansion wave or extinction event[27]. Thus, there is no need for a lineage-based continuity definition or arbitrary levels of acceptable admixture. Spatial models are also a natural choice in the study of selection, as selection pressures are inherently linked to the environment (e.g. presence of pathogens[34]) and space-dependent demographic processes interact with natural selection (Chapters 5 and 6).

7.4.2 Disadvantages

Spatial models also have some obvious disadvantages, as already mentioned in Chapters 1, 5 and 6. They have high computational costs, are challenging to develop from a coding perspective, and are intensive in terms of data - although the latter is mitigated in a mechanistic model where only a few free parameters are sufficient to explore the model. A further limitation is that it is difficult to represent sudden and/or large-scale changes (migrations, expansions or extinctions) in such models, although such events are common in human evolutionary history (e.g. the Neolithic transition[3] or the Bantu expansion[35]) and are often triggered by cultural or technological changes and not just by external environmental variables[36]. Since their origin is highly stochastic, difficult to predict and often not well-understood, this limitation is particularly hard to address without using other lines of evidence (e.g. from archaeology or linguistics). Our spatial framework certainly represents a more spatio-temporally continuous view of human population history than the reality, and we can only incorporate large-scale events through pre-defined effects (e.g. selection-related processes in Chapter 6) or by changing the interaction with environmental variables (as is currently explored in our group).

7.5 Concluding remarks

This thesis explored fundamental aspects of human evolutionary history - patterns of continuity and admixture and phases of stagnation and sudden changes - through the use of modelling and data analysis. The abundance of modern and ancient genetic data in today's "genomics era" enable the usage of not only simple, tree-like models, but also of complex, spatially explicit frameworks. The contrasting results from different areas and time periods highlighted key processes from the origins of our species' remarkable diversity, and have opened further questions to serve as the topic of future research.

7.6 Bibliography

1. Wilson, A. C., Bowman, B., Freiberger, M., Ryder, O. A. & Higuchi, R. DNA sequences from the quagga, an extinct member of the horse family. *Nature* **312,** 282 (1984).

2. Green, R. E. *et al.* Analysis of one million base pairs of Neanderthal DNA. *Nature* **444,** 330–336 (2006).

3. Lazaridis, I. *et al.* Genomic insights into the origin of farming in the ancient Near East. *Nature* **536,** 419–424 (2016).

4. Fu, Q. *et al.* Genome sequence of a 45,000-year-old modern human from western Siberia. *Nature* **514,** 445–449 (2014).

5. Wilde, S. *et al.* Direct evidence for positive selection of skin, hair, and eye pigmentation in Europeans during the last 5,000 y. *Proc. Natl. Acad. Sci.* **111,** 4832–4837 (2014).

6. Haak, W. *et al.* Massive migration from the steppe was a source for Indo-European languages in Europe. *Nature* **522,** 207–211 (2015).

7. Mathieson, I. *et al.* Genome-wide patterns of selection in 230 ancient Eurasians. *Nature* **528,** 499–503 (2015).

8. Raghavan, M. *et al.* Genomic evidence for the Pleistocene and recent population history of Native Americans. *Science* **349,** aab3884 (2015).

9. Lazaridis, I. *et al.* Ancient human genomes suggest three ancestral populations for present-day Europeans. *ArXiv13126639 Q-Bio* (2013).

10. Gallego-Llorente, M. *et al.* Ancient Ethiopian genome reveals extensive Eurasian admixture throughout East Africa. *Science* **350,** 820–822 (2015).

11. Fu, Q. *et al.* The genetic history of Ice Age Europe. *Nature* **534,** 200–205 (2016).

12. Jones, E. R. *et al.* Upper Palaeolithic genomes reveal deep roots of modern Eurasians. *Nat. Commun.* **6,** 8912 (2015).

13. Broushaki, F. *et al.* Early Neolithic genomes from the eastern Fertile Crescent. *Science* aaf7943 (2016). doi:10.1126/science.aaf7943

14. Hofmanová, Z. *et al.* Early farmers from across Europe directly descended from Neolithic Aegeans. *Proc. Natl. Acad. Sci.* **113,** 6886–6891 (2016).

15. Vernot, B. *et al.* Excavating Neandertal and Denisovan DNA from the genomes of Melanesian individuals. *Science* **352,** 235–239 (2016).

16. Martin, A. R. *et al.* Human Demographic History Impacts Genetic Risk Prediction across Diverse Populations. *Am. J. Hum. Genet.* **100,** 635–649 (2017).

17. Olalde, I. *et al.* Derived immune and ancestral pigmentation alleles in a 7,000-year-old Mesolithic European. *Nature* **507,** 225–228 (2014).

18. Allentoft, M. E. *et al.* Population genomics of Bronze Age Eurasia. *Nature* **522,** 167–172 (2015).

19. Callaway, E. Aboriginal genome analysis comes to grips with ethics. *Nature* **477,** 522–523 (2011).

20. Foley, R. A. & Lewin, R. *Principles of Human Evolution*. (John Wiley & Sons, 2013).

21. Raghavan, M. *et al.* Upper Palaeolithic Siberian genome reveals dual ancestry of Native Americans. *Nature* **505,** 87–91 (2014).

22. Green, R. E. *et al.* A Draft Sequence of the Neandertal Genome. *Science* **328,** 710–722 (2010).

23. Prüfer, K. *et al.* The complete genome sequence of a Neanderthal from the Altai Mountains. *Nature* **505,** 43–49 (2014).

24. Reich, D. *et al.* Genetic history of an archaic hominin group from Denisova Cave in Siberia. *Nature* **468,** 1053–1060 (2010).

25. Kuhlwilm, M. *et al.* Ancient gene flow from early modern humans into Eastern Neanderthals. *Nature* **530,** 429–433 (2016).

26. Fu, Q. *et al.* An early modern human from Romania with a recent Neanderthal ancestor. *Nature* **524,** 216–219 (2015).

27. Silva, N. M., Rio, J. & Currat, M. Investigating population continuity with ancient DNA under a spatially explicit simulation framework. *BMC Genet.* **18,** 114 (2017).

28. Brandt, G. *et al.* Ancient DNA Reveals Key Stages in the Formation of Central European Mitochondrial Genetic Diversity. *Science* **342,** 257–261 (2013).

29. Ghirotto, S. *et al.* Inferring Genealogical Processes from Patterns of Bronze-Age and Modern DNA Variation in Sardinia. *Mol. Biol. Evol.* **27,** 875–886 (2010).

30. Reich, D., Thangaraj, K., Patterson, N., Price, A. L. & Singh, L. Reconstructing Indian population history. *Nature* **461,** 489–494 (2009).

31. Moorjani, P. *et al.* Genetic evidence for recent population mixture in India. *Am J Hum Genet* **93,** 422–438 (2013).

32. Siska, V. *et al.* Genome-wide data from two early Neolithic East Asian individuals dating to 7700 years ago. *Sci. Adv.* **3,** e1601877 (2017).

33. Patterson, N. *et al.* Ancient Admixture in Human History. *Genetics* **192,** 1065–1093 (2012).

34. Piel, F. B. *et al.* Global distribution of the sickle cell gene and geographical confirmation of the malaria hypothesis. *Nat. Commun.* **1,** 104 (2010).

35. Patin, E. *et al.* Dispersals and genetic adaptation of Bantu-speaking populations in Africa and North America. *Science* **356,** 543–546 (2017).

36. Ammerman, A. J. & Cavalli-Sforza, L. L. *The Neolithic Transition and the Genetics of Populations in Europe*. (Princeton University Press, 2014).

Appendix A Appendix for Chapter 2

A.1 NGS sequencing statistics

Supplementary Table A.1 NGS data ouput from the test and HiSeq sequencing runs of Oase's libraries. "Rmdup" stands for results after the removal of clonal sequences and "rmdup30" after the removal of clonal sequencing and filtering for a mapping quality of at least 30. For more details, see section 2.6.2

Test sequencing run: NextSeq500 75PE

Library	Index	Pairs processed	Pairs merged	Mapped	Mapped rmdup	Mapped rmdup30	% endogenous	% duplicate
Bl004	4	833555	90192	26909	19998	14450	2.39	99.74
Bl288	288	1427469	902205	39728	8319	5945	0.58	99.71
eBb440	440	2382154	1608042	65978	11716	7856	0.49	82.24
eB200	200	3363366	2071394	82522	26945	18967	0.80	67.34
Oa1	220	23178331	17636104	8578143	8350749	6323583	36.02	2.65
Oa1b	610	40844664	28871250	15960082	15392302	11747066	37.68	3.55
Oa2	625	30550222	25577980	8511774	8315297	5644337	27.22	2.30
Oa3	687	51178692	36425021	17406697	16871246	12850859	32.96	3.07
Oa4	702	42278773	23253547	10360615	5558135	3488379	13.14	46.35
Oa5a	256	18453200	13055325	6153955	5999221	4519979	32.51	2.51
Oa5b	179	39033310	24724703	10894541	10446189	7788599	26.76	4.11
Oa6	475	6051604	4574323	2178206	2130496	1610837	35.20	2.19
1st sequencing run: HiSeq2500 50PE								
Oa1	220	218694705	166017467	81852475	76877139	61173573	35.15	6.07

Oa1b	610	219167211	155020497	86015028	78051448	61891296	35.61	9.25
Oa2	625	232139408	188593251	62873165	59956670	42397661	25.82	4.63
Oa3	687	207228837	148098807	71308759	67093026	53343783	32.37	5.91
Oa5a	256	246437576	174618955	83193552	77483404	61356779	31.44	6.86
Oa5b	179	236407674	151145092	67184491	58126474	44864529	24.58	13.48
Oa6	475	225576048	166619533	79427338	72109421	57074209	31.96	9.21
2nd sequencing run: HiSeq2500 50SE								
Oa1b	610	524609573	-	111235622	98002020	79427596	18.68	11.89
Oa3	687	443122797	-	112693437	103055243	84286502	23.25	8.55
Oa6	475	528482155	-	240654915	190258590	150359621	36.00	20.94
3rd sequencing run: HiSeq2500 50SE								
Oa1a	220	526882575		225577941	201793258	166711206	31.64	10.54
Oa5a	256	484243893		188043200	165783996	136752731	28.24	11.83
Oa5b	179	486687877		146261487	102429996	81378707	16.72	29.96
4rd sequencing run: HiSeq2500 50PE								
Oa1	610	591410490	341733401	203388411	183506479	151144450	44.22	9.77
Oa3	687	633224854	396530235	170367066	153152386	126245658	31.83	10.1
Oa5a	256	623366099	349413704	173617097	154964944	127357534	36.44	10.74

Appendix A Appendix for Chapter 2

Supplementary Table A.2 NGS data mapping to the mitochondrial reference (rCRS). “Rmdup” stands for results after the removal of clonal sequences and “rmdup30” after the removal of clonal sequencing and filtering for a mapping quality of at least 30. For more details, see section 2.6.2

Library	Index	Pairs processed	Pairs merged	Mapped	Mapped rmdup	Mapped rmdup30	mtDNA coverage
Oa1	220	218694705	166017467	67665	24856	24529	69.9x
Oa1b	610	219167211	155020497	85185	26178	25968	76.3x
Oa2	625	232139408	188593251	54760	24757	20528	61.4x
Oa3	687	207228837	148098807	60494	23985	23672	65.9x
Oa5a	256	246437576	174618955	80862	26018	25725	73.2x
Oa5b	179	236407674	151145092	70813	23900	23707	62.2x
Oa6	475	225576048	166619533	71971	25149	24856	70.5x
merged				168985	168985	168985	479.61x

A.2 Mitochondrial genome

Supplementary Table A.3 Polymorphic positions in the consensus mitochondrial genome of Oase 2 with regards the rCRS. Haplogroup assignment was performed using Haplogrep.

Defining haplogroup positions		Others (not expected)		Haplogroup	Quality
Polymorphism	**Coverage**	**Polymorphism**	**Coverage**	N	97.39%
73G	328	4113G	513		
263G	450	8155A	437		
750G	396	9456G	471		
1438G	472	16519C	357		
2706G	324				
4769G	509				
7028T	485				
8860G	400				
11719A	486				
12705T	591				
14766T	527				
15326G	370				
16223T	456				

A.3 Outgroup f_3 statistics for Oase 1 using modern populations

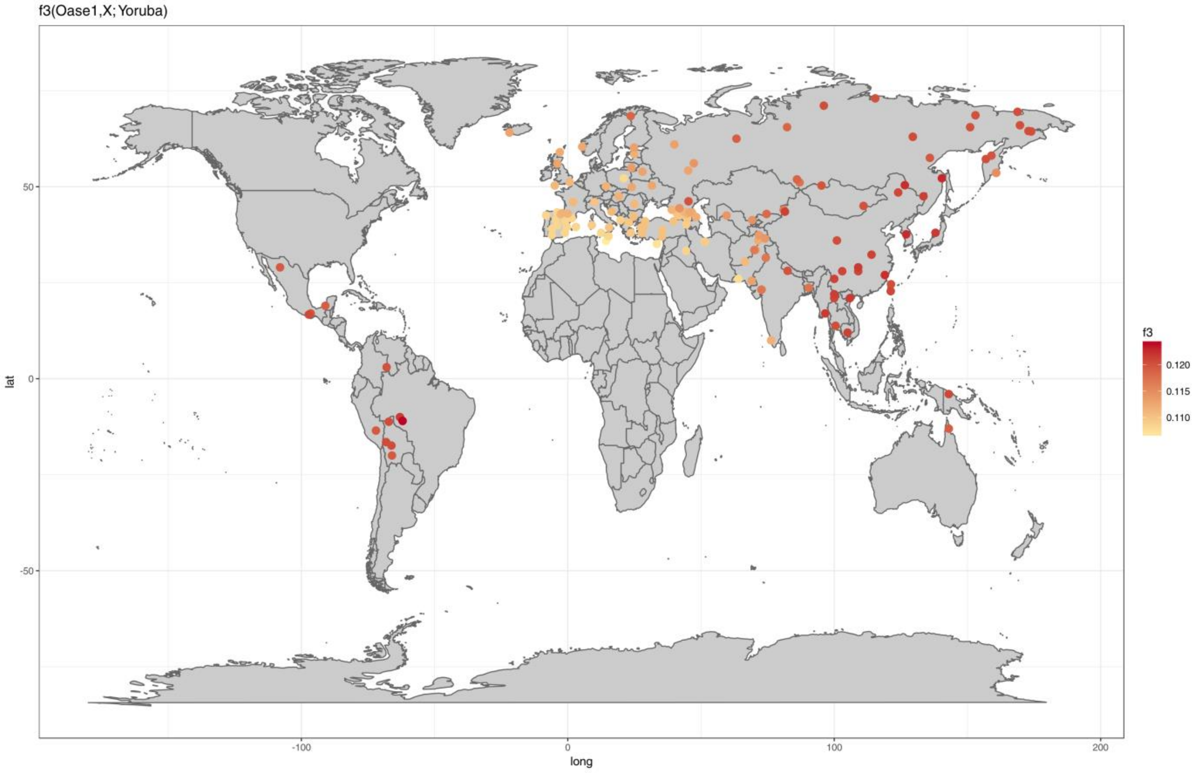

Supplementary Figure A.1 Outgroup f_3 statistics of the form f_3(Oase 1, X; Yoruba), 150 modern populations with the highest score displayed.

A.4 Outgroup f_3 statistics for Oase 2 on SNPs called in Oase 1

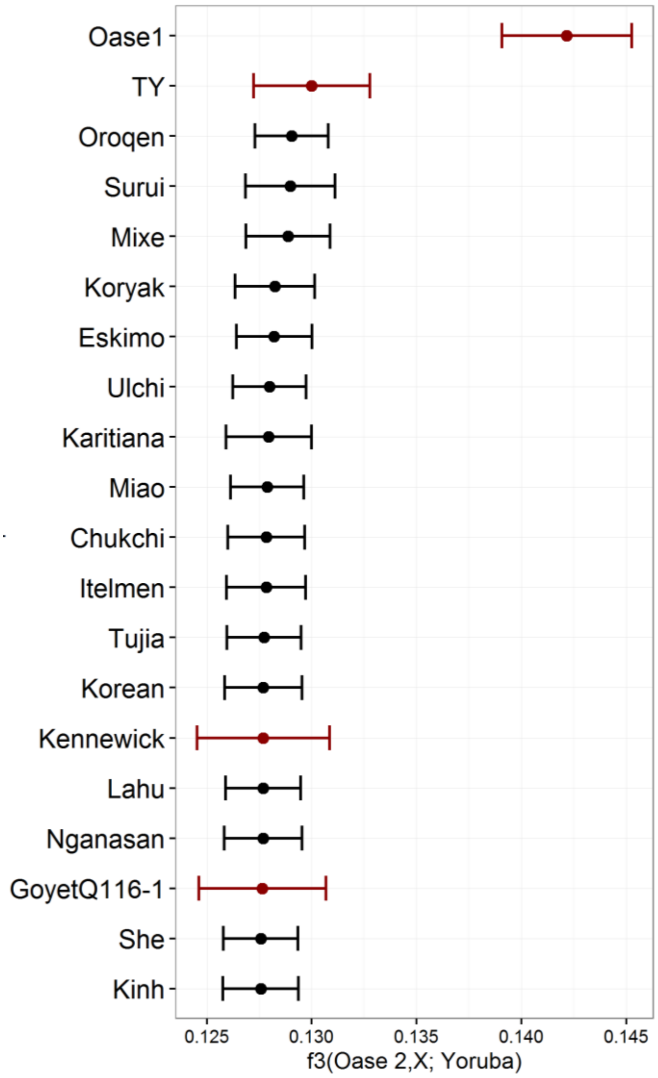

Supplementary Figure A.2 Outgroup f_3 statistics of the form f_3 (Oase 2, X; Yoruba), using only SNPs called in Oase 1. 20 populations with the highest score displayed. Ancient populations displayed in red and moderns in black.

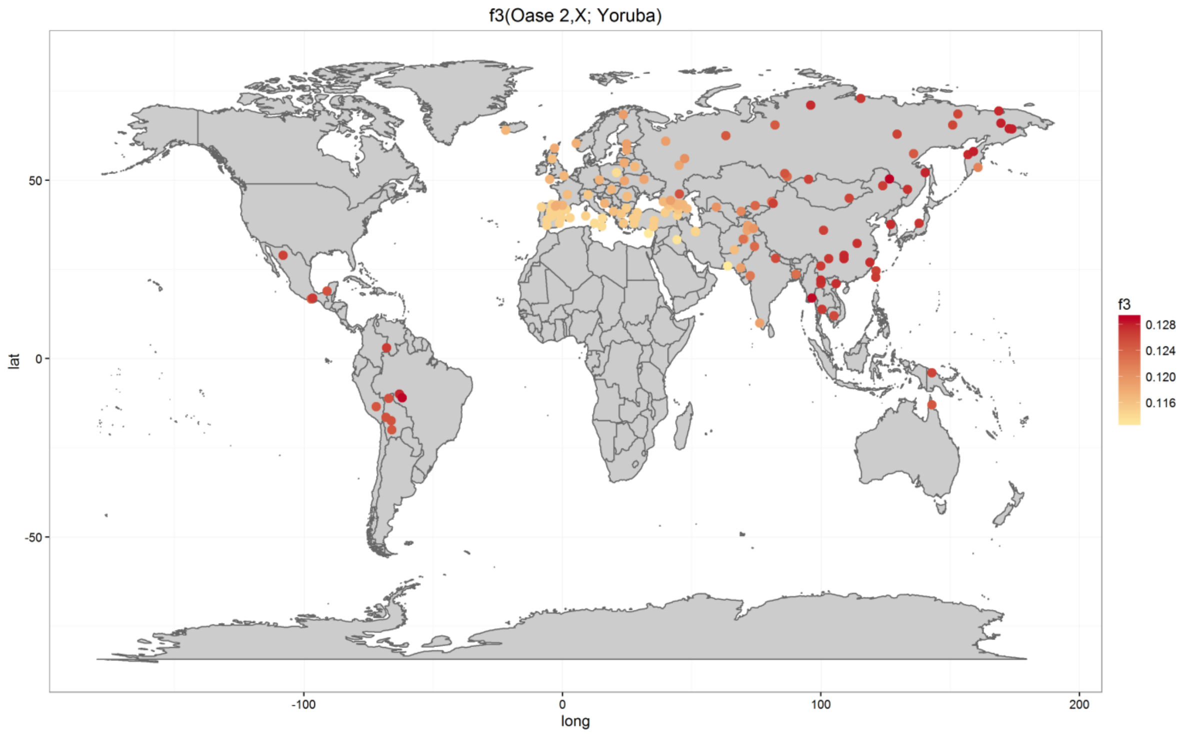

Supplementary Figure A.3 Outgroup f_3 statistics of the form f_3 (Oase 2, X; Yoruba), using only SNPs called in Oase 1. 150 modern populations with the highest score displayed.

A.5 African origins

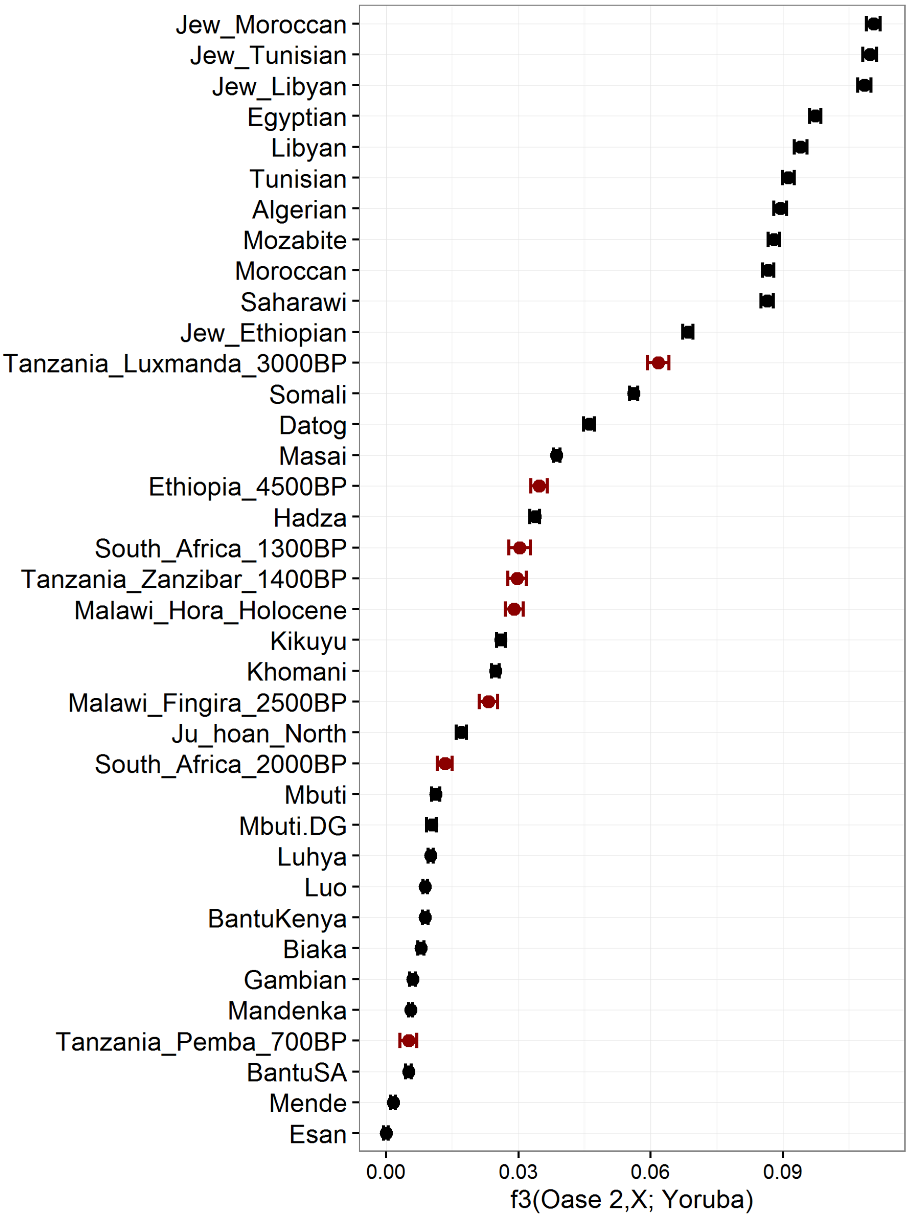

Supplementary Figure A.4 Outgroup f_3 statistics of the form f_3(Oase 2, X; Yoruba), where X is a modern (black) or ancient (red) African population.

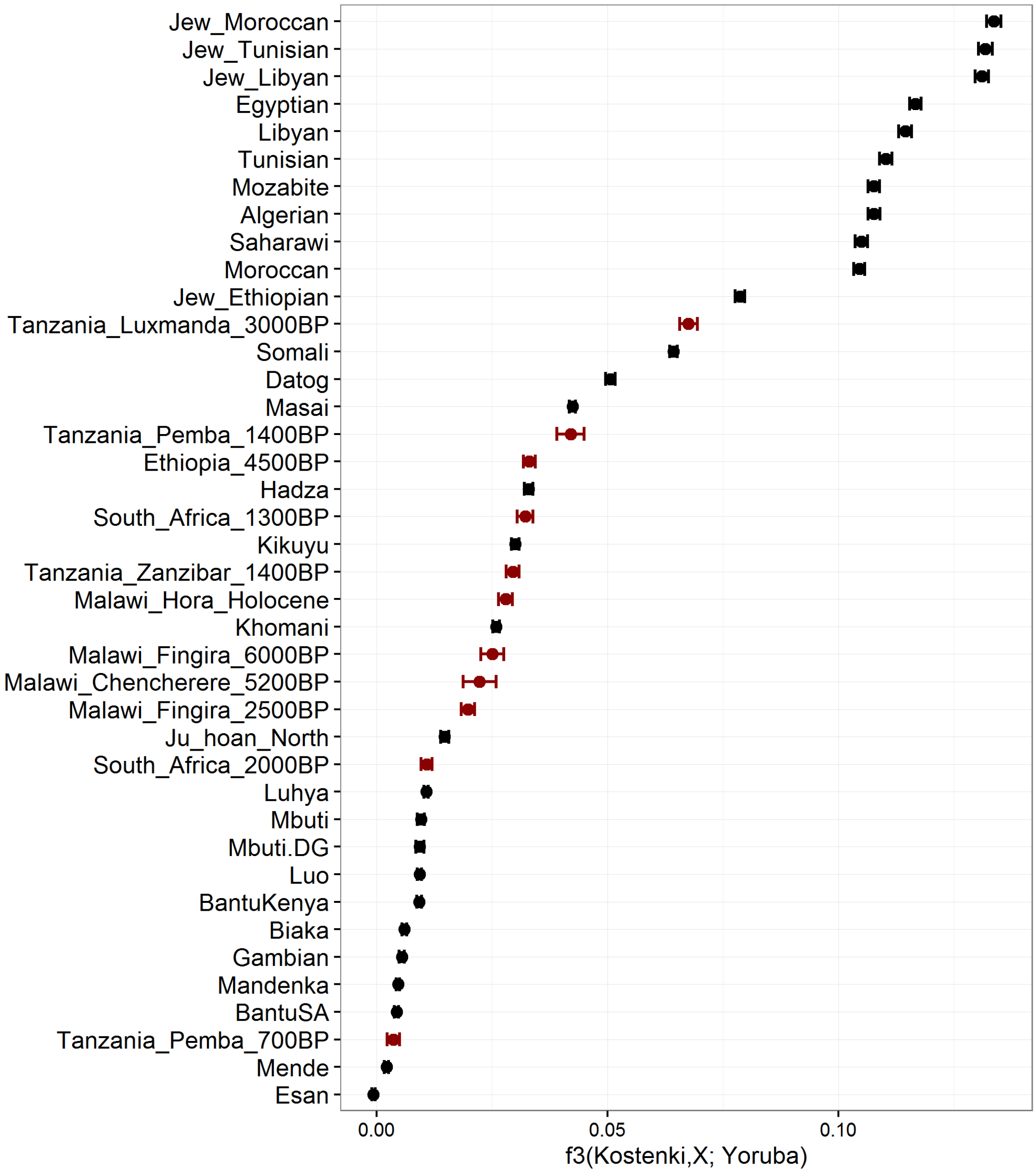

Supplementary Figure A.5 Outgroup f_3 statistics of the form f_3(Kostenki, X; Yoruba), where X is a modern (black) or ancient (red) African population.

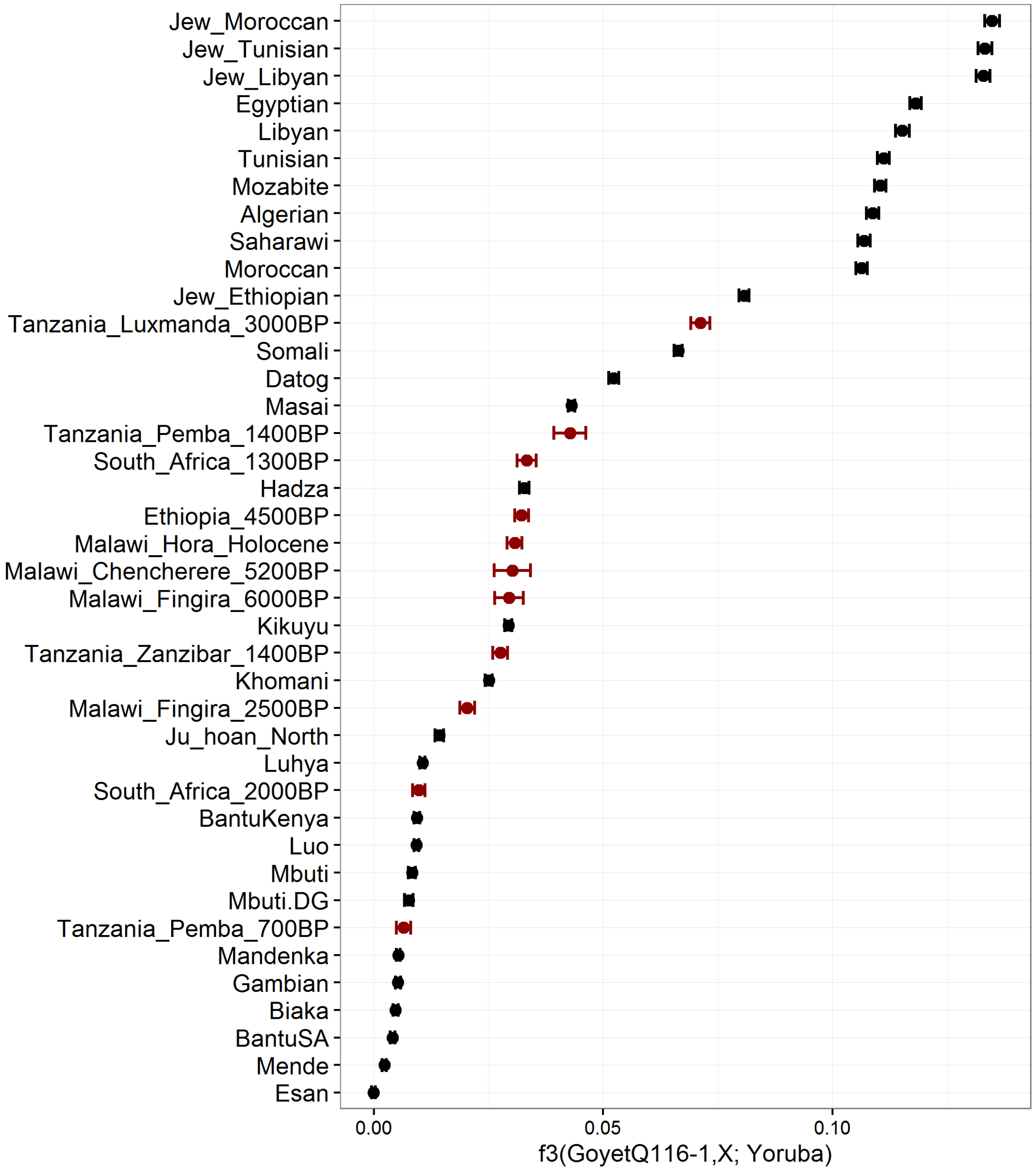

Supplementary Figure A.6 Outgroup f_3 statistics of the form f_3(GoyetQ116-1, X; Yoruba), where X is a modern (black) or ancient (red) African population.

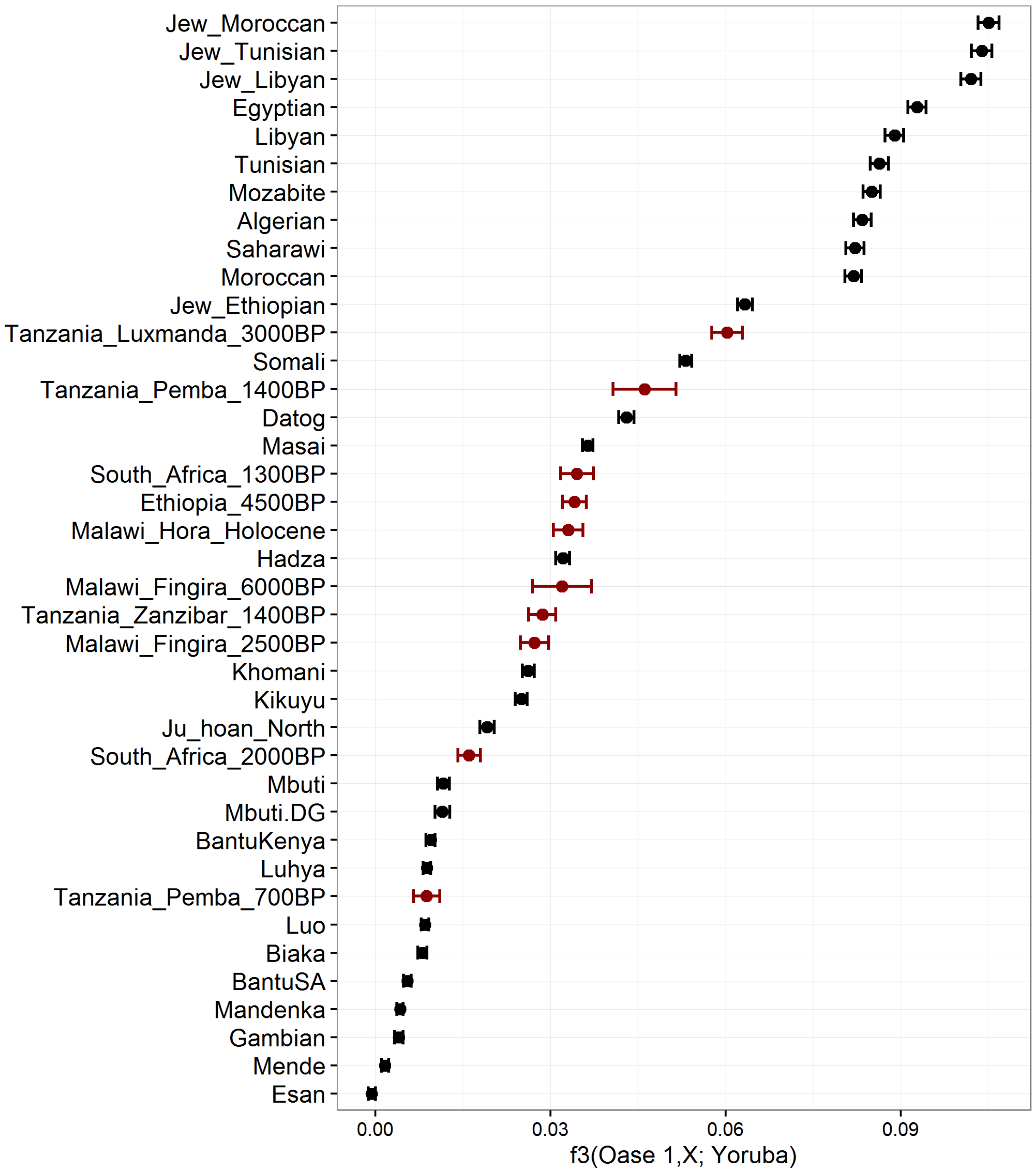

Supplementary Figure A.7 Outgroup f_3 statistics of the form f_3(Oase 1, X; Yoruba), where X a modern (black) or ancient (red) African population.

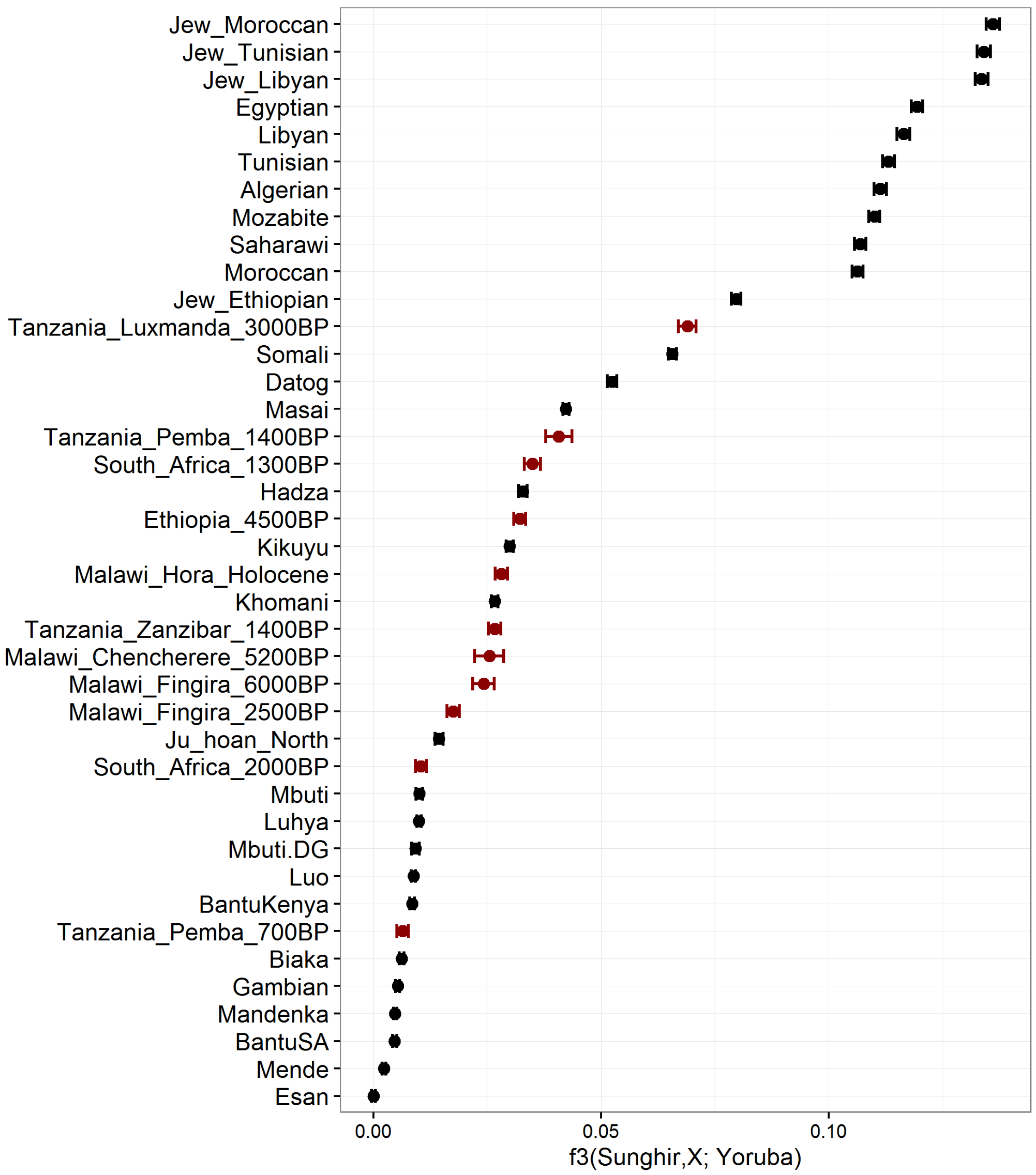

Supplementary Figure A.8 Outgroup f_3 statistics of the form f_3(Sunghir, X; Yoruba), where X is a modern (black) or ancient (red) African population

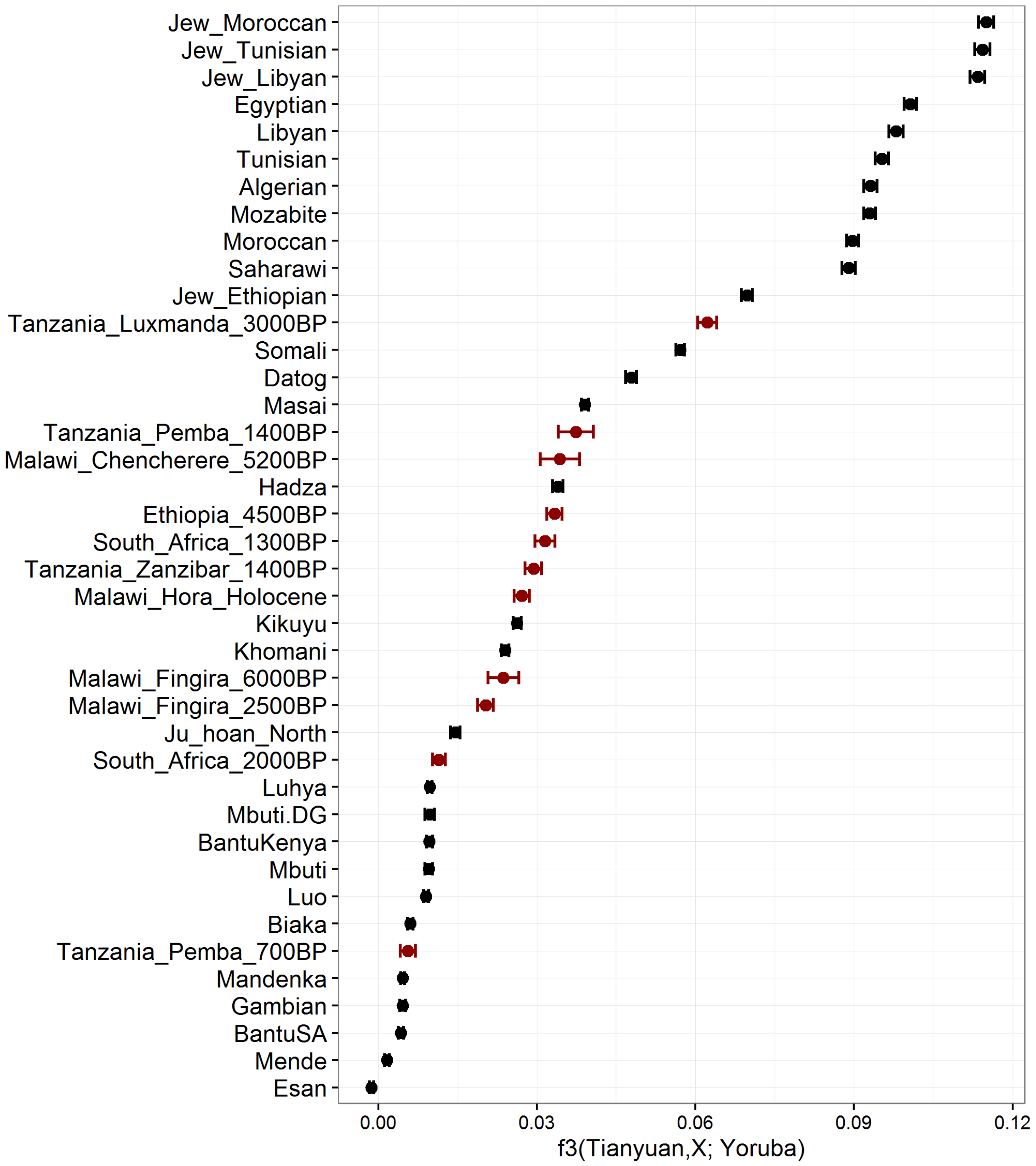

Supplementary Figure A.9 Outgroup f_3 statistics of the form f_3(Tianyuan, X; Yoruba), where X is a modern (black) or ancient (red) African population.

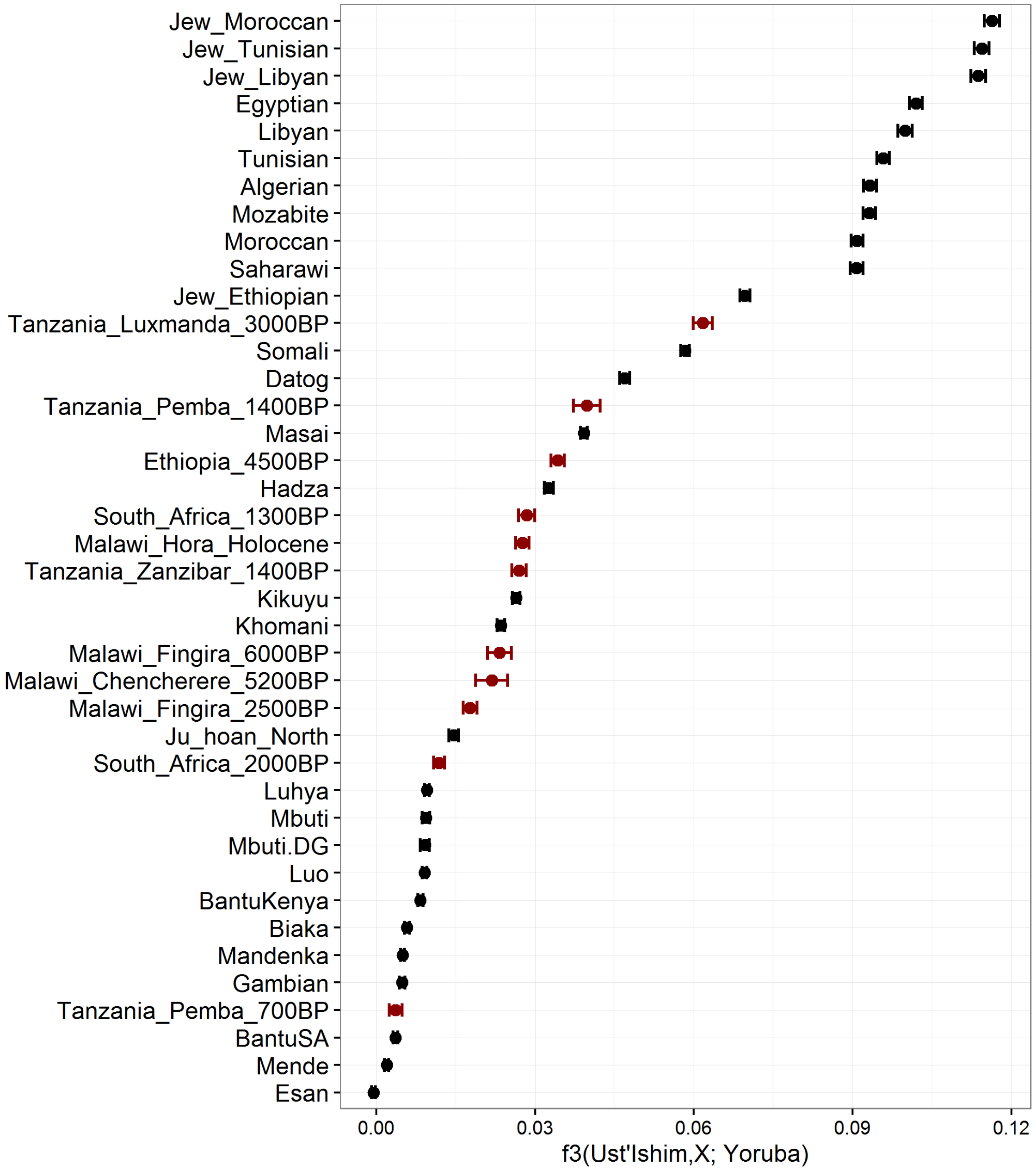

Supplementary Figure A.10 Outgroup f_3 statistics of the form f_3(Ust’Ishim, X; Yoruba), where X is a modern (black) or ancient (red) African population.

A.6 Comparison of Upper Palaeolithic genomes using D statistics

Supplementary Table A.4 D statistics of the form D(X, Y; Z, Yoruba), where X, Y and Z traverse all possible permutations of the following samples: Oase 1, Oase 2, Kostenki, Sunghir and Ust'Ishim, using all SNPs.

	X	**Y**	**Z**	**D**	**Z**	**SNP1**	**SNP2**	**nSNP**	
Kostenki	Kostenki	Ust'Ishim	Oase 2	0.0234	3.543	30547	29151	582106	**Oase 2**
	Ust'Ishim	Oase 2	Kostenki	-0.0134	-1.849	29738	30547	582106	
	Oase 2	Kostenki	Ust'Ishim	-0.01	-1.397	29151	29738	582106	
	Kostenki	Ust'Ishim	Oase 1	0.0189	2.168	6122	5895	119179	**Oase 1**
	Ust'Ishim	Oase 1	Kostenki	-0.031	-3.542	5755	6122	119179	
	Oase 1	Kostenki	Ust'Ishim	0.0121	1.305	5895	5755	119179	
Sunghir	Sunghir	Ust'Ishim	Oase 2	0.0234	3.41	30712	29309	584445	**Oase 2**
	Ust'Ishim	Oase 2	Sunghir	-0.0175	-2.439	29655	30712	584445	
	Oase 2	Sunghir	Ust'Ishim	-0.0059	-0.813	29309	29655	584445	
	Sunghir	Ust'Ishim	Oase 1	0.0286	3.658	6166	5823	119337	**Oase 1**
	Ust'Ishim	Oase 1	Sunghir	-0.0356	-4.17	5742	6166	119337	
	Oase 1	Sunghir	Ust'Ishim	0.007	0.849	5823	5742	119337	

Supplementary Table A.5 D statistics of the form D(X, Y; Z, Yoruba), where X, Y and Z traverse all possible permutations of the following samples: Oase 1, Oase 2, Kostenki, Sunghir and Ust'Ishim; using only SNPs called in Oase 1.

	X	**Y**	**Z**	**D**	**Z**	**SNP1**	**SNP2**	**nSNP**	
Kostenki	Kostenki14	Ust_Ishim	Oase 2	0.0216	2.647	6071	5814	131947	**Oase 2**
	Ust_Ishim	Oase 2	Kostenki14	-0.015	-1.758	5891	6071	131947	
	Oase 2	Kostenki14	Ust_Ishim	-0.0065	-0.778	5814	5891	131947	
	Kostenki14	Ust_Ishim	Oase 1	0.0194	2.193	6104	5872	118938	**Oase 1**
	Ust_Ishim	Oase 1	Kostenki14	-0.0309	-3.494	5738	6104	118938	
	Oase 1	Kostenki14	Ust_Ishim	0.0115	1.241	5872	5738	118938	
Sunghir	Sunghir	Ust_Ishim	Oase 2	0.0223	2.831	6143	5875	132452	**Oase 2**
	Ust_Ishim	Oase 2	Sunghir	-0.0195	-2.368	5908	6143	132452	
	Oase 2	Sunghir	Ust_Ishim	-0.0028	-0.33	5875	5908	132452	
	Sunghir	Ust_Ishim	Oase 1	0.0289	3.655	6148	5803	119096	**Oase 1**
	Ust_Ishim	Oase 1	Sunghir	-0.0356	-4.2	5725	6148	119096	
	Oase 1	Sunghir	Ust_Ishim	0.0067	0.806	5803	5725	119096	

A.7 Convergence of G-PhoCS Monte Carlo chains

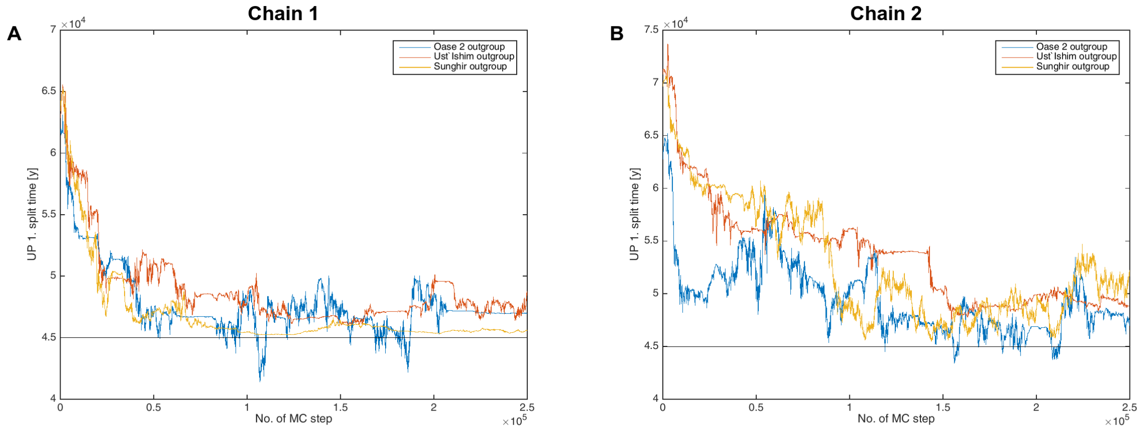

Supplementary Figure A.11 Traces of split times between the pair of Upper Palaeolithic genomes that merge first, from simulations with all three Upper Palaeolithic genomes (Oase 2, Ust'Ishim and Sunghir). A. and B. show the two independent Monte Carlo chains. Black line marks the age of Ust'Ishim, the oldest sample in the simulation. The first 100,000 steps were discarded as burn-in.

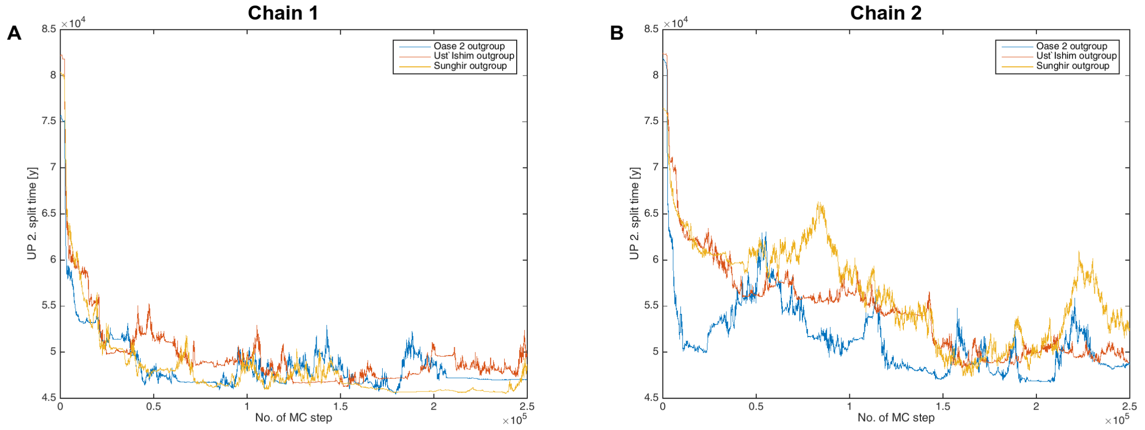

Supplementary Figure A.12 Traces of split times between the outgroup Upper Palaeolithic genome and the pair of Upper Palaeolithic genomes that merged first, from simulations with all three Upper Palaeolithic genomes (Oase 2, Ust'Ishim and Sunghir). A. and B. show the two independent Monte Carlo chains. Black line marks the age of Ust'Ishim, the oldest sample in the simulation. The first 100,000 steps were discarded as burn-in.

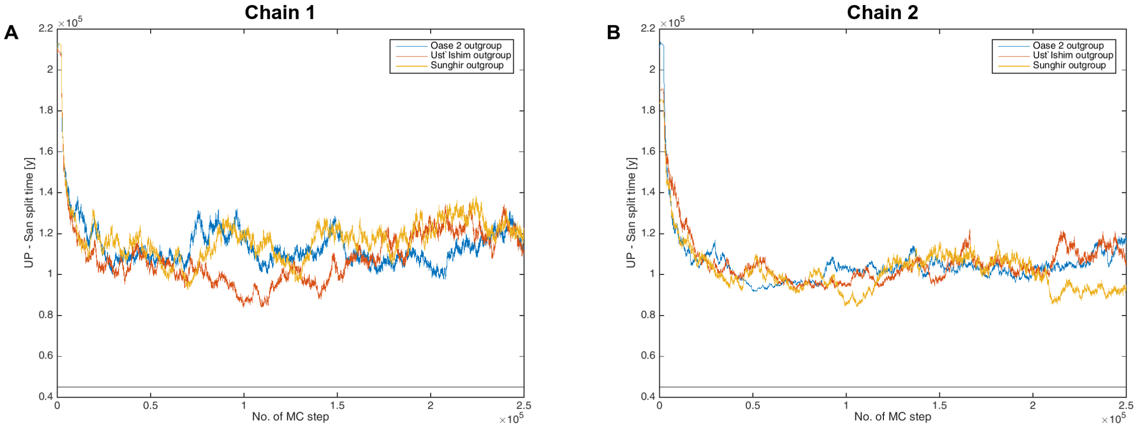

Supplementary Figure A.13 Traces of split times between the San and the common ancestor of all Upper Palaeolithic samples, from simulations with all three Upper Palaeolithic genomes (Oase 2, Ust'Ishim and Sunghir). A. and B. show the two independent Monte Carlo chains. Black line marks the age of Ust'Ishim, the oldest sample in the simulation. The first 100,000 steps were discarded as burn-in.

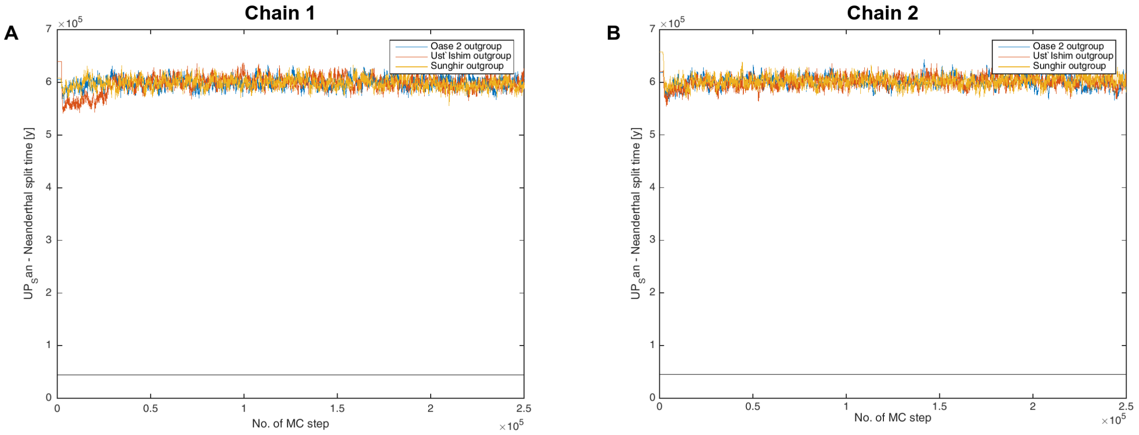

Supplementary Figure A.14 Traces of split times between the Altai Neanderthal and the common ancestor of all Upper Palaeolithic samples and the San, from simulations with all three Upper Palaeolithic genomes (Oase 2, Ust'Ishim and Sunghir). A. and B. show the two independent Monte Carlo chains. Black line marks the age of Ust'Ishim, the oldest sample in the simulation. The first 100,000 steps were discarded as burn-in.

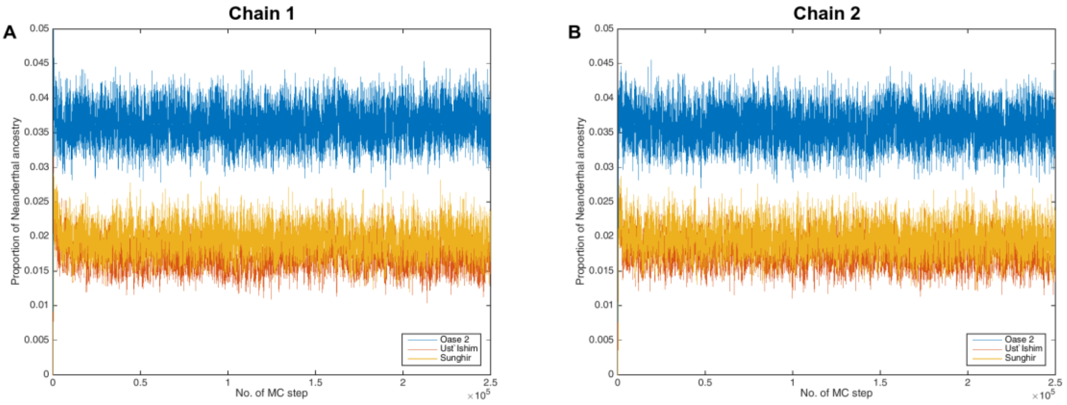

Supplementary Figure A.15 Traces of the proportion of Neanderthal ancestry for all three Upper Palaeolithic genomes (Oase 2, Ust’Ishim and Sunghir), from simulations where Oase 2 was the outgroup. A. and B. show the two independent Monte Carlo chains.

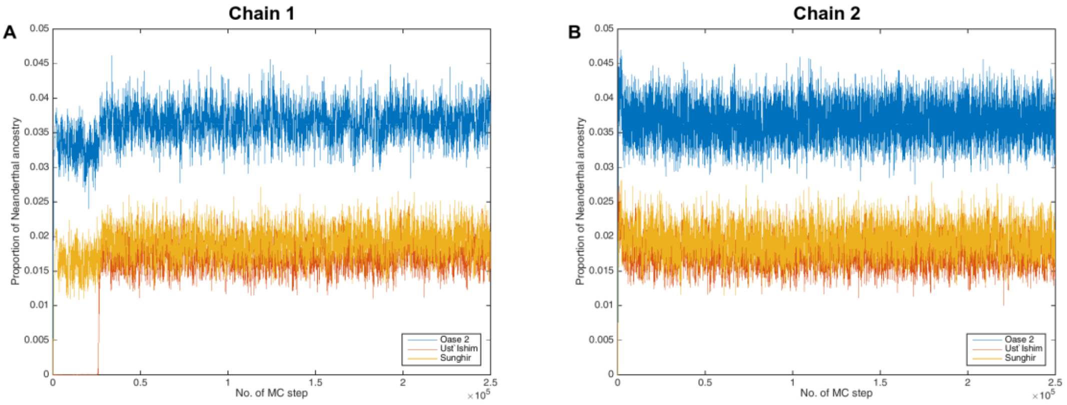

Supplementary Figure A.16 Traces of the proportion of Neanderthal ancestry for all three Upper Palaeolithic genomes (Oase 2, Ust’Ishim and Sunghir), from simulations where Sunghir was the outgroup. A. and B. show the two independent Monte Carlo chains.

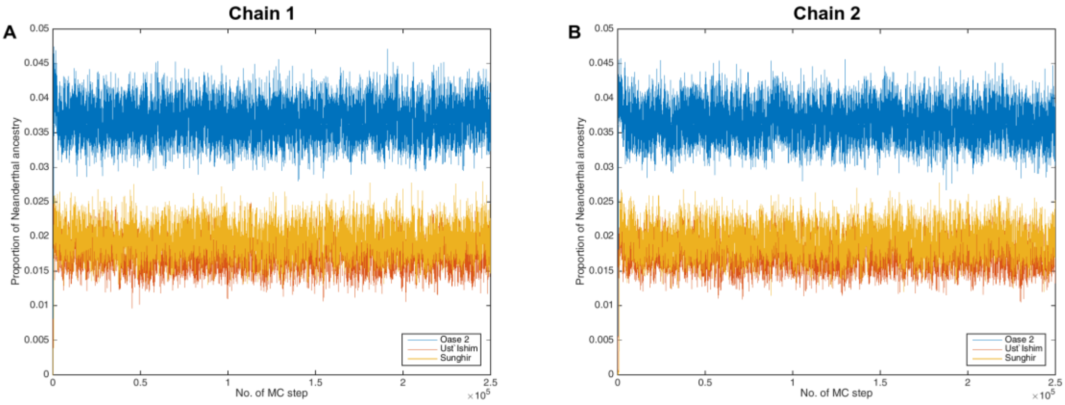

Supplementary Figure A.17 Traces of the proportion of Neanderthal ancestry for all three Upper Palaeolithic genomes (Oase 2, Ust'Ishim and Sunghir), from simulations where Ust'Ishim was the outgroup. A. and B. show the two independent Monte Carlo chains.

A.8 Detailed G-PhoCS results

Supplementary Table A.6 Results of coalescent modelling on a tree consisting of Oase 2, Ust'Ishim, San and the Altai Neanderthal. N denotes estimated population sizes, t split times and m proportions of Neanderthal ancestry.

	Mean	Median	Standard deviation	0.025 quantile	0.975 quantile
$N_{Neanderthal}$	3,902	3,900	74	3,758	4,050
N_{San}	17,729	17,473	1,724	14,995	21,635
N_{Oase}	3,740	3,511	1,174	2,186	6,433
$N_{Ust'Ishim}$	9,644	9,026	5,756	2,171	23,578
$N_{Oase\text{-}Ust'Ishim}$	2,622	2,538	593	1,706	3,841
$N_{Oase\text{-}Ust'Ishim\text{-}San}$	35,321	35,446	1,235	32,740	37,503
$N_{Oase\text{-}Ust'Ishim\text{-}San\text{-}Neanderthal}$	20,883	20,883	228	20,439	21,328
$t_{Oase\text{-}Ust'Ishim}$	53,051	52,340	4,572	47,407	62,646
$t_{Oase\text{-}Ust'Ishim\text{-}San}$	98,963	96,400	8,076	88,760	117,619
$t_{Oase\text{-}Ust'Ishim\text{-}San\text{-}Neanderthal}$	597,646	597,300	9,898	578,931	617,706
$m_{Neanderthal\text{-}>Oase}$	3.70%	3.70%	0.24%	3.25%	4.18%
$m_{Neanderthal\text{-}> Ust'Ishim}$	1.73%	1.73%	0.21%	1.33%	2.15%

Supplementary Table A.7 Results of coalescent modelling on a tree consisting of Oase 2, Sunghir, San and the Altai Neanderthal. N denotes estimated population sizes, t split times and m proportions of Neanderthal ancestry.

	Mean	Median	Standard deviation	0.025 quantile	0.975 quantile
$N_{\mathbf{Neanderthal}}$	3,882	3,881	76	3,736	4,032
$N_{\mathbf{San}}$	23,357	23,314	2,380	18,856	28,159
$N_{\mathbf{Oase}}$	4,317	4,179	1,781	1,408	8,157
$N_{\mathbf{Sunghir}}$	1,587	1,565	498	731	2,634
$N_{\mathbf{Oase\text{-}Sunghir}}$	4,203	4,265	811	2,500	5,753
$N_{\mathbf{Oase\text{-}Sunghir\text{-}San}}$	31,522	31,462	1,477	28,715	34,482
$N_{\mathbf{Oase\text{-}Sunghir\text{-}San\text{-}Neanderthal}}$	20,833	20,833	239	20,362	21,302
$t_{\mathbf{Oase\text{-}Sunghir}}$	53,106	52,860	6,030	42,661	65,770
$t_{\mathbf{Oase\text{-}Sunghir\text{-}San}}$	127,848	128,063	11,341	105,134	150,073
$t_{\mathbf{Oase\text{-}Sunghir\text{-}San\text{-}Neanderthal}}$	592,248	592,240	10,196	572,254	612,760
$m_{\mathbf{Neanderthal\text{-}>Oase}}$	3.23%	3.23%	0.25%	2.75%	3.72%
$m_{\mathbf{Neanderthal\text{-}>Sunghir}}$	2.13%	2.13%	0.23%	1.68%	2.60%

Supplementary Table A.8 Results of coalescent modelling on a tree consisting of Sunghir, Ust'Ishim, San and the Altai Neanderthal. N denotes estimated population sizes, t split times and m proportions of Neanderthal ancestry.

	Mean	Median	Standard deviation	0.025 quantile	0.975 quantile
$N_{Neanderthal}$	3,837	3,837	74	3,692	3,982
N_{San}	25,356	25,329	2,228	20,785	29,753
$N_{Sunghir}$	1,527	1,440	372	1,061	2,486
$N_{Ust'Ishim}$	15,676	13,665	8,766	4,153	37,374
$N_{Sunghir\text{-}Ust'Ishim}$	4,920	4,968	655	3,286	6,030
$N_{Sunghir\text{-}Ust'Ishim\text{-}San}$	29,689	29,632	1,324	27,230	32,679
$N_{Sunghir\text{-}Ust'Ishim\text{-}San\text{-}Neanderthal}$	21,091	21,089	233	20,630	21,548
$t_{Sunghir\text{-}Ust'Ishim}$	51,399	50,427	4,237	46,233	62,445
$t_{Sunghir\text{-}Ust'Ishim\text{-}San}$	141,476	141,563	10,222	116,054	160,026
$t_{Sunghir\text{-}Ust'Ishim\text{-}San\text{-}Neanderthal}$	584,077	584,003	9,765	564,947	603,323
$m_{Neanderthal\text{->}Sunghir}$	1.93%	1.93%	0.22%	1.50%	2.37%
$m_{Neanderthal\text{->} Ust'Ishim}$	1.59%	1.59%	0.20%	1.19%	1.99%

Supplementary Table A.9 Results of coalescent modelling on a tree with all three high quality Upper Palaeolithic genomes, with Sunghir as the outgroup out of the three. N denotes estimated population sizes, t split times and m proportions of Neanderthal ancestry.

	Mean	Median	Standard deviation	0.025 quantile	0.975 quantile
$N_{\text{Neanderthal}}$	3,931	3,932	75	3,785	4,078
N_{San}	19,070	18,932	2,037	15,338	23,270
N_{Oase}	2,807	2,656	654	1,943	4,437
$N_{\text{Ust'Ishim}}$	7,912	6,468	5,398	2,049	21,260
N_{Sunghir}	1,354	1,310	225	1,057	1,918
$N_{\text{Oase-Ust'Ishim}}$	9,075	7,263	7,506	757	29,766
$N_{\text{Oase-Ust'Ishim-Sunghir}}$	3,292	3,268	597	2,235	4,364
$N_{\text{Oase-Ust'Ishim-Sunghir-San}}$	34,837	34,943	1,486	31,988	37,618
$N_{\text{Oase-Ust'Ishim-Sunghir-San-Neanderthal}}$	20,701	20,695	231	20,249	21,159
$t_{\text{Oase-Ust'Ishim}}$	49,011	48,560	2,443	46,280	54,907
$t_{\text{Oase-Ust'Ishim-Sunghir}}$	49,643	49,140	2,529	46,670	56,047
$t_{\text{Oase-Ust'Ishim-Sunghir-San}}$	107,468	106,407	10,014	88,097	126,625
$t_{\text{Oase-Ust'Ishim-Sunghir-San-Neanderthal}}$	601,101	601,180	9,654	582,397	619,912
$m_{\text{Neanderthal->Oase}}$	3.66%	3.66%	0.22%	3.25%	4.09%
$m_{\text{Neanderthal-> Ust'Ishim}}$	1.75%	1.74%	0.17%	1.42%	2.08%
$m_{\text{Neanderthal->Sunghir}}$	1.93%	1.93%	0.19%	1.58%	2.31%

Supplementary Table A.10 Results of coalescent modelling on a tree with all three high quality Upper Palaeolithic genomes, with Ust’Ishim as the outgroup out of the three. N denotes estimated population sizes, t split times and m proportions of Neanderthal ancestry.

	Mean	Median	Standard deviation	0.025 quantile	0.975 quantile
$N_{\text{Neanderthal}}$	3,929	3,928	76	3,780	4,079
N_{San}	19,103	18,987	1,507	16,494	22,447
N_{Oase}	2,394	2,337	485	1,547	3,581
$N_{\text{Ust’Ishim}}$	8,391	6,608	5,778	2,108	23,418
N_{Sunghir}	1,158	1,146	154	870	1,557
$N_{\text{Oase- Sunghir}}$	12,243	10,366	9,613	382	36,830
$N_{\text{Oase- Sunghir –Ust’Ishim}}$	3,375	3,320	379	2,813	4,262
$N_{\text{Oase- Sunghir –Ust’Ishim-San}}$	34,857	34,928	1,067	32,507	36,765
$N_{\text{Oase- Sunghir –Ust’Ishim-San-Neanderthal}}$	20,701	20,704	224	20,265	21,146
$t_{\text{Oase- Sunghir}}$	47,306	47,113	1,718	44,113	51,583
$t_{\text{Oase-Sunghir –Ust’Ishim}}$	48,526	48,167	1,847	46,207	53,670
$t_{\text{Oase- Sunghir –Ust’Ishim-San}}$	107,739	106,103	6,288	98,893	123,096
$t_{\text{Oase- Sunghir –Ust’Ishim-San-Neanderthal}}$	600,627	600,653	9,799	580,864	620,076
$m_{\text{Neanderthal->Oase}}$	3.65%	3.65%	0.22%	3.24%	4.08%
$m_{\text{Neanderthal-> Ust’Ishim}}$	1.71%	1.71%	0.17%	1.37%	2.06%
$m_{\text{Neanderthal->Sunghir}}$	1.93%	1.93%	0.19%	1.56%	2.32%

Supplementary Table A.11 Results of coalescent modelling on a tree with all three high quality Upper Palaeolithic genomes, with Oase 2 as the outgroup out of the three. N denotes estimated population sizes, t split times and m proportions of Neanderthal ancestry.

	Mean	Median	Standard deviation	0.025 quantile	0.975 quantile
$N_{Neanderthal}$	3,925	3,925	74	3,780	4,072
N_{San}	19,390	19,425	2,356	15,101	23,872
N_{Oase}	2,944	2,618	1,036	1,716	5,261
$N_{Ust'Ishim}$	6,621	5,150	5,478	717	20,249
$N_{Sunghir}$	1,170	1,092	198	942	1,638
$N_{Sunghir-Ust'Ishim}$	8,486	6,933	6,993	438	26,946
$N_{Sunghir-Ust'Ishim-Oase}$	3,417	3,456	875	1,791	4,817
$N_{Sunghir-Ust'Ishim-Oase-San}$	34,641	34,640	1,739	31,398	38,027
$N_{Sunghir-Ust'Ishim-Oase-San-Neanderthal}$	20,707	20,707	235	20,239	21,158
$t_{Sunghir-Ust'Ishim}$	47,319	46,120	2,208	45,260	52,553
$t_{Sunghir-Ust'Ishim-Oase}$	49,739	48,487	4,015	45,660	58,516
$t_{Sunghir-Ust'Ishim-Oase-San}$	109,563	109,013	12,290	87,337	131,259
$t_{Sunghir-Ust'Ishim-Oase-San-Neanderthal}$	600,336	600,047	9,837	581,384	619,811
$m_{Neanderthal->Oase}$	3.60%	3.60%	0.22%	3.18%	4.03%
$m_{Neanderthal-> Ust'Ishim}$	1.73%	1.73%	0.18%	1.39%	2.08%
$m_{Neanderthal->Sunghir}$	1.94%	1.94%	0.19%	1.57%	2.33%

Appendix B Appendix for Chapter 3

B.1 Archaeological context

B.1.1 Kotias Klde

Kotias Klde (Supplementary Figure B.6) is a rockshelter located at 707 m above sea level (a.s.l.) on a limestone plateau above the Kvirila River in western Georgia. Excavations took place from 2003-2006 and in 2010. The exposed stratigraphy showed four layers without attaining bedrock. Below we provide a description of the stratigraphy from top to bottom.

Layer A1 was 30 cm deep and contained the remains of a shallow pit-house, 2.5/3.0 m in diameter, which was dug into the underlying layers (A2 and B). Though there were a few pottery shards of Bronze Age and later periods, most of the material at the base of the layer belonged to the local Late Neolithic period, generally referred to as 'Eneolithic'. These finds included a clay figurine[84]with nearby charcoal dated to 5,820 ± 40 uncal. BP (OS-90616).

Layer A2 contained a distinct lithic industry with transverse, trapezoid arrowheads. Special forms of denticulates known as "Lekalo" or "Kmlo" tools[85–87], often retouched on the ventral face, were represented in this assemblage. Flake scrapers, including the thumb-nail type, were also found. Blade cores and some production waste (debitage) reflect on-site blade reduction for secondary shaping of tools. A similar industry was reported in Neolithic sites of the region such as the Darkveti rockshelter, ca. 5 km away in the Kvirila river gorge[88], and

Paluri, which is situated further away on the Enguri river[86]. Charcoal from this layer was dated to 7,430 ± 40 uncal. BP (OS-63263).

Layer A2 contained the grave of a complete skeleton from a young adult male (ca. 30-35 years old) whom we have called “Kotias”. The grave was dug from this layer into layer B. The skeleton was laid in supine position and stones were placed over certain parts of the skeleton which crushed the skull and covered the knees and lower limb bones. The skull was angled with the right side facing upwards. Both the right and left hands, which lay along the side of the skeleton, covered the groin area. A 15 cm long bone splinter was found in the chest cavity of the specimen below the cervical vertebrae and above the clavicle on the right side. It cannot be affirmed, however, that this splinter was the cause of death. It appears that there were some pathological lesions on the right first rib. Other traumatic and degenerative pathological conditions were evident on the left calcaneus and talus. Attrition of the teeth was intense, especially when taking the relatively young age of the specimen into consideration. Two superimposed shallow hearths were exposed some 20 cm above the skeleton’s legs probably either indicating the sealing of the grave or a later occupation. A sample from one of the hearths was dated to 8,370 ± 55 uncal. BP (RTT 5220). A tibia from the skeleton was directly dated to 8,665 ± 65 uncal. BP (RTT 5246) and a mandibular fragment to 8,745 ± 40 uncal. BP (OxA-28256). A combined calibrated plot provided an interval of 9,529-9,895 cal. BP (95.4%, 2 s.d.).

Layer B, interspersed with limestone fragments, was 50-60cm thick and subdivided into three sub-layers (B1-B3) all of which contained evidence of Mesolithic industry and animal bones. A total of nine radiocarbon dates from animal bones and charcoal of this layer yielded a calibrated interval range of 10,300-13,000 cal. BP. Artefacts were made of flint, radiolarite, rare crystal rock, and obsidian (the latter was obtained from exposures some 80 km away). The main tool groups were backed and retouched bladelets. Numerous scalene triangles shaped by bi-polar retouch from blades and bladelets define the Mesolithic industry[89]. In addition, a few bone tools were recovered, including a handle made of a red deer antler hollowed for hafting a tool, as well as several point tips.

Layer C, consisting of yellow, compact clay/loamy sediment, was exposed to a very limited extent. The lithic industry was of Upper Palaeolithic age characterized by blade production and the presence of end-scrapers and burins. A total of 9 radiocarbon dates from animal bones and charcoal of this layer yielded a calibrated interval range of 22,200-23,600 cal. BP. The time gap between these two occupations (Layers B and C) indicates that the cave was not inhabited during the Last Glacial Maximum (LGM) and for quite some time after the LGM until the Younger Dryas and the first millennium of the Holocene.

B.1.2 Satsurblia

Satsurblia cave in western Georgia (Supplementary Figure B.6) was discovered in 1975 by A. N. Kalandadze[90] who excavated it sporadically during 1976, 1985–88 and 1990-1993[91]. A second series of excavations was conducted during 2008–2010, directed by Tengiz Meshveliani.

Further excavations in Satsurblia (2012-2013), directed by Tengiz Meshveliani and Ron Pinhasi, were conducted in two areas. Area A was situated in the north-western part of the cave, near the entrance (squares R−T 20−24) and Area B was to the rear of the cave (squares T−Z 4−7), adjacent to a trench excavated by K. Kalandadze in the 1980s. Both areas revealed stratigraphic sequences comprising Pleistocene (Upper Palaeolithic) and Holocene (Eneolithic and later) deposits. Excavations in 2012 and 2013 focused on Areas A and B with both yielding in situ Upper Palaeolithic layers that were extremely rich in finds (a circular fireplace, large quantities of charcoal and brunt bones, lithics, bone tools, shell ornaments, yellow ochre) and which continued to unknown depth. The Upper Palaeolithic sequence of Area A was divided into two main units: A/I and A/II. A/II contained a sequence of living surfaces which were dated (surface II and III) to 17,000-18,000 cal. BP and as such are the first well-dated evidence for human occupation in the southern Caucasus at the end of the

LGM. This fills a gap in the Upper Palaeolithic sequence, namely that between Unit C and Unit B in Dzudzuana Cave (western Georgia), dated to 27,000-24,000 cal. BP and 16,000 cal. BP - 13,200 cal. BP respectively.

Preliminary analyses of lithics from Satsurblia cave reveal a cultural variant which resembles Eastern Epi-Gravettian industries, dominated by bladelets and including varieties of microgravette points and bigger gravette points. A rectangular tool type was novel to excavations from the region and differed from the geometric trapezoid-rectangle tools of the proceeding Mesolithic cultures in size, shape and retouch[92] Direct AMS dating of human remains from Area B yielded the first securely dated Upper Palaeolithic human remains from the Caucasus. “Satsurblia” was sampled from a right temporal bone which was recovered in 2013 from square Y5 and dated to 11,415 ± 50 uncal. BP (OxA-34632). A combined calibrated plot provided an interval of 13,132-13,380 cal. BP (95.4%, 2 s.d.).

B.1.3 Grotte du Bichon

The small cave “Grotte du Bichon” is situated in the Swiss Jura Mountains, a few kilometres north of the city of La Chaux-de-Fonds (canton Neuchâtel), at an altitude of 845 m a.s.l. (Supplementary Figure B.6). During its first excavation, undertaken by speleologists in 1956, bones of a young man were discovered intermingled with the remains of a female brown bear (*Ursus arctos*) and nine flint projectile points, apparently stemming from the hunter’s weapons.

Both skeletons as well as the flints were located about 15 m from the entrance, at a recess of the cave, and were associated with charcoal concentrations but with no other archaeological material. Although a hunting accident was already envisioned at that time, without further indications the remains of the bear were considered not to be related to the human skeleton and therefore stored at the natural history museum of La Chaux-de-Fonds, while the human bones and the flints were kept in the archaeology museum of Neuchâtel (Laténium).

Only in 1991, during re-examination of the animal bone material, archaeozoologist Philippe Morel discovered an impact trace and two flint chips (probably a broken tip of an arrowhead) in a cervical vertebra of the bear, thus establishing a clear connection between the animal and the man[93]. This discovery prompted new excavations that were carried out between 1991 and 1995. During these new investigations, using modern excavation techniques (including water sieving), all of the missing long bones from the two skeletons were recovered, together with some more flint artefacts. The small lithic assemblage now contained 10 backed points, 16 backed bladelets and one retouched blade fragment, characteristic of final (Azilian) Palaeolithic industries. It seems that the cave was never used as a camp site as unretouched debitage products were not recovered. Four radiocarbon measurements performed on the bones from the bear and the man (two on each) and eight dates obtained from charcoal, from willow (*Salix sp.*) and from pine (*Pinus sylvestis*) ranged from 10,950 to 11,760 uncal. BP[94]. A new direct date on the human skeleton 11,855 ± 50 uncal. BP (OxA-27763) or 13,560-13,770 cal. BP (95.4% CI, previously unpublished) is in agreement with the dates of the charcoal and pine.

The human skeleton was determined to be of a young male, 20-23 years of age, of the Cro-magnon type. According to the cranio-facial architecture, it was characterized by classical cranio-facial disharmony, i.e. a relatively long skull associated with a low face and sub-rectangular eye-sockets, which are quite typical of the time period. The young man weighed a little over 60 kg and stood 1.64 m tall. Although of a relatively slender build, muscle attachments showed him to have been a strong runner and well adapted to mountainous terrain[95]. His upper limbs show a high degree of asymmetry, indicative of preferential use of the right arm[96]. Isotopic studies of carbon and nitrogen fractionations indicated a largely meat based terrestrial diet[97].

B.2 Supplementary figures

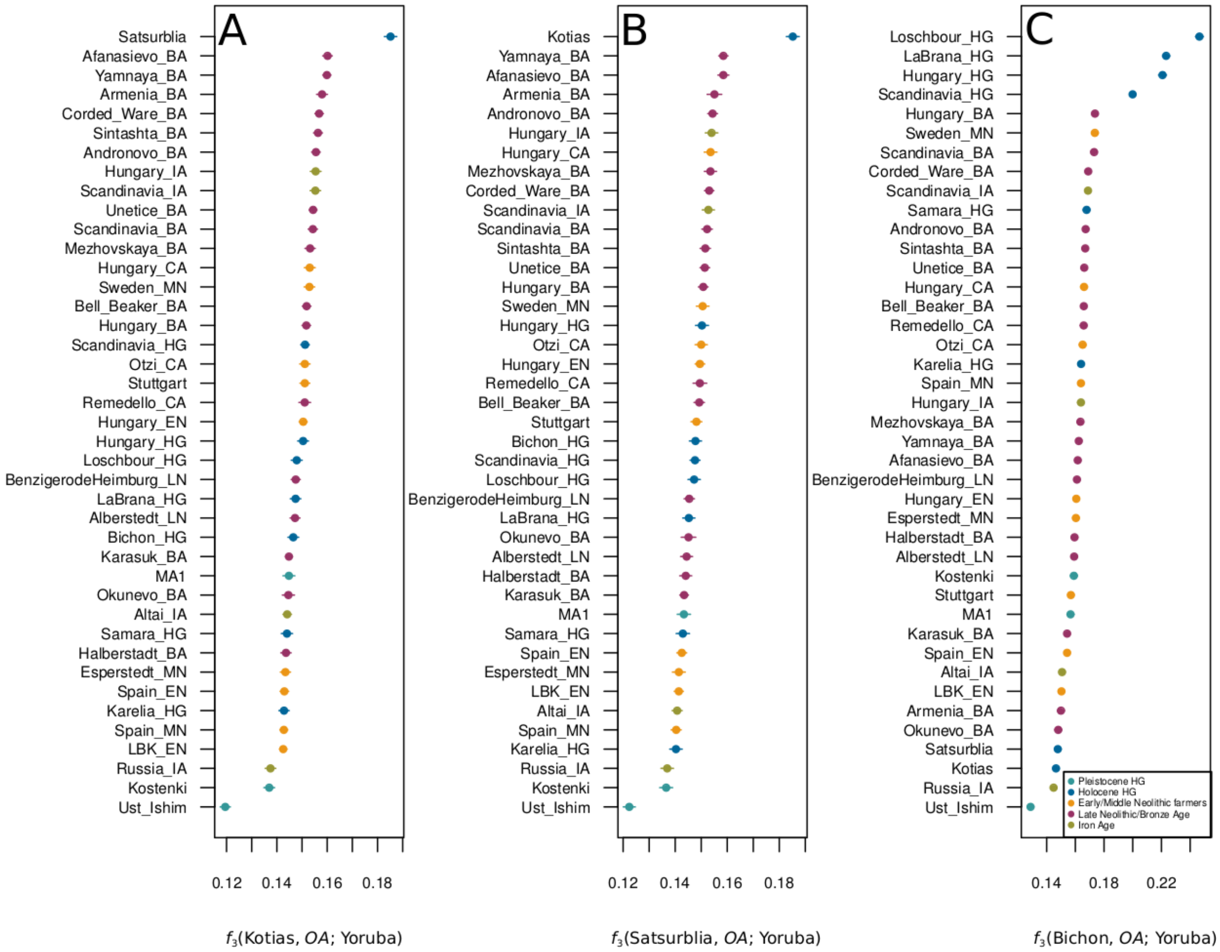

Supplementary Figure B.1 Outgroup f_3-statistics for Kotias, Satsurblia and Bichon which show the extent of shared drift with other ancient samples (OA) since they diverged from an African (Yoruba) outgroup. Satsurblia and Kotias share the most drift with each other while Bichon is closest to other western hunter-gatherers. Bars dissecting the points show standard error. HG, hunter-gatherer; EN, Early Neolithic; MN, Middle Neolithic; CA, Copper Age; BA, Bronze Age; IA, Iron Age.

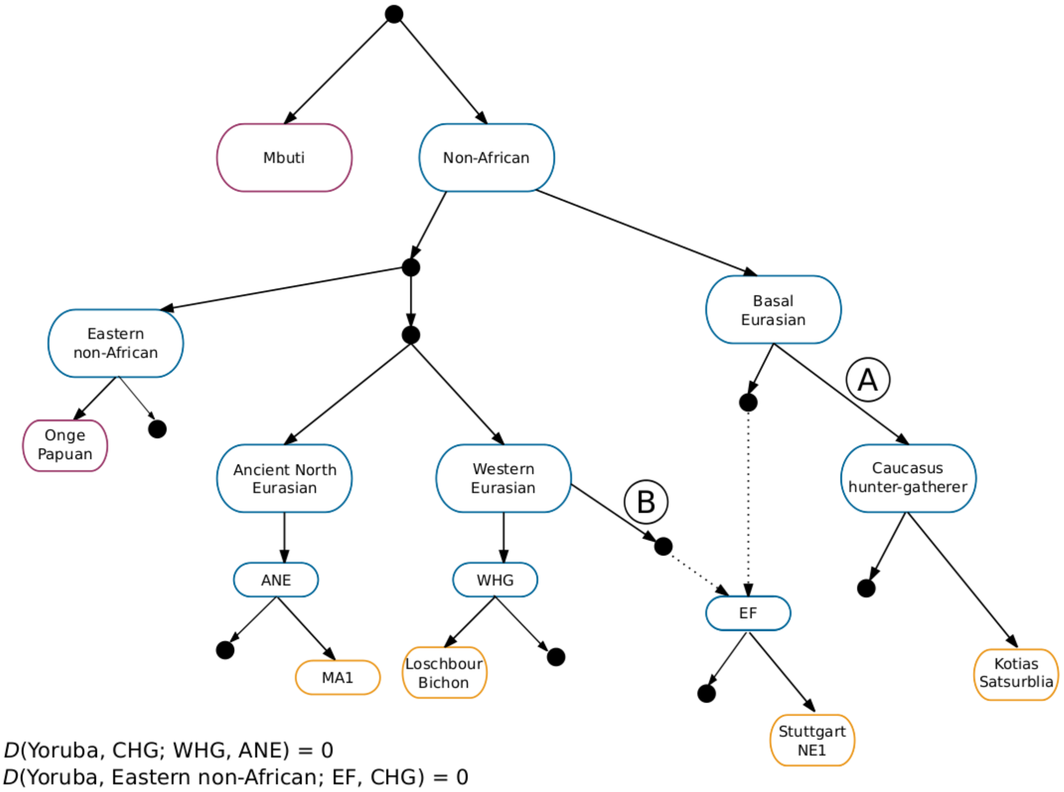

A. D(Yoruba, CHG; WHG, ANE) = 0
D(Yoruba, Eastern non-African; EF, CHG) = 0
f_3(WHG, CHG; EF)= 0 and f_3(CHG, EF; WHG) >> 0

B. D(Yoruba, WHG; CHG, EF) > 0
ADMIXTURE analysis (Fig. 1B) - the "blue" component which is maximized in WHG is found in EF

Supplementary Figure B.2 Inferred topology for ancient and modern populations. This was built on the model proposed by Lazaridis et al[2]. A. Caucasus hunter-gatherers descend from a basal Eurasian branch. This is supported by both D and f_3 statistics (Supplementary Table B.5,6,8). B. Early Europeans farmers have admixed with WHG. This is supported by D-statistics (Supplementary Table B.9) and ADMIXTURE analysis (Figure 3.1B). Ancient samples are shown in yellow, inferred populations in blue and modern populations in purple. Dotted lines show descent with admixture while solid lines depict descent without admixture.

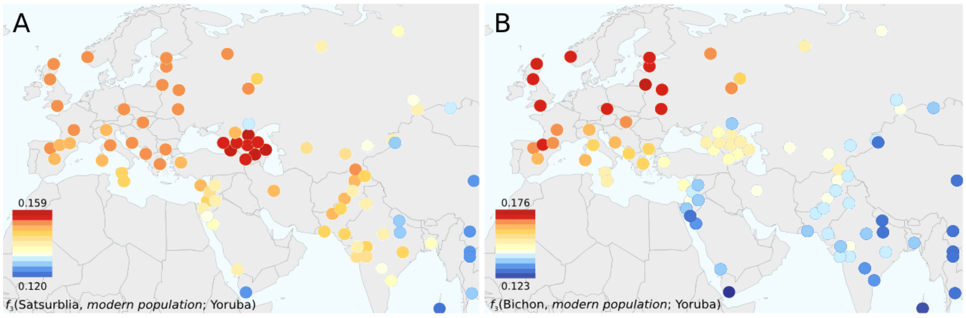
A
0.159
0.120
f_3(Satsurblia, *modern population*; Yoruba)
B
0.176
0.123
f_3(Bichon, *modern population*; Yoruba)

Supplementary Figure B.3 Outgroup f_3-statistics indicating the amount of shared drift between ancient samples and modern populations since they diverged from an African outgroup. Warmer colours indicate more shared drift than cooler colours. A. f_3(Satsurblia, *modern population*; Yoruba) which shows, similar to Kotias, that Satsurblia shares the most affinity to modern populations from the Caucasus. B. f_3 (Bichon, *modern population*; Yoruba) which shows that Bichon shares the most drift with modern populations from Northern Europe.

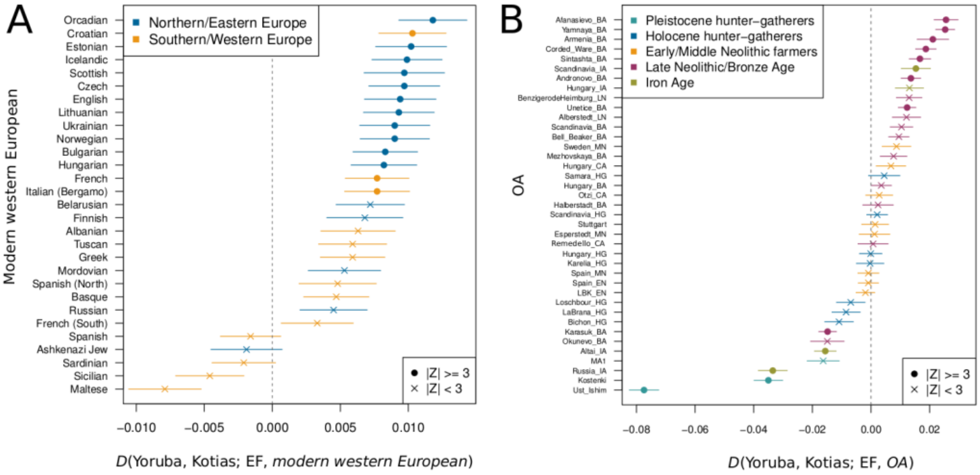

Supplementary Figure B.4 The impact of CHG on the European gene pool subsequent to the Neolithic expansion. A. *D*-statistics of the form *D*(Yoruba, Kotias; EF, *modern western European*) which suggest that there has been CHG admixture in northern/eastern Europe since the Neolithic period. Here EF are represented by Hungarian Neolithic samples[4]. B. *D*-statistics of the form *D*(Yoruba, Kotias; EF, *OA*) where OA represents other ancient Eurasian samples. EF are represented by Hungarian Neolithic samples[4]. Significantly positive statistics were found when OA were Late Neolithic individuals or individuals from the Yamnaya culture. These cultures may have acted as a conduit for CHG gene flow into western Europe. HG, hunter-gatherer; EN, Early Neolithic; MN, Middle Neolithic; CA, Copper Age; BA, Bronze Age; IA, Iron Age.

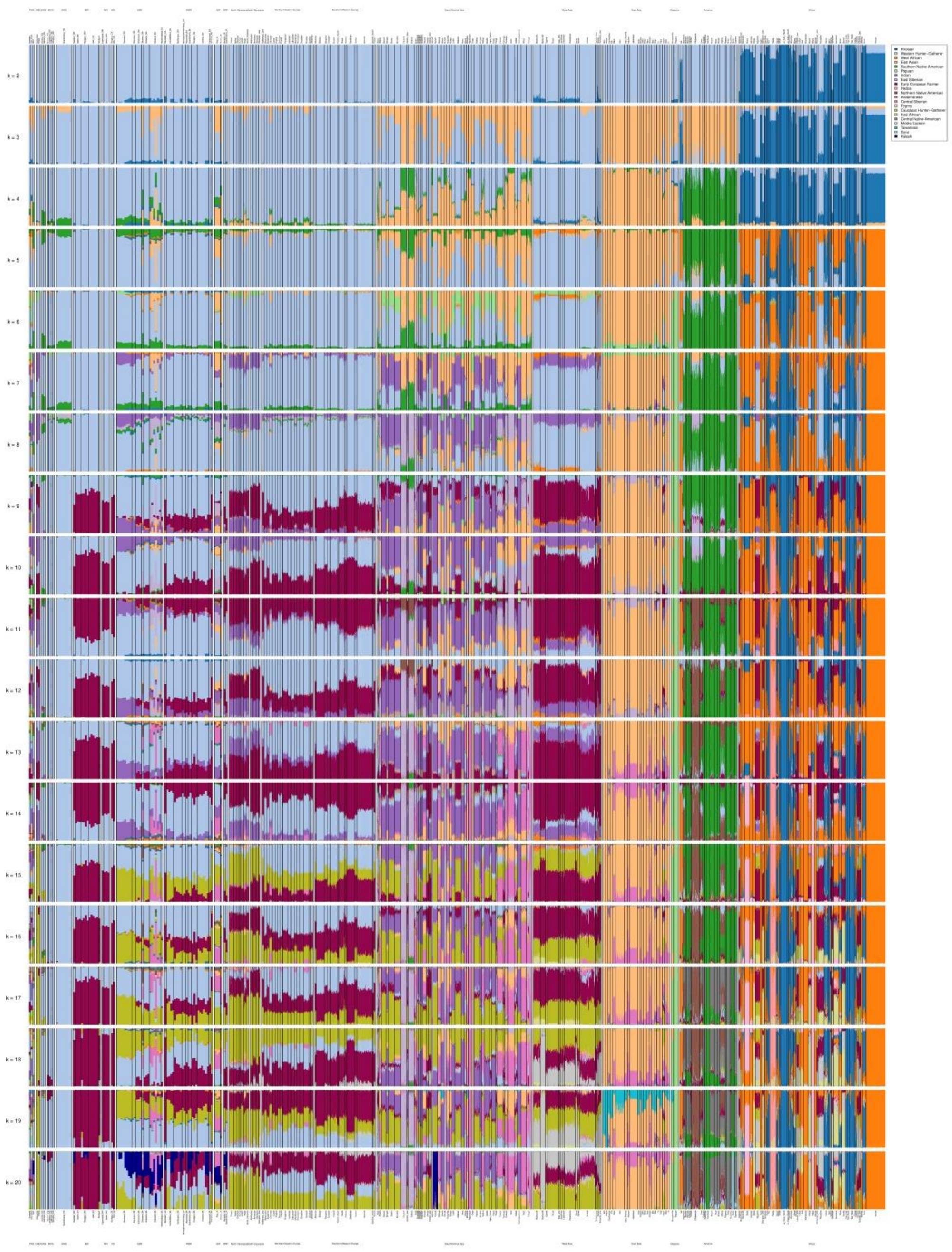

Supplementary Figure B.5 ADMIXTURE results for 2-20 clusters (*K*). Ancient samples are positioned on the left followed by modern individuals who are hierarchically clustered by population and region. Bichon resembles other western hunter-gatherers while the Caucasus hunter-gatherers Kotias and Satsurblia look unlike any other modern or ancient group.

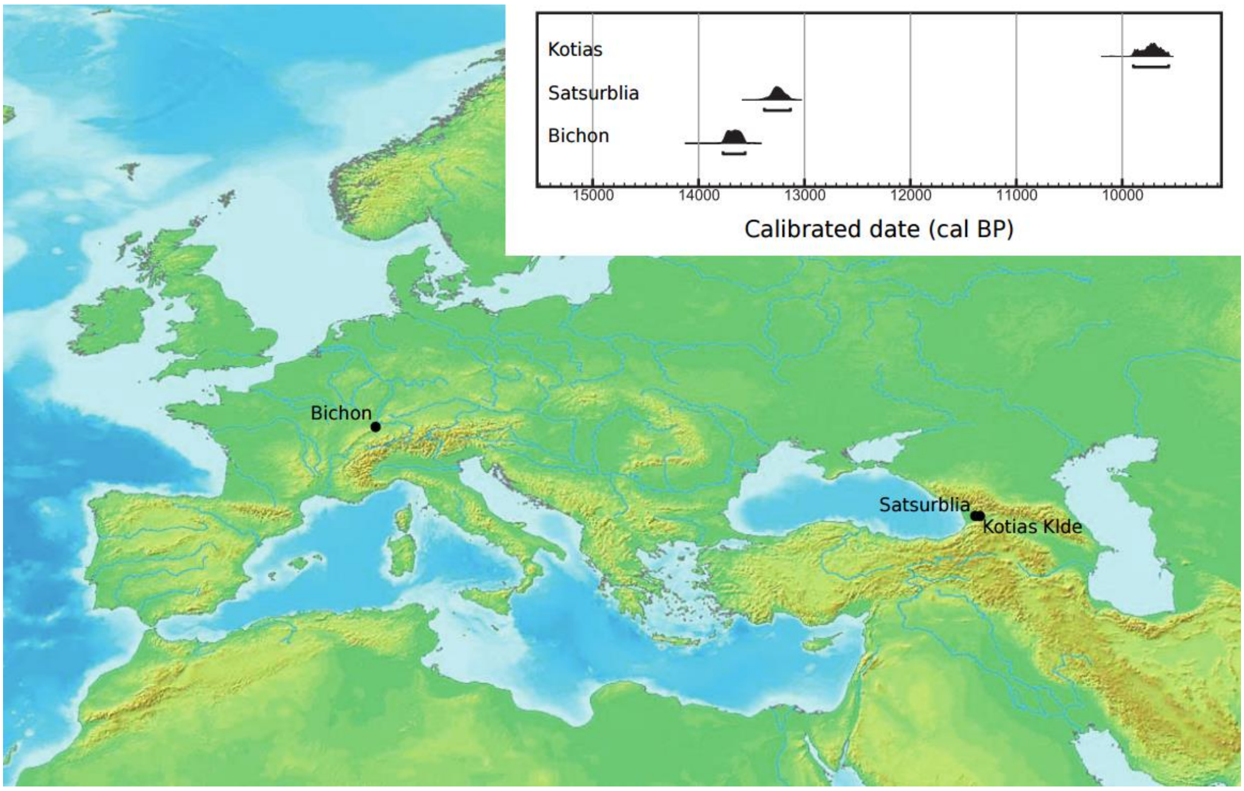

Supplementary Figure B.6 Sampling locations of Bichon (Bichon cave, Switzerland), Satsurblia (Satsurblia cave, Georgia) and Kotias (Kotias Klde cave, Georgia) accompanied by radiocarbon date curves.

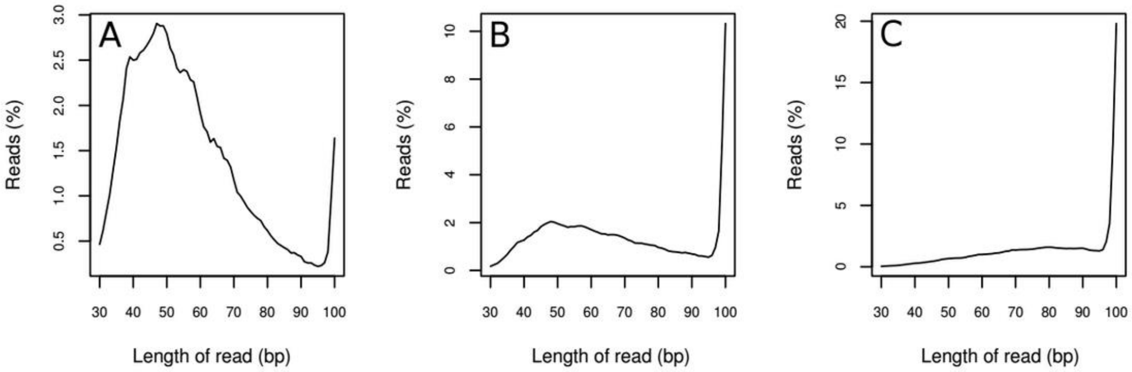

Supplementary Figure B.7 Sequence length distribution for (A) Kotias, (B) Satsurblia and (C) Bichon. All samples have sequences in the range expected for ancient DNA.

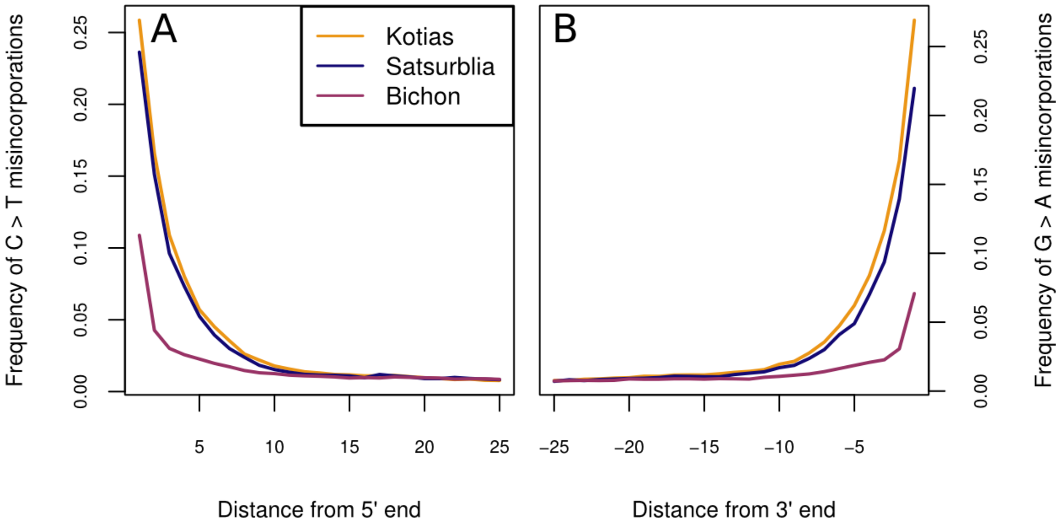

Supplementary Figure B.8 Damage patterns for Georgian and Swiss ancient samples. Plots show mismatch frequency relative to the reference genome as a function of read position. A. shows the frequency of C to T misincorporations at the 5' ends of reads while B. shows the frequency of G to A transitions at the 3' ends of reads.

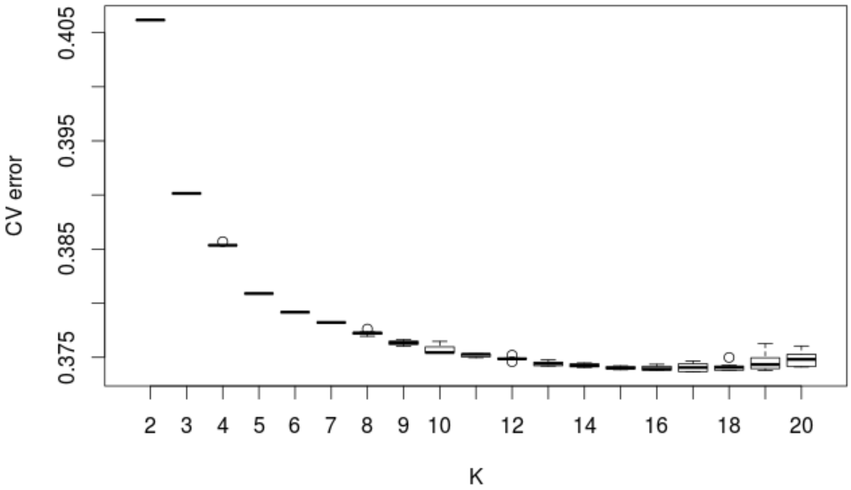

Supplementary Figure B.9 ADMIXTURE analysis cross validation (CV) error as a function of the number of clusters (K). The lowest mean value was attained at K=17.

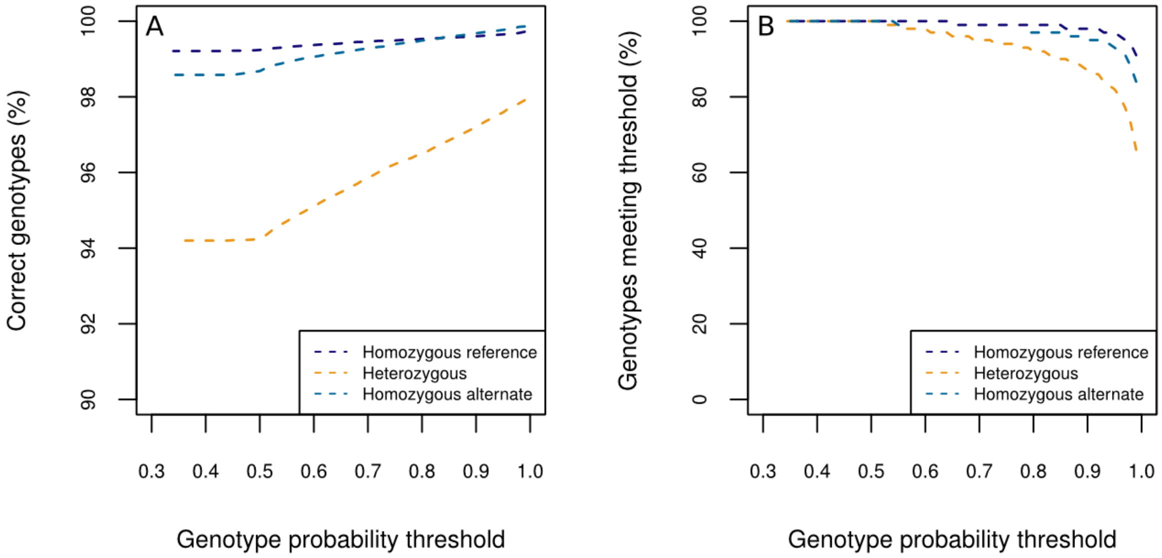

Supplementary Figure B.10 Accuracy of imputation for the Caucasus hunter-gatherer, Kotias. Genotypes are broken down into three categories - homozygous reference, heterozygous and homozygous alternate, all with respect to the reference genome. A. Genotypes imputed from a ~1x subsample of Kotias were compared to high coverage genotypes from the same sample and called "correct" if they matched. Heterozygous calls show the least accuracy. B. The proportion of genotypes retained for a range of genotype probabilities. Increasing the genotype probability threshold resulted in a reduction in the amount of genotypes meeting the threshold. These results are comparable to those found in [2].

B.3 Supplementary tables

Supplementary Table B.1 Ancient data used in analyses.

Group	Reference ID	Reference	Context/Culture	Region
Hunter-gatherers				
Ust_Ishim	Ust'-Ishim	15	Upper Palaeolithic	Siberia
Kostenki	Kostenki	13	Upper Palaeolithic	Russia
MA1	Mal'ta	7	Upper Palaeolithic	Siberia
Satsurblia	**Satsurblia**	**This study**	**Upper Palaeolithic**	**Georgia**
Bichon_HG	**Bichon**	**This study**	**Upper Palaeolithic**	**Switzerland**
Kotias	**Kotias**	**This study**	**Mesolithic**	**Georgia**
Loschbour_HG	Loschbour	2	Mesolithic	Luxembourg
LaBrana_HG	La Braña	3	Mesolithic	Spain
Karelia_HG	Karelia_HG	6	Mesolithic	Russia
Samara_HG	Samara_HG	6	Neolithic hunter-gatherer	Russia
Scandinavia_HG	Motala12, I0011, I0012, I0013, I0014, I0015, I0016, Ajvide58	2,5,6	Mesolithic and Neolithic hunter-gatherer/ Pitted Ware Culture	Sweden
Hungary_HG	KO1	4	Neolithic	Hungary
Early - Middle Neolithic				
Hungary_EN	NE1, NE5, NE6, NE7	4	Neolithic	Hungary
Stuttgart	Stuttgart	2	Neolithic	Germany
LBK_EN	I0025, I0026, I0046, I0054, I0100	6	Linearbandkeramik	Germany
Spain_EN	I0410, I0412, I0413	6	Epicardial	Spain
Esperstedt_MN	I0172	6	Esperstedt	Germany
Spain_MN	I0406, I0407, I0408	6	La Mina	Spain
Sweden_MN	Gökhem2	5	Funnelbeaker (TRB)	Sweden
Late Neolithic – Bronze Age				
Otzi_CA	Otzi	14	Alpine	Italy
Hungary_CA	CO1	4	Baden	Hungary
Remedello_CA	RISE489	8	Remedello	Italy
BenzigerodeHeimburg	I0058,I0059	6	Bell Beaker	Germany
Afanasievo_BA	RISE509, RISE511	8	Afanasievo	Russia
Yamnaya_BA	I0231, I0429, I0438, I0443, RISE547, RISE548, RISE550, RISE552	6,8	Yamnaya	Russia
Corded_Ware_BA	I0103, I0104, RISE00, RISE94	6,8	Corded Ware and Battle Axe	Germany/ Sweden/Estonia
Bell_Beaker_BA	I0108, I0111, I0112, RISE569	6,8	Bell Beaker	Germany/Czech Republic
Alberstedt_LN	I0118	6	Late Neolithic	Germany
Okunevo_BA	RISE516	8	Okunevo	Russia
Unetice_BA	I0047, I0116, I0117, I0164, RISE150, RISE577	6,8	Unetice	Germany/Poland/Czech Republic
Sintashta_BA	RISE392, RISE394, RISE395	8	Sintashta	Russia
Scandinavia_BA	RISE97, RISE98	8	Nordic Late Neolithic	Sweden
Andronovo_BA	RISE500, RISE503, RISE505	8	Andronovo	Russia
Karasuk_BA	RISE493, RISE495, RISE496, RISE497, RISE499, RISE502	8	Karasuk	Russia

Mezhovskaya_BA	RISE523	8	Mezhovskaya	Russia
Armenia_BA	RISE423	8	Middle Bronze Age	Armenia
Halberstadt_BA	I0099	6	Late Bronze Age	Germany
Hungary_BA	BR1, BR2, RISE479	4,8	Bronze Age	Hungary
Iron Age				
Hungary_IA	IR1	4	Pre-Scythian Mezőcsát	Hungary
Scandinavia_IA	RISE174	8	Iron Age	Sweden
Altai_IA	RISE600, RISE601, RISE602	8	Iron Age	Russia
Russia_IA	RISE504	8	Iron Age	Russia

Supplementary Table B.2 Number of SNPs from the Human Origins panel covered for those ancient samples that were recalled.

OA	SNPs
Kotias	510,034
Bichon	390,923
Ust'Ishim	591,238
Loschbour	571,054
Stuttgart	564,978
NE1	571,383
BR2	577,811
Ajv58	518,352
BR1	292,301
CO1	357,082
Gok2	400,285
KO1	401,740
La Braña	555,761
MA1	419,966
NE5	337,709
NE6	385,959
NE7	373,846
Otzi	541,031
Satsurblia	416,997

Appendix B Appendix for Chapter 3

Supplementary Table B.3 D-statistics of the form D(Yoruba, OA; Satsurblia, Kotias) which show that Satsurblia and Kotias tend to form a clade to the exclusion of other ancient samples (OA) (|Z|<3). Significant statistics are highlighted in bold.

OA	*D*(Yoruba,*OA*;Satsurblia,Kotias)	Z-score	P-value
Ust_Ishim	-0.0062	-1.042	0.149
Kostenki	-0.0018	-0.268	0.394
Bichon	-0.0010	-0.150	0.440
Hungary_HG	0.0016	0.233	0.408
Okunevo_BA	0.0021	0.264	0.396
Hungary_CA	0.0022	0.327	0.372
Mezhovskaya_BA	0.0028	0.456	0.324
Hungary_EN	0.0028	0.605	0.273
Halberstadt_BA	0.0032	0.450	0.326
Loschbour_HG	0.0036	0.578	0.282
Andronovo_BA	0.0040	0.845	0.199
LBK_EN	0.0042	0.889	0.187
Armenia_BA	0.0052	0.663	0.254
Hungary_BA	0.0052	1.160	0.123
MA1_HG	0.0061	0.832	0.203
Otzi_CA	0.0061	0.941	0.173
Remedello_CA	0.0066	0.880	0.189
Yamnaya_BA	0.0066	1.468	0.071
Karasuk_BA	0.0076	1.865	0.031
Samara_HG	0.0076	0.923	0.178
Russian_IA	0.0079	1.184	0.118
Spain_EN	0.0079	1.515	0.065
BenzigerodeHeimburg_LN	0.0082	1.395	0.082
Karelia_HG	0.0088	1.216	0.112
Hungary_IA	0.0089	1.278	0.101
Afanasievo_BA	0.0104	1.882	0.030
Stuttgart	0.0104	1.745	0.041
Scandinavia_BA	0.0105	1.917	0.028
Esperstedt_MN	0.0107	1.485	0.069
Spain_MN	0.0114	2.171	0.015
Bell_Beaker_BA	0.0116	2.434	0.007
Scandinavia_IA	0.0117	1.798	0.036
Sweden_MN	0.0117	1.783	0.037
Unetice_BA	0.0122	2.630	0.004
LaBrana_HG	0.0125	2.080	0.019
Alberstedt_LN	0.0133	1.877	0.030
Sweden_HG	0.0135	2.724	0.003
Corded_Ware_BA	0.0136	2.893	0.002
Altai_IA	0.0140	2.775	0.003
Sintashta_BA	**0.0184**	**3.627**	**1.43E-04**

Supplementary Table B.4 D-statistics of the form D(Yoruba, OA; Bichon, WHG) which show that Bichon and western hunter-gatherers tend to form a clade to the exclusion of other ancient samples (OA) as the majority of statistics do not deviate significantly from zero (|Z|<3). Significant statistics are highlighted in bold.

OA	D(Yoruba,OA; Bichon,Loschbour)	Z-score	P-value	D(Yoruba,OA; Bichon,La Braña)	Z-score	P-value
Afanasievo_BA	0.0073	1.059	0.145	0.0009	0.115	0.454
Alberstedt_LN	0.0142	2.607	0.005	0.0039	0.698	0.243
Altai_IA	0.0106	2.172	0.015	-0.0071	-1.467	0.071
Andronovo_BA	0.0086	1.219	0.111	0.0030	0.394	0.347
Armenia_BA	0.0133	2.710	0.003	-0.0025	-0.496	0.310
Bell_Beaker_BA	0.0073	1.777	0.038	-0.0003	-0.069	0.472
BenzigerodeHeimburg_LN	0.0071	1.094	0.137	-0.0007	-0.103	0.459
Corded_Ware_BA	0.0137	1.806	0.036	0.0197	2.384	0.009
Esperstedt_MN	0.0121	1.669	0.048	-0.0036	-0.469	0.320
Halberstadt_BA	0.0081	1.418	0.078	-0.0012	-0.208	0.418
Hungary_BA	0.0082	1.516	0.065	-0.0055	-1.005	0.157
Hungary_CA	0.0135	2.701	0.003	-0.0014	-0.259	0.398
Hungary_EN	0.0136	2.251	0.012	0.0035	0.544	0.293
Hungary_HG	0.0126	1.831	0.034	0.0018	0.240	0.405
Hungary_IA	0.0048	1.041	0.149	-0.0033	-0.667	0.252
Karasuk_BA	0.0067	0.923	0.178	-0.0096	-1.187	0.118
Karelia_HG	0.0132	1.819	0.035	-0.0081	-1.050	0.147
Kostenki	0.0105	2.301	0.011	0.0052	1.071	0.142
Kotias	0.0101	1.187	0.118	-0.0346	-4.079	0.000
LBK_EN	0.0033	0.481	0.315	-0.0095	-1.289	0.099
MA1_HG	0.0054	1.140	0.127	-0.0001	-0.019	0.492
Mezhovskaya_BA	0.0098	1.537	0.062	0.0015	0.215	0.415
Okunevo_BA	0.0139	2.132	0.017	-0.0061	-0.896	0.185
Otzi_CA	0.0163	2.244	0.012	0.0104	1.335	0.091
Remdello_CA	0.0075	1.200	0.115	0.0044	0.690	0.245
Russia_IA	0.0045	0.660	0.255	-0.0040	-0.579	0.281
Samara_HG	0.0101	2.055	0.020	0.0046	0.937	0.174
Satsurblia	0.0053	0.714	0.238	0.0015	0.207	0.418
Scandinavia_BA	0.0036	0.544	0.293	-0.0003	-0.049	0.480
Scandinavia_IA	0.0031	0.376	0.353	-0.0039	-0.467	0.320
Sintashta_BA	0.0036	0.531	0.298	-0.0069	-0.993	0.160
Spain_EN	0.0063	1.203	0.114	0.0024	0.423	0.336
Spain_MN	0.0104	1.926	0.027	0.0028	0.500	0.309
Stuttgart	0.0131	2.212	0.014	-0.0041	-0.693	0.244
Sweden_HG	**0.0236**	**4.463**	**4.04E-06**	**-0.0185**	**-3.439**	**2.92E-04**
Sweden_MN	0.0111	1.669	0.048	-0.0025	-0.350	0.363
Unetice_BA	**0.0154**	**3.371**	**3.74E-04**	-0.0008	-0.159	0.437
Ust_Ishim	0.0065	1.523	0.064	-0.0021	-0.451	0.326
Yamnaya_BA	0.0055	0.891	0.186	0.0013	0.205	0.419

Supplementary Table B.5 f_3-statistics which elucidate the topology between CHG, WHG and EF.

Tree	Pop1	Pop2	Outgroup	f_3	Standard error	Z-score
f_3(CHG, EF; WHG) 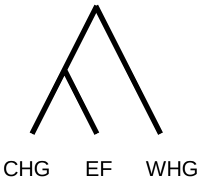	Kotias	NE1	Bichon	0.105	0.007	14.493
	Kotias	Stuttgart	Bichon	0.111	0.007	15.616
	Kotias	NE1	Loschbour	0.151	0.008	18.273
	Kotias	Stuttgart	Loschbour	0.161	0.008	19.018
f_3(WHG, EF; CHG) 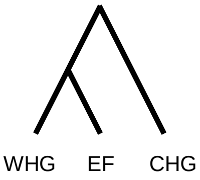	Bichon	NE1	Kotias	0.055	0.006	9.480
	Loschbour	NE1	Kotias	0.061	0.006	10.206
	Bichon	Stuttgart	Kotias	0.049	0.006	8.543
	Loschbour	Stuttgart	Kotias	0.052	0.006	9.285
f_3(WHG, CHG; EF) 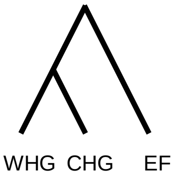	Kotias	Bichon	NE1	0.010	0.004	2.384
	Kotias	Loschbour	NE1	0.006	0.004	1.489
	Kotias	Bichon	Stuttgart	0.018	0.004	4.019
	Kotias	Loschbour	Stuttgart	0.015	0.004	3.313

Supplementary Table B.6 Parameters estimates from G-PhoCS. Mean and 95% HDP intervals for all estimated variables (split times, population sizes, migration rates and migration proportions) models with four possible trees, with EF represented by either Stuttgart or NE1, and with or without an outgroup (San).

Parameter	Stuttgart, San	Stuttgart, no outgroup	NE1, San	NE1, no outgroup
θ_{San}	69,578 (28,507–149,950)		65,565 (28,937–140,883)	
$\theta_{\mathrm{Loschbour}}$	8,514 (1,242–27,458)	8,714 (1,230–27,819)	8201 (1058–27105)	8,294 (1,179–27,274)
$\theta\tau_{\mathrm{Bichon}}$	7,641 (939–26,320)	7,676 (799–26,376)	7,896 (817–26,525)	7,648 (742–26,287)
$\theta\tau_{\mathrm{Kotias}}$	7,267 (1,096–24,384)	7,208 (1,182–25,058)	5,098 (1,206–17,066)	4,672 (899–18,650)
θ_{EF}	8,996 (1,810–27,407)	7,715 (1,207–25,545)	9,273 (2,199–27,020)	8,037 (1,706–25,676)
$\theta_{\mathrm{Loschbour+Bichon}}$	4,240 (1,201–10,339)	1,824 (390–4,593)	4,686 (1,562–10,541)	2,296 (611–5,428)
$\theta_{\mathrm{Kotias+EF}}$	5,313 (913–16,765)	2613 (607–11,510)	8,570 (1,227–25,662)	7,176 (966–23,764)
$\theta_{\mathrm{Loschbour+Bichon+Kotias+EF}}$	8312 (4,622–11,876)	13,086 (11,690–14,642)	9,214 (5,642–12,959)	13,021 (11,614–14,524)
$\theta_{\mathrm{Loschbour+Bichon+Kotias+EF+San}}$	15,567 (13,408–17,961)		15,103 (13,007–17,381)	
$\tau_{\mathrm{Loschbour+Bichon}}$	17,616 (13,993–28,855)	18,115 (13,955–29,124)	17,235 (13,917–27,110)	16,729 (13,893–24,470)
$\tau_{\mathrm{Kotias+EF}}$	23,962 (11,439–43,045)	20,360 (12,607–32,806)	31,800 (17,814–53,626)	22,990 (11,510–39,768)
$\tau_{\mathrm{Loschbour+Bichon+Kotias+EF}}$	46,441 (27,010–75,773)	33,806 (21,634–52,601)	52171 (30,555–84,651)	37,341 (21,923–61,832)
$\tau_{\mathrm{Loschbour+Bichon+Kotias+EF+San}}$	233,172 (157,714–309,530)		259,090 (189,055–335,442)	
$m_{\mathrm{Loschbour\text{->}EF}}$	230,977 (20,299–778,204)	282,893 (20,052–877,763)	200,098 (19,826–700,477)	210,978 (16,845–728,345)
propm$_{\mathrm{Loschbour\text{->}EF}}$	0.09 (0.01–0.34)	0.12 (0.01–0.39)	0.08 (0.01–0.31)	0.07 (0.01–0.28)

Supplementary Table B.7 D-statistics of the form D(Yoruba, CHG; WHG, OA) which show that western hunter-gatherers and eastern hunter-gatherers as well as the latter and the ancient north Eurasian MA1 form a clade to the exclusion of CHG (|Z|<3). WHG, western hunter-gatherer; OA, other ancient sample.

WHG	OA	*D*(Yoruba, Kotias; *WHG*, *OA*)	Z-score	P-value	SNPs	D(Yoruba, Satsurblia; *WHG*, *OA*)	Z-score	P-value	SNPs
Bichon	MA1	-0.0067	-1.002	0.158	250,841	-0.0114	-1.498	0.067	200,555
KO1	MA1	-0.0203	-2.831	0.002	250,957	-0.0218	-2.595	0.005	203,919
La Braña	MA1	-0.0092	-1.364	0.086	345,849	-0.0078	-1.085	0.139	279,481
Loschbour	MA1	-0.0102	-1.606	0.054	352,019	-0.0135	-1.888	0.030	286,844
Bichon	Samara_HG	0.0080	1.195	0.116	125,261	0.0129	1.554	0.060	100,667
KO1	Samara_HG	0.0039	0.517	0.303	124,626	0.0011	0.111	0.456	101,788
La Braña	Samara_HG	0.0131	1.913	0.028	171,183	0.0100	1.222	0.111	139,082
Loschbour	Samara_HG	0.0130	1.864	0.031	174,650	0.0119	1.515	0.065	142,960
Bichon	Karelia_HG	0.0136	2.188	0.014	199,889	0.0035	0.446	0.328	161,076
KO1	Karelia_HG	-0.0019	-0.270	0.394	202,463	-0.0079	-0.941	0.173	165,909
La Braña	Karelia_HG	0.0087	1.379	0.084	278,296	0.0035	0.479	0.316	227,050
Loschbour	Karelia_HG	0.0089	1.447	0.074	285,238	0.0008	0.106	0.458	234,780

Supplementary Table B.8 CHG and ANE ancestry in distinct is modern Northern Europeans. Significant statistics are highlighted in bold.

Modern Northern European	*D*(Yoruba, MA1; Kotias, *modern Northern European*)	Z-score	P-value
Belarusian	**0.0286**	**5.693**	**6.24E-09**
English	**0.0253**	**4.965**	**3.44E-07**
Estonian	**0.0351**	**6.941**	**1.95E-12**
Finnish	**0.0331**	**6.392**	**8.19E-11**
Icelandic	**0.0278**	**5.516**	**1.73E-08**
Lithuanian	**0.034**	**6.534**	**3.20E-11**
Mordovian	**0.0314**	**6.297**	**1.52E-10**
Norwegian	**0.0271**	**5.423**	**2.93E-08**
Orcadian	**0.0267**	**5.365**	**4.05E-08**
Russian	**0.0307**	**6.221**	**2.47E-10**
Scottish	**0.0285**	**5.532**	**1.58E-08**

Supplementary Table B.9 D-statistics of the form D(Yoruba, X; CHG, EF) which show that CHG and EF do not form a clade to the exclusion of WHG (Z >3) but do form a clade to the exclusion of MA1 and eastern non-Africans (|Z| < 3). Significant statistics are highlighted in bold.

X	**CHG**	**EF**	***D*(Yoruba,*X*;*CHG*,*EF*)**	**Z-score**	**P-value**
Bichon	**Kotias**	**Stuttgart**	**0.0244**	**3.902**	**4.77E-05**
Bichon	**Kotias**	**NE1**	**0.0336**	**5.450**	**2.52E-08**
Bichon	**Satsurblia**	**Stuttgart**	**0.0229**	**3.622**	**1.46E-04**
Bichon	**Satsurblia**	**NE1**	**0.0351**	**5.433**	**2.77E-08**
La Braña	**Kotias**	**Stuttgart**	**0.0216**	**3.711**	**1.03E-04**
La Braña	**Kotias**	**NE1**	**0.0362**	**6.203**	**2.77E-10**
La Braña	**Satsurblia**	**Stuttgart**	**0.0277**	**4.262**	**1.01E-05**
La Braña	**Satsurblia**	**NE1**	**0.0447**	**7.050**	**8.95E-13**
Loschbour	**Kotias**	**Stuttgart**	**0.0341**	**5.737**	**4.82E-09**
Loschbour	**Kotias**	**NE1**	**0.0477**	**7.815**	**2.75E-15**
Loschbour	**Satsurblia**	**Stuttgart**	**0.0369**	**5.834**	**2.71E-09**
Loschbour	**Satsurblia**	**NE1**	**0.0520**	**8.185**	**1.36E-16**
MA1	Kotias	Stuttgart	-0.0153	-2.380	0.009
MA1	Kotias	NE1	-0.0083	-1.362	0.087
MA1	Satsurblia	Stuttgart	-0.0096	-1.423	0.077
MA1	Satsurblia	NE1	-0.0006	-0.084	0.467
Onge	Kotias	NE1	-0.0024	-0.558	0.288
Onge	Kotias	Stuttgart	-0.0030	-0.678	0.249
Onge	Satsurblia	NE1	0.0009	0.202	0.420
Onge	Satsurblia	Stuttgart	-0.0004	-0.085	0.466
Papuan	Kotias	NE1	-0.0009	-0.199	0.421
Papuan	Kotias	Stuttgart	0.0021	0.454	0.325
Papuan	Satsurblia	NE1	0.0001	0.029	0.488
Papuan	Satsurblia	Stuttgart	0.0019	0.393	0.347

Appendix B Appendix for Chapter 3

Supplementary Table B.10 Lowest statistics for the test f_3(*Target; Source*$_1$*, Source*$_2$). Ancient Samples are highlighted in bold. Populations for which source populations could not be determined (Z > -3) are italicized.

Target	Region of target	Source$_1$	Source$_2$	Lowest f_3	Standard error	Z-score
Altaian	Central Asia/Siberia	**Scandinavia_HG (I0013)**	Ulchi	-0.020	0.001	-23.378
Kalmyk	Central Asia/Siberia	**LBK_EN (I0054)**	Ulchi	-0.017	0.001	-22.109
Kyrgyz	Central Asia/Siberia	**Spain_EN (I0410)**	Ulchi	-0.025	0.001	-30.837
Mansi	Central Asia/Siberia	**Scandinavia_HG (I0015)**	Nganasan	-0.021	0.001	-17.357
Selkup	Central Asia/Siberia	**Scandinavia_HG (I0015)**	Nganasan	-0.023	0.001	-20.470
Tajik Pomiri	Central Asia/Siberia	**LBK_EN (I0026)**	Karitiana	-0.012	0.001	-8.257
Tubalar	Central Asia/Siberia	**Scandinavia_HG (Motala12)**	Korean	-0.012	0.001	-12.045
Turkmen	Central Asia/Siberia	**LBK_EN (I0046)**	Nganasan	-0.025	0.001	-20.594
Tuvinian	Central Asia/Siberia	**LBK_EN (I0046)**	Nganasan	-0.012	0.001	-12.131
Uzbek	Central Asia/Siberia	**LBK_EN (I0046)**	Hezhen	-0.027	0.001	-27.451
Dai	*East Asia*	***Hungary_EN (NE6)***	*Ami*	*0.000*	*0.001*	*-0.074*
Lahu	*East Asia*	***LBK_EN (I0046)***	*Dai*	*0.014*	*0.001*	*13.381*
Naxi	*East Asia*	***Spain_EN (I0410)***	*She*	*0.001*	*0.001*	*1.429*
Thai	East Asia	**LBK_EN (I0026)**	Ami	-0.005	0.001	-4.801
Tu	East Asia	**Scandinavia_HG (Motala12)**	Korean	-0.009	0.001	-10.881
Uygur	East Asia	**LBK_EN (I0046)**	She	-0.028	0.001	-30.514
Xibo	East Asia	**LBK_EN (I0025)**	Korean	-0.007	0.001	-6.628
Bulgarian	Eastern Europe	**Hungary_EN (NE6)**	**Samara_HG**	-0.015	0.002	-6.927
Czech	Eastern Europe	**Hungary_EN (NE6)**	**Samara_HG**	-0.016	0.002	-6.924
Hungarian	Eastern Europe	**Hungary_EN (NE6)**	**Samara_HG**	-0.015	0.002	-6.804
Ukrainian	Eastern Europe	**Hungary_EN (NE6)**	**Samara_HG**	-0.015	0.002	-6.339
Adygei	North Caucasus	**LBK_EN (I0026)**	Karitiana	-0.008	0.002	-5.094
Balkar	North Caucasus	**LBK_EN (I0046)**	Nganasan	-0.012	0.001	-9.455
Chechen	North Caucasus	**LBK_EN (I0100)**	Karitiana	-0.007	0.001	-4.741
Kumyk	North Caucasus	**LBK_EN (I0100)**	Karitiana	-0.013	0.001	-8.589
Lezgin	North Caucasus	**LBK_EN (I0046)**	**MA1**	-0.010	0.002	-4.737
Nogai	North Caucasus	**LBK_EN (I0046)**	Nganasan	-0.024	0.001	-21.062
North Ossetian	North Caucasus	**LBK_EN (I0046)**	Nganasan	-0.011	0.001	-8.067
Belarusian	Northern Europe	**Hungary_EN (NE6)**	**Samara_HG**	-0.014	0.002	-6.121
Chuvash	Northern Europe	**LBK_EN (I0046)**	Nganasan	-0.021	0.001	-17.147
English	Northern Europe	**Hungary_EN (NE6)**	**Samara_HG**	-0.015	0.002	-6.330
Estonian	Northern Europe	**Kotias**	**Loschbour**	-0.012	0.002	-7.432
Finnish	Northern Europe	**Hungary_EN (NE6)**	**Samara_HG**	-0.012	0.002	-4.709
Icelandic	Northern Europe	**Hungary_EN (NE6)**	**Samara_HG**	-0.013	0.002	-5.491
Lithuanian	Northern Europe	**Hungary_EN (NE6)**	**Samara_HG**	-0.012	0.002	-5.106
Mordovian	Northern Europe	**LBK_EN (I0100)**	**MA1**	-0.013	0.002	-5.958
Norwegian	Northern Europe	**Hungary_EN (NE6)**	**Samara_HG**	-0.013	0.002	-5.562
Orcadian	Northern Europe	**Hungary_EN (NE6)**	**Samara_HG**	-0.013	0.002	-5.527
Russian	Northern Europe	**Hungary_EN (NE6)**	**Samara_HG**	-0.013	0.002	-6.125
Scottish	Northern Europe	**Loschbour**	Iraqi Jew	-0.011	0.001	-8.567
Balochi	South Asia	**Kotias**	Kharia	-0.006	0.001	-7.351
Bengali	South Asia	**Kotias**	Kharia	-0.011	0.001	-13.990
Brahui	South Asia	**Kotias**	Kharia	-0.004	0.001	-5.154
Burusho	South Asia	**Satsurblia**	Korean	-0.012	0.001	-11.349
GujaratiA	South Asia	**Kotias**	Kharia	-0.011	0.001	-12.005
GujaratiB	South Asia	**Kotias**	Kharia	-0.012	0.001	-12.427

GujaratiC	South Asia	**Kotias**	Kharia	-0.010	0.001	-10.205
GujaratiD	South Asia	**Kotias**	Kharia	-0.007	0.001	-7.217
Hazara	South Asia	**Spain_EN (I0410)**	Korean	-0.025	0.001	-27.520
Iranian	South Asia	**LBK_EN (I0026)**	Guarani	-0.011	0.001	-7.943
Kalash	*South Asia*	***Kotias***	*Cabecar*	*0.016*	*0.001*	*11.166*
Kharia	*South Asia*	*Lahu*	*Mala*	*0.001*	*0.000*	*2.675*
Kusunda	*South Asia*	***LBK_EN (I0054)***	*Naxi*	*0.010*	*0.001*	*9.149*
Lodhi	South Asia	**Kotias**	Kharia	-0.008	0.001	-10.559
Makrani	South Asia	**LBK_EN (I0046)**	Vishwabrahmin	-0.004	0.001	-5.672
Mala	South Asia	**Kotias**	Kharia	-0.007	0.001	-10.147
Onge	*South Asia*	*Cambodian*	*Papuan*	*0.130*	*0.002*	*61.297*
Pathan	South Asia	**Kotias**	Kharia	-0.011	0.001	-13.879
Punjabi	South Asia	**Kotias**	Kharia	-0.010	0.001	-12.115
Sindhi	South Asia	**Kotias**	Kharia	-0.012	0.001	-15.623
Tiwari	South Asia	**Kotias**	Kharia	-0.012	0.001	-17.322
Vishwabrahmin	South Asia	**Kotias**	Kharia	-0.008	0.001	-12.198
Abkhasian	South Caucasus	**Kotias**	**LBK_EN (I0046)**	-0.010	0.002	-5.847
Armenian	South Caucasus	**Satsurblia**	**LBK_EN (I0046)**	-0.010	0.002	-5.040
Georgian	South Caucasus	**Satsurblia**	**LBK_EN (I0046)**	-0.011	0.002	-5.469
Albanian	Southern Europe	**LBK_EN (I0046)**	**MA1**	-0.013	0.002	-5.833
Basque	Southern Europe	**LBK_EN (I0026)**	**Bichon**	-0.009	0.002	-4.861
Croatian	Southern Europe	**Hungary _EN (NE6)**	**Samara_HG**	-0.015	0.002	-6.644
Greek	Southern Europe	**LBK_EN (I0100)**	**MA1**	-0.013	0.002	-6.343
Italian (Bergamo)	Southern Europe	**Hungary _EN (NE6)**	**Samara_HG**	-0.013	0.002	-5.762
Maltese	Southern Europe	**LBK_EN (I0100)**	**MA1**	-0.010	0.002	-4.834
Sardinian	Southern Europe	**LBK_EN (I0026)**	**Bichon**	-0.007	0.002	-3.666
Sicilian	Southern Europe	**Hungary _EN (NE6)**	**Samara_HG**	-0.012	0.002	-5.216
Spanish	Southern Europe	**Hungary _EN (NE6)**	**Samara_HG**	-0.014	0.002	-6.580
Spanish (North)	Southern Europe	**Hungary _EN (NE6)**	**Scandinavia_HG (I0012)**	-0.013	0.002	-5.526
Tuscan	Southern Europe	**LBK_EN (I0100)**	**MA1**	-0.011	0.002	-5.366
BedouinA	West Asia	**LBK_EN (I0046)**	Mende	-0.019	0.001	-18.211
BedouinB	*West Asia*	***LBK_EN (I0046)***	*Mende*	*0.005*	*0.001*	*4.030*
Cypriot	West Asia	**Satsurblia**	**LBK_EN (I0046)**	-0.008	0.002	-3.774
Druze	West Asia	**LBK_EN (I0046)**	Dinka	-0.005	0.001	-4.151
Jordanian	West Asia	**LBK_EN (I0046)**	Dinka	-0.016	0.001	-13.288
Lebanese	West Asia	**Spain_EN (I0410)**	Luo	-0.013	0.001	-12.029
Palestinian	West Asia	**LBK_EN (I0046)**	Dinka	-0.014	0.001	-13.743
Saudi	West Asia	**LBK_EN (I0046)**	Dinka	-0.007	0.001	-5.134
Syrian	West Asia	**LBK_EN (I0046)**	Mende	-0.013	0.001	-10.934
Turkish	West Asia	**LBK_EN (I0046)**	Nganasan	-0.015	0.001	-13.709
Yemen	West Asia	**Spain_EN (I0410)**	Mende	-0.025	0.001	-21.821
French	Western Europe	**Hungary _EN (NE6)**	**Samara_HG**	-0.015	0.002	-6.810
French (South)	Western Europe	**Hungary _EN (NE6)**	**Scandinavia_HG (I0012)**	-0.012	0.002	-5.624

Appendix B Appendix for Chapter 3

Supplementary Table B.11 Highest *D*-statistics for *D*(Yoruba, *X*; Onge, *Indian population*) where we let X be every possible non-African population and ancient sample in the Human Origins dataset.

Indian population	X	***D*(Yoruba, *X*; Onge, *Indian population*)**	Z-score	P-value
GujaratiC	Kotias	0.0540	15.925	2.13E-57
GujaratiD	Kotias	0.0503	15.311	3.23E-53
Lodhi	Kotias	0.0448	14.829	4.76E-50
Mala	Kotias	0.0368	12.339	2.79E-35
Vishwabrahmin	Kotias	0.0393	13.025	4.41E-39
GujaratiA	Afanasievo_BA	0.0623	20.594	1.55E-94
GujaratiB	Afanasievo_BA	0.0576	20.032	1.45E-89
Tiwari	Afanasievo_BA	0.0602	23.159	5.90E-119
Kharia	Mala	0.0240	13.062	2.71E-39

Supplementary Table B.12 Summary of the results for all samples sequenced during the screening phase of the project. Samples were sequenced using 50 base pair (bp) single-end sequencing on a MiSeq platform. Adapter trimmed reads were aligned to the GRCh37 build of the human genome with the mitochondrial sequence replaced by the revised Cambridge reference sequence and clonal reads were removed using SAMtools (see methods). Samples highlighted in bold were selected for further sequencing.

Sample ID	Lab ID	Skeletal element	Mass of powder (g)	Total reads	Aligned non-clonal reads	Human DNA (%)
Bichon	**Bichon**	**Petrous**	**0.250**	**3,501,019**	**2,504,728**	**71.54**
Kotias	KK1.C1	Molar Crown	0.335	584,353	385,012	65.89
Kotias	**KK1.R1**	**Molar Root**	**0.335**	**255,035**	**196,060**	**76.88**
Satsurblia	SATP.1	Petrous	0.373	3,333,552	307,444	9.22
Satsurblia	**SATP.3**	**Petrous**	**0.372**	**2,228,960**	**306,748**	**13.76**

Appendix B Appendix for Chapter 3

Supplementary Table B.13 Summary of the results for samples sequenced during the deep sequencing phase of the project. All sequencing was performed on a HiSeq 2000 platform using 100 bp single-end sequencing. Adapter trimmed reads were aligned to the GRCh37 build of the human genome with the mitochondrial sequence replaced by the revised Cambridge reference sequence and clonal reads were removed using SAMtools. Coverage was calculated using GATK (see methods).

Sample ID	Lab ID	Sequencing facility	Number of lanes	Total reads	Aligned non-clonal reads	Human DNA (%)	Coverage (x)
Bichon	Bichon	BGI*	7	1,139,300,766	352,921,957	30.98	9.50
Kotias	KK1.R1	BC^	6	1,327,399,258	849,496,700	64.00	15.38
Satsurblia	SATP.3	BC^	3	419,683,577	66,338,333	15.81	1.44

* Beijing Genomics Institute, China; ^ Beckmann Coulter Inc., USA

Supplementary Table B.14 Mitochondrial contamination estimates. %C, percentage contamination excluding sites with potentially damaged bases; %C + MD, percentage contamination including sites with potentially damaged bases. Estimates are derived from the proportion of secondary bases at haplogroup-defining positions in the mitochondrial genome.

Sample	%C	%C+MD
Kotias	0.07	0.32
Satsurblia	0.11	0.57
Bichon	0.16	0.62

Supplementary Table B.15 Establishing the background error rate for X chromosome contamination estimates. “Test 1” and “test 2” were performed as in[52]. The number of primary alleles (p) and secondary alleles (s) in ancient male samples at X chromosome sites found to be polymorphic in European populations and adjacent sites 4 bases upstream and downstream are reported.

Test	Sample	Allele	-4	-3	-2	-1	0	1	2	3	4
1	Kotias	p	1,856,365	1,854,061	1,849,192	1,842,313	1,773,694	1,841,046	1,847,342	1,853,194	1,855,144
	Kotias	s	4,582	4,483	4,593	5,453	10,001	5,570	4,574	4,497	4,525
	Satsurblia	p	36,003	36,133	36,182	35,863	34,645	35,978	36,204	36,022	36,293
	Satsurblia	s	90	57	84	97	155	86	61	72	68
	Bichon	p	980,753	980,819	979,916	978,924	948,648	978,001	979,943	980,432	980,784
	Bichon	s	2,458	2,411	2,429	2,743	4,164	2,692	2,391	2,457	2,504
2	Kotias	p	223,214	223,081	222,624	222,014	214,334	221,873	222,412	222,897	223,050
	Kotias	s	618	519	567	651	1215	657	559	531	559
	Satsurblia	p	11,201	11,238	11,264	11,171	10,793	11,201	11,269	11,202	11,291
	Satsurblia	s	30	22	23	33	44	25	14	28	17
	Bichon	p	143,919	143,956	143,754	143,676	139,533	143,524	143,777	143,841	143,950
	Bichon	s	319	343	370	422	616	387	360	365	355

Supplementary Table B.16 Contingency table for X chromosome contamination estimates. “Test 1” and “test 2” were performed as in[52]. The table reports the number of primary alleles (p) and secondary alleles (s) in ancient male samples at X chromosome sites found to be polymorphic in European populations and the average of adjacent sites 4 bases upstream and downstream as well as the observed probability of error (e).

Sample		Test 1 Polymorphic sites	Test 1 Average of adjacent sites	Test 2 Polymorphic sites	Test 2 Average of adjacent sites
Kotias	p	1,773,694	1,849,832.125	214,334	222,645.625
	s	10,001	4,784.625	1,215	582.625
	e	0.006	0.003	0.006	0.003
Satsurblia	p	34,645	36,084.75	10,793	11,229.625
	s	155	76.875	44	24
	e	0.004	0.002	0.004	0.002
Bichon	p	948,648	979,946.500	139,533	143,799.625
	s	4,164	2,510.625	616	365.125
	e	0.004	0.003	0.004	0.003

Appendix B Appendix for Chapter 3

Supplementary Table B.17 X chromosome contamination estimates. Estimates are based on “test 1” and “test 2”11. Associated p-values for contingency tables used in this analysis were calculated using Fisher’s exact test.

Sample	Test	Contamination (%)	P-value
Kotias	1	0.99	$< 2.2 \times 10^{-16}$
	2	0.99	$< 2.2 \times 10^{-16}$
Satsurblia	1	0.56	5.22×10^{-8}
	2	0.58	0.0011
Bichon	1	0.54	$< 2.2 \times 10^{-16}$
	2	0.45	$< 2.2 \times 10^{-16}$

Supplementary Table B.18 Molecular sex assignment of ancient samples. Ry, the ratio of the fraction of Y chromosome reads to the fraction of reads aligning to both sex chromosomes.

Sample	R_y	Standard error	95% Confidence interval	Assignment
Kotias	0.0840	0.0001	0.0839-0.0842	Male
Satsurblia	0.0878	0.0002	0.0873-0.0882	Male
Bichon	0.0928	0.0001	0.0926-0.0930	Male

.

Appendix B Appendix for Chapter 3

Supplementary Table B.19 Mitochondrial haplogroups and haplotypes for Kotias, Satsurblia and Bichon. Mutations reported here are with respect to the Reconstructed Sapiens Reference Sequence[98]. Mutations found in our samples which are present in the reported haplogroup are shown here unless marked in bold or underlined. Bold mutations are those expected for the prescribed haplogroup but not found in the sample. Underlined mutations are those present in our samples but not associated with the determined haplogroup.

Sample	Coverage	Haplogroup	Haplotype
Kotias	425x	H13c	73A, 146T, 152T, 195T, 247G, 769G, 825T, 1018G, 2706A, 2758G, 2885T, 3594C, 4104A, 4312C, 4769A, 7028C, 7146A, 7256C, **7521G**, 8206A, 8468C, 8655C, 8701A, 9540T, 10289G, 10398A, 10664C, 10688G, 10810T, 10873T, 10915T, 11719G, 11914G, 12705C, 13105A, 13276A, 13506C, 13650C, 14766C, 14872T, **16129G**, 16187C, 16189T, 16223C, 16230A, 16278C, 16311T, 16519T
Satsurblia	144x	K3	146T, 150T, 152T, **235G**, 247G, 560T, 769G, 825T, 1018G, 1097T, 1811G, 2758G, 2885T, 3480G, 3594C, 4104A, 4312C, 4769A, 6027T, 7146A, 7256C, 7498A, 7521G, 7657C, **8188G**, 8468C, 8655C, 8701A, 9055A, 9540T, 9698C, **9852T**, 10398A, 10550G, 10664C, 10688G, 10810T, 10873T, 10915T, 11299C, 11467G, 11914G, 12308G, 12372A, 12705C, 13105A, 13276A, 13506C, 13650C, 14167T, 14198A, 14212C, 14798C, 15924G, **16093C**, 16129G, 16148T, **16153A**, 16187C, 16189T, 16223C, 16224C, 16230A, 16278C
Bichon	314x	U5b1h	146T, 150T, 152T, 195T, 247G, **384G**, 769G, 825T, 1018G, 2758G, 2885T, 3197C, 3594C, 4104A, 4312C, **5656G,** 7028C, 7146A, 7256C, **7521G**, 7768G, 8468C, 8655C, 8701A, 9477A, 9540T, 10398A, 10664C, 10688G, 10810T, 10873T, 10915T, 11467G, 11914G, 12308G, 12372A, 12705C, 13105A, 13276A, 13506C, 13617C, 13650C, 14182C, 16129G, 16187C, 16223C, 16230A, 16270T, 16278C, 16311T, 16519T

Appendix B Appendix for Chapter 3

Supplementary Table B.20 Y-chromosomal haplogroups for ancient male samples. Haplogroups were determined by Yfitter55. The “maximum likelihood haplogroup” is described by55, as being the best guess haplogroup while the “confidence haplogroup” is described as the conservative guess haplogroup.

Sample	Major haplogroup	Maximum likelihood haplogroup	Confidence haplogroup
Kotias	J	J	J
Satsurblia	J	J2a	J2
Bichon	I	I2a*	I2

Supplementary Table B.21 Genotypes for SNP panel used in 8-plex prediction system. Observed genotypes are shown for Bichon and Kotias while imputed genotypes with probability greater than 0.85 are reported for Satsurblia unless otherwise marked. Coverage refers to coverage of observed high quality alleles with a depth ≥ 4x. Genotypes are reported with respect to the GRCh37 build of the human genome. Skin colour determination was inconclusive for all samples.

Gene	Marker	Genotype Bichon	Coverage Bichon	Genotype Kotias	Coverage Kotias	Genotype Satsurblia	Coverage Satsurblia
SLC45A2	rs16891982	CC	4C	CC	21C	CC*	-
IRF4	rs12203592	CC	13C	CC	19C	CC*	7C
SLC24A4	rs12896399	GT	5G,5T	GT	4G,9T	GG	-
OCA2	rs1545397	AA	8A	AA	5A	AA	-
HERC2	rs12913832	AG	6A,3G	AA	15A	AG^	2A,2G
SLC24A5	rs1426654	GG	25G	AA	13A	AA*	4A
MC1R	rs885479	GG	16G	GG	10G	-	-
ASIP	rs6119471	CC	10C	CC	24C	CC	-

* genotype supported by observed and imputed data

^ genotype supported by observed data

Supplementary Table B.22 Genotypes for positions that define common haplotypes in the region surrounding the *SLC24A5* gene. Observed genotypes are shown for Kotias and Bichon while imputed genotypes with probability greater than 0.85 are reported for Satsurblia. Coverage refers to coverage of observed high quality alleles with a depth ≥ 4x. Genotypes are reported with respect to the GRCh37 build of the human genome. Markers of the C11 haplogroup are shown in bold. This haplogroup is found in 97% of individuals with the derived rs1426654 variant76. Kotias and Satsurblia exhibit the the C11 haplogroup while Bichon does not.

Marker	Ancestral allele	Selected allele	Genotype Bichon	Coverage Bichon	Genotype Kotias	Coverage Kotias	Genotype Satsurblia	Coverage Satsurblia
rs1834640	G	A	AA	8A	AA	15A	AA	-
rs2675345	G	A	GG	5G	AA	12A	AA	-
rs2469592	G	A	GG	11G	AA	25A	AA	-
rs2470101	C	T	CT	10C,1T	TT	16T	TT	-
rs938505	T	C	TT	9T	CT	6C,1T	CC	-
rs2433354	T	C	TT	9T	CC	9C,1T	CC	-
rs2459391	G	A	GG	18G	AA	26A	AA	-
rs2433356	A	G	AA	4A	GG	22G,1A	GG	-
rs2675347	G	A	GG	7G	AA	19A	AA	-
rs2675348	G	A	GG	9G	AA	19A	AA	-
rs1426654	G	A	GG	25G	AA	13A	AA*	4A
rs2470102	G	A	GG	9G	AA	12A	AA	-
rs16960631	A	G	AA	12A	AA	17A	AA	-
rs2675349	G	A	-	-	AA	6A	AA	-
rs3817315	T	C	TT	18T	CC	12C	CC	-
rs7163587	T	C	TT	11T	CC	19C	CC	-

* genotype supported by observed and imputed data

Appendix B Appendix for Chapter 3

Supplementary Table B.23 Genotypes for the SNP panel used in the Hirisplex prediction system. Observed genotypes are shown for Kotias and Bichon while imputed genotypes with a probability of greater than 0.85 are reported for Satsurblia unless otherwise marked. Coverage refers to coverage of observed high quality alleles with a depth ≥ 4x. Genotypes are reported with respect to the GRCh37 build of the human genome.

Gene	SNP	Genotype Bichon	Coverage Bichon	Genotype Kotias	Coverage Kotias	Genotype Satsurblia	Coverage Satsurblia
MC1R	N29insA	CC	8C	-	-	-	-
MC1R	rs11547464	GG	16G	GG	28G	GG	-
MC1R	rs885479	GG	16G	GG	10G	-	-
MC1R	rs1805008	CC	15C	CC	14C	CC	-
MC1R	rs1805005	GG	10G	GG	9C	GG	-
MC1R	rs1805006	CC	10C	CC	13C	CC	-
MC1R	rs1805007	CC	17C	CC	22C	CC	-
MCIR	rs1805009	GG	12G	GG	19G	GG	-
MC1R	Y1520CH	CC	15C	CC	19C	-	-
MC1R	rs2228479	GG	12G	GG	15G,2A	GG	-
MC1R	rs1110400	TT	14T	TT	16T	TT	-
SLC45A2	rs28777	CC	8C	CC	25C	CC	-
SLC45A2	rs16891982	CC	4C	CC	21C	CC	-
KITLG	rs12821256	TT	8T	TT	11T	-	-
EXOC2	rs4959270	CC	5C	CC	8C	AA	-
IRF4	rs12203592	CC	13C	CC	19C	CC*	7C
TYR	rs1042602	CC	11C	CC	19C	CC	-
OCA2	rs1800407	CC	11C	CC	8C	CC	-
SLC24A4	rs2402130	AA	18A	AA	24A	AA	-
HERC2	rs12913832	AG	6A,3G	AA	15A	AG^	2A,2G
PIGU/ASIP	rs2378249	AA	10A	AA	21A	GA	-
SLC24A4	rs12896399	GT	5G,5T	GT	4G,9T	GG	-
TYR	rs1393350	GG	14G	GG	14G	GG	-
TYRP1	rs683	CA	3C,2A	AA	4A	AA	-

* genotype supported by observed and imputed data

^ genotype supported by observed data

Supplementary Table B.24 Hirisplex phenotypic predictions with accompanying associated probabilities for Bichon, Kotias and Satsurblia.

			Bichon	Kotias	Satsurblia
Eye colour	Associated probability	Blue	0.007	< 0.001	0.014
		Intermediate	0.027	0.003	0.033
		Brown	0.967	0.997	0.952
	Prediction		**Brown**	**Brown**	**Brown**
Hair colour/shade	Associated probability	Blonde hair	0.022	0.005	0.032
		Brown hair	0.275	0.164	0.259
		Red hair	< 0.001	< 0.001	< 0.001
		Black hair	0.704	0.831	0.709
		Light hair	0.030	0.006	0.060
		Dark hair	0.970	0.994	0.940
	Prediction		**Black/Dark**	**Black/Dark**	**Black/Dark**

Appendix A

Appendix C Appendix for Chapter 4

C.1 Osteology

The fragmented remains of seven individuals were unearthed from the floor of the dwelling, none of which were recovered in their primary burial anatomical position.

- Skull A (DevilsGate4) – juvenile, 6-7 years (genetically determined to be female)
- Skull Д – (DevilsGate3) – female, 50-60 years old
- Skull Б (DevilsGate2) – male, 20-25 years old
- Skull E (DevilsGate1) – female, 40-50 years old
- Skull Ж (DevilsGate5) – complete skull of a young person, 18-20 years old (believed to be a male based on morphology but genetically determined to be female)
- Skull B – sub-adult, 12-13 years old (no aDNA analysis)
- Skull Г – male, ~50 years old (no aDNA analysis)

Complete and fragmented skulls were recovered from four of these individuals, three adults and one subadult (12-13 years of age) [59]. Of the three adult skulls, two were believed to be from males (although one of these was genetically determined to be a female, see Supp. S.7.) and one of a female

The skulls all have a short, high and wide cranial vault, a wide, high and flat face, with a slight protrusion of the nasal bones and with narrow orbits. The mandible is very wide and is characteristic of hunter-gatherers[59]. The craniometric features are in general agreement with the genetics in terms of suggesting some level of regional continuity between the Devil's Gate individuals and later populations in the Russian Far East.

C.2 Archaeology

Devil's Gate (Chertovy Vorota) is a karst cave situated in the mountainous part of Primorye Province, 12 km from the town Dalnegorsk (Primorsky Krai, Russian Far East), 660 meters above sea level and ~35m above the Krivaya River. The cave was first excavated in 1973 by a Soviet team under the directorship of Tatarnikov V.A[60]. This is the only known Neolithic cave site in Primorye[61] .

The large cave has a rectangular entrance and consists of a 45m long and 10m wide gallery of which the total area excavated was ~200 m^2. Most of the cave's area was occupied as a dwelling space[61]. The site contains a single occupational layer which belongs to the 'Rudninskaya' Neolithic culture. In the central part of the hall, excavations revealed the remains of a rectangular pit dwelling around 45 m^2 in area which was walled by wooden poles[61].

Cultural material recovered included stone, bone and antler tools, pottery, bone and shell ornaments, as well as good preservation of other organics including wood and textile artefacts[13]. The lithic assemblage includes retouched scrapers, arrows, knives, drills, and other tools. The bone tools include needles of various sizes, harpoons, and bases of insert tools. The composition of the tool assemblages is typical and indicative of a subsistence which is based on hunting and fishing[61].

Excavations also yielded 14 clay vessels made of local materials and a large number of shards. The pottery is flat-bottomed and conical-shaped with comb pattern decoration[13]; the method of construction was coiling. The vessels were decorated by stamping and appliqué.

Prior to radiometric dating, the cultural layer at the cave was indirectly assigned to the 5th millennium BC based on the artefacts, which are similar to those recovered from a settlement situated near the Rudnaya River in the Dalnegorsk district[62].

The excavations yielded fragments of textiles, fishing nets, cords and mats made of plant fabrics and wooden artefacts made of birch bark. A large number of bones of animals, acorns, fruits and birch bark were found in the center[62]. The assemblage also includes numerous ornaments including bone pendants from boar canines and beads made of shell, bone and stone.

Animal bones belong mostly to brown and black bears, wild boar, red deer, and badger. The fauna also comprises of the remains of birds (grouse, ptarmigan, dove and duck) and freshwater and anadromous fish (salmon)[60]. The assemblage does not include any domestic plant or faunal remains which suggests that the inhabitants of the site belonged to a hunter-gatherer-fisher population who manufactured utilitarian low-quality domestic pottery.

C.3 Phenotypic prediction

To explore pigmentation, we first looked at the genes *SLC45A2* and *SLC24A5*, contributing to light skin pigmentation in modern-day Europeans[37,63–67]. Selected genotypes in these two genes (rs16891982 and rs1426654 for *SLC45A2* and *SLC24A5*, respectively) are known to have been under strong positive selection in Europeans and are almost fixed in modern populations in the region. Our results imply that DevilsGate1 was unlikely to have been homozygous for either of the selected alleles, as is typical for non-Europeans. The rs12913832 variant of the *HERC2* gene was also investigated, where a mutation is found in nearly all people with blue eyes. Our sample was likely homozygous for the ancestral allele, implying brown eyes.

A variant of the *LCT* gene (rs4988235), where the derived genotype is associated with lactose tolerance in adult Europeans[41], was examined. We found that DevilsGate1 was unlikely to possess the derived genotype similar to modern-day East Asian populations.

A number of mutations associated with phenotypes in East Asians were also looked at, first two locations within the *OCA2* gene (rs1800414 and rs74653330) that give signals of positive selection[68–70] and are wide-spread and associated with decreased melanin levels in East Asians[71–73]. The results for the variant rs1800414 were inconclusive, but DevilsGate1 likely did not carry the derived variant at rs74653330. We also looked at two loci with a high frequency differentiation between East Asians and non-East Asians and showing signals of positive selection (rs12821256, rs1407995, rs885479 on the KITLG, DCT and SLC24A2 genes, respectively)[37] or otherwise associated with pigmentation (rs1042602, rs1834640, rs26722 on the TYR, RPL7AP62/SLC24A5 and SLC24A2 genes, respectively)[74]. DevilsGate1 was most likely homozygous for the East Asian variant at both rs12821256 and rs1407995 and did not possess the alleles rare in East Asia at rs885479, rs1042602, rs1834640 and rs26722.

Our next target was the *EDAR* gene. This region also shows signals of positive selection in East Asian populations, with the selected allele linked to certain phenotypic changes (e.g. in tooth morphology[40], hair thickness[38,39] and sweat gland density[75]), also confirmed using a mouse model. The haplotype with the selected allele is very common in East Asian, Northeast Asian and Native American populations and is estimated to have emerged in central China around 30,000 years ago[75]. Our sample likely carried at least one copy of the derived allele, giving increased odds of straight, thick hair as well as shovel-shaped incisors.

The mutation rs671 on *ALDH2* was also studied. The derived variant, of intermediate frequencies (roughly up to 50%) in various East Asian populations[76,77], is associated with alcohol flush and increased risk of hangovers, alcoholism and Esophageal Cancer[42,78]. Our sample probably did not carry the derived allele.

Then, three East Asian phenotypic traits were investigated. DevilsGate1 most likely had at least one copy of the risk allele for common salt-sensitive hypertension[79] at rs4961 on the ADD1 gene, common in Asia. She was most likely not homozygous for the risk allele at rs1799971 on the OPRM1 gene, associated with increased craving and stronger effects for alcohol[80] and for opioids[81] in Asian populations, although the results from association studies on this marker are mixed. The derived variant at rs17822931 on the ABCC11 gene is associated with weaker than usual body odour[82] and dry ear wax type[83] (for the latter, when homozygous) in East Asians and is indicative of east Asian ancestry. DevilsGate1's genotype could not be determined but she most likely possessed at least one copy of the derived allele.

Finally, eight loci associated with an increased risk for Type 2 diabetes in East Asian populations was studied (rs1535500, rs6017317, rs6467136, rs9470794, rs3786897, rs6815464, rs7041847, rs831571)[84]. She was likely heterozygous at two loci associated with increased susceptibility to Type 2 diabetes in East Asians (rs1535500 and rs9470794) and had at least one copy of the disease-associated variant at a third location (rs6815464). Our results at rs3786897 were completely uninformative and at other locations, she most likely had at least one copy of the normal variant.

Detailed results of the phenotypic inference are shown in Supplementary Table C.32..

C.4 Supplementary figures

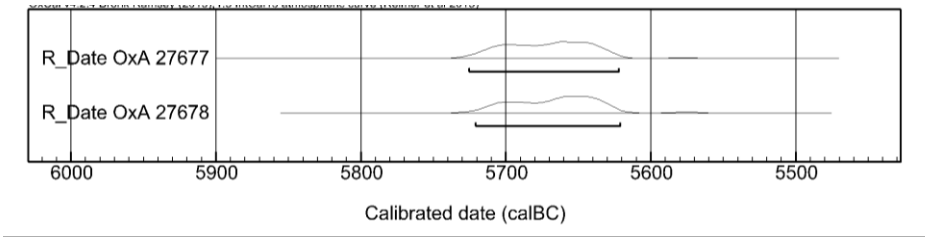

Supplementary Figure C.1 Calibrated range of the two human specimens from Devil's Gate (OxCal v. 4.2.4)

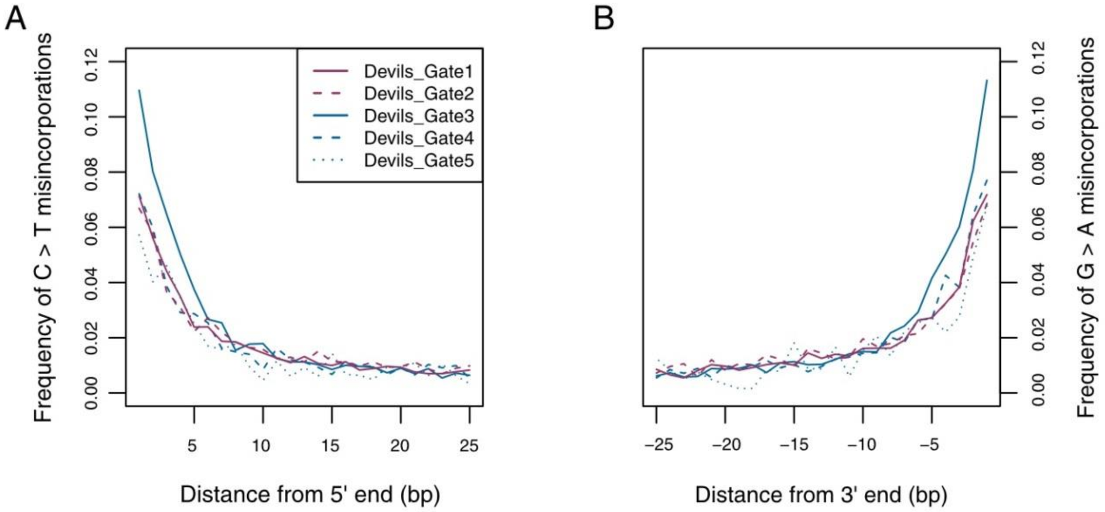

Supplementary Figure C.2 Damage patterns for Devil's Gate samples. Plots show mismatch frequency relative to the reference genome as a function of read position. A) shows the frequency of C to T misincorporations at the 5' ends of reads while B) shows the frequency of G to A transitions at the 3' ends of reads.

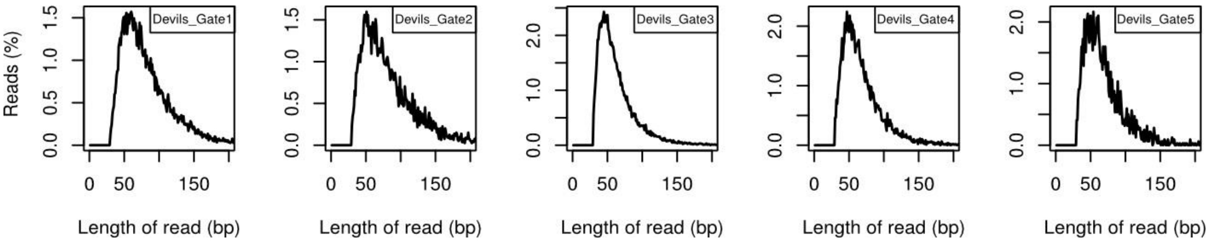

Supplementary Figure C.3 Sequence length distribution for samples from Devil's Gate. All samples have sequences in the range expected for ancient DNA.

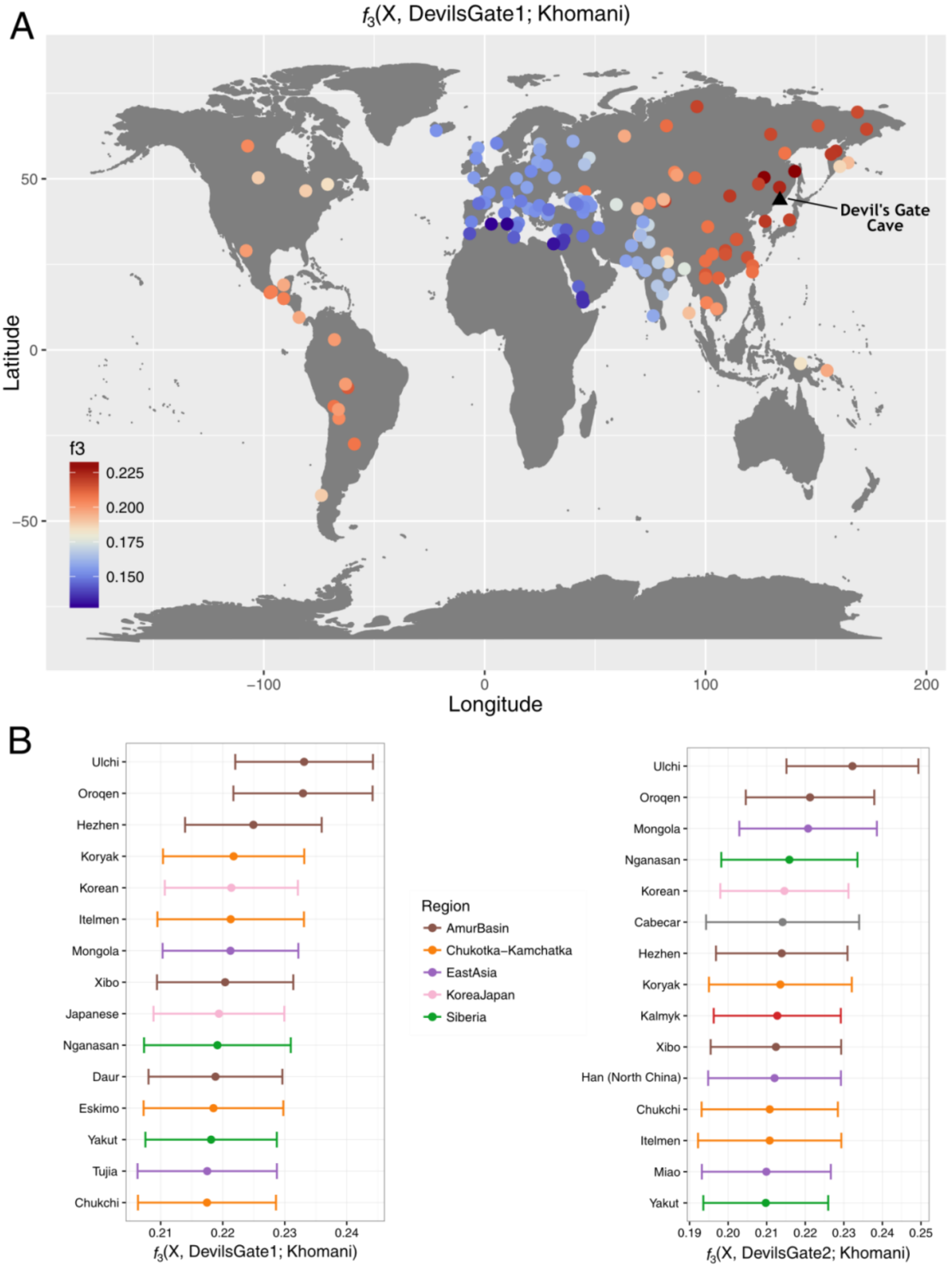

Supplementary Figure C.4 Outgroup f3 statistics on PMDtools-filtered data. Outgroup f3 measuring shared drift between samples from Devil's Gate (black triangle shows sampling location) and modern populations with respect to an African outgroup (Khomani), using only reads with a PMD score of at least 3(9). (A) Map of the whole world. (B) 15 populations with the highest shared drift with Devil's Gate, color coded by regions as on Figure PCA. Error bars represent one standard error.

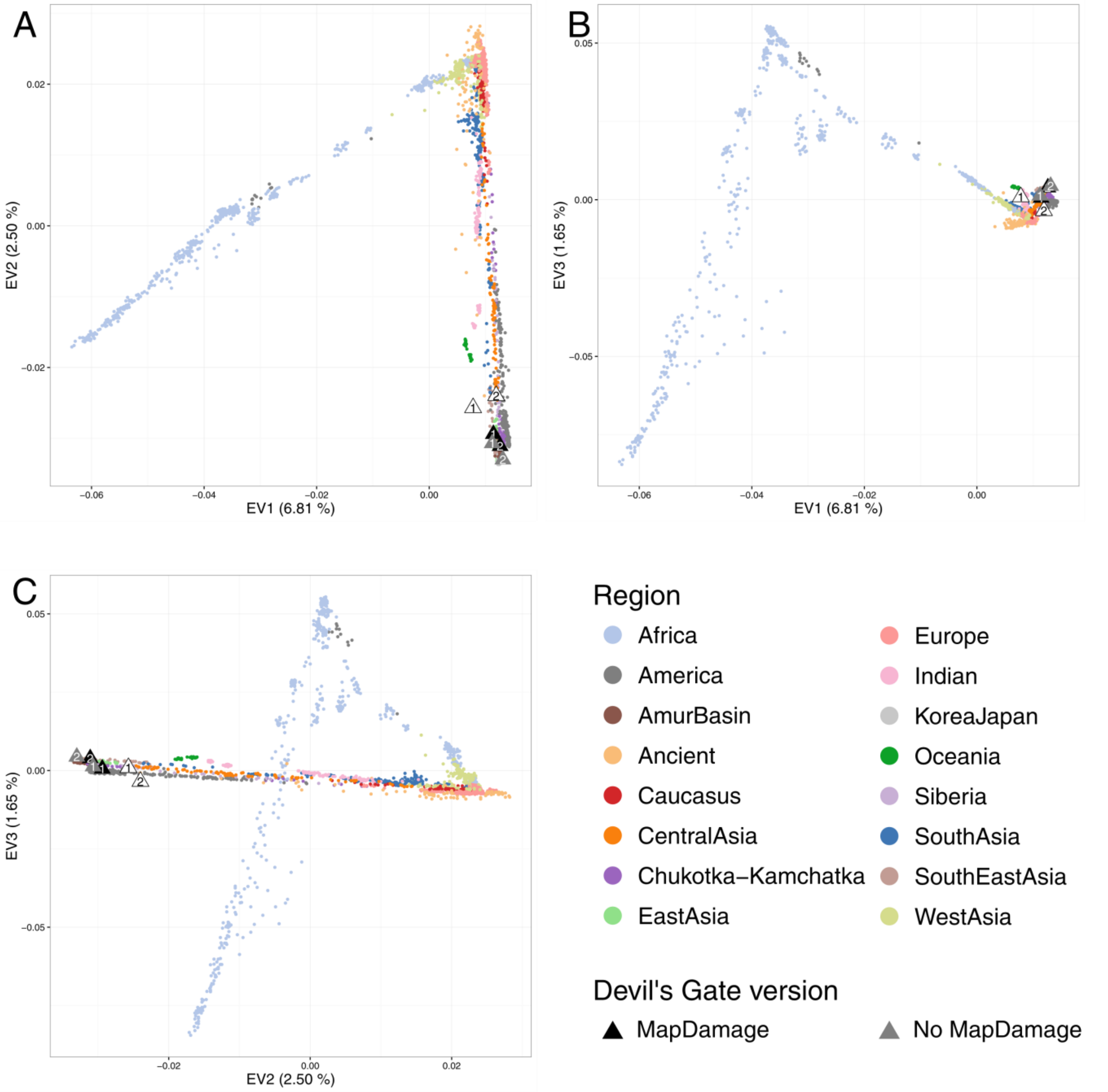

Supplementary Figure C.5 Principal component analysis on all SNPs using the worldwide panel. Black (MapDamage treated), gray (not MapDamage treated) and white (PMD-filtered, not MapDamage treated) symbols mark DevilsGate1 and DevilsGate2, projected upon the principal components as defined by the modern panel. Proportion of variance explained is displayed in parentheses on the axis. A) Component 1 and 2. B) Component 1 and 3. C) Component 2 and 3.

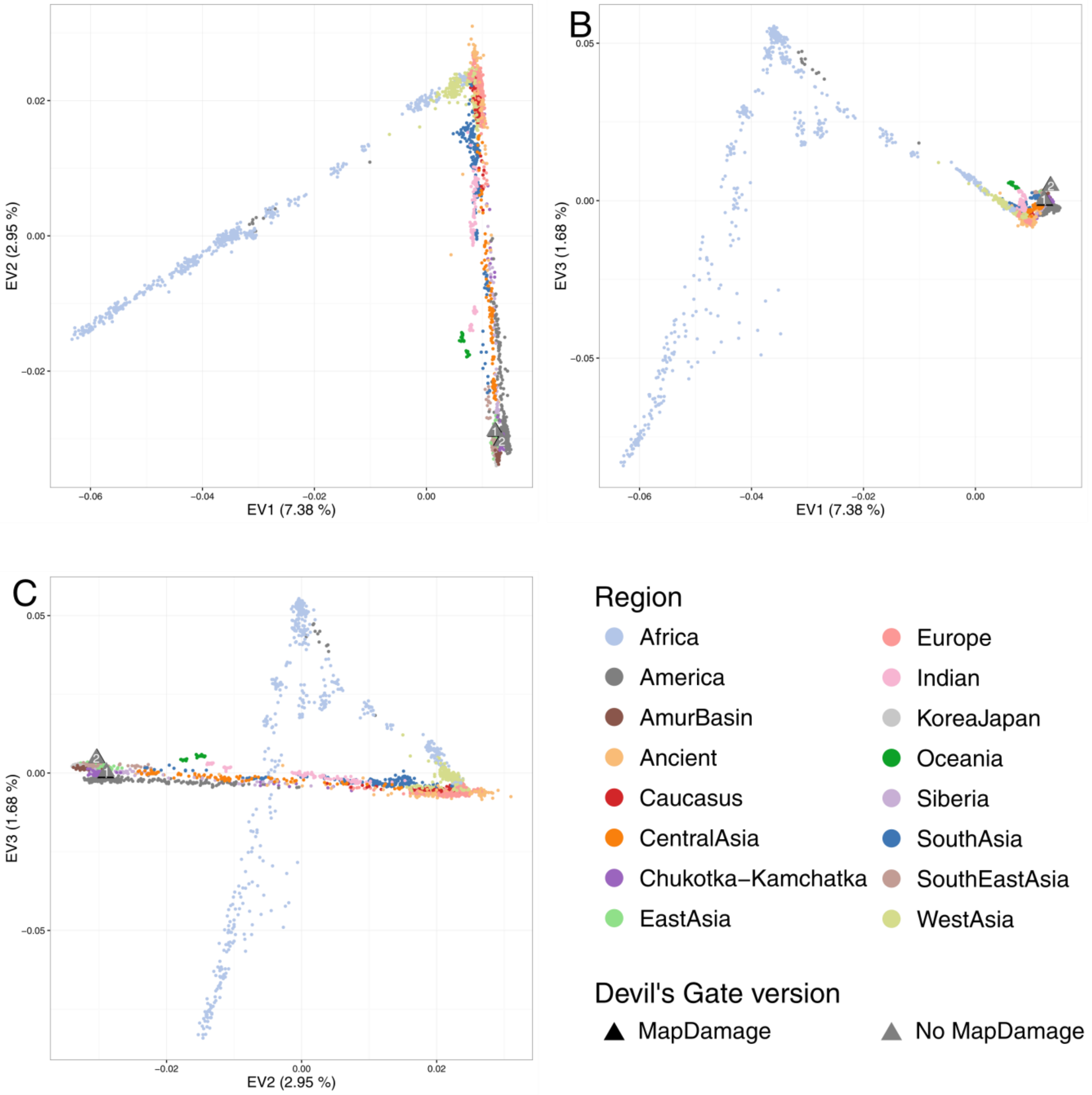

Supplementary Figure C.6 Principal component analysis on transversion SNPs using the worldwide panel. Black (MapDamage treated) and gray (not MapDamage treated) symbols mark DevilsGate1 and DevilsGate2, projected upon the principal components as defined by the modern panel. Proportion of variance explained is displayed in parentheses on the axis. A) Component 1 and 2. B) Component 1 and 3. C) Component 2 and 3.

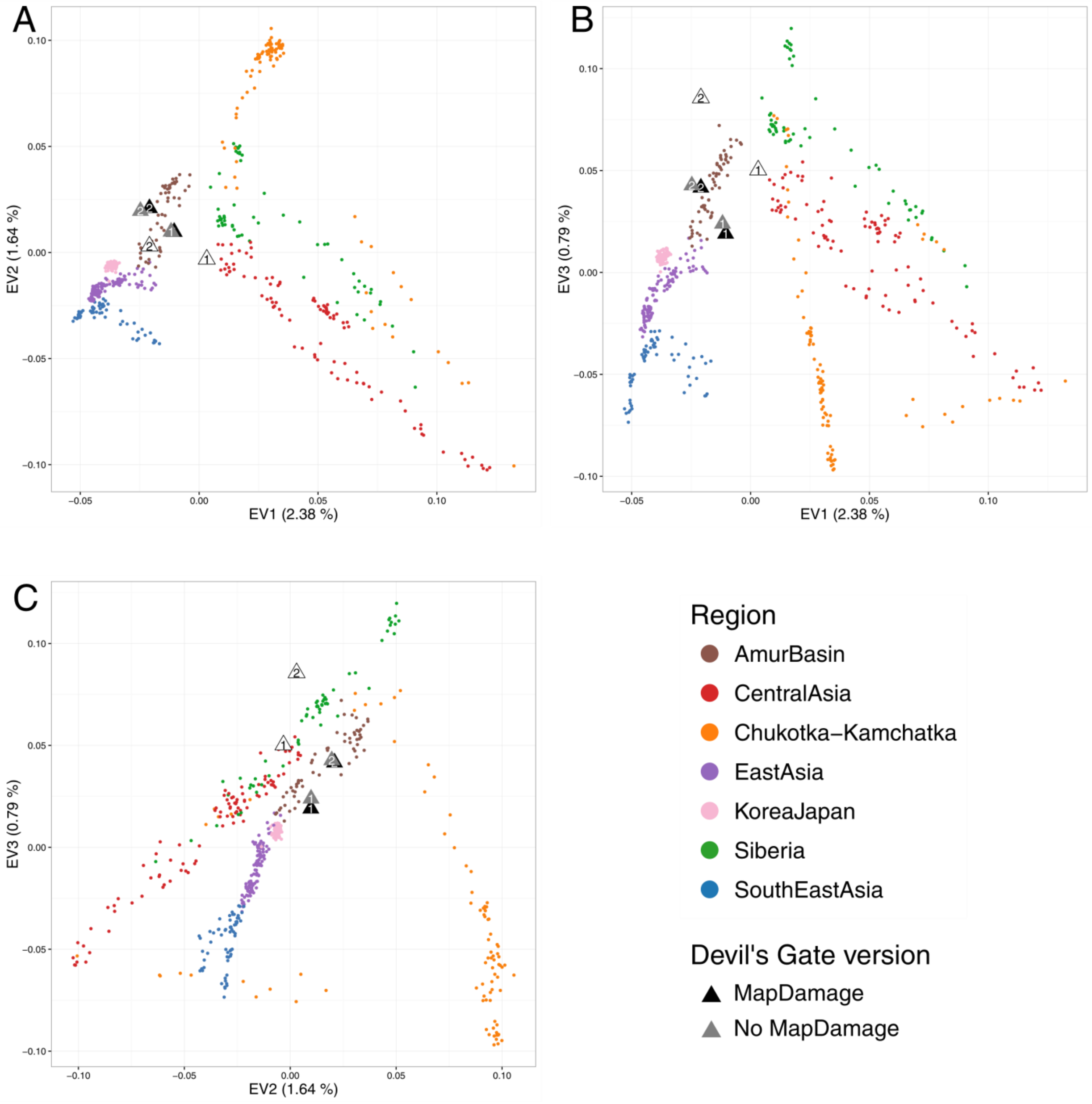

Supplementary Figure C.7 Principal component analysis on all SNPs using the regional panel. Black (MapDamage treated), gray (not MapDamage treated) and white (PMD-filtered, not MapDamage treated) symbols mark DevilsGate1 and DevilsGate2, projected upon the principal components as defined by the modern panel. Proportion of variance explained is displayed in parentheses on the axis. A) Component 1 and 2. B) Component 1 and 3. C) Component 2 and 3.

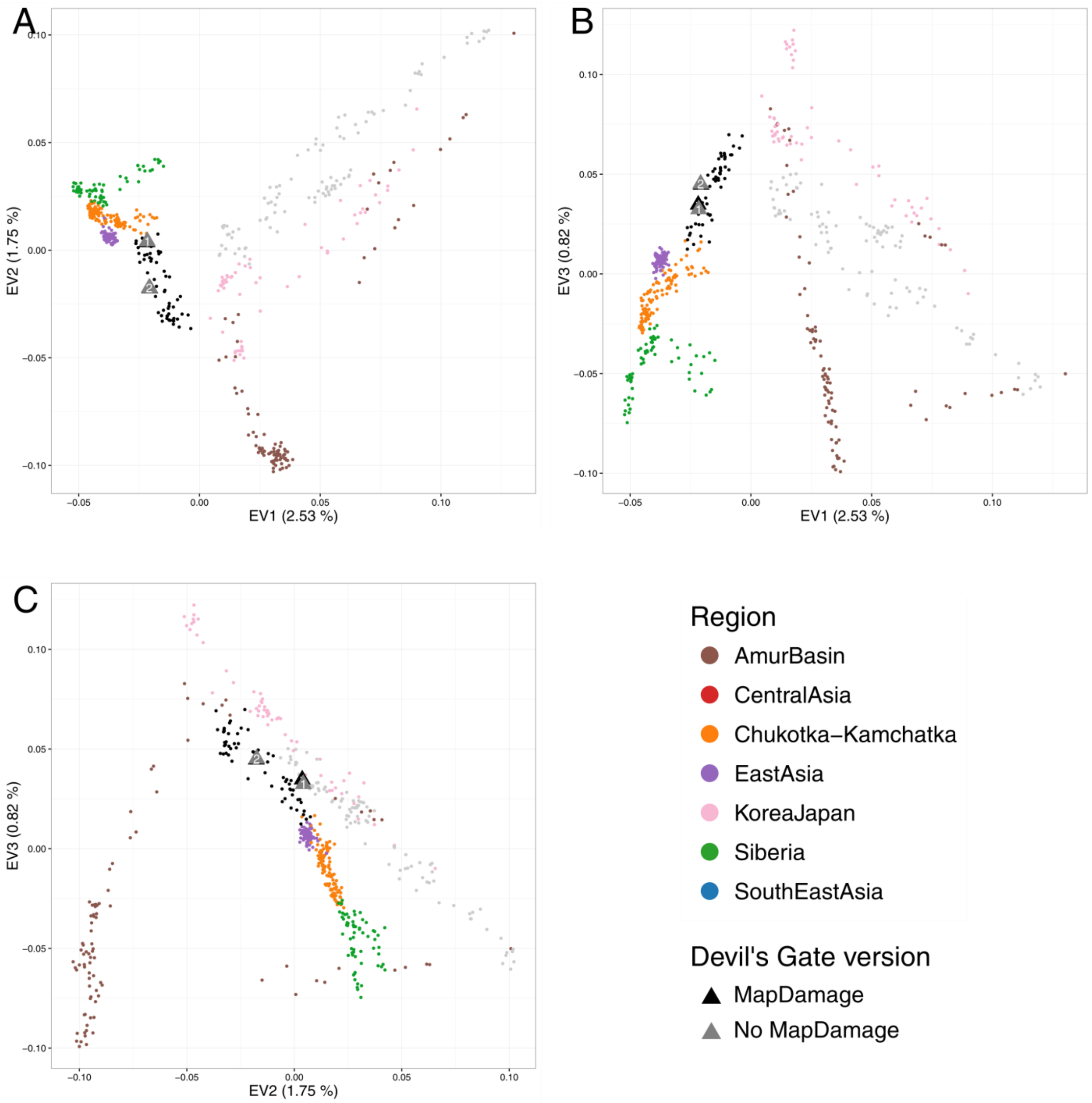

Supplementary Figure C.8 Principal component analysis on transversion SNPs using the regional panel. Black (MapDamage treated) and gray (not MapDamage treated) symbols mark DevilsGate1 and DevilsGate2, projected upon the principal components as defined by the modern panel. Proportion of variance explained is displayed in parentheses on the axis. A) Component 1 and 2. B) Component 1 and 3. C) Component 2 and 3.

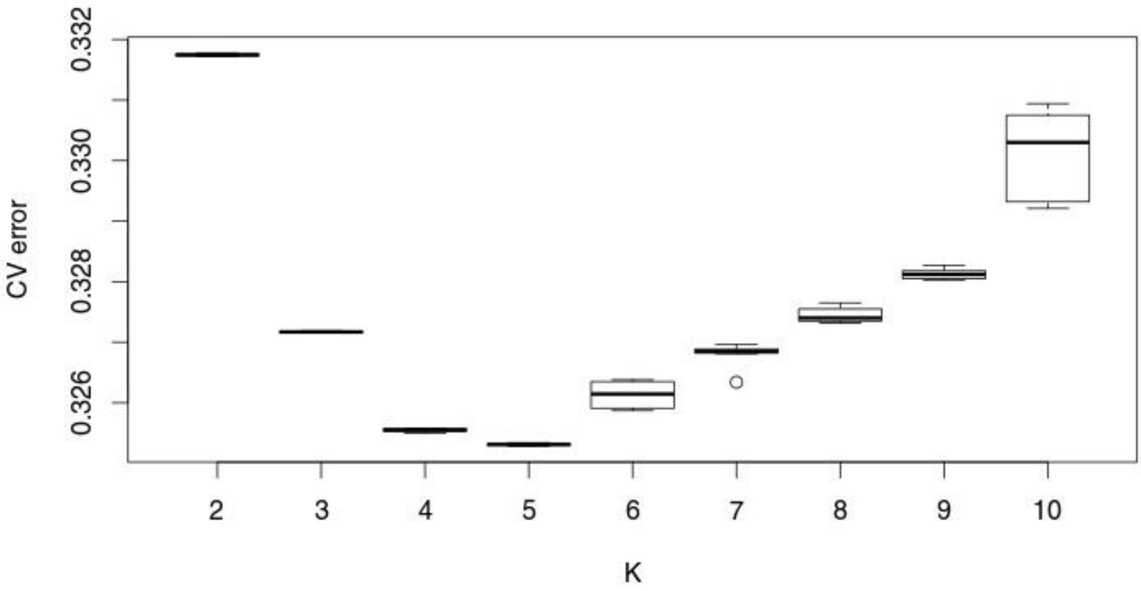

Supplementary Figure C.9 ADMIXTURE analysis cross validation (CV) error as a function of the number of clusters (K) for the regional panel, using all SNPs (top row) or transversions only (bottom row) and with (left column) or without (right column) MapDamage treatment. The lowest mean value was attained at K=5.

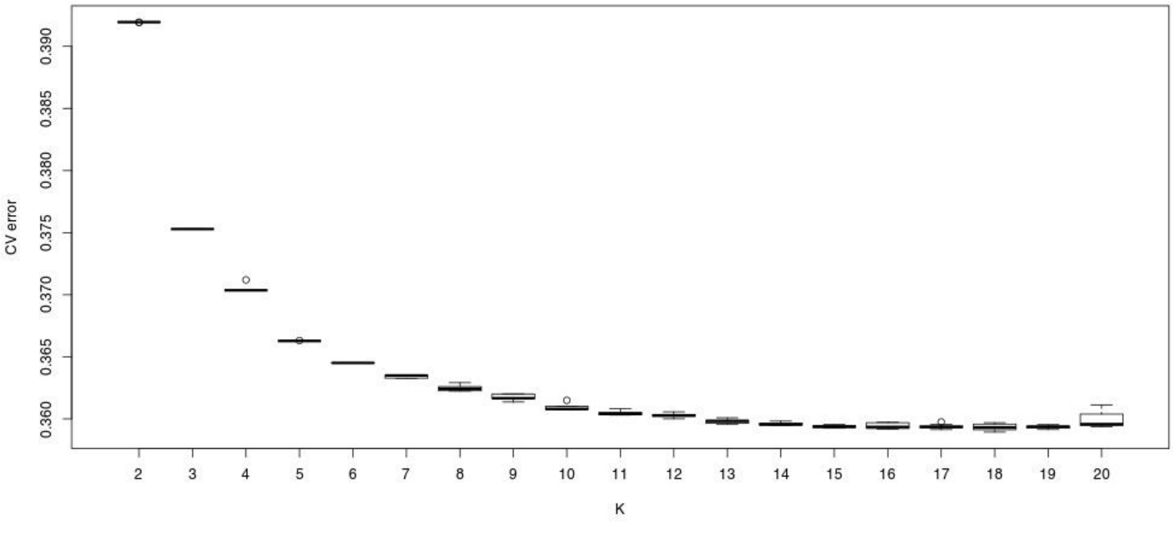

Supplementary Figure C.10 ADMIXTURE analysis cross validation (CV) error as a function of the number of clusters (K) for the world panel, using all SNPs (top row) or transversions only (bottom row) and with (left column) or without (right column) MapDamage treatment. The lowest mean value was attained at K=18.

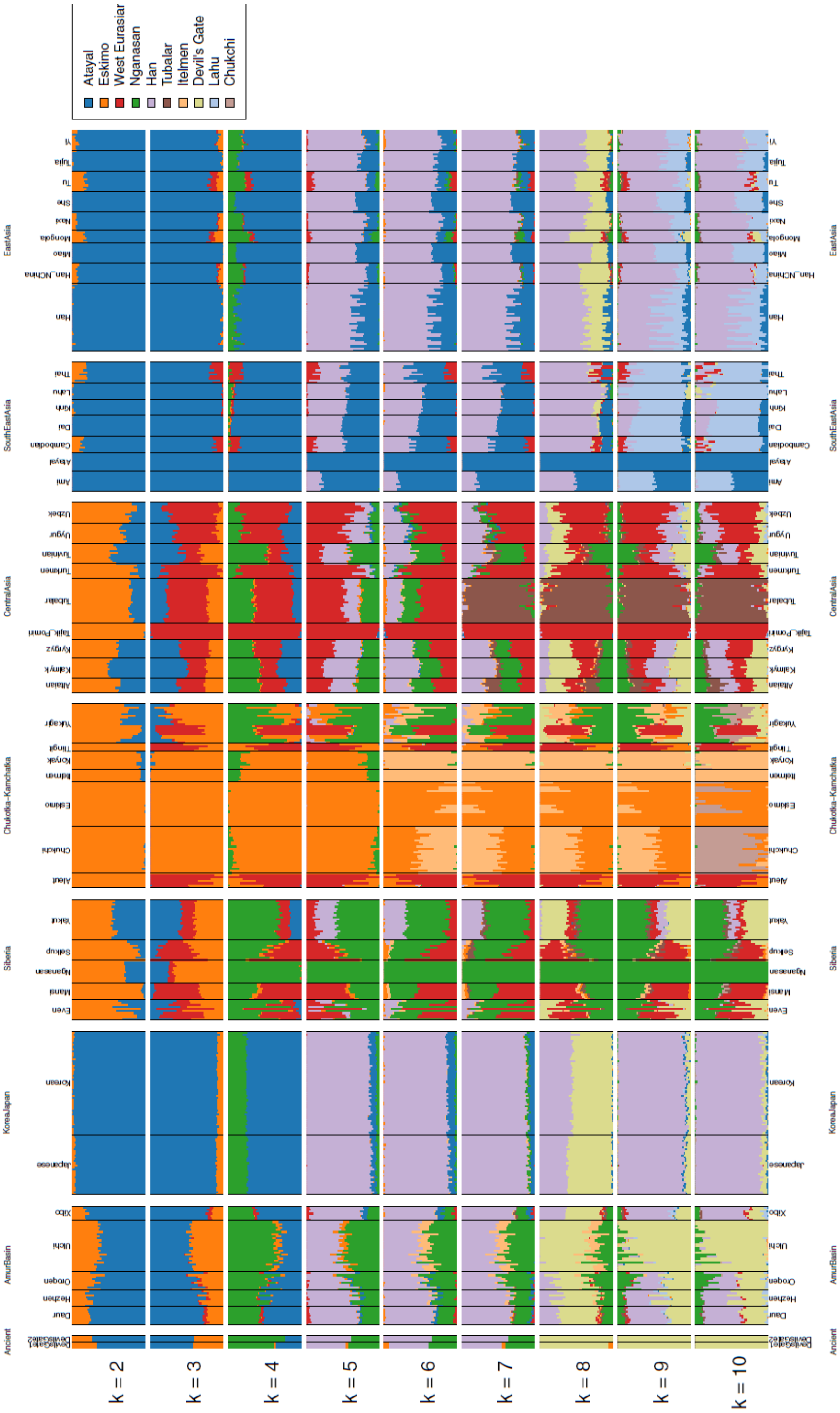

Supplementary Figure C.11 Results from ADMIXTURE analysis using the regional panel, all SNP-s and setting the number of clusters to K=2 to K=10. Minimal cross-validation error was attained at K=5.

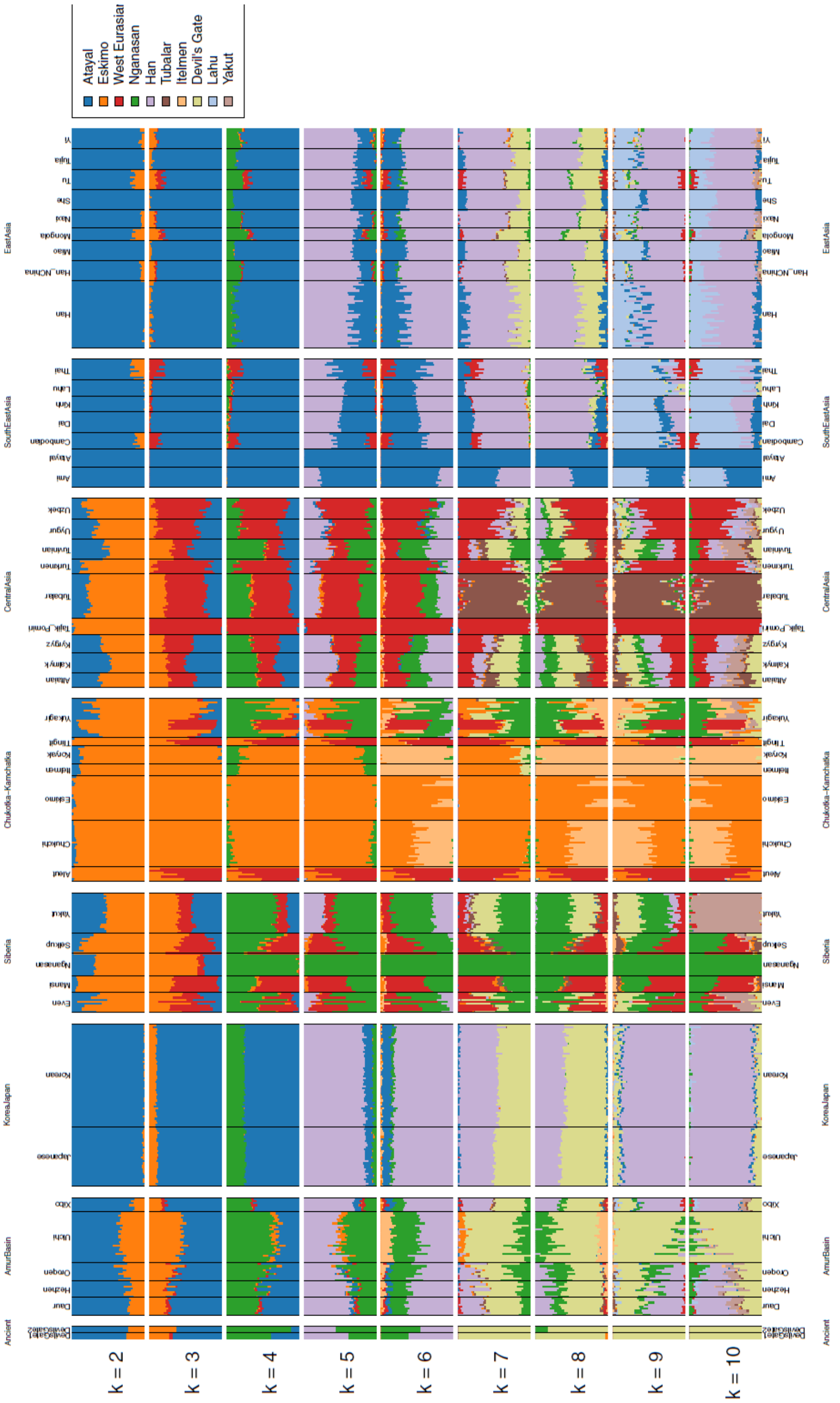

Supplementary Figure C.12 Results from ADMIXTURE analysis using the regional panel, transversion SNP-s and setting the number of clusters to K=2 to K=10. Minimal cross-validation error was attained at K=5.

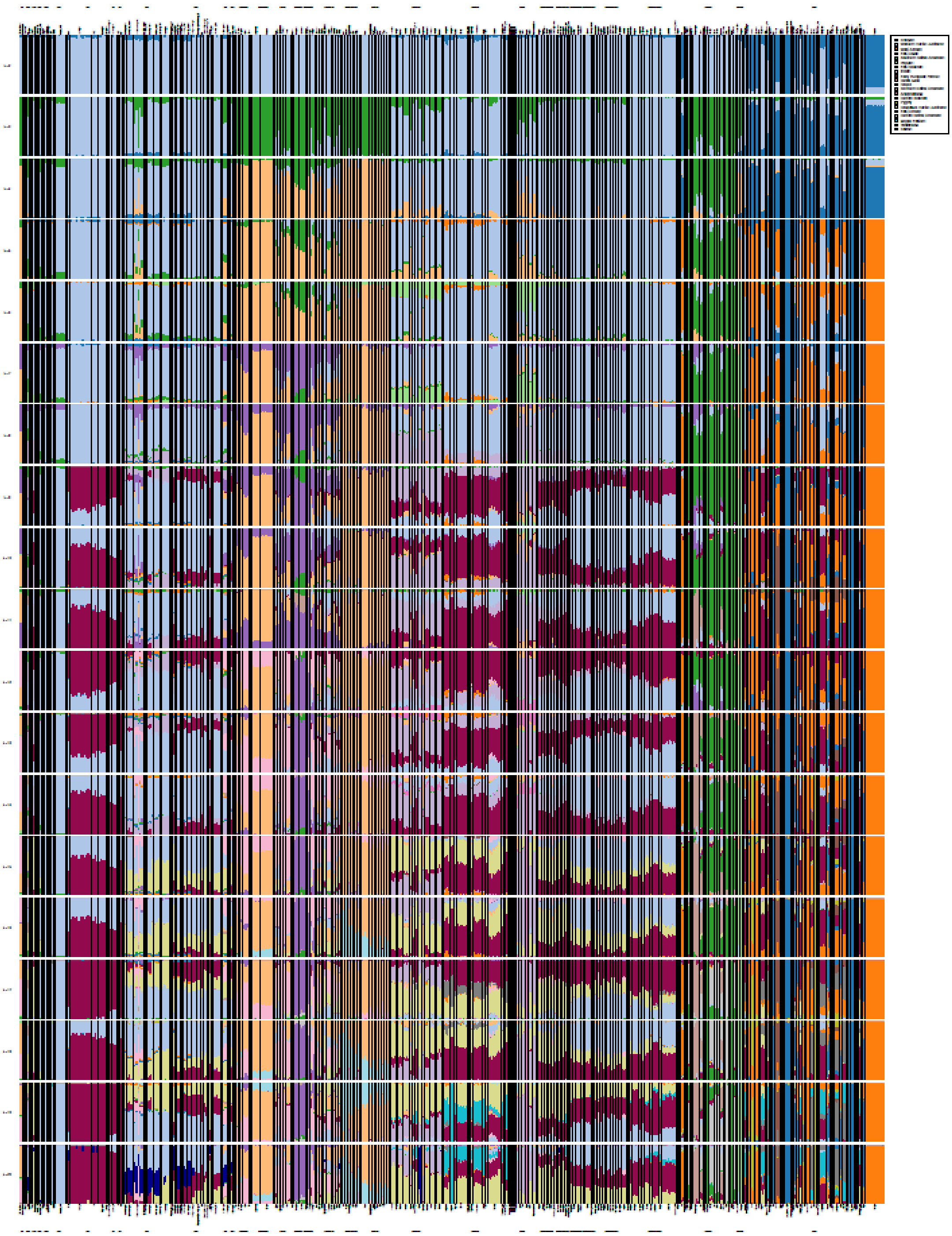

Supplementary Figure C.13 Results from ADMIXTURE analysis using the total panel, all SNP-s and setting the number of clusters to K=2 to K=20. Minimal cross-validation error was attained at K=5.

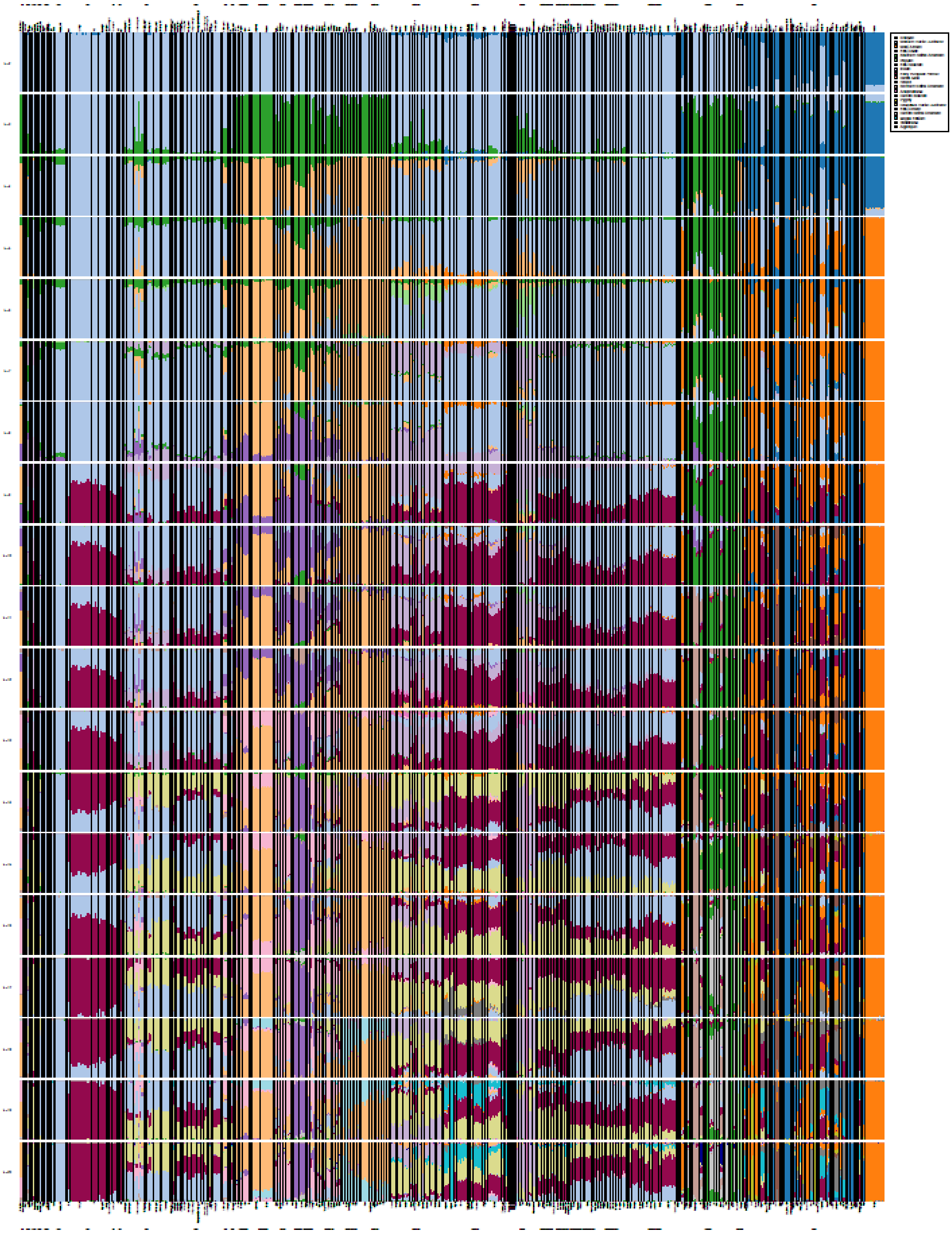

Supplementary Figure C.14 Results from ADMIXTURE analysis using the total panel, transversion SNP-s and setting the number of clusters to K=2 to K=20. Minimal cross-validation error was attained at K=5.

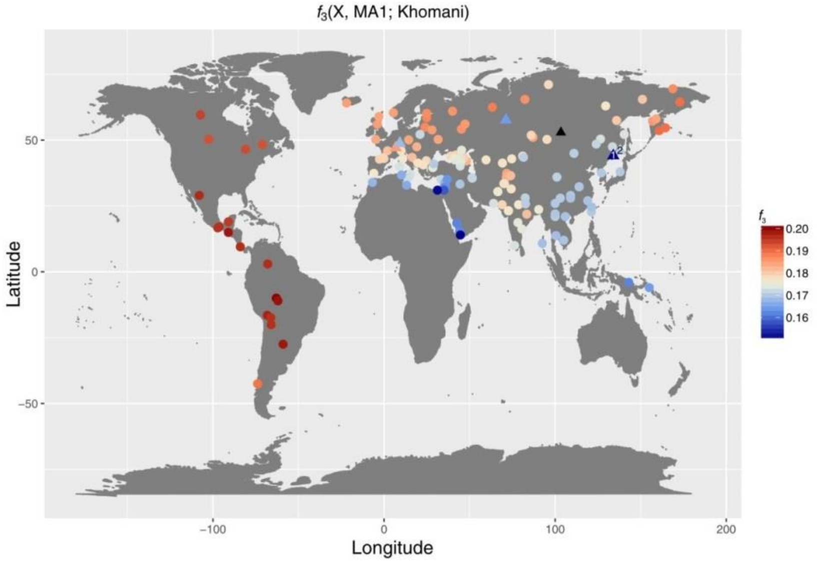

Supplementary Figure C.15 Outgroup f3 scores of the form f3(X, MA1; Khomani), with modern populations and selected ancient samples (Ust'Ishim, Kotias, Loschbour and Stuttgart), using all SNPs, with f3 > 0.15 displayed. The black triangle marks the location of MA1.

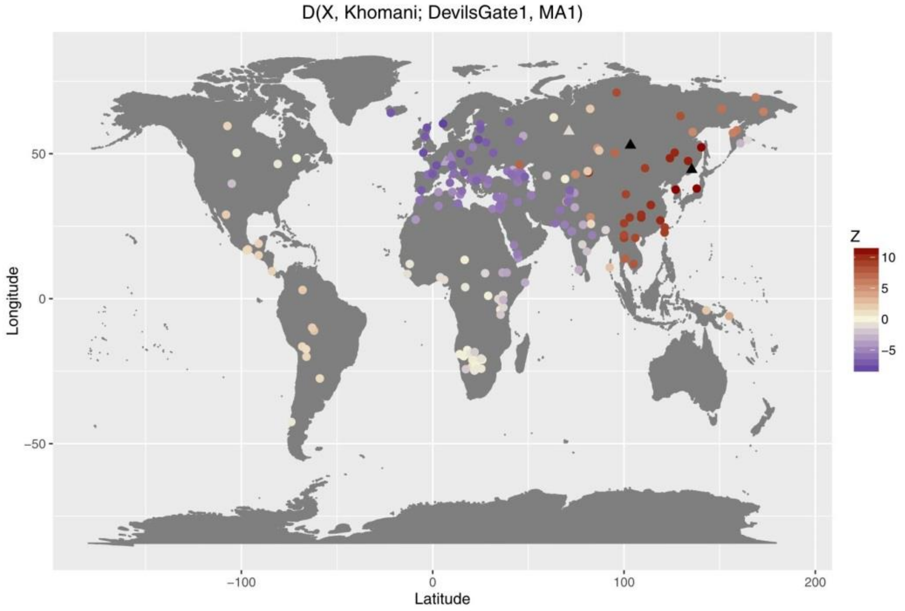

Supplementary Figure C.16 D scores of the form D(X, Khomani; MA1, DevilsGate1), with all modern populations in our panel and selected ancient samples, using all SNPs. (Ust'Ishim, Kotias, Loschbour and Stuttgart) displayed. The black triangles mark the location of MA1 and Devil's Gate.

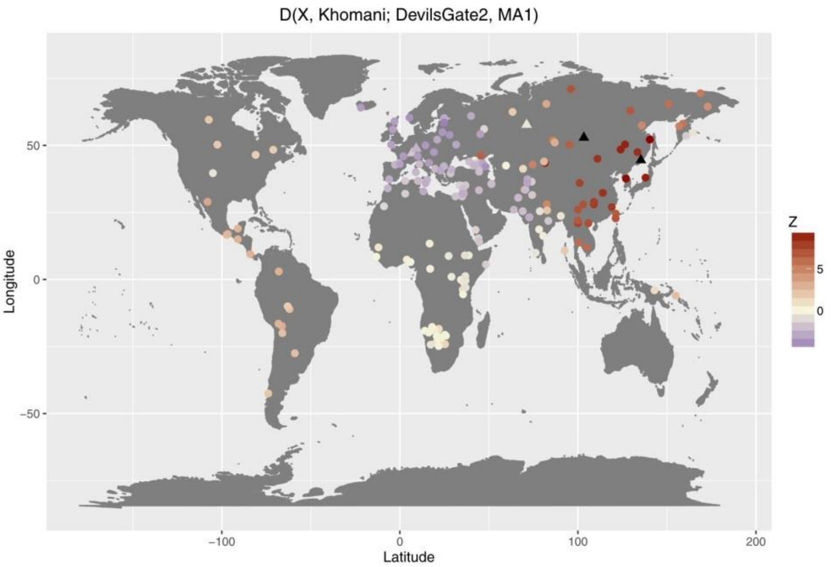

Supplementary Figure C.17 D scores of the form D(X, Khomani; MA1, DevilsGate1), with all modern populations in our panel and selected ancient samples, using all SNPs. (Ust'Ishim, Kotias, Loschbour and Stuttgart) displayed. The black triangles mark the location of MA1 and Devil's Gate.

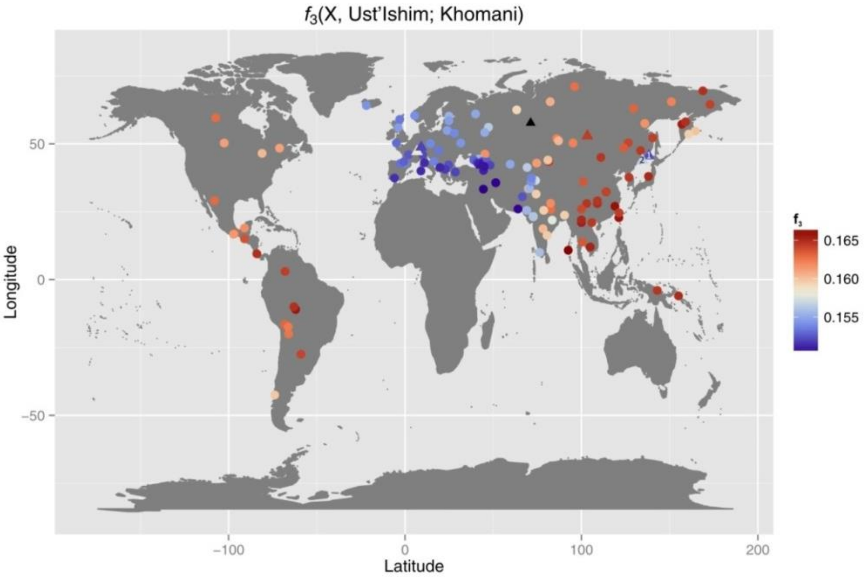

Supplementary Figure C.18 Outgroup f3 scores of the form f3(X, Ust'Ishim; Khomani), with modern populations and selected ancient samples (MA1, Kotias, Loschbour and Stuttgart), using all SNPs, with f3 > 0.15 displayed. The black triangle marks the location of Ust'Ishim.

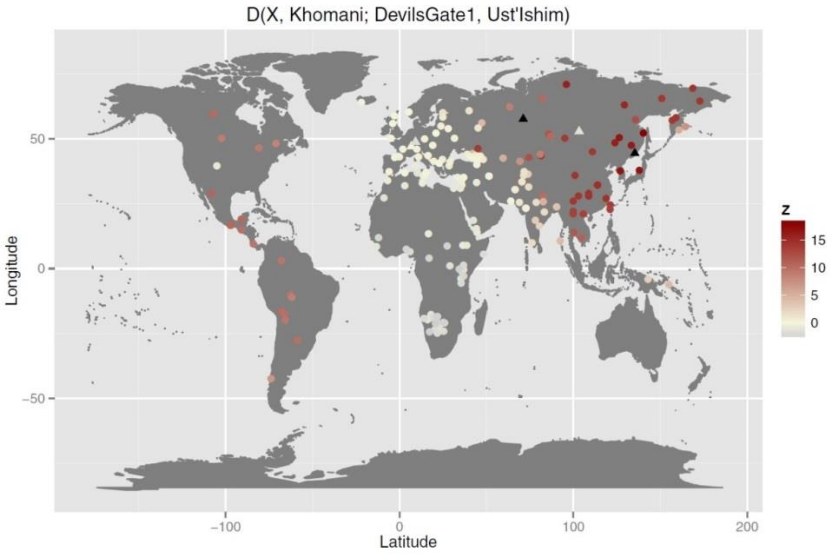

Supplementary Figure C.19 D scores of the form D(X, Khomani; Ust'Ishim, DevilsGate1), with all modern populations in our panel and selected ancient samples, using all SNPs. (MA1, Kotias, Loschbour and Stuttgart) displayed. The black triangles mark the location of MA1 and Devil's Gate.

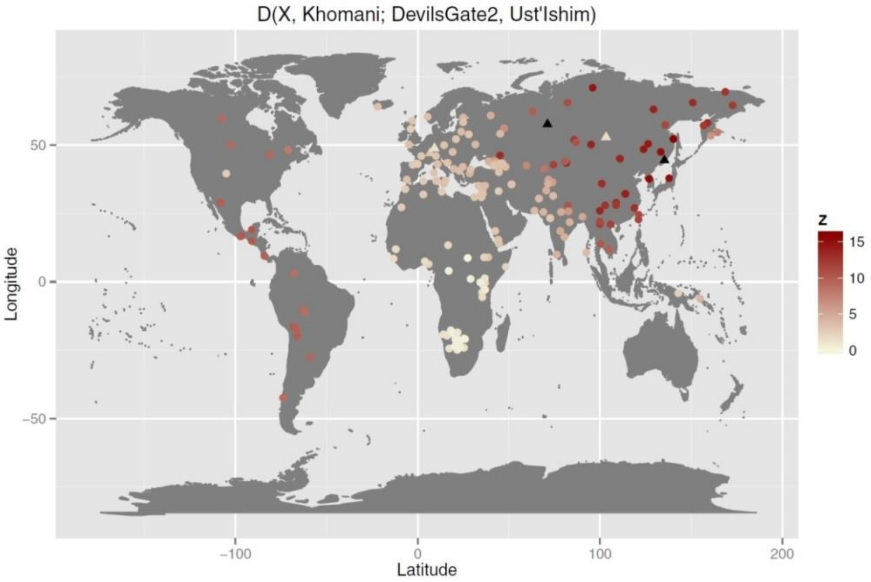

Supplementary Figure C.20 D scores of the form D(X, Khomani; Ust'Ishim, DevilsGate2), with all modern populations in our panel and selected ancient samples, using all SNPs. (MA1, Kotias, Loschbour and Stuttgart) displayed. The black triangles mark the location of MA1 and Devil's Gate.

C.5 Supplementary tables

Supplementary Table C.1 Details of sample preparation and sequencing. Extraction codes: 1*, DNA extracted from first lysis buffer' 2* DNA extracted from second lysis buffer; bp, base pairs. High quality non-clonal reads refers to reads with mapping quality >=30 and of length >=30. Coverage: average genomic depth of coverage.

Sample	Library ID	Extraction	Skeletal element	Sequencing Instrument	Sequencing facility	Sequencing length and type	Reads	Aligned reads	%	High quality non-clonal	Coverage (x)
DevilsGate4	MOS2A.E1	1*	molar	Illumina MiSeq	TrinSeq, Dublin	150bp paired end	7,096,341	25,455	0.36	10792	0.0002
	MOS2C.E1	1*	cranial fragment	Illumina MiSeq	TrinSeq, Dublin	150bp paired end	433,003	1,510	0.35		
DevilsGate3	MOS3.2A.E1	1*	molar (root)	Illumina MiSeq	TrinSeq, Dublin	150bp paired end	535,857	14,895	2.78	31184	0.0006
	MOS3.3A.E1	1*	molar (crown)	Illumina MiSeq	TrinSeq, Dublin	150bp paired end	560,654	26,440	4.72		
DevilsGate2	MOS4A.E1	1*	molar	Illumina HiSeq	Beijing Genomics Institute, China	50bp single end	6,775,617	132,363	1.95	1,469,128	0.0333
	MOS4A.E1	1*	molar	Illumina HiSeq	Beijing Genomics Institute, China	50bp single end	108,566,893	2,003,142	1.85		
	MOS4A.E1	1*	molar	Illumina MiSeq	TrinSeq, Dublin	150bp paired end	618,270	11,689	1.89		
	MOS4A.E2	2*	molar	Illumina MiSeq	TrinSeq, Dublin	150bp paired end	338,589	7,172	2.12		
	MOS4.C3.E1	1*	cranial fragment	Illumina MiSeq	TrinSeq, Dublin	150bp paired end	532,719	2,822	0.53		
DevilsGate1	MOS5A.E1	1*	molar	Illumina HiSeq	Beijing Genomics Institute, China	50bp single end	3,775,905	127,260	3.37	2,625,622	0.0759
	MOS5A.E1	1*	molar	Illumina HiSeq	Beijing Genomics Institute, China	50bp single end	34,240,237	1,129,604	3.30		
	MOS5A.E1	1*	molar	Illumina MiSeq	TrinSeq, Dublin	150bp paired end	584,305	20,133	3.45		
	MOS5A.E2	2*	molar	Illumina MiSeq	TrinSeq, Dublin	150bp paired end	444,709	18,755	4.22		
	MOS5B.R1.E2	2*	molar (root)	Illumina MiSeq	TrinSeq, Dublin	70bp single end	2,632,825	216,661	8.23		
	MOS5B.R1.E2	2*	molar (root)	Illumina HiSeq	Theragen BiO Institute	100 bp paired end	60,490,976	2,043,091	3.38		
DevilsGate5	MOS6.C1.E1	1*	cranial fragment	Illumina MiSeq	TrinSeq, Dublin	150bp paired end	518,401	5,457	1.05	3,187	0.0001

Appendix C Appendix for Chapter 4

Supplementary Table C.2 Regional groups for the Human Origins panel.

Population	Region	Population	Region	Population	Region
Abkhasian	SouthCaucasus	Gambian	Africa	Koryak	Chukotka-Kamchatka
AA	America	Punjabi	SouthAsia	Itelmen	Chukotka-Kamchatka
Turkish	WestAsia	Esan	Africa	Cochin Jew	Indian
Chukchi	Chukotka-Kamchatka	Bengali	SouthAsia	Kumyk	NorthCaucasus
Eskimo	Chukotka-Kamchatka	Mende	Africa	Kusunda	SouthAsia
Nganasan	Siberia	Brahui	SouthAsia	Lebanese	WestAsia
Oromo	Africa	Balochi	SouthAsia	Lezgin	NorthCaucasus
Albanian	SouthernEurope	Hazara	SouthAsia	Libyan Jew	Africa
Tlingit	Chukotka-Kamchatka	Makrani	SouthAsia	Lithuanian	NorthernEurope
Aleut	Chukotka-Kamchatka	Sindhi	SouthAsia	Lodhi	Indian
Algerian	Africa	Pathan	SouthAsia	Mala	Indian
Altaian	CentralAsia	Kalash	SouthAsia	Maltese	SouthernEurope
Armenian	SouthCaucasus	Burusho	SouthAsia	Mansi	Siberia
Ashkenazi Jew	EasternEurope	Mbuti	Africa	Georgian	SouthCaucasus
Aymara	America	Biaka	Africa	Mixtec	America
Masai	Africa	French	WesternEurope	Mixe	America
Somali	Africa	Papuan	Oceania	Mordovian	NorthernEurope
Luo	Africa	Druze	WestAsia	Moroccan Jew	Africa
Kikuyu	Africa	BedouinB	WestAsia	Korean	KoreaJapan
Balkar	NorthCaucasus	BedouinA	WestAsia	Atayal	SouthEastAsia
Hadza	Africa	Bougainville	Oceania	Ami	SouthEastAsia
Basque	SouthernEurope	Sardinian	SouthernEurope	Czech	EasternEurope
Belarusian	NorthernEurope	Palestinian	WestAsia	Icelandic	NorthernEurope
Kyrgyz	CentralAsia	Piapoco	America	Luhya	Africa
Bolivian	America	Cambodian	SouthEastAsia	GujaratiD	Indian
Quechua	America	Japanese	KoreaJapan	GujaratiB	Indian
Taa East	Africa	Han	EastAsia	GujaratiA	Indian
Hoan	Africa	Orcadian	NorthernEurope	GujaratiC	Indian
Taa West	Africa	Surui	America	Chipewyan	America
Taa North	Africa	Mayan	America	Wambo	Africa
Gui	Africa	Russian	NorthernEurope	Xuun	Africa
Naro	Africa	Mandenka	Africa	Haiom	Africa
Gana	Africa	Yoruba	Africa	Damara	Africa
Kgalagadi	Africa	Yakut	Siberia	Himba	Africa
Ju hoan South	Africa	BantuSA	Africa	Nama	Africa
Ju hoan North	Africa	Karitiana	America	Even	Siberia
Khwe	Africa	Pima	America	Nogai	NorthCaucasus
Shua	Africa	Tujia	EastAsia	Norwegian	NorthernEurope

Tshwa	Africa	Bergamo	SouthernEurope	North Ossetian	NorthCaucasus
Tswana	Africa	Tuscan	SouthernEurope	Ojibwa	America
Bulgarian	EasternEurope	Yi	EastAsia	Onge	Indian
Cabecar	America	Miao	EastAsia	Khomani	Africa
Chechen	NorthCaucasus	Oroqen	AmurBasin	Saharawi	Africa
Thai	SouthEastAsia	Daur	AmurBasin	Sandawe	Africa
Chilote	America	Mongola	EastAsia	Saudi	WestAsia
Chuvash	NorthernEurope	Hezhen	AmurBasin	Selkup	Siberia
Yukagir	Chukotka-Kamchatka	Xibo	AmurBasin	Turkish Jew	WestAsia
Cree	America	Mozabite	Africa	French South	WesternEurope
Croatian	SouthernEurope	Han NChina	EastAsia	Sicilian	SouthernEurope
Cypriot	WestAsia	Uygur	CentralAsia	Syrian	WestAsia
Dinka	Africa	Dai	SouthEastAsia	Tajik Pomiri	CentralAsia
Egyptian	Africa	Lahu	SouthEastAsia	Guarani	America
Estonian	NorthernEurope	She	EastAsia	Tiwari	Indian
Ethiopian Jew	Africa	Naxi	EastAsia	Tubalar	CentralAsia
Georgian Jew	SouthCaucasus	Tu	EastAsia	Tunisian	Africa
Algonquin	America	Adygei	NorthCaucasus	Tunisian Jew	Africa
Greek	SouthernEurope	BantuKenya	Africa	Tuvinian	CentralAsia
Kaqchikel	America	Hungarian	EasternEurope	Ukrainian	EasternEurope
Scottish	NorthernEurope	Iranian	SouthAsia	Ulchi	AmurBasin
English	NorthernEurope	Iranian Jew	SouthAsia	Uzbek	CentralAsia
Finnish	NorthernEurope	Iraqi Jew	WestAsia	Turkmen	CentralAsia
Spanish	SouthernEurope	Jordanian	WestAsia	Vishwabrahmin	Indian
Spanish North	SouthernEurope	Kalmyk	CentralAsia	Yemen	WestAsia
Kinh	SouthEastAsia	Kharia	Indian	Yemenite Jew	WestAsia
				Zapotec	America

Appendix C Appendix for Chapter 4

Supplementary Table C.3 Samples from the Personal Genome Project Korea (http://opengenome.net/)

Sample ID	Population	Region
KPGP-00001	Korean	KoreaJapan
KPGP-00002	Korean	KoreaJapan
KPGP-00006	Korean	KoreaJapan
KPGP-00032	Korean	KoreaJapan
KPGP-00033	Korean	KoreaJapan
KPGP-00039	Korean	KoreaJapan
KPGP-00056	Korean	KoreaJapan
KPGP-00086	Korean	KoreaJapan
KPGP-00088	Korean	KoreaJapan
KPGP-00090	Korean	KoreaJapan
KPGP-00117	Korean	KoreaJapan
KPGP-00120	Korean	KoreaJapan
KPGP-00121	Korean	KoreaJapan
KPGP-00122	Korean	KoreaJapan
KPGP-00124	Korean	KoreaJapan
KPGP-00125	Korean	KoreaJapan
KPGP-00127	Korean	KoreaJapan
KPGP-00128	Korean	KoreaJapan
KPGP-00129	Korean	KoreaJapan
KPGP-00131	Korean	KoreaJapan
KPGP-00132	Korean	KoreaJapan
KPGP-00134	Korean	KoreaJapan
KPGP-00136	Korean	KoreaJapan
KPGP-00137	Korean	KoreaJapan
KPGP-00138	Korean	KoreaJapan
KPGP-00139	Korean	KoreaJapan
KPGP-00141	Korean	KoreaJapan
KPGP-00142	Korean	KoreaJapan
KPGP-00144	Korean	KoreaJapan
KPGP-00145	Korean	KoreaJapan
KPGP-00205	Korean	KoreaJapan
KPGP-00220	Korean	KoreaJapan
KPGP-00224	Korean	KoreaJapan
KPGP-00227	Korean	KoreaJapan
KPGP-00228	Korean	KoreaJapan
KPGP-00229	Korean	KoreaJapan
KPGP-00230	Korean	KoreaJapan
KPGP-00232	Korean	KoreaJapan
KPGP-00233	Korean	KoreaJapan
KPGP-00235	Korean	KoreaJapan
KPGP-00254	Korean	KoreaJapan
KPGP-00255	Korean	KoreaJapan
KPGP-00256	Korean	KoreaJapan
KPGP-00265	Korean	KoreaJapan
KPGP-00266	Korean	KoreaJapan

Supplementary Table C.4 Ancient samples used in the study.

Sample ID	Population	Country	Broad group	Publication
DevilsGate1	DevilsGate	Russia	DG	This study
DevilsGate2	DevilsGate	Russia	DG	This study
KK1	KK1	Georgia	CHG	Jones et al. 2015
SATP_md	SATP	Georgia	CHG	Jones et al. 2015
Bichon	Bichon	Luxembourg	WHG	Jones et al. 2015
BR1_md	BR1	Hungary	WBR	Lazaridis et al. 2014
BR2	BR2	Hungary	WBR	Lazaridis et al. 2014
CO1_md	CO1	Hungary	CO	Lazaridis et al. 2014
HDma1_md	HDma1	Hungary	WBR	Lazaridis et al. 2014
IR1_md	IR1	Hungary	WIR	Lazaridis et al. 2014
KO1_md	KO1	Hungary	WHG	Lazaridis et al. 2014
Kostenki	Kostenki	Russia	PHG	Lazaridis et al. 2014
LaBrana_md	LaBrana	Spain	WHG	Lazaridis et al. 2014
LBK_hg19_1000g	Stuttgart	Germany	EEF	Lazaridis et al. 2014
Loschbour_hg19_1000g	Loschbour	Germany	WHG	Lazaridis et al. 2014
MA1_nf	MA1	Russia	PHG	Lazaridis et al. 2014
Gok2_md	Gok	Sweden	EEF	Lazaridis et al. 2014
Ajv58_md	Ajv	Sweden	SHG	Lazaridis et al. 2014
Motala12_ancient	Motala12	Sweden	SHG	Lazaridis et al. 2014
NE1	NE	Hungary	EEF	Lazaridis et al. 2014
NE5_md	NE	Hungary	EEF	Lazaridis et al. 2014
NE6_md	NE	Hungary	EEF	Lazaridis et al. 2014
NE7_md	NE	Hungary	EEF	Lazaridis et al. 2014
otzi_nf	otzi	Italy	CO	Lazaridis et al. 2014
Ust_Ishim	Ust_Ishim	Russia	PHG	Lazaridis et al. 2014
RISE00	baCw	Estonia	WBR	Allentoft et al. 2015
RISE150	baUne	Poland	WBR	Allentoft et al. 2015
RISE174	irSca	Sweden	WIR	Allentoft et al. 2015
RISE392	baSin	Russia	EBR	Allentoft et al. 2015
RISE394	baSin	Russia	EBR	Allentoft et al. 2015
RISE395	baSin	Russia	EBR	Allentoft et al. 2015
RISE423	baArm	Armenia	WBR	Allentoft et al. 2015
RISE479	baHu	Hungary	WBR	Allentoft et al. 2015

RISE489	baRem	Italy	WBR	Allentoft et al. 2015
RISE493	baKarasuk	Russia	EBR	Allentoft et al. 2015
RISE495	baKarasuk	Russia	EBR	Allentoft et al. 2015
RISE496	baKarasuk	Russia	EBR	Allentoft et al. 2015
RISE497	baKarasuk	Russia	EBR	Allentoft et al. 2015
RISE499	baKarasuk	Russia	EBR	Allentoft et al. 2015
RISE500	baAndrov	Russia	EBR	Allentoft et al. 2015
RISE502	baKarasuk	Russia	EBR	Allentoft et al. 2015
RISE503	baAndrov	Russia	EBR	Allentoft et al. 2015
RISE504	irRus	Russia	EIR	Allentoft et al. 2015
RISE505	baAndrov	Russia	EBR	Allentoft et al. 2015
RISE509	baAfan	Russia	EBR	Allentoft et al. 2015
RISE511	baAfan	Russia	EBR	Allentoft et al. 2015
RISE516	baOku	Russia	EBR	Allentoft et al. 2015
RISE523	baMezh	Russia	EBR	Allentoft et al. 2015
RISE547	baYam	Russia	EBR	Allentoft et al. 2015
RISE548	baYam	Russia	EBR	Allentoft et al. 2015
RISE550	baYam	Russia	EBR	Allentoft et al. 2015
RISE552	baYam	Russia	EBR	Allentoft et al. 2015
RISE569	baBb	Czech Republic	WBR	Allentoft et al. 2015
RISE577	baUne	Czech Republic	WBR	Allentoft et al. 2015
RISE600	irAltai	Russia	EIR	Allentoft et al. 2015
RISE601	irAltai	Russia	EIR	Allentoft et al. 2015
RISE602	irAltai	Russia	EIR	Allentoft et al. 2015
RISE94	baSca	Sweden	WBR	Allentoft et al. 2015
RISE97	baSca	Sweden	WBR	Allentoft et al. 2015
RISE98	baSca	Sweden	WBR	Allentoft et al. 2015
I0011	Motala_HG	Sweden	SHG	Haak et al. 2015
I0012	Motala_HG	Sweden	SHG	Haak et al. 2015
I0013	Motala_HG	Sweden	SHG	Haak et al. 2015
I0014	Motala_HG	Sweden	SHG	Haak et al. 2015
I0015	Motala_HG	Sweden	SHG	Haak et al. 2015
I0016	Motala_HG	Sweden	SHG	Haak et al. 2015
I0022	LBK_EN	Germany	EEF	Haak et al. 2015
I0025	LBK_EN	Germany	EEF	Haak et al. 2015
I0026	LBK_EN	Germany	EEF	Haak et al. 2015
I0046	LBK_EN	Germany	EEF	Haak et al. 2015
I0047	Unetice_EBA	Germany	WBR	Haak et al. 2015
I0048	LBK_EN	Germany	EEF	Haak et al. 2015
I0054	LBK_EN	Germany	EEF	Haak et al. 2015
I0056	LBK_EN	Germany	EEF	Haak et al. 2015
I0057	LBK_EN	Germany	EEF	Haak et al. 2015
I0058	BenzigerodeHeimburg_LN	Germany	WBR	Haak et al. 2015

I0059	BenzigerodeHeimburg_LN	Germany	WBR	Haak et al. 2015
I0061	Karelia_HG	Russia	EHG	Haak et al. 2015
I0099	Halberstadt_LBA	Germany	WBR	Haak et al. 2015
I0100	LBK_EN	Germany	EEF	Haak et al. 2015
I0103	Corded_Ware_LN	Germany	WBR	Haak et al. 2015
I0104	Corded_Ware_LN	Germany	WBR	Haak et al. 2015
I0108	Bell_Beaker_LN	Germany	WBR	Haak et al. 2015
I0111	Bell_Beaker_LN	Germany	WBR	Haak et al. 2015
I0112	Bell_Beaker_LN	Germany	WBR	Haak et al. 2015
I0116	Unetice_EBA	Germany	WBR	Haak et al. 2015
I0117	Unetice_EBA	Germany	WBR	Haak et al. 2015
I0118	Alberstedt_LN	Germany	WBR	Haak et al. 2015
I0124	Samara_HG	Russia	EHG	Haak et al. 2015
I0164	Unetice_EBA	Germany	WBR	Haak et al. 2015
I0172	Esperstedt_MN	Germany	MN	Haak et al. 2015
I0174	Starcevo_EN	Hungary	EBR	Haak et al. 2015
I0176	LBKT_EN	Hungary	WBR	Haak et al. 2015
I0231	Yamnaya	Russia	EBR	Haak et al. 2015
I0406	Spain_MN	Spain	MN	Haak et al. 2015
I0407	Spain_MN	Spain	MN	Haak et al. 2015
I0408	Spain_MN	Spain	MN	Haak et al. 2015
I0409	Spain_EN	Spain	EEF	Haak et al. 2015
I0410	Spain_EN	Spain	EEF	Haak et al. 2015
I0412	Spain_EN	Spain	EEF	Haak et al. 2015
I0413	Spain_EN	Spain	EEF	Haak et al. 2015
I0429	Yamnaya	Russia	EBR	Haak et al. 2015
I0438	Yamnaya	Russia	EBR	Haak et al. 2015
I0443	Yamnaya	Russia	EBR	Haak et al. 2015
I0659	LBK_EN	Germany	EEF	Haak et al. 2015
I0795	LBK_EN	Germany	EEF	Haak et al. 2015
I0821	LBK_EN	Germany	EEF	Haak et al. 2015

Supplementary Table C.5 Abbreviations of ancient groups used in the study

Abbreviation	Full name
CHG	Caucasus Hunter-Gatherer
CO	Copper Age
DG	Devil's Gate
EBR	Bronze Age (East)
EEF	Early European Farmer
EHG	Eastern Hunter-Gatehrer
EIR	Iron Age (East)
MN	Middle Neolithic
PHG	Paleolithic Hunter-Gatherer
SHG	Scandinavian Hunter-Gatherer
WBR	Bronze Age (West)
WHG	Western Hunter-Gatherer
WIR	Iron Age (West)
EN	Early Neolithic
MN	Middle Neolithic
LN	Late Neolithic
BA / ba	Bronze Age
IR / ir	Iron Age
NE	Neolithic
LBK	Linearbandkeramik
baCw	Corded Ware (Bronze Age)
baUne	Unetice (Bronze Age)
irSca	Iron Age
baSin	Sintashta (Bronze Age)
baArm	Armenia (Bronze Age)
baHu	Hungary (Bronze Age)
baRem	Remedello (Bronze Age)
baKarasuk	Karasuk (Bronze Age)
baAndrov	Andronovo (Bronze Age)
irRus	Russia (Iron Age)
baAfan	Afanasievo (Bronze Age)
baOku	Okunevo (Bronze Age)
baMezh	Mezhovskaya (Bronze Age)
baYam	Yamnaya (Bronze Age)
baBb	Bell Beaker (Bronze Age)
baUne	Unetice (Bronze Age)
irAltai	Altai (Iron Age)
baSca	Battle Axe (Bronze Age)

Supplementary Table C.6 Result of the t-tests to compare the proportion of Devil's Gate-related ancestry in the Ulchi to the proportions of the European Hunter-Gatherer-related component in modern European populations. Proportions were estimated as those reported by ADMIXTURE runs on all SNPs from the regional panel at k=8 for the Ulchi and the global panel at k=18 for modern European populations.

Population	t	df	p-value
Lithuanian	3.10	27.23	2.22E-03
Estonian	3.73	27.23	4.49E-04
Finnish	5.69	27.78	2.16E-06
Belarusian	6.41	29.84	2.30E-07
Icelandic	6.61	27.05	2.13E-07
Norwegian	7.04	25.89	9.09E-08
Scottish	7.33	24.54	6.32E-08
Orcadian	7.82	25.50	1.54E-08
Russian	8.04	25.00	1.07E-08
Basque	8.39	24.99	4.84E-09
Ukrainian	8.16	30.03	2.07E-09
English	8.78	27.69	8.67E-10
Mordovian	9.07	26.63	6.21E-10
Czech	9.19	26.51	4.94E-10
Spanish_North	9.43	26.75	2.71E-10
French_South	10.09	25.59	1.03E-10
French	10.93	27.14	9.51E-12
Hungarian	11.11	27.66	5.20E-12
Croatian	12.17	29.96	1.99E-13
Spanish	14.04	25.67	7.43E-14
Chuvash	14.87	27.93	4.28E-15
Bergamo	17.13	26.43	3.93E-16
Sardinian	18.50	25.07	1.98E-16
Bulgarian	16.47	30.71	4.30E-17
Tuscan	20.54	25.69	9.15E-18
Albanian	20.26	26.86	4.23E-18
Sicilian	23.87	28.01	1.84E-20
Ashkenazi_Jew	25.70	27.08	7.41E-21
Greek	17.48	42.92	1.94E-21
Maltese	23.52	30.72	1.66E-21

Appendix C Appendix for Chapter 4

Supplementary Table C.7 Results of t-tests to compare the proportion of Devil’s Gate-related ancestry in the Ulchi to the proportions of the Early European Farmer-related component in modern European populations. Proportions were estimated as those reported by ADMIXTURE runs on all SNPs from the regional panel at k=8 for the Ulchi and the global panel at k=18 for modern European populations.

Population	**t**	**df**	**p-value**
Sardinian	0.47	25.16	0.32
Sicilian	8.76	24.57	2.49E-09
Maltese	8.29	29.30	1.79E-09
Ashkenazi_Jew	9.18	26.53	5.07E-10
Tuscan	10.18	27.07	4.68E-11
Bergamo	11.24	25.77	9.81E-12
Albanian	10.70	28.22	9.60E-12
Greek	10.97	29.28	3.46E-12
Spanish	12.16	24.71	3.20E-12
Basque	12.26	24.86	2.44E-12
French_South	12.24	26.65	9.55E-13
Spanish_North	12.46	26.26	7.78E-13
Bulgarian	15.18	27.67	3.02E-15
Croatian	18.20	25.98	1.31E-16
French	16.43	30.71	4.60E-17
Hungarian	20.15	25.25	2.23E-17
English	20.51	25.55	1.09E-17
Orcadian	22.06	25.16	2.78E-18
Scottish	21.76	26.53	9.55E-19
Czech	21.23	27.43	7.37E-19
Norwegian	22.93	25.60	6.86E-19
Icelandic	23.01	26.05	3.89E-19
Belarusian	24.98	26.71	2.34E-20
Mordovian	28.00	24.66	1.65E-20
Ukrainian	22.60	30.61	5.94E-21
Russian	28.15	25.76	3.57E-21
Estonian	27.67	26.50	2.19E-21
Finnish	24.83	29.43	1.36E-21
Lithuanian	26.52	28.89	3.94E-22
Chuvash	30.50	26.10	3.04E-22

Supplementary Table C.8 Result of the t-tests to compare the proportion of Devil's Gate-related ancestry in the Ulchi to the proportions of the Bronze Age Steppe-related component in modern European populations. Proportions were estimated as those reported by ADMIXTURE runs on all SNPs from the regional panel at k=8 for the Ulchi and the global panel at k=18 for modern European populations.

Population	t	df	p-value
Scottish	23.15	23.08	8.92E-18
Ashkenazi_Jew	22.34	27.59	1.65E-19
Russian	25.40	25.02	1.10E-19
Bulgarian	23.54	26.73	1.06E-19
Mordovian	23.92	26.36	1.06E-19
Sicilian	24.60	26.09	7.05E-20
Chuvash	24.31	26.63	5.18E-20
Czech	25.60	25.80	3.63E-20
Ukrainian	24.14	27.17	3.40E-20
Hungarian	25.63	25.87	3.23E-20
Orcadian	26.85	24.98	3.02E-20
Albanian	23.04	28.56	2.71E-20
Estonian	25.97	25.95	2.12E-20
Norwegian	26.71	25.42	2.01E-20
Belarusian	24.71	27.39	1.46E-20
Lithuanian	25.61	26.58	1.44E-20
Croatian	25.15	27.16	1.19E-20
Maltese	22.09	30.95	8.29E-21
English	26.72	26.16	8.12E-21
Finnish	26.47	26.74	5.18E-21
Tuscan	24.51	28.68	4.39E-21
Bergamo	27.72	26.10	3.41E-21
Icelandic	26.04	27.68	2.62E-21
Spanish	31.43	25.01	6.37E-22
French	27.48	27.97	4.39E-22
Greek	19.81	38.63	3.91E-22
French_South	33.93	25.61	4.07E-23
Basque	36.02	25.09	1.98E-23
Sardinian	37.91	24.56	1.30E-23
Spanish_North	32.79	27.71	5.22E-24

Supplementary Table C.9 Result of the t-tests to compare the proportion of Devil's Gate-related ancestry in the Ulchi to the proportions of the European Hunter-Gatherer-related component in modern European populations. Proportions were estimated as those reported by ADMIXTURE runs on transversion SNPs from the regional panel at k=8 for the Ulchi and the global panel at k=18 for modern European populations.

Population	t	df	p-value
Lithuanian	2.31	29.31	1.41E-02
Estonian	3.55	28.19	6.87E-04
Finnish	4.93	29.72	1.46E-05
Scottish	6.11	18.20	4.29E-06
Icelandic	5.61	28.84	2.38E-06
Belarusian	5.87	29.97	1.01E-06
Norwegian	6.19	27.57	5.90E-07
Russian	7.35	25.17	5.03E-08
Orcadian	7.20	26.92	4.88E-08
Ukrainian	7.62	29.91	8.55E-09
Basque	8.10	25.58	7.88E-09
Czech	8.50	25.73	3.02E-09
Mordovian	8.16	28.99	2.65E-09
English	8.29	29.77	1.59E-09
Spanish_North	8.92	26.55	9.11E-10
French_South	9.19	28.34	2.69E-10
French	10.33	26.95	3.60E-11
Hungarian	10.28	27.57	3.07E-11
Croatian	11.83	27.20	1.54E-12
Spanish	13.23	25.87	2.55E-13
Chuvash	13.74	28.53	2.09E-14
Bergamo	16.07	28.46	4.14E-16
Sardinian	17.71	25.66	3.35E-16
Bulgarian	15.79	31.03	1.12E-16
Tuscan	19.18	26.57	2.17E-17
Albanian	18.23	28.96	1.04E-17
Sicilian	22.16	30.29	1.41E-20
Ashkenazi_Jew	23.84	28.45	1.21E-20
Greek	16.76	42.78	1.04E-20
Maltese	22.67	30.64	5.21E-21

Appendix C Appendix for Chapter 4

Supplementary Table C.10 Result of the t-tests to compare the proportion of Devil's Gate-related ancestry in the Ulchi to the proportions of the Early European Farmer-related component in modern European populations. Proportions were estimated as those reported by ADMIXTURE runs on transversion SNPs from the regional panel at k=8 for the Ulchi and the global panel at k=18 for modern European populations.

Population	**t**	**df**	**p-value**
Sardinian	-0.62	25.76	0.72805655
Maltese	7.45	28.83	1.70E-08
Sicilian	8.09	25.51	8.29E-09
Ashkenazi_Jew	8.10	27.88	4.18E-09
Tuscan	8.75	30.72	3.84E-10
Albanian	9.64	27.18	1.45E-10
Bergamo	9.94	27.50	6.64E-11
Greek	9.77	29.94	3.97E-11
Basque	10.76	24.93	3.72E-11
Spanish	11.00	24.88	2.41E-11
Spanish_North	10.65	27.87	1.24E-11
French_South	10.60	29.57	6.90E-12
Bulgarian	13.84	28.44	1.82E-14
Croatian	17.17	24.70	1.52E-15
French	15.06	31.35	3.31E-16
Hungarian	18.59	26.23	6.30E-17
English	18.49	26.71	4.77E-17
Scottish	19.11	26.12	3.54E-17
Orcadian	20.35	25.45	1.45E-17
Norwegian	21.09	25.73	4.63E-18
Czech	19.84	27.44	4.17E-18
Icelandic	21.83	25.49	2.56E-18
Belarusian	23.22	27.37	7.57E-20
Mordovian	26.44	24.70	6.21E-20
Ukrainian	20.62	31.45	3.93E-20
Russian	26.63	25.39	2.24E-20
Finnish	23.05	29.54	9.79E-21
Estonian	25.12	29.58	8.24E-22
Chuvash	29.23	26.20	7.92E-22
Lithuanian	24.21	31.17	4.45E-22

Appendix C Appendix for Chapter 4

Supplementary Table C.11 Results of the t-tests to compare the proportion of Devil's Gate-related ancestry in the Ulchi to the proportions of the Bronze Age Steppe-related component in modern European populations. Proportions were estimated as those reported by ADMIXTURE runs on transversion SNPs from the regional panel at k=8 for the Ulchi and the global panel at k=18 for modern European populations.

Population	t	df	p-value
Scottish	22.61	23.35	1.11E-17
Ashkenazi_Jew	20.11	29.94	3.06E-19
Chuvash	23.96	25.52	2.55E-19
Russian	24.67	25.02	2.22E-19
Sicilian	23.42	26.47	1.58E-19
Bulgarian	22.13	28.35	9.80E-20
Ukrainian	23.39	27.09	8.45E-20
Albanian	21.84	28.93	7.98E-20
Mordovian	22.76	27.90	7.37E-20
Estonian	24.54	26.72	3.69E-20
Hungarian	24.70	26.60	3.60E-20
Croatian	24.27	27.32	2.53E-20
Belarusian	23.63	28.04	2.33E-20
Maltese	21.46	30.83	2.14E-20
Czech	24.36	27.93	1.17E-20
Tuscan	22.13	30.98	7.64E-21
Norwegian	25.87	27.01	6.79E-21
Lithuanian	24.52	28.29	6.62E-21
Orcadian	25.23	27.70	5.93E-21
English	25.26	27.71	5.71E-21
Bergamo	26.24	27.43	2.85E-21
Icelandic	24.89	28.87	2.35E-21
Finnish	24.51	29.86	1.24E-21
Spanish	30.49	25.13	1.13E-21
Greek	19.79	37.44	1.00E-21
French	26.27	28.56	7.50E-22
Basque	34.42	25.75	2.31E-23
French_South	32.01	27.24	1.86E-23
Spanish_North	32.34	27.05	1.84E-23
Sardinian	36.24	25.50	9.26E-24

Supplementary Table C.12 Outgroup f_3 statistics for Devil's Gate. f_3 statistics of the form f_3(DevilsGate, X; Khomani) for all populations X in our panel compared to DevilsGate1, using all SNPs. Top 50 populations with at least 1000 overlapping SNPs.

Population	**Region**	f_3	**SE**	**Z**	**SNPs**
Ulchi	AmurBasin	0.22782	0.00371	61.352	27588
Oroqen	AmurBasin	0.22282	0.00374	59.564	27566
Hezhen	AmurBasin	0.22265	0.00374	59.507	27558
Korean	KoreaJapan	0.22231	0.00361	61.613	27595
Japanese	KoreaJapan	0.22185	0.00359	61.879	27587
Daur	AmurBasin	0.22065	0.00366	60.345	27566
Xibo	AmurBasin	0.22058	0.00368	59.915	27558
Nganasan	Siberia	0.22042	0.00380	57.983	27533
Han_NChina	EastAsia	0.21828	0.00364	60.011	27568
Eskimo	Chukotka-Kamchatka	0.21823	0.00388	56.196	27558
Koryak	Chukotka-Kamchatka	0.21769	0.00389	55.959	27537
Chukchi	Chukotka-Kamchatka	0.21704	0.00384	56.586	27572
Itelmen	Chukotka-Kamchatka	0.21698	0.00397	54.605	27521
Miao	EastAsia	0.21694	0.00367	59.106	27573
Mongola	EastAsia	0.21648	0.00365	59.348	27554
She	EastAsia	0.21648	0.00365	59.308	27564
Tujia	EastAsia	0.21642	0.00368	58.744	27565
Yakut	Siberia	0.21615	0.00360	60.074	27581
Yi	EastAsia	0.21603	0.00368	58.784	27565
Han	EastAsia	0.21571	0.00362	59.637	27592
Naxi	EastAsia	0.21379	0.00367	58.255	27562
Ami	SouthEastAsia	0.21378	0.00377	56.758	27554
Lahu	SouthEastAsia	0.21317	0.00374	57.078	27547
Dai	SouthEastAsia	0.21274	0.00370	57.456	27561
Atayal	SouthEastAsia	0.21243	0.00386	55.044	27534
Tu	EastAsia	0.21242	0.00356	59.709	27580
Yukagir	Chukotka-Kamchatka	0.21172	0.00356	59.478	27574
Tuvinian	CentralAsia	0.21127	0.00360	58.642	27571
Kinh	SouthEastAsia	0.21105	0.00371	56.926	27555
Kalmyk	CentralAsia	0.21084	0.00356	59.265	27576
Mixe	America	0.20943	0.00415	50.499	27498
Karitiana	America	0.20837	0.00413	50.444	27474
Cabecar	America	0.20821	0.00444	46.926	27434

Surui	America	0.20817	0.00439	47.376	27445
Piapoco	America	0.20720	0.00430	48.201	27461
Kaqchikel	America	0.20669	0.00405	51.069	27472
Pima	America	0.20640	0.00400	51.546	27494
Guarani	America	0.20542	0.00400	51.345	27480
Zapotec	America	0.20521	0.00391	52.556	27510
Mixtec	America	0.20483	0.00400	51.210	27510
Aymara	America	0.20459	0.00398	51.410	27473
Cambodian	SouthEastAsia	0.20457	0.00363	56.370	27555
Altaian	CentralAsia	0.20412	0.00355	57.472	27553
Even	Siberia	0.20387	0.00355	57.401	27571
Thai	SouthEastAsia	0.20324	0.00357	56.940	27560
Kyrgyz	CentralAsia	0.20292	0.00355	57.177	27571
Bolivian	America	0.20282	0.00398	51.024	27500
Mayan	America	0.20213	0.00385	52.492	27536
Quechua	America	0.20067	0.00398	50.410	27504
Chipewyan	America	0.20057	0.00383	52.353	27554

Supplementary Table C.13 Outgroup f_3 statistics for Devil's Gate. f_3 statistics of the form f_3(DevilsGate, X; Khomani) for all populations X in our panel compared to DevilsGate1, using transversions only. Top 50 populations with at least 1000 overlapping SNPs.

Population	**Region**	f_3	**SE**	**Z**	**SNPs**
Ulchi	AmurBasin	0.23347	0.00780	29.921	5355
Oroqen	AmurBasin	0.22914	0.00783	29.255	5352
Daur	AmurBasin	0.22881	0.00781	29.317	5354
Japanese	KoreaJapan	0.22774	0.00760	29.968	5356
Korean	KoreaJapan	0.22699	0.00760	29.885	5356
Hezhen	AmurBasin	0.22674	0.00792	28.641	5350
Xibo	AmurBasin	0.22592	0.00772	29.275	5348
Han_NChina	EastAsia	0.22367	0.00745	30.026	5353
Miao	EastAsia	0.22279	0.00772	28.873	5355
Nganasan	Siberia	0.22234	0.00792	28.090	5347
Yi	EastAsia	0.22222	0.00777	28.591	5352
Han	EastAsia	0.22186	0.00750	29.587	5356
Tujia	EastAsia	0.22096	0.00790	27.985	5352

Lahu	SouthEastAsia	0.22091	0.00794	27.817	5349
Mongola	EastAsia	0.22066	0.00794	27.782	5351
Yakut	Siberia	0.21992	0.00750	29.306	5355
Naxi	EastAsia	0.21966	0.00779	28.204	5351
Dai	SouthEastAsia	0.21876	0.00766	28.555	5349
She	EastAsia	0.21874	0.00772	28.324	5351
Ami	SouthEastAsia	0.21843	0.00786	27.790	5353
Eskimo	Chukotka-Kamchatka	0.21802	0.00790	27.598	5349
Chukchi	Chukotka-Kamchatka	0.21793	0.00800	27.243	5353
Tuvinian	CentralAsia	0.21713	0.00766	28.357	5354
Tu	EastAsia	0.21705	0.00758	28.624	5355
Atayal	SouthEastAsia	0.21703	0.00788	27.539	5344
Koryak	Chukotka-Kamchatka	0.21677	0.00800	27.113	5349
Kalmyk	CentralAsia	0.21529	0.00743	28.992	5353
Guarani	America	0.21527	0.00815	26.411	5343
Yukagir	Chukotka-Kamchatka	0.21513	0.00748	28.761	5355
Itelmen	Chukotka-Kamchatka	0.21325	0.00830	25.693	5345
Cabecar	America	0.21318	0.00881	24.185	5326
Kinh	SouthEastAsia	0.21305	0.00793	26.878	5350
Surui	America	0.21245	0.00855	24.847	5325
Kaqchikel	America	0.21225	0.00822	25.815	5339
Mixe	America	0.21216	0.00816	26.002	5342
Piapoco	America	0.21213	0.00849	24.981	5337
Altaian	CentralAsia	0.21110	0.00764	27.625	5350
Karitiana	America	0.21098	0.00831	25.398	5337
Cambodian	SouthEastAsia	0.21080	0.00768	27.468	5350
Kyrgyz	CentralAsia	0.21062	0.00745	28.255	5353
Zapotec	America	0.21027	0.00795	26.446	5344
Pima	America	0.20808	0.00803	25.926	5344
Chipewyan	America	0.20677	0.00770	26.845	5349
Mayan	America	0.20666	0.00762	27.107	5349
Thai	SouthEastAsia	0.20664	0.00734	28.174	5350
Even	Siberia	0.20651	0.00734	28.122	5354
Aymara	America	0.20601	0.00782	26.334	5337
irRus_atoft	Ancient	0.20595	0.01411	14.597	2598
Bolivian	America	0.20476	0.00777	26.366	5345
Mixtec	America	0.20465	0.00779	26.268	5344

Supplementary Table C.14 Outgroup f_3 statistics for Devil's Gate. f_3 statistics of the form f_3(DevilsGate, X; Khomani) for all populations X in our panel compared to DevilsGate2, using all SNPs. Top 50 populations with at least 1000 overlapping SNPs.

Population	**Region**	f_3	**SE**	**Z**	**SNPs**
Ulchi	AmurBasin	0.23607	0.00544	43.389	11004
Nganasan	Siberia	0.23088	0.00573	40.331	10992
Hezhen	AmurBasin	0.23040	0.00539	42.721	10995
Korean	KoreaJapan	0.22999	0.00526	43.716	11006
Japanese	KoreaJapan	0.22962	0.00532	43.160	11004
Oroqen	AmurBasin	0.22896	0.00552	41.503	10995
Xibo	AmurBasin	0.22803	0.00542	42.095	10997
Koryak	Chukotka-Kamchatka	0.22664	0.00564	40.200	10986
Daur	AmurBasin	0.22629	0.00533	42.496	10999
Mongola	EastAsia	0.22540	0.00530	42.560	10993
Han_NChina	EastAsia	0.22527	0.00542	41.598	10998
Itelmen	Chukotka-Kamchatka	0.22466	0.00572	39.247	10979
Han	EastAsia	0.22403	0.00533	42.008	11005
Yakut	Siberia	0.22394	0.00532	42.081	11001
She	EastAsia	0.22388	0.00546	41.043	10997
Chukchi	Chukotka-Kamchatka	0.22261	0.00555	40.103	11003
Tujia	EastAsia	0.22241	0.00544	40.881	10994
Naxi	EastAsia	0.22207	0.00528	42.033	10999
Tu	EastAsia	0.22164	0.00536	41.365	11000
Miao	EastAsia	0.22153	0.00533	41.585	10997
Yi	EastAsia	0.22148	0.00544	40.746	10999
Eskimo	Chukotka-Kamchatka	0.22095	0.00571	38.702	10998
Tuvinian	CentralAsia	0.21957	0.00538	40.812	10999
Cabecar	America	0.21867	0.00680	32.179	10949
Yukagir	Chukotka-Kamchatka	0.21812	0.00525	41.521	11002
Atayal	SouthEastAsia	0.21789	0.00558	39.034	10978
Kalmyk	CentralAsia	0.21743	0.00531	40.959	11003
Aymara	America	0.21741	0.00626	34.741	10960
Dai	SouthEastAsia	0.21736	0.00525	41.413	10994
Ami	SouthEastAsia	0.21727	0.00540	40.226	10982
Kaqchikel	America	0.21678	0.00619	34.996	10963
Lahu	SouthEastAsia	0.21613	0.00541	39.927	10990
Surui	America	0.21595	0.00651	33.160	10946

Kinh	SouthEastAsia	0.21588	0.00534	40.414	10988
Mixe	America	0.21577	0.00608	35.515	10976
Pima	America	0.21503	0.00617	34.854	10976
Altaian	CentralAsia	0.21488	0.00521	41.237	10989
Karitiana	America	0.21446	0.00628	34.139	10962
Zapotec	America	0.21434	0.00589	36.412	10978
Piapoco	America	0.21349	0.00634	33.654	10957
Mixtec	America	0.21293	0.00609	34.951	10979
Bolivian	America	0.21290	0.00602	35.347	10966
Guarani	America	0.21285	0.00614	34.688	10958
Quechua	America	0.21094	0.00605	34.875	10966
Mayan	America	0.21037	0.00578	36.401	10989
Even	Siberia	0.21013	0.00527	39.907	10996
Kyrgyz	CentralAsia	0.20993	0.00508	41.325	10998
Thai	SouthEastAsia	0.20913	0.00528	39.592	10992
Selkup	Siberia	0.20830	0.00512	40.666	10998
Cambodian	SouthEastAsia	0.20822	0.00529	39.362	10989

Supplementary Table C.15 Outgroup f_3 statistics for Devil’s Gate. f_3 statistics of the form f_3(DevilsGate, X; Khomani) for all populations X in our panel compared to DevilsGate2, using transversions only. Top 50 populations with at least 1000 overlapping SNPs.

Population	**Region**	f_3	**SE**	**Z**	**SNPs**
Ulchi	AmurBasin	0.24518	0.01164	21.070	2217
Oroqen	AmurBasin	0.24251	0.01131	21.447	2215
Hezhen	AmurBasin	0.24163	0.01171	20.633	2217
Korean	KoreaJapan	0.24137	0.01124	21.484	2218
Xibo	AmurBasin	0.24064	0.01173	20.522	2215
Han_NChina	EastAsia	0.24002	0.01192	20.138	2216
Tujia	EastAsia	0.23879	0.01160	20.578	2215
Eskimo	Chukotka-Kamchatka	0.23836	0.01240	19.216	2216
Japanese	KoreaJapan	0.23811	0.01141	20.868	2217
Cabecar	America	0.23782	0.01415	16.805	2205
Itelmen	Chukotka-Kamchatka	0.23771	0.01225	19.400	2212
Nganasan	Siberia	0.23767	0.01214	19.576	2216
Yakut	Siberia	0.23753	0.01136	20.908	2216

Naxi	EastAsia	0.23722	0.01167	20.335	2216
Chukchi	Chukotka-Kamchatka	0.23711	0.01195	19.849	2218
Koryak	Chukotka-Kamchatka	0.23654	0.01218	19.415	2215
Han	EastAsia	0.23615	0.01131	20.878	2218
Miao	EastAsia	0.23458	0.01144	20.507	2217
Daur	AmurBasin	0.23442	0.01154	20.318	2217
Lahu	SouthEastAsia	0.23296	0.01196	19.475	2213
Mixe	America	0.23293	0.01250	18.632	2212
Surui	America	0.23242	0.01421	16.357	2206
Kaqchikel	America	0.23207	0.01311	17.705	2207
Ami	SouthEastAsia	0.23188	0.01192	19.455	2211
Atayal	SouthEastAsia	0.23166	0.01244	18.625	2210
Tu	EastAsia	0.23114	0.01118	20.680	2217
Yi	EastAsia	0.23107	0.01140	20.277	2218
Karitiana	America	0.23102	0.01322	17.479	2210
Aymara	America	0.23076	0.01291	17.881	2208
Piapoco	America	0.23072	0.01342	17.191	2207
Tuvinian	CentralAsia	0.23056	0.01133	20.357	2216
Mongola	EastAsia	0.22985	0.01145	20.073	2215
Altaian	CentralAsia	0.22889	0.01133	20.200	2214
She	EastAsia	0.22883	0.01165	19.643	2217
Dai	SouthEastAsia	0.22878	0.01152	19.866	2213
Yukagir	Chukotka-Kamchatka	0.22835	0.01103	20.701	2216
Pima	America	0.22794	0.01266	18.009	2209
Quechua	America	0.22685	0.01242	18.268	2211
Kalmyk	CentralAsia	0.22680	0.01133	20.023	2216
Kinh	SouthEastAsia	0.22504	0.01141	19.729	2213
Guarani	America	0.22467	0.01262	17.799	2204
Bolivian	America	0.22436	0.01204	18.630	2208
Zapotec	America	0.22407	0.01211	18.508	2212
Chipewyan	America	0.22249	0.01159	19.202	2214
Mayan	America	0.22150	0.01203	18.411	2216
Kusunda	SouthAsia	0.22142	0.01145	19.336	2217
Even	Siberia	0.22126	0.01102	20.073	2217
Cambodian	SouthEastAsia	0.22106	0.01115	19.826	2214
Thai	SouthEastAsia	0.22053	0.01114	19.801	2216
Mixtec	America	0.22035	0.01207	18.252	2213

Supplementary Table C.16 D scores for the Ulchi. D statistics of the form D(Ulchi, DevilsGate1; X, Khomani) for all populations X in our panel, using all SNPs, sorted by |Z| and top 30 populations displayed.

Population	D	Z	SNPs1	SNPs2	SNPs
Nganasan	-0.0466	-6.658	1485	1630	34815
Yukagir	-0.0413	-6.448	1478	1605	34815
Koryak	-0.0475	-6.412	1481	1628	34815
Selkup	-0.0410	-6.172	1462	1587	34815
Itelmen	-0.0463	-6.089	1477	1620	34815
Even	-0.0365	-5.699	1471	1583	34815
Tuvinian	-0.0372	-5.680	1486	1601	34815
Chukchi	-0.0407	-5.655	1485	1611	34815
Oroqen	-0.0380	-5.604	1500	1619	34815
Altaian	-0.0357	-5.488	1477	1586	34815
Han	-0.0353	-5.457	1496	1605	34815
Hezhen	-0.0370	-5.403	1501	1616	34815
Yakut	-0.0343	-5.331	1492	1598	34815
Naxi	-0.0355	-5.261	1491	1601	34815
Kinh	-0.0360	-5.203	1489	1600	34815
Tubalar	-0.0323	-5.179	1462	1560	34815
Kharia	-0.0322	-5.068	1451	1547	34815
MA1	-0.0668	-5.020	978	1118	24644
Kalmyk	-0.0337	-5.012	1488	1592	34815
Tu	-0.0335	-5.004	1494	1597	34815
Sindhi	-0.0291	-4.963	1424	1509	34815
Thai	-0.0327	-4.955	1481	1581	34815
Tujia	-0.0328	-4.857	1498	1600	34815
Xibo	-0.0337	-4.773	1504	1608	34815
Daur	-0.0330	-4.745	1502	1605	34815
Mongola	-0.0331	-4.733	1498	1601	34815
Dai	-0.0323	-4.718	1493	1593	34815
GujaratiA	-0.0310	-4.668	1420	1511	34815
Lodhi	-0.0287	-4.666	1433	1518	34815
Mansi	-0.0313	-4.658	1464	1559	34815

Supplementary Table C.17 D scores for the Ulchi. D statistics of the form D(Ulchi, DevilsGate1; X, Khomani) for all populations X in our panel, using transversion SNPs, sorted by |Z|, populations where |Z|>2 displayed.

Population	D	Z	SNPs1	SNPs2	SNPs
Koryak	-0.0469	-3.299	290	318	6702
MA1	-0.0928	-3.155	183	221	4655
Itelmen	-0.0472	-3.150	288	316	6702
Mbuti	-0.0333	-2.897	224	239	6702
Chukchi	-0.0395	-2.665	291	315	6702
Yukagir	-0.0344	-2.466	293	313	6702
Kharia	-0.0316	-2.328	284	303	6702
Kinh	-0.0346	-2.319	293	314	6702
Nganasan	-0.0351	-2.282	294	315	6702
Eskimo	-0.0337	-2.252	293	314	6702
Kikuyu	-0.0244	-2.070	247	259	6702
Ju_hoan_South	-0.0206	-2.050	215	224	6702
Selkup	-0.0291	-2.034	291	308	6702

Supplementary Table C.18 D scores for the Ulchi. D statistics of the form D(Ulchi, DevilsGate2; X, Khomani) for all populations X in our panel, using all SNPs, sorted by |Z|, populations where |Z|>2 displayed.

Population	D	Z	SNPs1	SNPs2	SNPs
Koryak	-0.0469	-3.299	290	318	6702
MA1	-0.0928	-3.155	183	221	4655
Itelmen	-0.0472	-3.150	288	316	6702
Mbuti	-0.0333	-2.897	224	239	6702
Chukchi	-0.0395	-2.665	291	315	6702
Yukagir	-0.0344	-2.466	293	313	6702
Kharia	-0.0316	-2.328	284	303	6702
Kinh	-0.0346	-2.319	293	314	6702
Nganasan	-0.0351	-2.282	294	315	6702
Eskimo	-0.0337	-2.252	293	314	6702
Kikuyu	-0.0244	-2.070	247	259	6702
Ju_hoan_South	-0.0206	-2.050	215	224	6702
Selkup	-0.0291	-2.034	291	308	6702

Supplementary Table C.19 . D scores for the Ulchi. D statistics of the form D(Ulchi, DevilsGate2; X, Khomani) for all populations X in our panel, using transversion SNPs, sorted by |Z|, top 30 populations displayed.

Population	D	Z	SNPs1	SNPs2	SNPs
HDma1	-0.4466	-2.347	2	6	69
Chechen	0.0401	2.017	121	112	2750
Moroccan_Jew	0.0435	2.017	120	110	2750
Balkar	0.0427	2.031	122	112	2750
Himba	0.0415	2.032	102	94	2750
Egyptian	0.0368	2.045	118	109	2750
Iraqi_Jew	0.0437	2.050	120	110	2750
Ukrainian	0.0442	2.057	122	111	2750
North_Ossetian	0.0401	2.061	121	111	2750
Tunisian_Jew	0.0435	2.061	119	109	2750
baArm	0.1539	2.070	25	18	622
Druze	0.0402	2.070	119	110	2750
Iranian_Jew	0.0424	2.075	120	110	2750
Mala	0.0388	2.075	122	113	2750
Tubalar	0.0398	2.100	126	117	2750
Russian	0.0420	2.102	122	112	2750
Sardinian	0.0422	2.102	121	111	2750
AA	0.0356	2.103	105	98	2750
Libyan_Jew	0.0436	2.118	118	108	2750
Tuscan	0.0442	2.123	121	111	2750
Jordanian	0.0420	2.133	120	110	2750
Bulgarian	0.0440	2.134	120	110	2750
English	0.0443	2.143	122	112	2750
Iranian	0.0430	2.147	120	110	2750
Yakut	0.0409	2.155	128	118	2750
Georgian	0.0437	2.174	120	110	2750
Maltese	0.0450	2.187	121	110	2750
Starcevo	0.2091	2.206	21	14	424
baAndrov	0.0838	2.224	73	62	1686
baAfan	0.0955	2.245	72	59	1636

Supplementary Table C.20 Admixture f_3(Source1, Source2; Target) for the Ulchi with Z < -1, using all SNPs. All pairs without a sample from DevilsGate gave Z > -1, regardless of whether all SNPs were used or only those called in DevilsGate1 or DevilsGate2.

Source1	**Source2**	**Target**	**f3**	**SE**	**Z**	**SNPs**
DevilsGate1MapDamage	MA1	Ulchi	-0.00647	0.00502	-1.287	15582
DevilsGate1	MA1	Ulchi	-0.00596	0.00506	-1.179	15582

Supplementary Table C.21 Admixture f_3(Source1, Source2; Target) for the Ulchi with Z < -1, using only transversion SNPs. All pairs without a sample from Devil's Gate gave Z > -1, regardless of whether all SNPs were used or only those called in DevilsGate1 or DevilsGate2.

Source1	**Source2**	**Target**	**f3**	**SE**	**Z**	**SNPs**
DevilsGate2	Motala12	Ulchi	-0.02081	0.01448	-1.438	1606
DevilsGate1MapDamage	Karelia_HG	Ulchi	-0.01955	0.01201	-1.628	2337
DevilsGate1	Karelia_HG	Ulchi	-0.01923	0.01191	-1.614	2337
DevilsGate1MapDamage	MA1	Ulchi	-0.01698	0.01075	-1.58	3004
DevilsGate1	MA1	Ulchi	-0.01462	0.01076	-1.359	3004
DevilsGate1MapDamage	Itelmen	Ulchi	-0.00533	0.00406	-1.313	4365
DevilsGate1MapDamage	Koryak	Ulchi	-0.00451	0.00355	-1.273	4368
DevilsGate1	Itelmen	Ulchi	-0.00517	0.00407	-1.27	4365

Supplementary Table C.22 Admixture f_3(Source1, Source2; Target) for the Sardinians, using all SNPs and showing the 10 most significantly negative pairs.

Source1	**Source2**	**Target**	**f3**	**SE**	**Z**	**SNPs**
Spain_EN	baArm	Sardinian	-0.028907	0.008386	-3.447	1984
Loschbour	baRem	Sardinian	-0.026789	0.00903	-2.967	2648
LaBrana	baRem	Sardinian	-0.03462	0.011897	-2.91	2512
Loschbour	Iraqi_Jew	Sardinian	-0.004893	0.001722	-2.842	9435
Spain_EN	Chuvash	Sardinian	-0.004701	0.001816	-2.588	5574
Xibo	Spain_EN	Sardinian	-0.006728	0.002612	-2.576	5571
Stuttgart	LaBrana	Sardinian	-0.012009	0.004766	-2.519	8627
Yemenite_Jew	Loschbour	Sardinian	-0.004339	0.001785	-2.43	9435
LBK_EN	irAltai	Sardinian	-0.007362	0.003034	-2.426	5214
Stuttgart	Karelia_HG	Sardinian	-0.014699	0.006069	-2.422	5212

Supplementary Table C.23 Admixture f_3(Source1, Source2; Target) for the Lithuanians using all SNPs and showing the 10 most significantly negative pairs.

Source1	**Source2**	**Target**	**f3**	**SE**	**Z**	**SNPs**
Loschbour	Iraqi_Jew	Lithuanian	-0.014007	0.002063	-6.788	8617
Loschbour	Lezgin	Lithuanian	-0.012662	0.001965	-6.445	8629
Palestinian	Loschbour	Lithuanian	-0.010899	0.00172	-6.338	8660
Loschbour	Druze	Lithuanian	-0.010408	0.001667	-6.243	8653
Turkish	Loschbour	Lithuanian	-0.009566	0.001532	-6.243	8660
Loschbour	Armenian	Lithuanian	-0.011644	0.001879	-6.196	8634
Loschbour	Georgian_Jew	Lithuanian	-0.012235	0.00201	-6.088	8626
Loschbour	Georgian	Lithuanian	-0.011701	0.001983	-5.9	8632
Loschbour	Chechen	Lithuanian	-0.011107	0.00189	-5.875	8630
Loschbour	Adygei	Lithuanian	-0.010003	0.001713	-5.839	8637

Supplementary Table C.24 Admixture f_3 for the Koreans. f_3 statistics of the form f_3(X, Y; Korean) for all populations X in our panel, using all SNPs. 30 populations with the lowest statistics are displayed.

Source1	**Source2**	**Target**	**f3**	**SE**	**Z**	**SNPs**
DevilsGate2	Ami	Korean	-0.00766	0.00204	-3.752	9259
DevilsGate2	Lahu	Korean	-0.00752	0.00213	-3.530	9260
DevilsGate2	Kinh	Korean	-0.00666	0.00180	-3.703	9260
DevilsGate2	Dai	Korean	-0.00647	0.00168	-3.846	9259
DevilsGate2	Miao	Korean	-0.00608	0.00157	-3.865	9258
DevilsGate2	Atayal	Korean	-0.00586	0.00254	-2.309	9260
DevilsGate2	Tujia	Korean	-0.00523	0.00152	-3.442	9259
DevilsGate2	She	Korean	-0.00499	0.00178	-2.800	9259
DevilsGate1	Kinh	Korean	-0.00490	0.00124	-3.937	23147
DevilsGate1	Han	Korean	-0.00471	0.00077	-6.127	23152
DevilsGate2	Cambodian	Korean	-0.00463	0.00188	-2.461	9259
DevilsGate2	Han	Korean	-0.00430	0.00107	-4.033	9261
DevilsGate2	Thai	Korean	-0.00410	0.00189	-2.176	9260
DevilsGate2	Yi	Korean	-0.00404	0.00165	-2.445	9260
DevilsGate1	Dai	Korean	-0.00324	0.00126	-2.580	23151
DevilsGate1	Tujia	Korean	-0.00308	0.00113	-2.729	23149
DevilsGate1	She	Korean	-0.00288	0.00118	-2.437	23148
Nganasan	Dai	Korean	-0.00197	0.00037	-5.388	404831
Ulchi	Kinh	Korean	-0.00193	0.00025	-7.878	405402

Ulchi	Han	Korean	-0.00191	0.00015	-12.951	406842
Ulchi	Dai	Korean	-0.00189	0.00022	-8.429	405330
Ulchi	Atayal	Korean	-0.00184	0.00033	-5.647	404628
Ulchi	She	Korean	-0.00183	0.00021	-8.874	404851
Nganasan	She	Korean	-0.00182	0.00035	-5.205	404475
Nganasan	Ami	Korean	-0.00181	0.00043	-4.163	404413
Ulchi	Ami	Korean	-0.00178	0.00031	-5.789	404789
Nganasan	Han	Korean	-0.00172	0.00022	-7.895	405829
Nganasan	Kinh	Korean	-0.00155	0.00037	-4.245	404849
Koryak	Ami	Korean	-0.00150	0.00046	-3.252	404317
Nganasan	Atayal	Korean	-0.00149	0.00052	-2.866	404368
Nganasan	Tujia	Korean	-0.00148	0.00031	-4.743	404802

Supplementary Table C.25 Admixture f_3 for the Koreans. f_3 statistics of the form f_3(X, Y; Korean) for all populations X in our panel, using transversions only. 30 populations with the lowest statistics are displayed.

Source1	**Source2**	**Target**	**f3**	**SE**	**Z**	**SNPs**
DevilsGate1	Kinh	Korean	-0.01010	0.00262	-3.856	4538
DevilsGate2	She	Korean	-0.00854	0.00376	-2.271	1869
DevilsGate2	Dai	Korean	-0.00772	0.00376	-2.050	1869
DevilsGate1	She	Korean	-0.00502	0.00237	-2.118	4538
DevilsGate2	Han	Korean	-0.00473	0.00222	-2.129	1869
DevilsGate1	Han	Korean	-0.00346	0.00149	-2.322	4538
Nganasan	Dai	Korean	-0.00193	0.00042	-4.631	75295
Ulchi	Ami	Korean	-0.00179	0.00035	-5.140	75290

Eskimo	Ami	Korean	-0.00175	0.00048	-3.677	75250
Nganasan	She	Korean	-0.00174	0.00041	-4.277	75239
Ulchi	Dai	Korean	-0.00172	0.00026	-6.573	75361
Ulchi	Atayal	Korean	-0.00172	0.00038	-4.504	75256
Ulchi	Han	Korean	-0.00171	0.00017	-10.034	75662
Ulchi	Kinh	Korean	-0.00171	0.00029	-5.884	75391
Nganasan	Han	Korean	-0.00169	0.00025	-6.739	75494
Ulchi	She	Korean	-0.00162	0.00026	-6.189	75312
Nganasan	Ami	Korean	-0.00162	0.00051	-3.184	75231
Koryak	Ami	Korean	-0.00157	0.00054	-2.889	75202
Nganasan	Tujia	Korean	-0.00156	0.00038	-4.141	75300
Itelmen	Han	Korean	-0.00150	0.00028	-5.319	75370
Koryak	Han	Korean	-0.00139	0.00025	-5.548	75437
Chukchi	Han	Korean	-0.00137	0.00024	-5.656	75624
Yakut	Ami	Korean	-0.00131	0.00036	-3.672	75356
Ulchi	Miao	Korean	-0.00128	0.00024	-5.335	75355
Ulchi	Tujia	Korean	-0.00126	0.00024	-5.373	75380
Nganasan	Atayal	Korean	-0.00125	0.00060	-2.082	75216
Itelmen	Ami	Korean	-0.00124	0.00059	-2.110	75183
Itelmen	She	Korean	-0.00123	0.00047	-2.636	75192
Nganasan	Kinh	Korean	-0.00119	0.00043	-2.752	75319
Chukchi	Ami	Korean	-0.00117	0.00047	-2.487	75268
Yukagir	Han	Korean	-0.00116	0.00020	-5.763	76050

Supplementary Table C.26 Admixture f_3 for the Koreans. f_3 statistics of the form f_3(X, Y; Korean) for all populations X in our panel, using SNPs called in DevilsGate1. 30 populations with the lowest statistics are displayed.

Source1	**Source2**	**Target**	**f3**	**SE**	**Z**	**SNPs**
DevilsGate1	Kinh	Korean	-0.00490	0.00124	-3.942	23147
DevilsGate1	Han	Korean	-0.00471	0.00077	-6.131	23152
DevilsGate1	Dai	Korean	-0.00324	0.00125	-2.586	23151
DevilsGate1	Tujia	Korean	-0.00308	0.00112	-2.748	23149
DevilsGate1	She	Korean	-0.00288	0.00121	-2.376	23148
Nganasan	Atayal	Korean	-0.00221	0.00084	-2.632	23199
Ulchi	Han	Korean	-0.00208	0.00024	-8.575	23352
Ulchi	Kinh	Korean	-0.00203	0.00039	-5.232	23263
Ulchi	Dai	Korean	-0.00194	0.00037	-5.228	23255
Ulchi	She	Korean	-0.00190	0.00034	-5.628	23224
Ulchi	Atayal	Korean	-0.00182	0.00054	-3.374	23206
Ulchi	Miao	Korean	-0.00176	0.00035	-4.968	23238
Koryak	Han	Korean	-0.00171	0.00035	-4.951	23275
Nganasan	Han	Korean	-0.00170	0.00037	-4.642	23305
Nganasan	She	Korean	-0.00167	0.00054	-3.099	23207
Chukchi	Han	Korean	-0.00162	0.00034	-4.764	23344
Ulchi	Ami	Korean	-0.00162	0.00048	-3.377	23228
Nganasan	Tujia	Korean	-0.00161	0.00050	-3.203	23237
Ulchi	Tujia	Korean	-0.00150	0.00033	-4.609	23253
Itelmen	She	Korean	-0.00149	0.00060	-2.488	23193
Nganasan	Dai	Korean	-0.00142	0.00059	-2.401	23232
Nganasan	Miao	Korean	-0.00141	0.00054	-2.642	23224

Itelmen	Han	Korean	-0.00138	0.00039	-3.501	23258
Itelmen	Miao	Korean	-0.00134	0.00061	-2.197	23197
Itelmen	Tujia	Korean	-0.00132	0.00055	-2.386	23206
Yukagir	Han	Korean	-0.00124	0.00028	-4.383	23468
Eskimo	Han	Korean	-0.00123	0.00035	-3.498	23309
Yakut	Han	Korean	-0.00117	0.00028	-4.224	23428
Yakut	She	Korean	-0.00116	0.00039	-2.945	23238
Yukagir	She	Korean	-0.00110	0.00042	-2.611	23248
Chukchi	Tujia	Korean	-0.00098	0.00048	-2.025	23241

Supplementary Table C.27 Admixture f_3 for the Koreans. f_3 statistics of the form f_3(X, Y; Korean) for all populations X in our panel, using SNPs called in DevilsGate2. 30 populations with the lowest statistics are displayed.

Source1	**Source2**	**Target**	**f3**	**SE**	**Z**	**SNPs**
DevilsGate2	Ami	Korean	-0.00766	0.00204	-3.757	9259
DevilsGate2	Lahu	Korean	-0.00752	0.00205	-3.673	9260
DevilsGate2	Kinh	Korean	-0.00666	0.00180	-3.694	9260
DevilsGate2	Dai	Korean	-0.00647	0.00171	-3.778	9259
DevilsGate2	Miao	Korean	-0.00608	0.00164	-3.696	9258
DevilsGate2	Atayal	Korean	-0.00586	0.00245	-2.388	9260
DevilsGate2	Tujia	Korean	-0.00523	0.00152	-3.445	9259
DevilsGate2	She	Korean	-0.00499	0.00167	-2.988	9259
DevilsGate2	Cambodian	Korean	-0.00463	0.00189	-2.445	9259
DevilsGate2	Han	Korean	-0.00430	0.00107	-4.030	9261
DevilsGate2	Thai	Korean	-0.00410	0.00183	-2.236	9260
DevilsGate2	Yi	Korean	-0.00404	0.00159	-2.536	9260

Japanese	irRus	Korean	-0.00361	0.00158	-2.280	4274
Koryak	Ami	Korean	-0.00278	0.00106	-2.631	9284
Itelmen	Tujia	Korean	-0.00272	0.00079	-3.441	9280
Ulchi	Ami	Korean	-0.00269	0.00063	-4.302	9296
Ulchi	Dai	Korean	-0.00264	0.00054	-4.865	9299
Chukchi	Tujia	Korean	-0.00250	0.00065	-3.836	9303
Ulchi	Han	Korean	-0.00247	0.00032	-7.773	9350
Ulchi	Tujia	Korean	-0.00247	0.00043	-5.709	9308
Koryak	Tujia	Korean	-0.00243	0.00072	-3.381	9287
Itelmen	Han	Korean	-0.00243	0.00055	-4.419	9307
Koryak	Kinh	Korean	-0.00240	0.00090	-2.651	9294
Itelmen	Ami	Korean	-0.00225	0.00111	-2.017	9279
Koryak	Han	Korean	-0.00223	0.00052	-4.270	9315
Eskimo	Tujia	Korean	-0.00221	0.00070	-3.162	9300
Nganasan	Tujia	Korean	-0.00218	0.00071	-3.070	9295
Itelmen	Dai	Korean	-0.00216	0.00096	-2.258	9286
Ulchi	Kinh	Korean	-0.00212	0.00056	-3.810	9311
Itelmen	Kinh	Korean	-0.00210	0.00098	-2.144	9289
Ulchi	Atayal	Korean	-0.00208	0.00075	-2.794	9294

Supplementary Table C.28 Admixture f_3 for the Japanese. f_3 statistics of the form f_3(X, Y; Japanese) for all populations X in our panel, using all SNPs. Significant (|Z|>2) statistics are displayed.

Source1	**Source2**	**Target**	**f3**	**SE**	**Z**	**SNPs**
DevilsGate2	Ami	Japanese	-0.00548	0.00218	-2.511	9014
DevilsGate2	Lahu	Japanese	-0.00526	0.00227	-2.316	9012
DevilsGate2	Dai	Japanese	-0.00432	0.00183	-2.362	9013
DevilsGate1	Han	Japanese	-0.00219	0.00092	-2.374	22677

Supplementary Table C.29 Admixture f_3 for the Japanese. f_3 statistics of the form f_3(X, Y; Japanese) for all populations X in our panel, using transversions only. Significant (|Z|>2) statistics are displayed.

Source1	**Source2**	**Target**	**f3**	**SE**	**Z**	**SNPs**
DevilsGate1	Kinh	Japanese	-0.00901	0.00273	-3.307	4412

Supplementary Table C.30 Admixture f_3 for the Japanese. f_3 statistics of the form f_3(X, Y; Japanese) for all populations X in our panel, using SNPs called in DevilsGate1. Significant (|Z|>2) statistics are displayed.

Source1	**Source2**	**Target**	**f3**	**SE**	**Z**	**SNPs**
DevilsGate1	Han	Japanese	-0.00219	0.00093	-2.364	22677

Supplementary Table C.31 Admixture f_3 for the Japanese. f_3 statistics of the form f_3(X, Y; Japanese) for all populations X in our panel, using SNPs called in DevilsGate2. Significant (|Z|>2) statistics are displayed.

Source1	**Source2**	**Target**	**f3**	**SE**	**Z**	**SNPs**
DevilsGate2	Ami	Japanese	-0.00548	0.00217	-2.526	9014
DevilsGate2	Lahu	Japanese	-0.00526	0.00221	-2.382	9012
DevilsGate2	Dai	Japanese	-0.00432	0.00188	-2.303	9013

Supplementary Table C.32 Phenotypes of interest. Results of imputed SNPs with known biological function. Genotype probabilities are color coded: blue for <0.1, red for >0.9 and black for the rest.

Identifier	Gene	Allele0	Allele1	GP Homozygous Allele0	Heterozygous	GP Homozygous Allele1	Category	Comments
MAEA	rs6815464	C	G	0.257	0.743	**0**	Type II diabetes	homozygous for the normal allele G.
PEPD	rs3786897	A	G	0.112	0.749	0.139	Type II diabetes	Undetermined (A is the risk allele)
ZNFAND3	rs9470794	T	C	**0.999**	**0.001**	**0**	Type II diabetes	homozygous for the normal allele T.
GCC1-PAX4	rs6467136	A	G	**0.063**	**0.937**	**0**	Type II diabetes	heterozygous for the risk allele G.
FITM2-R3HDML-HNF4A	rs6017317	T	G	**0.868**	0.131	**0**	Type II diabetes	homozygous for the normal allele
KNCK16	rs1535500	G	T	**0.024**	**0.955**	**0.022**	Type II diabetes	heterozygous for the risk allele T.
ABCC11	rs17822931	C	T	**0.068**	0.388	0.544	Body odour and ear wax type	also an indicator for Asian ancestry.
OPRM1	rs1799971	A	G	0.305	0.652	**0.043**	Alcohol / opioid response	alcohol / opioid and a stronger response.
ADD1	rs4961	G	T	**0.001**	0.185	**0.814**	Salt-sensitive hypertension	Asian populations are polymorphic).
LCT	rs4988235	G	A	**1**	**0**	**0**	Lactose tolerance	Likely to be lactose intolerant as an adult
ALDH2	rs671	G	A	**0.84735**	0.153165	**0**	Alcohol flush	Normal risk of Esophageal Cancer.
EDAR	rs3827760	A	G	0.1356	0.7546	0.1159	Hair and other phenotypic traits	thicker hair as well as shovel-shaped incisors
MC1R	rs885479	G	A	0.192	0.64	0.168	Pigmentation	associated with red hair and skin pigmentation)
SLC24A2	rs26722	C	T	0.508	0.432	**0.06**	Pigmentation	(East Asian populations are polymorphic)
RPL7AP62, SLC24A5	rs1834640	A	G	**0.007**	0.67	0.323	Pigmentation	have the ancestral allele A, which is rare in East Asia.
TYR	rs1042602	C	A	0.722	0.262	**0.015**	Pigmentation	skin and hair pigmentation and the abscence of freckles.
DCT	rs1407995	T	C	**0.839**	0.161	**0**	Pigmentation	most commonly found in East Asians.
KITLG	rs12821256	T	C	**0.997**	**0.003**	**0**	Pigmentation	higher probability of blond hair in Europeans)
OCA2	rs74653330	C	T	**0.9821**	**0.0189**	**0**	Pigmentation	associated with decreased melanin in East Asians.
OCA2	rs1800414	T	C	**0.23943**	0.53135	0.2323	Pigmentation	associated with melanin levels in East Asians)
HERC2	rs12913832	A	G	**0.90511**	**0.09589**	**0.001**	Pigmentation	Brown eye pigmmentation, 80% of the time
SLC45A2	rs16891982	C	G	**0.39341**	0.5438	**0.0592**	Pigmentation	derived. This is typical of non-Europeans.
SLC24A5	rs1426654	A	G	**0.002**	0.77512	0.22486	Pigmentation	derived. This is typical of non-Europeans.

Appendix D Appendix for Chapter 5

D.1 Relationship between potential ABC summary statistics

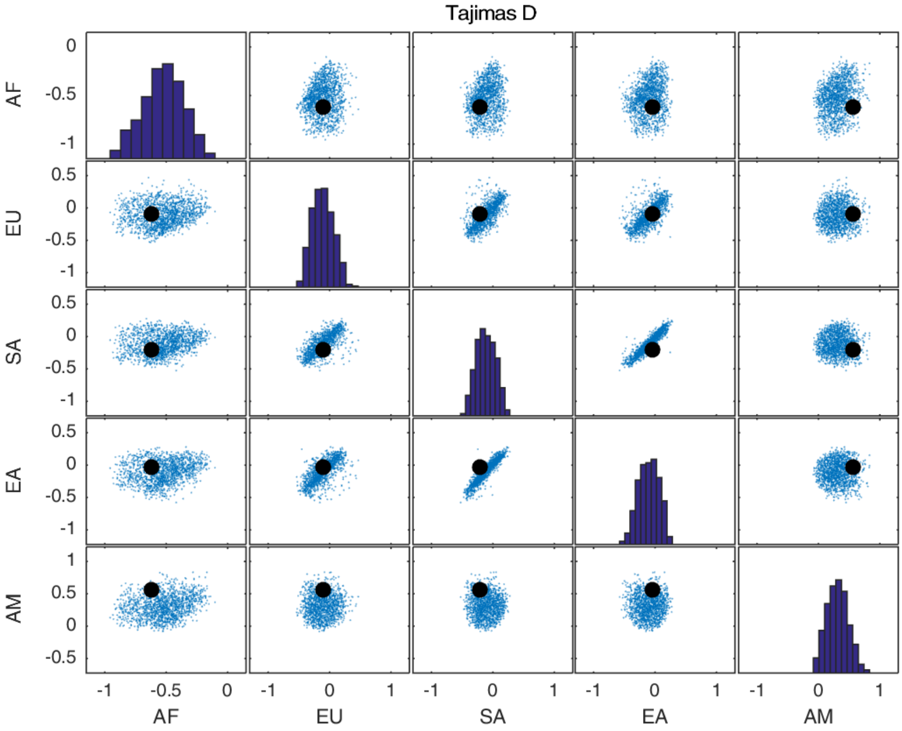

Supplementary Figure D.1 Pairwise plots of mean Tajima's D over continental groups. Each dot represents one of the 64,772 simulations where all sampled cells were populated by present time. Abbreviations are as follows: AF – Africa, EU – Europe, SA – South Asia, EA – East Asia and AM – America, including populations as detailed in Table 5.1. Black dots represent estimates from the 1000 Genomes data (Table 5.2).

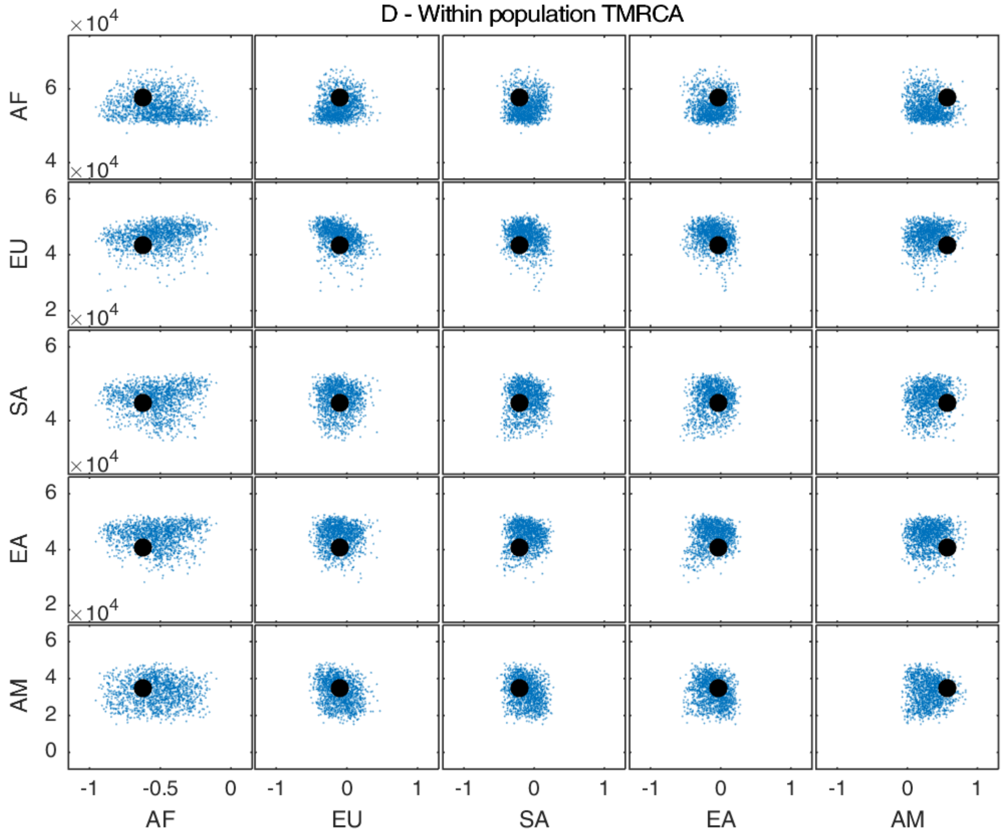

Supplementary Figure D.2 Mean Tajima's D as a function of mean within-population TMRCA over continental groups. Each dot represents one of the 64,772 simulations where all sampled cells were populated by present time. Abbreviations are as follows: AF – Africa, EU – Europe, SA – South Asia, EA – East Asia and AM – America, including populations as detailed in Table 5.1. Black dots represent estimates from the 1000 Genomes data (Table 5.2).

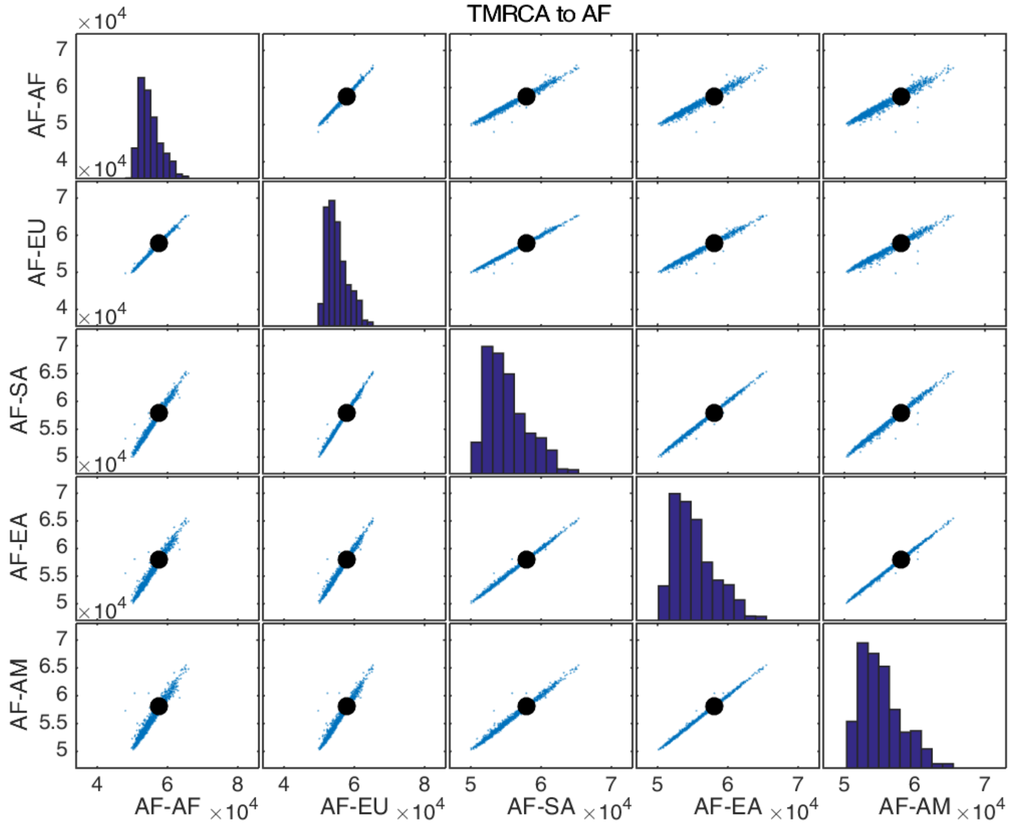

Supplementary Figure D.3 Mean TMRCA between Africa (AF) and the other continental groups. Each dot represents one of the 64,772 simulations where all sampled cells were populated by present time. Abbreviations are as follows: AF – Africa, EU – Europe, SA – South Asia, EA – East Asia and AM – America, including populations as detailed in Table 5.1. Black dots represent estimates from the 1000 Genomes data (Table 5.2).

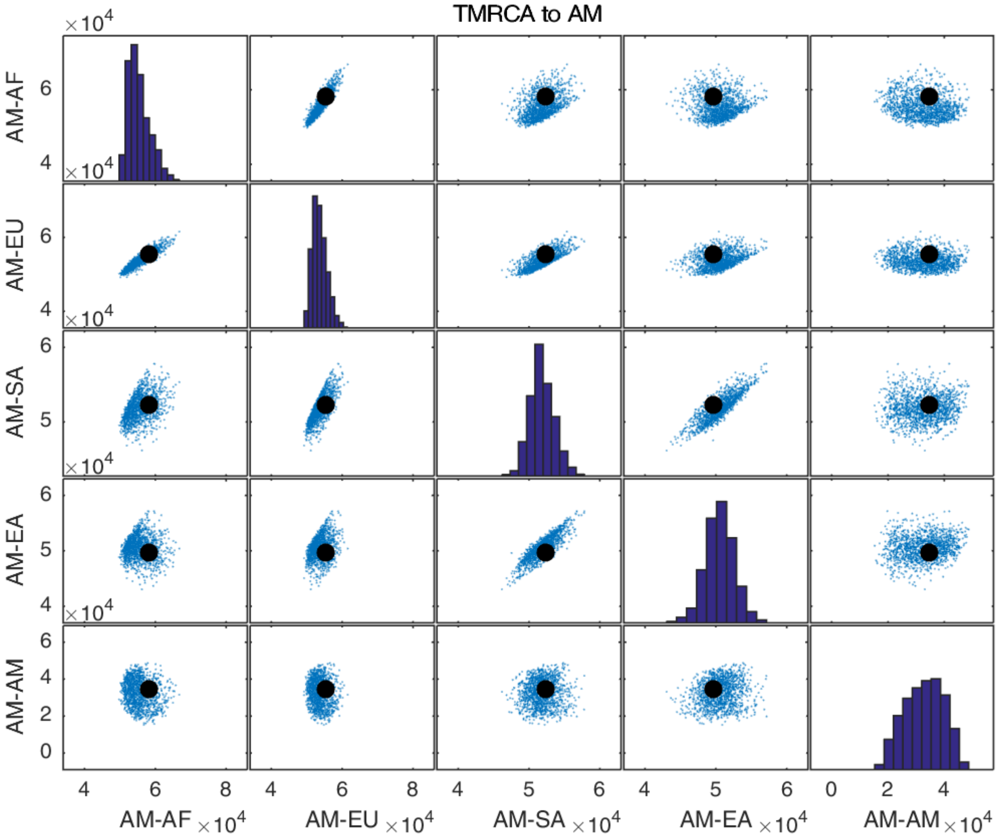

Supplementary Figure D.4 Mean TMRCA between America (AM) and the other continental groups. Each dot represents one of the 64,772 simulations where all sampled cells were populated by present time. Abbreviations are as follows: AF – Africa, EU – Europe, SA – South Asia, EA – East Asia and AM – America, including populations as detailed in Table 5.1. Black dots represent estimates from the 1000 Genomes data (Table 5.2).

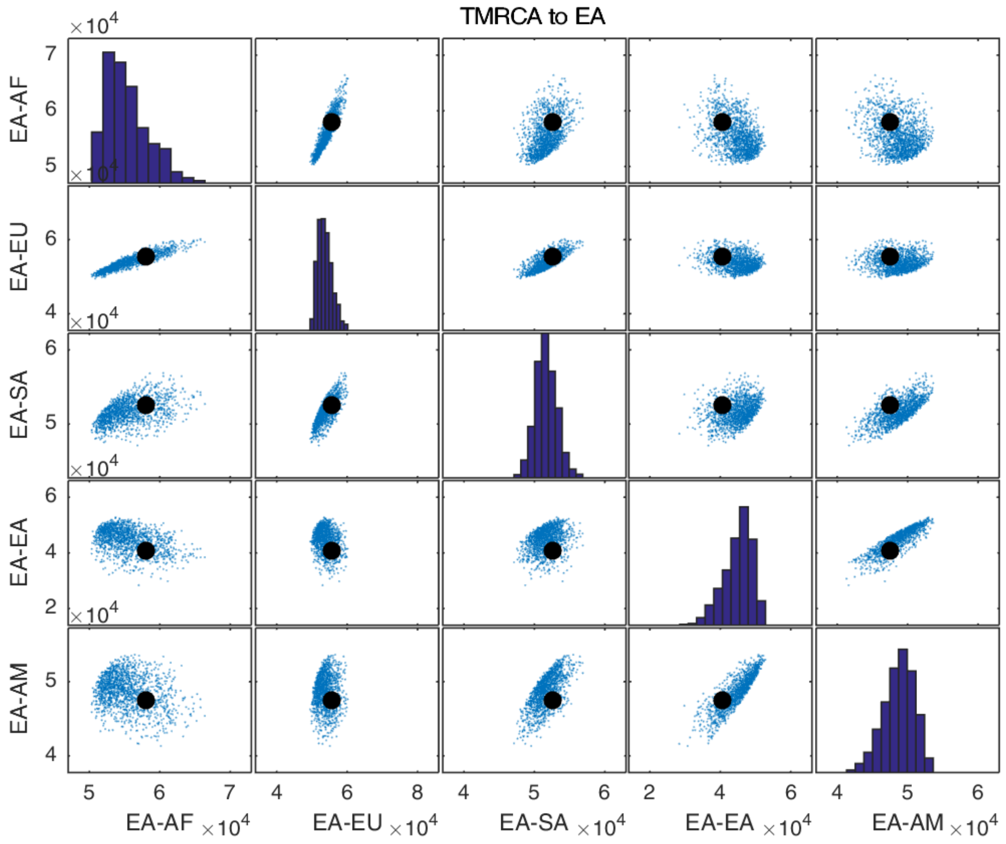

Supplementary Figure D.5 Mean TMRCA between East Asia (EA) and the other continental groups. Each dot represents one of the 64,772 simulations where all sampled cells were populated by present time. Abbreviations are as follows: AF – Africa, EU – Europe, SA – South Asia, EA – East Asia and AM – America, including populations as detailed in Table 5.1. Black dots represent estimates from the 1000 Genomes data (Table 5.2).

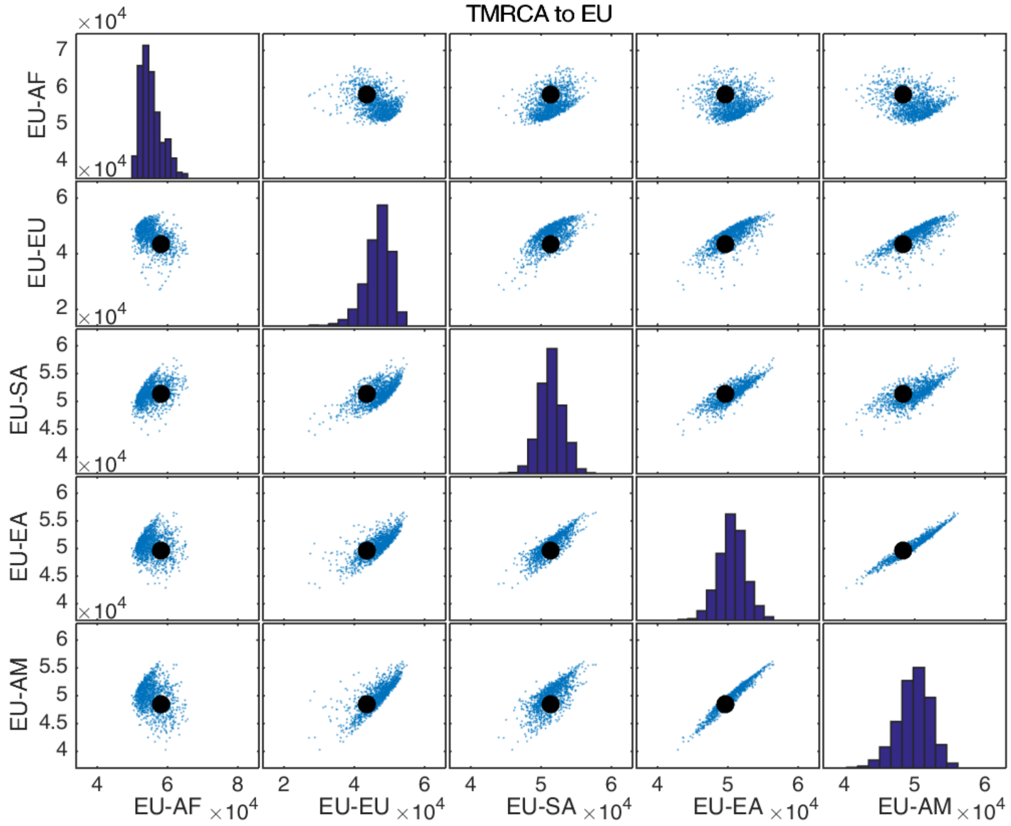

Supplementary Figure D.6 Mean TMRCA between Europe (EU) and the other continental groups. Each dot represents one of the 64,772 simulations where all sampled cells were populated by present time. Abbreviations are as follows: AF – Africa, EU – Europe, SA – South Asia, EA – East Asia and AM – America, including populations as detailed in Table 5.1. Black dots represent estimates from the 1000 Genomes data (Table 5.2).

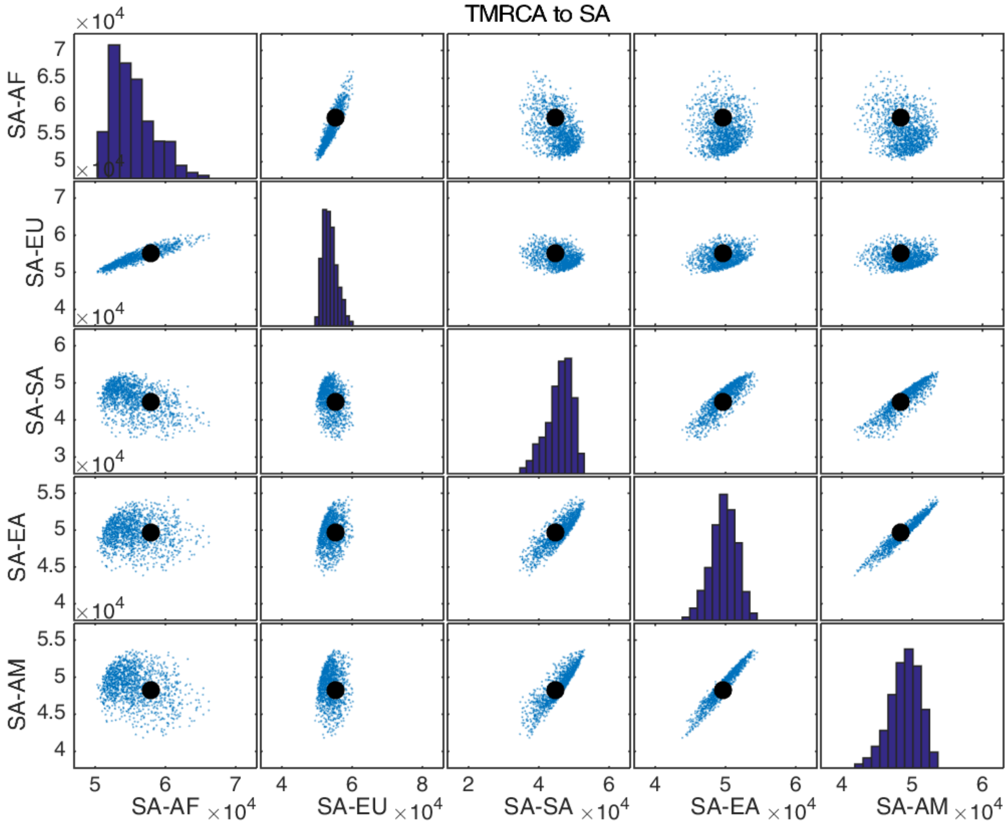

Supplementary Figure D.7 Mean TMRCA between South Asia (SA) and the other continental groups. Each dot represents one of the 64,772 simulations where all sampled cells were populated by present time. Abbreviations are as follows: AF – Africa, EU – Europe, SA – South Asia, EA – East Asia and AM – America, including populations as detailed in Table 5.1. Black dots represent estimates from the 1000 Genomes data (Table 5.2)

Appendix E Appendix for Chapter 6

E.1 Fit using SSE for thalassemia

We initially investigated fitting the distribution of thalassemia variants using the same, frequency-based error function as for sickle-cell disease (6.4.3.1). The resulting origins for Cd39 (Supplementary Figure E.2) were similar to, but noisier than those inferred using the classification error presented in the main text. Furthermore, since the Cd39 frequencies were higher in North Africa than in Southern Europe (Table 6.6), the former was a more likely origin than the latter. For FSC-6, on the other hand, the obtained distribution was fundamentally different, the complement of that inferred for Cd39 (Supplementary Figure E.3). It was absent in Europe and western North Africa, near the sampled regions, as opposed to the North African origin inferred using classification error. After observing the frequencies, we found that this behaviour was driven by the low frequencies of the variant in the data, which lead to the complete absence of FSC-6 in sampled countries appear as an outcome favoured over frequencies that were too high (Supplementary Figure E.1). For IVS-I-1, we also obtained fundamentally different distributions using the two error functions. Classification error implied an origin in Eastern Europe, whereas the frequency-based error function was undetermined, apart from showing that the origin should not be in North Africa (Supplementary Figure E.4). Again this is due to the low frequencies of the variant which resulted in a marginal change between its presence or absence in Europe; only the very low frequencies in North Africa were picked up.

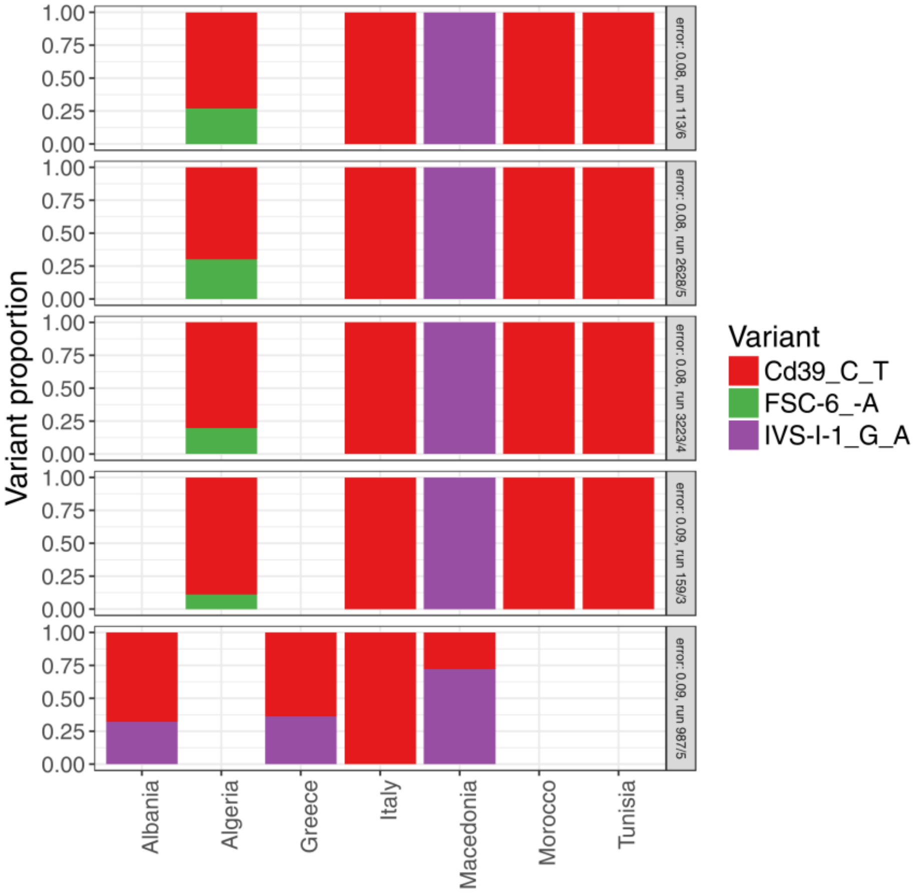

Supplementary Figure E.1 Distribution of thalassemia variants in monitored countries from the five sets of origins with the lowest frequency-based error. In countries not reached by any variant, no data is shown.

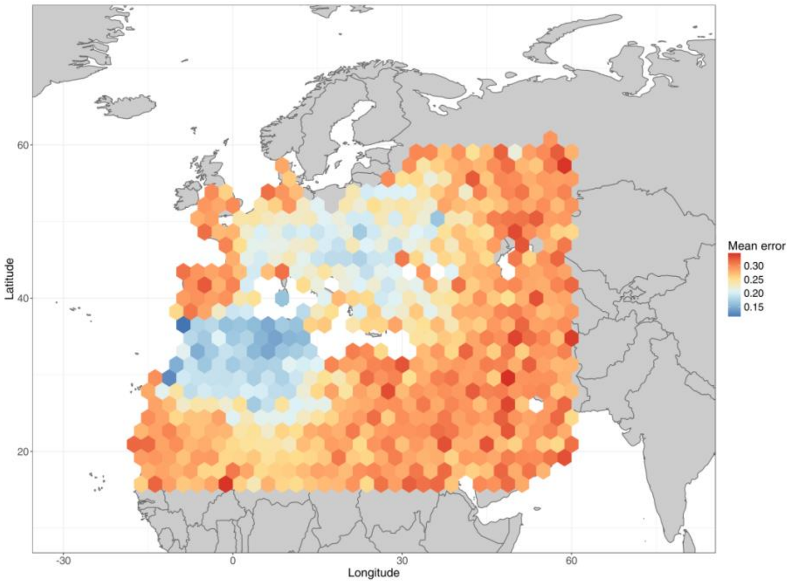

Supplementary Figure E.2 Most likely origins for the Cd39 variant using the frequency-based error function. The figure shows the mean classification error (sum of misclassified variantsper country) for simulations where the variant originated from that cell, averaged over 2.5° bins in both latitude and longitude.

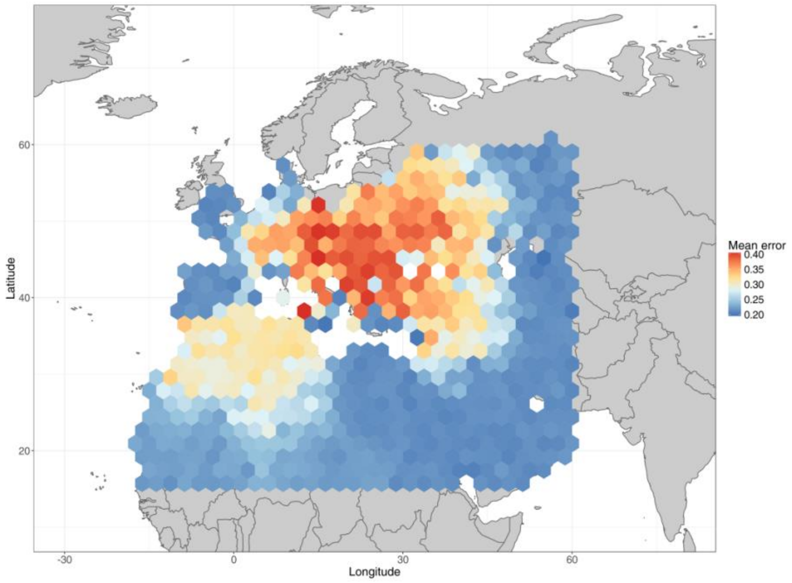

Supplementary Figure E.3 Most likely origins for the FSC-6 variant. The figure shows the mean classification error (sum of misclassified variants per country) for simulations where the variant originated from that cell, averaged over 2.5° bins in both latitude and longitude.

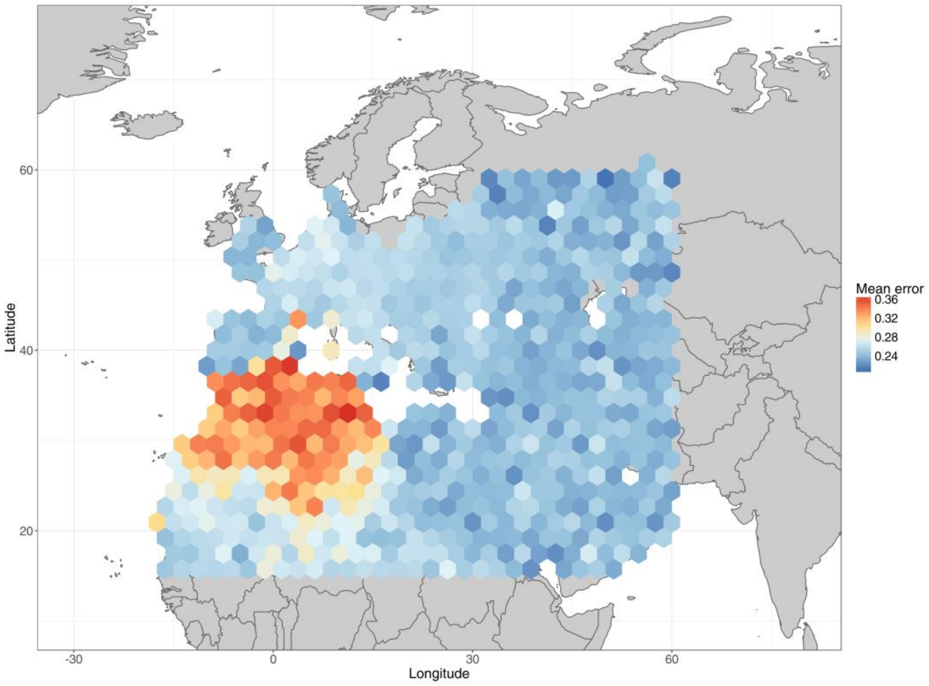

Supplementary Figure E.4 Most likely origins for the IVS-I-1 variant. The figure shows the mean classification error (sum of misclassified variants per country) for simulations where the variant originated from that cell, averaged over 2.5° bins in both latitude and longitude.

E.2 Sensitivity analysis

To investigate how sensitive our results are, I reran the best-fitting set of spatial origins for sickle-cell disease (Figure 6.10) using a range of parameters. I recorded the number of individuals per layer in each country in our dataset and calculated the proportion of individuals carrying the derived allele, as well as the prevalence of the most common variant among all derived variants. Since the distribution of variants we obtained for thalassemia was qualitatively similar to that for sickle-cell disease, I expect the results from the sensitivity analysis to transfer. Regarding the single-origin hypothesis of sickle-cell disease, multiple starting times and demographic parameters were explored and the selection coefficient proved to not influence the spread of haplotypes (E.2.1). Therefore, those results should also not be affected by changes in the estimates of these parameters.

E.2.1 Selection coefficient

I first focused on the selection coefficient *s* and explored values between 0.05 and 0.25, since the relative fitnesses of $w_0 = 0.868$ for the ancestral and $w_1 = 1.0$ for all derived variants, which we used for our main results correspond to a selection coefficient $s = \frac{1}{w_1} - 1 \approx 0.152$. We found that although the prevalence of the selected trait depends on the selection coefficient, as expected, the relative proportion of the major variant is largely independent. Furthermore, the presence of the selected trait was also hardly dependent on the selection coefficient, implying that the speed of the spatial spread was also not sensitive to it.

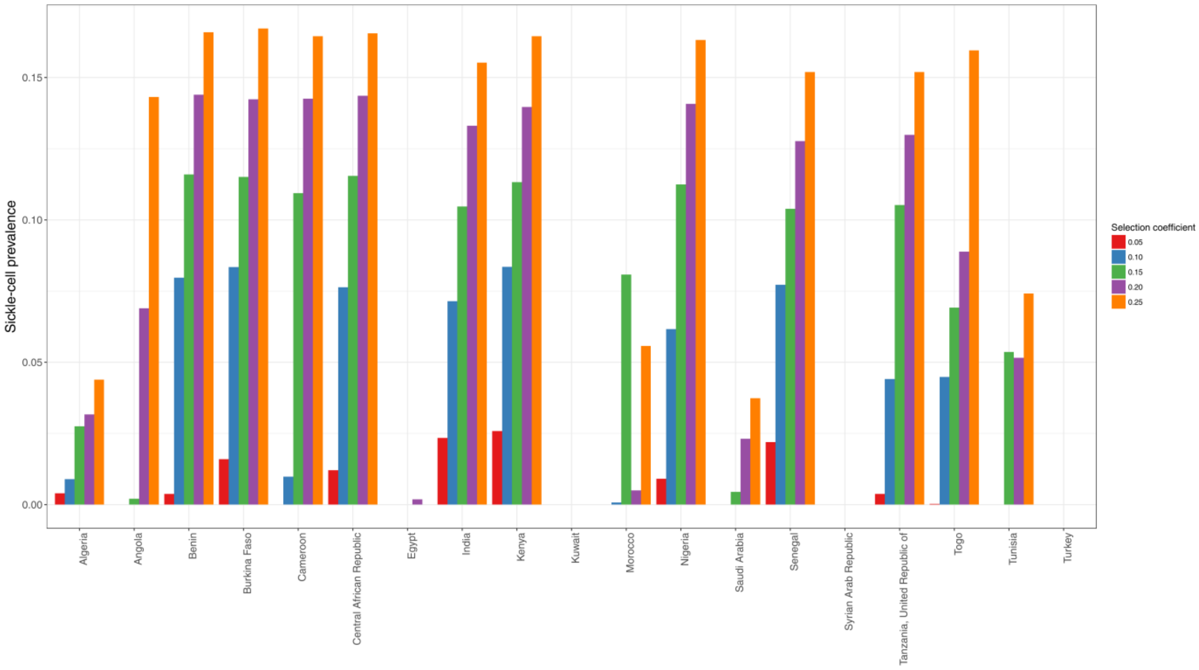

Supplementary Figure E.5 Prevalence of the sickle-cell trait in countries in our dataset, for five different selection coefficients (0.05, 0.1, 0.15, 0.2 and 0.25).

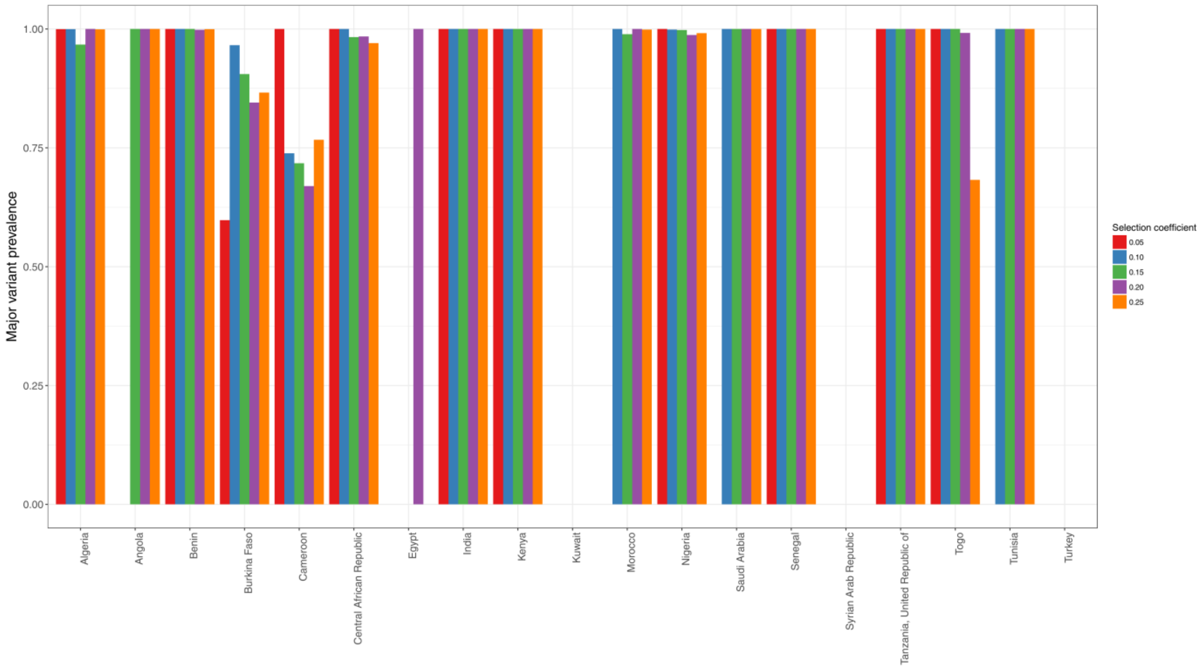

Supplementary Figure E.6 Prevalence of the major sickle-cell variant in countries in our dataset, for five different selection coefficients (0.05, 0.1, 0.15, 0.2 and 0.25).

E.2.2 Demographic parameters

I then examined whether alternative, plausible demographic parameters result in similar behaviours. I explored the three best-fitting parameter sets from Raghavan et al[12] (Table 6.1) and found that for countries with an established presence of malaria, neither the prevalence of the derived allele nor that of the major variant varied considerably. For countries at the edge of the ranges of variants, particularly in North African, the demographic parameters sometimes made a difference as they influenced how far a variant could spread: out of those explored, parameter set 2 resulted in the quickest spread.

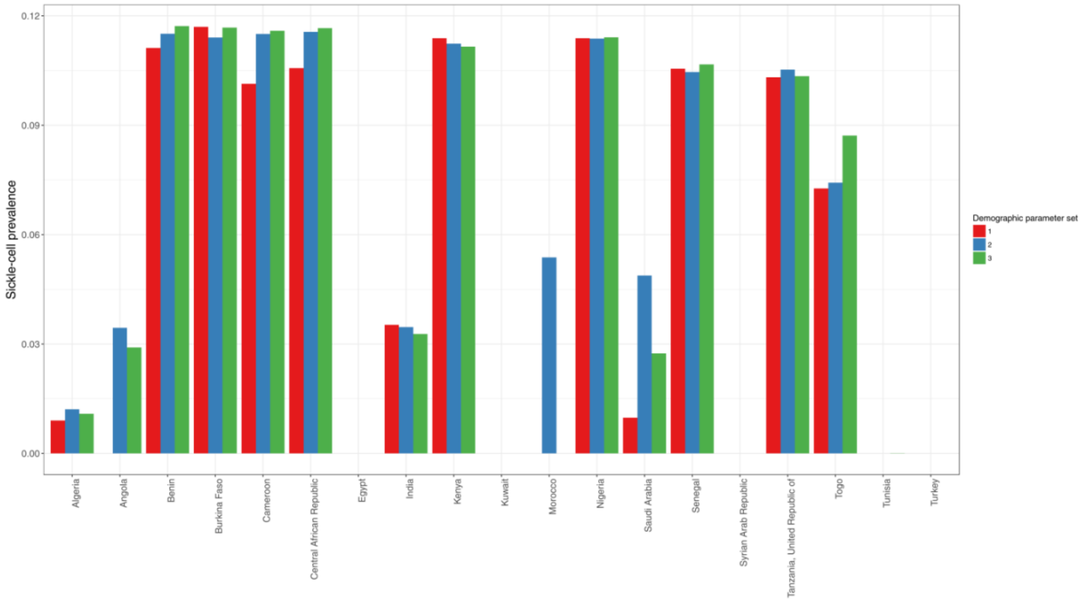

Supplementary Figure E.7 Prevalence of the sickle-cell trait in countries in our dataset, for the three best-fitting parameter sets from Raghavan et al[12] (Table 6.1).

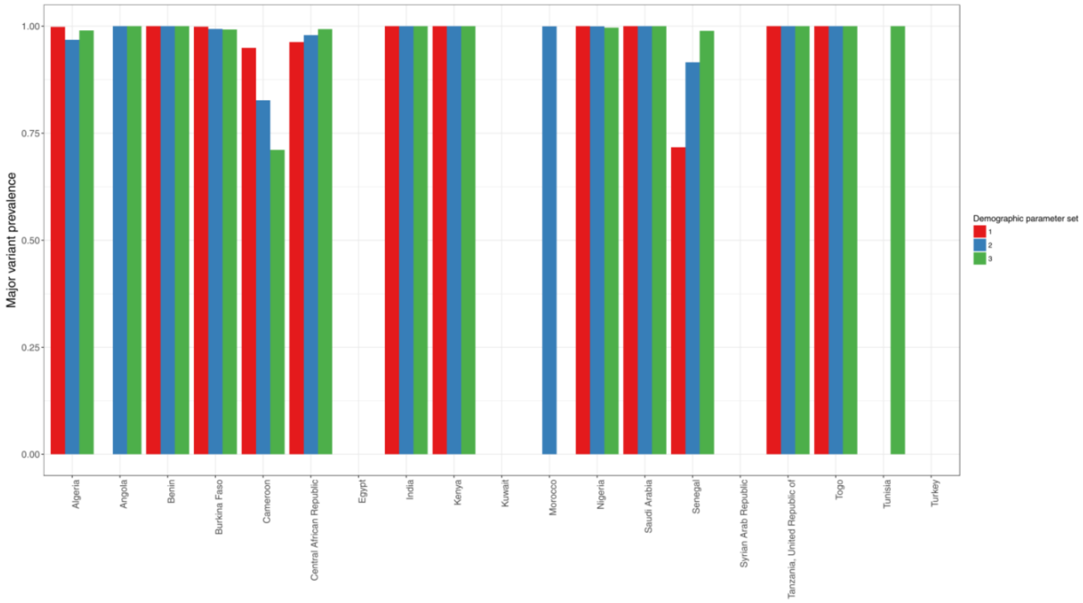

Supplementary Figure E.8 Prevalence of the major sickle-cell variant in countries in our dataset, for the three best-fitting parameter sets from Raghavan et al[12] (Table 6.1).

E.2.3 Starting time of selection

I finally looked at the starting time of selection, considering 100 to 500 generations ago (2,500 years ago to 12,500 years ago), in steps of 100 generations (2,500 years). The prevalence of sickle-cell disease in some countries was sensitive to this quantity. This is not surprising, given that the time it takes for the variant to spread on such large spatial scales, encompassing a whole continent, is on the same order of magnitude as our parameter sweep. However, the proportion of the major variant within derived variants was robust to this parameter, although with sensitivity through the presence of the protective variant.

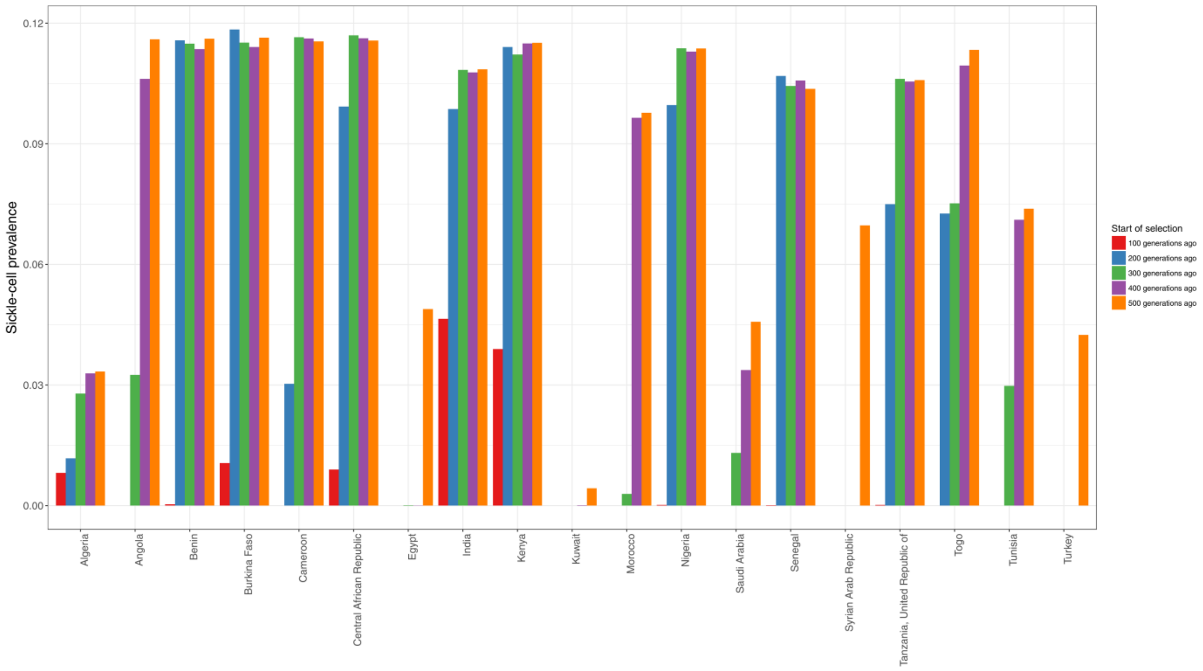

Supplementary Figure E.9 Prevalence of the sickle-cell trait in countries in our dataset, for five starting times of selection (100 to 500 generations ago, in 100 generation steps).

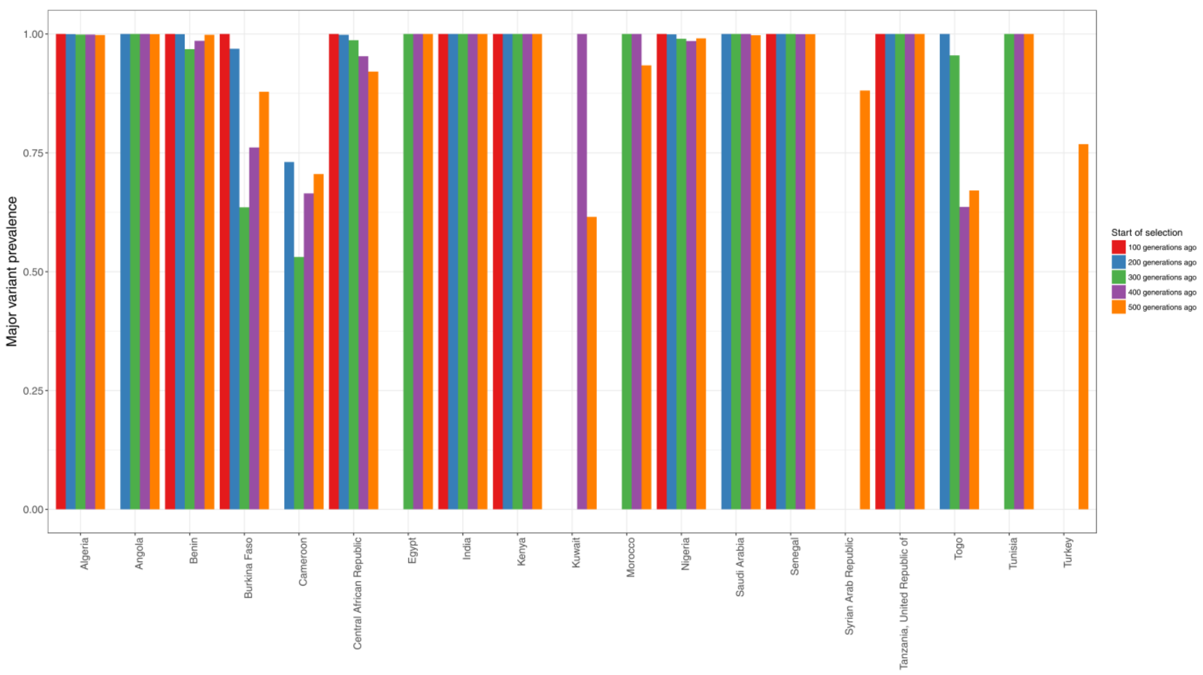

Supplementary Figure E.10 Prevalence of the major sickle-cell variant in countries in our dataset, for five starting times of selection (100 to 500 generations ago, in 100 generation steps).